UNIVERSITÀ
DEGLI STUDI
FIRENZE

Ph.D. in

Agricultural and Environmental Sciences

CYCLE XXXVIII

Purple non-sulfur bacteria: ideal microbial cell factories for the biotransformation of agro-industrial wastes into high-added-value molecules

Academic Discipline (SSD) AGRI-08/A

Doctoral Candidate

Dott. Bernabò Luca

Supervisor

Prof.ssa Granchi Lisa

Coordinator

Prof. Viti Carlo

2022/2025

Table of contents.

PART I

Introduction

Chapter I

Microbial Biorefineries: From Biomass to Biofuels and Biopolymers

1.1 The Biorefinery Concept

In recent decades, the rapid growth of the global population and the consequent increase in urbanization have led to a significant rise in the generation of organic solid waste, which currently represents one of the largest categories of waste produced worldwide. Additionally, the intensive exploitation of finite natural resources, such as petroleum, is seriously threatening the long-term sustainability of our economic system (Munir et al., 2018).

Traditionally, organic solid waste has been either incinerated or disposed of in landfills, options that are both environmentally harmful. Incineration, for instance, results in the emission of various toxic compounds, including sulfur dioxide (SO_2), nitrogen dioxide (NO_2), carbon monoxide (CO), carbon dioxide (CO_2), as well as the production of highly toxic ash residues (Shah et al., 2022). On the other hand, landfilling leads to the anaerobic decomposition of organic waste, producing large quantities of methane (CH_4), a greenhouse gas (GHG) with a global warming potential 28 times higher than that of CO_2 over 100 years. It is estimated that approximately 11 % of anthropogenic methane emissions originate from landfills. Furthermore, landfill leachate, resulting from the decomposition of organic matter, can contaminate groundwater and act as a vector for disease-causing pathogens (Pengadeth et al., 2024).

A considerable portion of organic solid waste is composed of agro-industrial residues, which arise from losses occurring at various stages of the agri-food supply chain. These losses are typically due to excessive processing, the generation of by-products, transportation inefficiencies, and poor production planning. Despite being produced in large quantities, the absence of viable recovery and reuse strategies means that most agro-industrial waste is improperly managed, predominantly ending up in landfills (Freitas et al., 2021).

To address these environmental challenges, it is necessary to transition from the traditional linear economic model of extract-produce-use-dispose to a circular economy. The circular economy aims to maximize resource efficiency by reducing waste,

conserving raw materials, and establishing closed loops of products and materials. This model also provides social, economic, and environmental benefits (Shah et al., 2022).

Within this context, the concept of biorefinery emerges. A biorefinery is an integrated industrial system that combines various processes to produce a wide range of high-value products from biomass and organic solid waste using different types of conversion technologies. Biorefineries are designed to generate minimal waste, thus reducing the overall environmental burden (Ragini et al., 2025; Shah et al., 2022).

Microorganisms play a key role in biomass conversion processes within biorefineries. They can utilize organic and inorganic compounds present in plant-based materials as sources of carbon and electrons for growth and reproduction. Through their metabolic activities, microorganisms transform organic matter into other compounds, which may be waste products for them but are valuable for humans, such as biofuels and biopolymers. Additionally, they can produce commercially important secondary metabolites, including enzymes, pigments, antibiotics, and vitamins (Baral et al., 2018; Paes & Almeida, 2014).

Hence, microorganisms can be harnessed as true "living factories" capable of converting biological waste into useful products, contributing to the development of sustainable and circular biorefinery systems.

1.2 Microorganisms: Key Players in Biorefinery Technologies

Since ancient times, humanity has recognized the value of microorganisms, particularly for their role in the transformation of plant biomass. A notable example is alcoholic fermentation, which has been used for millennia in the production of alcoholic beverages (Decker et al., 2023). Today, the connection between microbiology and the valorization of organic residues is more relevant than ever, especially in the context of sustainability and technological innovation.

Microorganisms offer significant advantages: they grow rapidly, can be easily isolated, and enable the efficient recovery of valuable compounds. In addition, their vast diversity, largely still unexplored due to the limitations of conventional cultivation techniques, represents a major scientific opportunity (Saini & Mishra, 2024).

This microbial richness opens up new pathways for developing bioproducts and biochemicals, with applications in key sectors such as food, energy, and healthcare. In this context, microorganisms emerge as key players in bioeconomy, contributing to the creation of a more sustainable future and the enhancement of human well-being.

Microorganisms, owing to their remarkable metabolic versatility, can valorize waste-derived raw materials through a variety of biochemical pathways. Among these, enzymatic hydrolysis (mediated by cellulases, hemicellulases, pectinases, and ligninases) facilitates the depolymerization of lignocellulosic substrates into fermentable sugars. This process can be complemented by fermentation techniques, aerobic and anaerobic digestion, and transesterification routes, all conducted under tightly controlled operational conditions (Gaur et al., 2024; Thapa et al., 2020).

These microbial processes enable the synthesis of a broad spectrum of high-value compounds, including simple sugars, fatty acids (such as arachidonic acid and γ-linolenic acid), organic acids, and biofuels. In addition, microbial metabolism yields further value-added products such as pigments, amino acids, proteins, and polymers, which find diverse applications across the pharmaceutical, nutraceutical, food, feed, cosmetic, and biopolymer industries (Gaur et al., 2024).

The target compounds are subsequently recovered through sequential extraction techniques, which allow for the efficient separation of desired products from by-products, thereby maximizing overall process yield and efficiency (Gaur et al., 2024).

Among the most widely utilized microorganisms in the biorefinery of organic residues are, without doubt, microalgae, fungi, and bacteria.

1.3 Biofuels production from renewable resources using microorganisms

The continuous intensification of human activities, particularly in the industrial and transport sectors, has led to a growing reliance on fossil-based fuels. These non-renewable resources not only face depletion but also contribute significantly to environmental degradation. Consequently, the scientific community has increasingly focused its attention on the exploration of alternative energy sources, such as biofuels. (Trivedi & Joshi, 2025).

The term biofuel generally refers to liquid or gaseous fuels produced from biomass through processes that may involve thermochemical conversion or biological pathways, the latter relying on the metabolic activity of various microorganisms (Melin et al., 2022). Biological strategies for biofuel production include fermentation, anaerobic digestion, and photobiological processes, through which microorganisms such as bacteria, yeast, filamentous fungi, algae, and cyanobacteria convert carbohydrates, lipids, or lignocellulosic substrates into fuels such as bio-ethanol, bio-butanol, bio-diesel, bio-methane, or bio-hydrogen (bio-H_2) (Gaur et al., 2024).

Biofuels are categorized into different generations based on the type of biomass used as feedstock and the technologies applied in their production. First-generation biofuels are derived from edible biomass, whereas second-generation biofuels utilize non-food-based feedstocks. Third-generation biofuels involve the use of microorganisms as direct biofuel producers, while fourth-generation biofuels rely on genetic engineering strategies to enhance production efficiency (Pandey et al., 2019). Third-generation biofuels offer significant advantages over previous generations, including higher biomass productivity compared to agricultural crops and the ability to cultivate microbial biomass on marginal lands, such as non-arable or saline environments, where traditional agriculture is not viable (Trivedi & Joshi, 2025).

Microbially derived biofuels can exist in both liquid and gaseous forms. Liquid biofuels offer practical advantages such as ease of storage, transport, and direct utilization in existing vehicles, including cars, lorries, trains, and aircraft. In contrast, gaseous biofuels require energy-intensive processes like compression or liquefaction to reduce their volume, making them more suitable for localized use in stationary systems. The replacement of fossil fuels with selected liquid biofuels is considered technically feasible, as it allows for the continued use of current infrastructure and engine technologies with minimal adaptation (Antoni et al., 2007).

1.4 Bioplastics production from renewable resources using microorganisms

Plastics are a diverse group of synthetic polymers that are mainly derived from fossil fuels. Their industrial-scale production began in the 1950s, with an annual output of around two million tonnes. Since then, global plastic production has grown exponentially, reaching 400.3 million tonnes per year by 2022. Projections indicate that this figure could double within the next two decades (Daggubati et al., 2025; Walker & Fequet, 2023).

Although plastic materials have significantly contributed to improving the quality of life across numerous sectors, their low unit cost and high versatility have led to excessive and often unsustainable use (Schmaltz et al., 2020). As a result, there has been a massive accumulation of plastic waste, with significant environmental and public health implications. Currently, it is estimated that approximately 80 % of plastics produced are not recycled, ending up in landfills or being released into the environment, where they persist for extremely long periods due to their non-biodegradable nature (Xuyang et al., 2025).

Unlike biodegradable materials, most plastics do not break down through microbial activity; instead, they fragment over time when exposed to environmental factors. Ultraviolet (UVB) radiation is one of the main agents of photochemical degradation, altering the structure of plastic polymers and promoting the formation of smaller and smaller fragments. This process, known as photodegradation, leads to the formation of microplastics, particles smaller than 5 mm, which present a significant challenge for waste management and treatment systems (Hale et al., 2020; Xuyang et al., 2025).

Compared to larger plastic debris, microplastics are characterized by greater environmental persistence, more challenging detection, and an enhanced ability to penetrate food chains. Their presence has been documented across a wide range of ecosystems and organisms, highlighting the potential risk to both animal and human health (Tirkey & Upadhyayet, 2021; Xuyang et al., 2025).

Therefore, the current challenge lies in identifying alternative materials that can perform similarly to conventional, petrochemical-based plastics while avoiding the associated drawbacks. These materials must be economically sustainable and derived from renewable sources.

Bioplastics are a potential solution to conventional plastics. Thanks to their biodegradability and/or biocompatibility, they offer several advantages, including a lower carbon footprint, reduced energy costs during production, and decreased release of persistent waste into the environment. Although bioplastics are a viable alternative to conventional plastics, their production is still in its infancy. The main limitation to their widespread adoption is the production cost, which remains uncompetitive compared to traditional plastics (Alias et al., 2022).

Consequently, current research focuses on using low-cost (ideally zero-cost) raw materials, such as agro-industrial waste, to produce various types of bioplastics (Chaudry et al., 2025; Montiel-Corona & Buitrón, 2021). Like the classification applied to biofuels, bioplastics can be produced from first-, second- and third-generation feedstocks. Second- and third-generation bioplastics are of particular interest in the context of this thesis as they are obtained through microbial fermentation processes (Martínez-Burgos et al., 2023)

Microorganisms can be exploited to produce bioplastics in two main ways: by producing monomers that are subsequently polymerized, or by directly synthesizing biopolymers, which are then extracted from the cells.

Biomonomers produced via the microbial fermentation of biomass can be broadly classified into two categories: aliphatic and aromatic. Aliphatic biomonomers include lactic acid, dicarboxylic acids (e.g., succinic, fumaric, and malic acids), ω-amino acids (e.g., γ-aminobutyric acid, or GABA), diols, and diamines. Aromatic biomonomers include shikimic acid, phenylpropanoids, and benzoic acid derivatives (Kawaguchi, Ogino, & Kondo, 2017).

Some microorganisms can synthesize biopolymers directly through fermentative processes, either as part of their natural metabolic repertoire or via genetic engineering strategies. The production of biopolymers by microbes is preferable to monomer synthesis as it avoids the use of additional, costly processes involving environmentally hazardous chemical catalysts (Lee et al., 2011). The main categories of biopolymers obtainable via microbial fermentation include polysaccharides (bacterial cellulose, levan, microbial hyaluronic acid, xanthan gum, microbial β-glucan, alginate, pullulan, and chitosan); polyamides (poly-γ-glutamic acid, γ-PGA); and polyesters (polyhydroxyalkanoates, PHA) (Nambiar et al., 2024; Reshmy et al., 2021; Sharma et al., 2024).

1.5 Limitations and Perspectives of Microbial Biomass Fermentation for Biofuels and Bioplastics

Transitioning from the current linear economic model to a circular one is crucial in mitigating greenhouse gas emissions and limiting their negative impact on climate change. Biorefineries are currently the most tangible and effective tool for achieving this objective. These facilities convert biomass into energy, bioplastics, and other valuable products, thereby reducing the release of potentially harmful substances into the environment and benefiting ecosystems, human, and animal health.

Microorganisms are central to this process; as true “living factories”, they transform organic waste into biofuels, bioplastics, enzymes, and organic acids (Monclaro et al., 2024). However, despite the promising potential of microbial metabolism in biorefineries, its large-scale industrial implementation is hindered by several limitations. The high cost and complexity of feedstock pretreatment is foremost among these limitations. For instance, lignocellulosic biomass is highly recalcitrant due to the crystalline nature of cellulose, its encapsulation within hemicellulose, its high degree of polymerization, its small particle size, and its protective lignin layer. This structural complexity significantly

reduces the surface area available for enzymatic hydrolysis, thereby decreasing overall process efficiency (Reshmy et al., 2021).

Although pretreatment methods improve the digestibility of lignocellulosic biomass, physical and chemical approaches are often associated with high operational costs and considerable environmental risks due to the use of potentially hazardous substances. Consequently, biological pretreatments are becoming increasingly popular. These methods exploit enzymes, such as cellulases, hemicellulases, and ligninases, which are secreted by various types of microorganisms and break down the biomass, releasing fermentable sugars that can be converted into high-value compounds (Mankar et al., 2021; Sharma, Xu, & Qin, 2019).

Since a single microbial strain cannot provide all the required enzymes, co-cultivation of bacteria and fungi is being investigated. These systems are more effective than monocultures due to their metabolic complementarity and greater tolerance to inhibitors (Sharma, Xu, & Qin, 2019). Complementary strategies include metabolic engineering, which transfers the ability to degrade biomass into strains lacking this function, and the use of food waste and agro-industrial wastewaters. These substrates are less recalcitrant than lignocellulosic biomass, rich in fermentable sugars, and do not compete with agricultural resources intended for food or feed, since they are by-products of existing processes (Dahiya et al., 2018; Nazzaro et al., 2018).

Another limitation is that microorganisms do not naturally produce biofuels or bioplastics in significant amounts. Genetic and metabolic engineering can optimize metabolic fluxes, reduce undesired metabolic by-products, and increase yields to near-stoichiometric levels. In this context, genome-scale metabolic models (GEMs) are innovative tools for *in silico* simulating cellular metabolism, identifying bottlenecks, and predicting the impact of genetic modifications or substrate availability. Analytical tools such as Flux Balance Analysis (FBA) can be used to optimize metabolic flux towards desired products, minimize the formation of unwanted by-products, and improve process efficiency (Gu et al., 2019; Van der Hauwaert et al., 2024).

Finally, the choice of microorganism is critical. Among the most promising candidates are purple non-sulfur bacteria (PNSB), which exhibit remarkable metabolic versatility. Notably, they can produce key metabolites such as bio-H_2 and PHA. Under specific operational conditions, these microorganisms can produce both bio-H_2 and PHA simultaneously, enabling the integrated generation of energy and materials in a single biological process. Their unique combination of metabolic flexibility and ability to

valorize waste substrates positions PNSB as key players in the development of sustainable, multifunctional biorefineries consistent with the principles of the circular economy and ecological transition (Montiel-Corona & Buitrón, 2021).

Chapter II

Hydrogen Production via Biological Processes

2.1 A Brief Introduction to Hydrogen as an Energy Carrier

H_2 is the most abundant and lightest element in the universe, accounting for around 90 % of visible matter. On Earth, however, it is not found in its free molecular form but is always chemically bound to other elements to form substances such as water, natural gas, and petroleum (Abdin et al., 2020). Molecular H_2, which is necessary for energy production, only occurs naturally in environments such as volcanic emissions, fumaroles, and petroleum seeps (Milkov, 2022). Consequently, there are no H_2 deposits comparable to those of fossil fuels. To be used, H_2 must first be extracted from the compounds in which it is found through processes that require energy input (Nikolaidis & Poullikkas, 2017).

Using H_2 as a fuel has significant advantages over conventional fossil sources. Firstly, the energy content of H_2 per unit of mass is approximately three times higher than that of petrol (Abdin et al., 2020). Furthermore, when it is burned, it produces only water vapor and no CO_2, making it environmentally clean (Xu et al., 2022). However, it also has certain disadvantages. Due to its extremely low atomic mass (it is the lightest element in the periodic table), H_2 has a low energy density per unit of volume. This means that significantly larger volumes are required to obtain the same amount of energy as with other fuels. This has important implications for infrastructure, necessitating the use of larger or higher-flow pipelines, as well as larger storage tanks (Cavaliere, 2025).

To overcome these limitations, H_2 can be compressed or liquefied, or converted into H_2-based fuels with a higher energy density. However, such processes, as well as the potential reconversion of hydrogen into energy, result in efficiency losses throughout the energy cycle (Cavaliere, 2025).

To fully understand the role that H_2 can play in future sustainable energy systems, it is important to emphasize that it is an energy carrier, not a primary energy source. Primary energy sources are natural resources that can be used directly for energy production. Examples of these include fossil fuels, such as coal, crude oil, and natural gas, which originate from the transformation of organic matter over millions of years, as well as renewable sources such as sunlight, wind, flowing water, and geothermal heat, which are naturally replenished. Nuclear energy is also considered a primary source because it

harnesses the energy contained within the nuclei of atoms, particularly uranium (Aba et al., 2024; Matias & Devezas, 2007).

By contrast, an energy carrier is a means through which energy can be stored, transported, and released as required. H_2 is considered an energy carrier because it does not occur naturally and must be produced from a primary energy source using an additional energy source. Another classic example of an energy carrier is electricity, which is generated from primary sources and then transmitted and distributed for end use (Aba et al., 2024).

Due to its nature as an energy carrier, H_2 can be a renewable energy storage system. One of the major problems of renewable energy is, in fact, its "non-programmability" characteristic. The production of renewable energy depends on natural phenomena, such as sunlight or wind power, which cannot be managed or predicted with absolute certainty, making constant production impossible. Intermittency in renewable energy production is a significant challenge for electricity grid operators, who must at all times ensure a perfect balance between energy production and demand (Arsad et al., 2022; Cavaliere, 2025).

Renewable energy can be stored in the form of H_2 at peak production times. This H_2 can then be converted back into electricity through fuel cells, turbines, or engines when renewable energy production is low, ensuring a constant energy supply. H_2 can also be stored and transported cost-effectively over long distances using existing natural gas infrastructure (Schrotenboer et al., 2022).

Using H_2 can pose risks, particularly at large scales, as it often requires specific equipment and procedures for handling. The H_2 molecule is extremely small, which increases the risk of leakage through seals and pipes, as well as structural failure. While H_2 is non-toxic, it is also extremely flammable, with a wide flammable range and low ignition energy. Its colorless, odorless flame makes it more difficult for people to detect fires or leaks (Calabrese et al., 2024).

2.2 Processes for Hydrogen Production

As discussed in the previous section, the primary challenge of using gaseous H_2 as a fuel is its scarcity in nature, which necessitates production methods that require an energy input.

A wide range of processes can be employed for H_2 production. These are broadly classified according to the feedstock used into four main categories: (1) fossil fuel-based

methods, (2) water electrolysis, (3) biomass-derived methods, and (4) biological processes (Dincer & Acar, 2015; Nikolaidis & Poullikkas, 2017).

Each category has different advantages and limitations in terms of energy efficiency, operational costs, feedstock availability, and environmental impact. Fossil fuel-based methods are technologically mature and widely implemented on an industrial scale, but they are associated with substantial greenhouse gas emissions. In contrast, renewable-based technologies, such as electrolysis powered by solar or wind energy, offer a more sustainable alternative, though they are currently less economically competitive (Longden et al., 2022).

The term bio-H_2 generally refers to H_2 produced from biomass through biological or thermochemical methods. The production of bio-H_2 through thermochemical processes is highly energy-intensive and cannot, therefore, be classified as a renewable primary energy source. By contrast, generating bio-H_2 biologically from biomass offers a low-energy, economically viable, and environmentally friendly alternative (Antoni et al., 2007). This process is based on microbial metabolism and relies on the catalytic activity of two key enzymes, hydrogenase and nitrogenase, to convert organic substrates and water molecules into bio-H_2 (Akhlaghi & Najafpour-Darzi, 2020). This approach will be examined in the following section, given its relevance to the aims of this thesis.

2.3 Biological Hydrogen Production

Biological hydrogen production (bio-H_2) is a promising technology for biomass valorization. It operates under ambient temperature and pressure, requiring less energy than thermochemical methods (Sinha & Pandey, 2011).

Relying on microbial metabolism, it can be broadly divided into two categories: light-independent and light-dependent processes. The former includes dark fermentation (DF), while the latter comprises direct and indirect biophotolysis and photofermentation (PF). Additionally, strategies that integrate DF and PF have been explored (Antoni et al., 2007; Xu et al., 2022).

Each method has specific advantages and limitations, as well as presenting challenges for industrial-scale implementation (Hallenbeck, 2014; Manish & Banerjee, 2008; Rai & Singh, 2016). These biological pathways offer sustainable and viable alternatives for bio-H_2 production and have strong potential for recovering biomass and organic waste within a circular economy framework.

2.3.1 Biophotolysis

Biophotolysis is a biological process carried out by microalgae (eukaryotic) and cyanobacteria (prokaryotic), both of which are capable of oxygenic photosynthesis and atmospheric CO_2 fixation, like higher plants. However, unlike higher plants, these microorganisms possess specific enzymes that allow bio-H_2 production under defined conditions (Hallenbeck, 2014).

Direct biophotolysis has been demonstrated exclusively in green microalgae (Hallenbeck, 2014). Under anoxic conditions and illumination, electrons are transferred linearly from water to ferredoxin (Fd) via photosystem II (PSII) and photosystem I (PSI). Reduced Fd then donates electrons to hydrogenase, which catalyzes the reduction of protons to molecular H_2 (Nagarajan et al., 2017). However, oxygenic photosynthesis simultaneously generates O_2 through PSII-mediated water oxidation, and hydrogenase is extremely O_2-sensitive. Consequently, H_2 production occurs only transiently after illumination, until O_2 accumulates to inhibitory levels (Nagarajan et al., 2017). To overcome this limitation, a strategy based on sulfur deprivation has been proposed: sulfur limitation triggers rapid PSII degradation and the consequent cessation of O_2 evolution, while PSI remains active, thereby sustaining H_2 production (Melis et al., 2000).

Indirect biophotolysis can occur in both microalgae and cyanobacteria and represents an efficient strategy for temporal or spatial separation of O_2 evolution from H_2 generation (Manish & Banerjee, 2008). In this process, carbohydrates synthesized during photosynthesis are subsequently fermented in the dark, providing reducing equivalents for hydrogenase-mediated H_2 release (Nagarajan et al., 2017). In nitrogen-fixing cyanobacteria, nitrogenase, rather than hydrogenase, plays the key role in H_2 production. Nitrogenase catalyses the reduction of atmospheric N_2 to NH_3 but is highly O_2-sensitive. Filamentous cyanobacteria overcome this by compartmentalizing H_2 evolution into heterocysts, specialized cells that maintain an anoxic environment where reductants derived from carbohydrate metabolism drive nitrogenase-dependent H_2 generation (Hallenbeck, 2014).

2.3.2 Dark Fermentation (DF)

Dark fermentation (DF) is among the most promising biological routes for sustainable bio-H_2 production, owing to its high productivity, low operating costs, and ability to process carbohydrate-rich waste (Hallenbeck, 2014). It proceeds under anoxic, light-independent conditions and is carried out by obligate or facultative anaerobes (Rai & Singh, 2016). The key metabolic intermediate is pyruvate, derived from glycolysis, which serves as the central node in hydrogen metabolism (Pengadeth et al., 2024).

The hydrogenase enzyme is essential in DF. In obligate anaerobes, pyruvate is oxidized to acetyl-CoA and CO_2 via pyruvate: ferredoxin oxidoreductase, reducing ferredoxin (Fd). Hydrogenase reoxidizes Fd, releasing H_2. At very low H_2 partial pressures (< 60 Pa), additional H_2 can be produced through NADH-ferredoxin reductase, which regenerates reduced Fd (Pengadeth et al., 2024). In facultative anaerobes, pyruvate is cleaved into acetyl-CoA and formate by pyruvate formate lyase; formate is then converted to CO_2 and H_2 by hydrogenases (Hallenbeck, 2014).

The fate of acetyl-CoA determines H_2 yield: the acetate pathway produces 4 mol H_2 per mol glucose (Eq. 1), while the butyrate pathway yields only 2 (Eq. 2) (Pengadeth et al., 2024).

$$C_6H_{12}O_6 + 2H_2O \rightarrow 2C_2H_4O_2 + 2CO_2 + 4H_2 \quad (1)$$

$$C_6H_{12}O_6 \rightarrow C_4H_8O_2 + 2CO_2 + 2H_2 \quad (2)$$

Nonetheless, current DF systems achieve less than 33 % of the theoretical maximum (12 mol H_2 per mol glucose), markedly lower than other biofuels (Hallenbeck, 2014). Enhancing yields requires strategies such as metabolic engineering, immobilized cells, or two-stage DF-photofermentation (PF), which valorizes DF by-products into additional H_2 (Rai & Singh, 2016).

Further details on DF are provided in Chapter I of Part V (Appendix) of this thesis, entitled *Recent advances in dark fermentative hydrogen production from vegetable waste: role of inoculum, consolidated bioprocessing, and machine learning*.

2.3.3 Photofermentation (PF)

Photofermentation (PF) is a biochemical process carried out by PNSB, which use solar energy to produce bio-H_2 from organic acids. These acids act as both a carbon source and an electron donor (reducing power) (Saravanan et al., 2021).

During PF, anoxygenic photosynthesis takes place, whereby no O_2 is produced (McKinlay, 2014). In this process, bacteriochlorophylls (BChl) act as both electron donors and acceptors, maintaining a closed cycle. When a photon is absorbed by the antenna complexes, the bacteriochlorophyll in the reaction center (RC) becomes excited, releasing an electron that reduces a quinone (Q). Once Q has undergone two reductions, it moves across the membrane, carrying protons from the cytoplasm to the cytochrome bc_1 complex. Here, electrons are transferred to cytochrome c_2, while protons are released into the periplasmic space. Finally, cytochrome c_2 reduces the oxidized donors in the RC,

thus completing the photosynthetic cycle. The generated proton gradient powers ATP synthase, which produces ATP (Adessi, La Cava & De Philippis, 2021).

The key enzyme in bio-H_2 production through PF is nitrogenase, responsible for the fixation of molecular nitrogen (N_2) into ammonium (NH_4^+) and capable of generating H_2 as an integral part of its catalytic cycle. Most PNSB encode the Mo-nitrogenase, characterized by a Fe-Mo cluster in the active site (Eq. 3). Some strains, however, also encode "alternative" nitrogenases, namely V-nitrogenase (Eq. 4) and Fe-nitrogenase (Eq. 5), in which molybdenum (Mo) is replaced by vanadium (V) or iron (Fe), respectively. These variants display different kinetics in H_2 production. In several bacteria, only one alternative nitrogenase is expressed alongside Mo-nitrogenase, whereas others encode all three forms. Furthermore, Mo-nitrogenase can also function in the absence of N_2 (Eq. 6) (McKinlay, 2014).

$$N_2 + 8Fd_{red} + 8H^+ + 16ATP \rightarrow 2NH_3 + H_2 + 8Fdox + 16ADP + 16P_i \quad (3)$$

$$N_2 + 12Fd_{red} + 12H^+ + 24ATP \rightarrow 2NH_3 + 3H_2 + 12Fdox + 24ADP + 24P_i \quad (4)$$

$$N_2 + 24Fd_{red} + 24H^+ + 48ATP \rightarrow 2NH_3 + 9H_2 + 24Fdox + 48ADP + 48P_i \quad (5)$$

$$8Fd_{red} + 8H^+ + 16ATP \rightarrow 4H_2 + 8Fd_{ox} + 16ADP + 16P_i \quad (6)$$

As previously noted, nitrogenase is highly sensitive to O_2. The main advantage of PNSB is their ability to catalyze H_2 production under anaerobic conditions without generating oxygen through photosynthesis, thus eliminating the need to protect hydrogen-producing enzymes from oxidative inactivation (McKinlay, 2014). However, nitrogenase activity is also limited by the presence of NH_4^+, since the synthesis and activation of this enzyme are energetically costly, and microorganisms repress its expression when nitrogen is available in an assimilable form (McKinlay, 2014). As waste biomass often contains high levels of nitrogen, preliminary treatments are therefore required to lower NH_4^+ concentrations (Corneli et al., 2017).

In terms of energy, nitrogenase is extremely demanding: four ATP molecules and two electrons (e^-) are required for each H_2 molecule produced. Additional energy is required for the reduction of Fd, which is the main electron donor to nitrogenase. However, ATP is not a limiting factor in PNSB, as it is generated through anoxygenic photosynthesis. Therefore, parameters related to light and photosynthetic efficiency, which directly influence productivity, are crucial (McKinlay, 2014).

The bio-H_2 yield achieved by PNSB is strongly influenced by the type of organic acid employed as a growth substrate. Eqs. (7)-(10) present the theoretical hydrogen yields

from PF of several organic acids typically found in agro-industrial effluents, including acetic (Eq. 7), malic (Eq. 8), butyric (Eq. 9), and lactic acids (Eq. 10). Although strain-specific variations have been reported, malate and lactate are generally regarded as the most favorable substrates for bio-H_2 production. In contrast, acetate and butyrate are more commonly directed towards the synthesis of alternative metabolites, such as polyhydroxyalkanoates (PHA) (Gosh et al., 2017).

$$C_2H_4O_2 + 2H_2O + Light \rightarrow 4H_2 + 2CO_2 \quad (7)$$

$$C_4H_6O_5 + 3H_2O + Light \rightarrow 6H_2 + 4CO_2 \quad (8)$$

$$C_4H_8O_2 + 6H_2O + Light \rightarrow 10H_2 + 4CO_2 \quad (9)$$

$$C_3H_6O_3 + 3H_2O + Light \rightarrow 6H_2 + 3CO_2 \quad (10)$$

Although PF can generate higher quantities of hydrogen than DF, technological limitations include low sunlight conversion efficiency, the need for complex anaerobic photobioreactors, and the limited availability of organic acids in industrial effluents. Additionally, the dark color of many effluents and the presence of toxic compounds, such as heavy metals, may necessitate pre-treatment to guarantee the process's effectiveness (Nikolaidis & Poullikkas, 2017).

2.3.4 Coupling Dark and Photofermentation Processes

Of the various bio-H_2 production routes, DF and PF are two promising strategies, each with specific advantages and limitations. However, integrating them synergistically offers one of the most effective solutions for optimizing H_2 yield and improving the system's overall sustainability.

The main limitation of DF is that only a fraction of the substrate is converted into bio-H_2, while the rest accumulates as different by-products, primarily volatile fatty acids (VFAs) such as acetic acid, butyric acid, propionic acid, and other organic acids. These by-products inhibit microbial growth, thereby limiting the process yield. The resulting effluent, therefore, has an acidic pH and cannot be reintroduced directly into the environment without proper treatment, as it would alter the pH of water bodies and damage aquatic ecosystems. Furthermore, the low pH renders the effluent highly corrosive to storage, transport, and treatment facilities (Rai & Singh, 2016).

The organic acids present in DF effluents can be further photo-fermented by PNSB, enabling additional bio-H_2 production and contributing to an increase in effluent pH.

The integration of DF and PF processes can theoretically achieve a hydrogen yield of up to 12 mol H_2 per mol of glucose (the maximum theoretical yield), corresponding to the sum of H_2 produced via reactions (1) and (3). However, this yield is not practically attainable due to enzymatic limitations and other physical constraints. Integration can be implemented through two main operational approaches: a sequential two-stage configuration or a single-stage co-culture system (Nikolaidis & Poullikkas, 2017; Rai & Singh, 2016).

In the sequential two-stage configuration, DF and PF are conducted as two distinct and successive phases. The main advantage of this approach lies in the ability to optimize operational conditions for each process individually, thereby maximizing overall efficiency. However, this method requires the use of two separate bioreactors, leading to increased costs associated with system operation and maintenance. Additionally, DF effluents often require pretreatment before they can be effectively utilized in the PF stage (Rai & Singh, 2016).

In the single-stage co-culture configuration, both DF and PF occur simultaneously within the same bioreactor. During DF, bio-H_2 and VFAs are produced; these VFAs are immediately utilized in situ by PNSB as substrates for additional bio-H_2 production. This integrated approach presents several advantages over the sequential mode. Firstly, pH regulation becomes unnecessary, as the acidification resulting from VFA production during DF is counterbalanced by their consumption during PF, which leads to alkalinization. Secondly, the immediate utilization of inhibitory metabolites by PNSB allows DF to proceed for a longer duration, reducing the accumulation of toxic compounds and enhancing overall bio-H_2 yield. Finally, the single-stage setup shortens fermentation times, improving process efficiency (Rai & Singh, 2016).

The integration of DF and PF faces several limitations, including metabolic incompatibility between strains, the formation of inhibitory compounds during substrate pretreatment, and the low light conversion efficiency of photosynthetic microorganisms. Although these approaches show promise, their industrial feasibility requires validation through pilot-scale studies (Rai & Singh, 2016).

Chapter III

Microbial production of Polyhydroxyalkanoates

3.1 Introduction to Bioplastics

The term bioplastic refers to polymers wholly or partially derived from biological resources using living organisms, such as plants or microorganisms (Anjum et al., 2016; Jayakumar et al., 2023). While bioplastic and biopolymer are often used interchangeably, some authors distinguish between the two: a biopolymer is a biologically derived macromolecule, whereas a bioplastic is an engineered formulation of one or more biopolymers with functional additives for industrial use (Lackner, Mukherjee, & Koller, 2023).

Bioplastics can be classified according to their origin and biodegradability. Bio-based bioplastics are derived from renewable biomass, such as plants, residues, and food waste, whereas fossil-based bioplastics are synthesized from non-renewable sources but are designed to biodegrade. It is important to note that the term “bioplastic” does not necessarily imply biodegradability; bio-based polymers such as PEF, PTT, and bio-PE are not biodegradable (European Bioplastics, n.d.). Biodegradation relies on the activity of microorganisms that break down polymers safely and completely (Narayan, 2017).

Among biopolymers, polyhydroxyalkanoates (PHA) are natural polyesters synthesized by many microorganisms as intracellular energy reserves under nutrient limitation. They are found in both Gram-positive and Gram-negative bacteria, as well as in some archaea (Koller et al., 2011; Sharma, Sehgal & Gupta, 2021). PHA combine several favorable features, including biocompatibility, biodegradability, thermoplasticity, water insolubility, UV resistance, and porosity (Sali & Mackey, 2021). Their degradation rate varies depending on the polymer structure and environmental conditions; however, the resulting metabolites are non-toxic and are naturally eliminated (Lim et al., 2017). These properties make PHAs promising substitutes for conventional plastics in agriculture, retail, and healthcare. Furthermore, they can be produced from agro-industrial waste via microbial conversion, thereby enhancing their sustainability (Montiel-Corona & Buitrón, 2021).

3.2 Molecular Structure and Classification of PHA

PHAs are natural polyesters made up of long chains containing between 600 and 35.000 hydroxy acid units that are linked by ester bonds. Each monomer consists of a carbon backbone and a side chain (R), which can be a saturated or unsaturated alkyl group, a substituted alkyl group or a branched alkyl group. The nature of this side chain plays a key role in determining important polymer characteristics, such as stereospecificity, crystallinity and biodegradability (Sharma, Sehgal, & Gupta, 2021; Tan et al., 2014). Additionally, each monomeric unit contains a chiral carbon atom whose configuration can significantly impact the polymer's mechanical performance and degradability (Caputo et al., 2022).

PHAs are classified based on the length of the carbon backbone: short-chain-length PHA (scl-PHA) contain monomers with up to five carbon atoms; medium-chain-length PHA (mcl-PHA) contain six to fourteen carbons; and long-chain-length PHA (lcl-PHA) contain more than fourteen carbon atoms (Sharma, Sehgal & Gupta, 2021). Moreover, a PHA polymer can be characterized either by a single repeating monomeric unit, known as a homopolymer, or by different monomeric units, forming a copolymer (Montiel-Corona & Buitrón, 2021).

Among the numerous types of PHA that have been studied, poly-β-hydroxybutyrate (PHB) was the first biopolymer of this family to be isolated and remains the most extensively characterized in the literature (Lenz & Marchessault, 2005; Turco et al., 2021).

3.3 PHA Granules in Bacterial Cells

PHAs accumulate within cells in the form of globular cytoplasmic inclusions of lipid nature, which are readily observed as electron-dense bodies by transmission electron microscopy (TEM) (Sudesh, Abe, & Doi, 2000). The inclusions have a size of approximately 0.3-2 μm along the short axis and 5-10 μm along the long axis, with a thickness ranging from 4 to 10 nm (Numata, Abe, & Iwata, 2009).

As shown in Fig. 1, the surface of PHA inclusions represents a highly complex environment, where proteins involved in biosynthesis (PHA synthase) as well as in degradation and/or mobilization (intracellular depolymerase) of PHA are found. The granule surface is composed of a phospholipid monolayer, which acts as a structural interface between the hydrophobic PHA core and the surrounding cytoplasm. In addition, other proteins known as phasins have also been identified on the surface of the granules

and are likely involved in the formation and stabilization of the granules (Sudesh, Abe, & Doi, 2000).

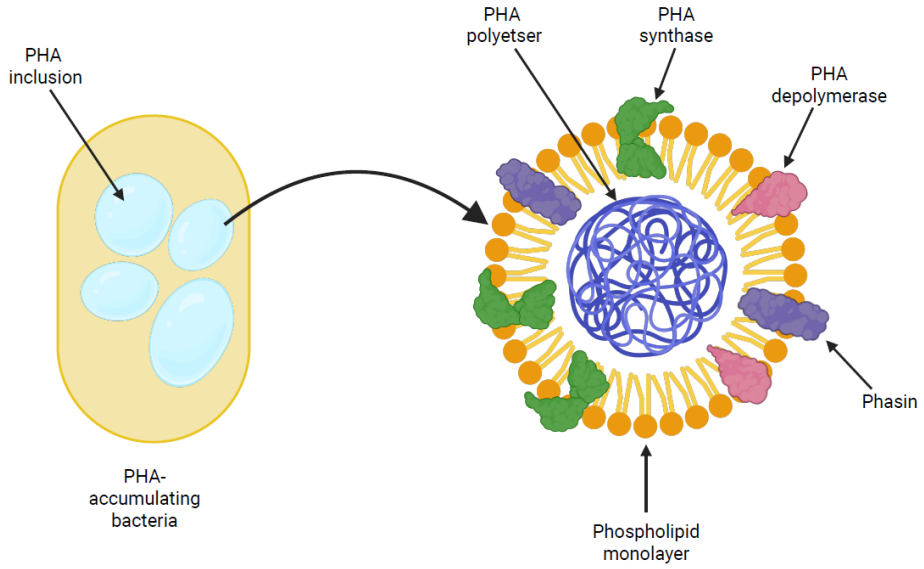

Figure 1. Schematic representation of intracellular PHA granules in PHA-accumulating bacteria. The magnified view shows the structural organization of a single PHA inclusion: a hydrophobic core of PHA polyester is surrounded by a phospholipid monolayer embedded with functional proteins such as PHA synthase, PHA depolymerase, and phasins, which are involved in polymer biosynthesis, degradation, and granule stabilization.

3.4 Poly-β-hydroxybutyrate (PHB): A model biopolymer among PHA

PHB is a scl-PHA and represents the most extensively studied polymer within the PHA family, due to its chemical and physical properties that make it suitable for a wide range of applications, both in industrial and biomedical fields (Yanti et al., 2021).

Its high crystallinity (50-80 %) is attributed to the stereochemical regularity of its structure, which consists of monomeric units of (R)-3-hydroxybutyrate. Its side chain (R group) comprises a methyl group (CH_3) as an alkyl substituent, conferring hydrophobic characteristics to the material. PHB exhibits low oxygen permeability and good thermoplastic properties; however, it has poor mechanical performance (Young's modulus and tensile strength) when compared to petrochemical-derived polymers such as polypropylene, making it rigid and brittle. The poor mechanical properties of PHB are attributed to its glass transition temperature (Tg), which ranges between 4 °C and 7 °C. This relatively high Tg causes the polymer to remain below or just above its Tg at room temperature, resulting in a glassy or semicrystalline state characterized by limited molecular mobility and consequent structural brittleness (dos Santos et al., 2017; Turco et al., 2021).

PHB also exhibits piezoelectricity, i.e., the ability to generate an electric charge in response to mechanical stress, making it suitable for applications in the medical field (Yanti et al., 2021).

One of the main technological limitations of PHB is that this polyester undergoes thermal degradation and depolymerization at temperatures close to its melting point, which is approximately 180 °C. This results in a narrow processing window, significantly restricting the use of PHB in conventional thermoplastic processing and requiring minimal residence times and strictly controlled operating conditions (Turco et al., 2021).

3.4.1 Biosynthesis of PHB

Prokaryotic organisms synthesize PHA as intracellular reserves of carbon and energy in response to environmental conditions characterized by an excess of carbon sources and a simultaneous limitation of essential nutrients, particularly nitrogen and phosphorus. PHA biosynthesis is mediated by three key enzymes: β-ketothiolase (PhaA), acetoacetyl-CoA reductase (PhaB), and PHA synthase (PhaC), encoded by the *phaA*, *phaB*, and *phaC* genes, respectively (Paduvari & Somashekara, 2025).

Under nitrogen-limiting conditions, the intracellular accumulation of reduced nicotinamide nucleotides (NADH and NADPH) leads to the inhibition of citrate synthase, the enzyme responsible for catalyzing the first step of the Krebs cycle. This metabolic inhibition prevents the entry of acetyl-CoA into the TCA cycle. As a result, acetyl-CoA accumulates intracellularly, accompanied by a concomitant decrease in free CoA. In this metabolic context, cells activate the PHA biosynthetic pathway, which enables the utilization of excess acetyl-CoA and the regeneration of CoA, thus maintaining cellular homeostasis (Yañez et al., 2020).

In the sugar-based pathway, which is considered the traditional route for producing scl-PHA, such as PHB, simple sugars undergo glycolysis to produce acetyl-CoA. Two acetyl-CoA molecules are then condensed by PhaA to form acetoacetyl-CoA. This is subsequently reduced by PhaB to (R)-3-hydroxyacyl-CoA, which is then polymerized into PHB by PhaC (Sharma, Sehgal, & Gupta, 2021).

Acetyl-CoA is the fundamental precursor for PHB synthesis. In PNSB, the metabolic pathways leading to the formation of this metabolite can be multiple and differ from strain to strain, even when using the same starting substrate. In the case of acetate, for example, *Rhodobacter sphaeroides* assimilates it via the ethylmalonyl-CoA pathway, *Rhodobacter capsulatus* via the TCA cycle, while *Rhodopseudomonas palustris* uses the glyoxylate cycle. Numerous studies have shown that acetate is one of the preferred substrates for

PHB synthesis in PNSB, thanks to its rapid conversion to acetyl-CoA. Other substrates, such as lactate and malate, can also be easily converted to acetyl-CoA through oxidation to pyruvate and subsequent oxidative decarboxylation. In contrast, substrates such as butyrate require more metabolic steps, resulting in greater energy consumption (Sali & Mackey, 2021).

3.5 Current Challenges and Future Prospects of Microbial PHA Production

The global production of biopolymers is growing steadily, driven by a shift towards materials with a reduced environmental impact. Projections suggest that the annual global production of bioplastics could reach around 7.43 million tons by 2028 (Ghasemlou, Barrow, & Adhikari, 2024). However, despite the significant potential of PHA in terms of biodegradability and versatility of application, they currently account for only around 2.5% of total global bioplastic production (European Bioplastics, n.d.).

The main obstacle to the industrial diffusion of PHA lies in the high production costs, currently ranging between $ 4 and $ 15/kg, still too far from the approximately $ 1.24/kg required for conventional plastics (Zytner et al., 2023). One of the most expensive aspects of PHA production is the carbon substrate used for microbial growth. This can account for up to 60% of the overall production cost (Gundlapalli & Ganesan, 2025). Using pure carbon sources, such as refined sugars and fatty acids, is uneconomical and should be avoided. Using agro-industrial waste and lignocellulosic biomasses is a promising alternative, as these waste materials have low or no commercial value (Getino, Martín, & Chamizo-Ampudia, 2024). However, such biomasses often require complex and costly pre-treatment, especially in the presence of high quantities of lignin. The careful selection of the residues used is therefore essential (Zytner et al., 2023).

In this sense, food waste, such as stale bread and bakery products, emerges as an ideal substrate for PHA biosynthesis. These wastes are widely available, have no or negligible lignocellulosic content, and are rich in carbohydrates (up to 70 %, mainly in the form of starch), thus reducing the need for expensive and impactful pre-treatment (Adessi et al., 2018; Montemurro et al., 2022; Nielsen et al., 2017).

In addition to choosing low-cost substrates, another strategy for reducing costs and increasing the efficiency of PHA production is selecting and optimizing the microorganisms involved in the process. To this end, four main lines of action have been proposed in the literature: (1) expanding the metabolic capacity of natural PHA producers by introducing exogenous genes, thereby enabling them to utilize complex or residual

substrates not accessible to native strains (Povolo et al., 2010); (2) incorporating PHA biosynthetic pathways into non-natural hosts with advantageous traits, such as high growth rates and tolerance to extreme environmental conditions (Chen & Jiang, 2018); (3) engineering copolymer composition to achieve specific properties, or eliminating competing metabolic routes to maximize polymer accumulation (Monroy & Buitrón, 2020; Srirangan et al., 2016); and (4) modifying the physical morphology of cells or PHA granules to increase production yields and reduce downstream processing (Brown et al., 2022; Gao et al., 2022; Jiang et al., 2015).

To achieve these goals, genome-scale metabolic models (GEMs) emerge as essential tools for guiding genetic engineering strategies aimed at promoting and optimizing PHA synthesis. Using simulations based on flux balance analysis (FBA), it is possible to analyse intracellular metabolic fluxes and identify pathways that compete with PHA biosynthesis for metabolic precursors and cofactors. These analyses allow the identification of specific genetic targets on which to intervene to redirect cellular metabolism and maximise PHA accumulation, thus making the process more efficient and economically sustainable (Simeonidis & Price, 2015).

Chapter IV

Purple Non-Sulfur Bacteria (PNSB) as Microbial Cell Factories for PHB and Bio-H_2 Production

4.1 Overview of Purple Phototrophic Bacteria (PPB)

Purple phototrophic bacteria (PPB) are a group of anoxygenic photosynthetic prokaryotes, meaning they can perform photosynthesis without producing O_2. Their name derives from their characteristic reddish-purple color, which is due to the presence of a complex of photosynthetic pigments (such as bacteriochlorophylls and carotenoids) produced under phototrophic growth conditions (Madigan & Jung, 2009).

In PPB, photosynthesis occurs exclusively under anoxic conditions, since the synthesis of photosynthetic pigments takes place in the absence of O_2 (Cohen-Bazire, Sistrom, & Stanier, 1957). Consequently, PPB's natural habitats require light and anoxic conditions simultaneously, circumstances that can be found in various aquatic environments, such as lakes, ponds, and estuaries (Madigan & Jung, 2009).

From physiological and taxonomic perspectives, PPB are generally classified into two main subgroups: purple sulfur bacteria (PSB) and purple non-sulfur bacteria (PNSB). This distinction was first made in early studies of the group based on their tolerance to sulfide and their ability to oxidize it to elemental sulfur. PSB can tolerate high concentrations of sulfide (in the millimolar range) and oxidize it to form intracellular sulfur globules. In contrast, PNSB do not exhibit the same level of tolerance or possess this accumulation capacity (Capson-Tojo et al., 2020).

Subsequent experiments have shown that PNSB are also capable of tolerating low concentrations of sulfide, typically below 0.5 mM, by oxidizing sulfide-containing compounds (S^{2-}) into elemental sulfur (S^0), tetrathionate ($S_4O_6^{2-}$), or sulphate (SO_4^{2-}). The main currently recognized distinction between PSB and PNSB lies in their different handling of elemental sulfur (S^0); while PSB can accumulate S^0 granules within the cell, PNSB (with some exceptions) lack this ability and instead excrete the produced S^0 outside the cell (Madigan & Jung, 2009).

A further distinguishing feature of PNSB compared to PSB is their ability to fix molecular nitrogen (N_2), a process mediated by the enzyme nitrogenase. Although some PSB may possess genes associated with nitrogen fixation, this function is neither

widespread nor widely expressed within the group, making it a trait primarily attributed to PNSB (Capson-Tojo et al., 2020; Madigan & Jung, 2009).

From a phylogenetic perspective, studies based on 16S rRNA gene sequencing have shown that PSB belong primarily to the phylum *Gammaproteobacteria*, while purple PNSB are distributed among the *Alphaproteobacteria* and *Betaproteobacteria* (Madigan & Jung, 2009).

4.2 Metabolic Traits of Purple Non-Sulfur Bacteria (PNSB)

Thanks to their extremely versatile metabolism, PNSB can be isolated from a wide range of organic matrices, including urban, agricultural, and industrial wastewater, as well as from lagoons used for the treatment of liquid organic wastes such as manure and sludge. In fact, they are capable of metabolizing numerous volatile organic compounds (VOCs), which are typical of these matrices, making them potentially useful for odor control, particularly in pig farming facilities (Schmidt et al., 2003).

Research has mainly focused on model species such as *R. palustris*, *Rhodospirillum rubrum*, *Rhodobacter capsulatus*, and *R. sphaeroides* (also known as *Cereibacter*) (Morrison & Bose, 2024).

PNSB are mixotrophic organisms and possess all the major known metabolic pathways, which provide them with a competitive advantage in unstable environments such as wastewater and aquatic ecosystems (Morrison & Bose, 2024). The four primary metabolic pathways are described below.

4.2.1 Photoheterotrophy

This metabolic model represents the preferred growth pathway for PNSB in light-exposed, organic-rich environments that are microaerobic or strictly anaerobic. In such settings, light provides energy while organic compounds supply carbon and electrons. Energy conversion occurs through anoxygenic photosynthesis, generating ATP via cyclic electron transport (see Chapter 2, Section 2.3, Subsection 2.3.3) (McKinlay, 2014).

PNSB can metabolize a broad range of organic compounds, including organic acids, fatty acids, alcohols, amino acids, and carbohydrates. Among these, organic acids such as malate, acetate, succinate, fumarate, and pyruvate are preferred, as they can directly enter the TCA cycle without requiring energy-intensive preliminary conversions (Morrison & Bose, 2024). Lactate can also be used, although it must first be converted into pyruvate by lactate dehydrogenase (Petushkova, Mayorova, & Tsygankov, 2021).

The use of sugars as carbon sources is uncommon among PNSB, although some species, such as *R. sphaeroides*, can grow on these substrates. Other PNSB, like *R. palustris*, are capable of degrading aromatic compounds, including chlorinated ones, highlighting their potential for bioremediation of contaminated environments (McKinlay, 2014).

When the available carbon source is more reduced than cellular biomass (approximately 4 moles of electrons per mole of carbon), a redox imbalance may occur due to the accumulation of NADH and NADPH, without regeneration of their oxidized forms (NAD^+ and $NADP^+$). In the absence of a terminal electron acceptor, this condition can inhibit cellular metabolism. To prevent this, PNSB can employ alternative strategies such as the use of external electron acceptors like CO_2 (*via* carbon fixation) or dimethyl sulfoxide (DMSO). Some species initiate PHB synthesis, storing excess carbon and electrons as intracellular reserves. Others utilize nitrogenase, which enables atmospheric N_2 fixation (even in its absence) while simultaneously producing bio-H_2 (the so-called photofermentation process). Hydrogenase may also support the dissipation of excess reducing equivalents through additional bio-H_2 production (Capson-Tojo *et al*., 2020; McKinlay, 2014).

4.2.2 Photoautotrophy

In this metabolic mode, which also operates under microaerobic or strictly anaerobic conditions, CO_2 serves as the main carbon source and is assimilated via the Calvin-Benson-Bassham (CBB) cycle. In PNSB, this pathway plays a dual role, supporting biomass synthesis through atmospheric CO_2 fixation and enabling the consumption of excess reducing power. Light acts as an energy source, while inorganic compounds serve as electron donors. These include ferrous iron (Fe^{2+}), molecular hydrogen (H_2), thiosulfate, other reduced sulfur compounds, nitrite (NO_2^-), and, in some cases, electrons supplied directly via cathodes in bioelectrochemical systems (Morrison & Bose, 2024).

4.2.3 Chemoautotrophy

Chemoautotrophy is a metabolic strategy in which energy is derived from the oxidation of inorganic compounds, such as H_2, ferrous ions (Fe^{2+}), or sulfur- and nitrogen-based compounds, rather than from light. The resulting electrons feed into the electron transport chain, which generates a proton gradient across the cell membrane. This gradient is then used by ATP synthase to produce ATP via oxidative phosphorylation. For the electron transport chain to function, a terminal electron acceptor is required: under aerobic

conditions, this is O_2, while under anaerobic conditions, PNSB can use alternative acceptors such as nitrate, sulphate, DMSO, or trimethylamine N-oxide. In this context, CO_2 serves as the carbon source and is assimilated via the CBB cycle for biomass production (McKinlay, 2014; Morrison & Bose, 2024).

4.2.4 Chemoeterotrophy

This growth mode also occurs in the absence of light and relies on electron donors, either organic or inorganic, to generate reducing power and energy. Organic compounds serve as the main carbon source (McKinlay, 2014).

In the presence of O_2, PNSB perform aerobic respiration, while under anoxic conditions they can switch to anaerobic respiration using alternative electron acceptors, such as DMSO. In the absence of a terminal electron acceptor, PNSB are also capable of fermenting sugars, although growth under these conditions is generally limited (Morrison & Bose, 2024).

4.3 PNSB as Biotechnological Tools for Bio-H_2 and PHB Production from Agro-Industrial Wastewater

Thanks to their metabolic versatility, the use of PNSB for the valorization of agro-industrial wastewater is receiving increasing attention. Under photoheterotrophic conditions, these microorganisms can direct excess reducing power towards either the photofermentative production of bio-H_2 or the intracellular accumulation of PHB (Morrison & Bose, 2024). Both processes use complex waste as substrates, contributing to the recovery of energy and materials, while reducing the organic load of effluents. Indeed, if released directly into aquatic environments, these effluents would promote eutrophication and acidification (Martinez-Burgos *et al*., 2021; Seifert, Waligorska, and Laniecki, 2010a; Zhang, Quijano, & Wang, 2024).

The production of bio-H_2 via PNSB is a well-established and widely studied process. In contrast, the study of PHB accumulation in these microorganisms is a relatively new and limited field of research. This is because, historically, PHB biosynthesis has been entrusted to model aerobic microorganisms such as *Cupriavidus necator*, which are already used in industry (Zhang et al., 2022). However, compared to these traditional aerobic producers, PNSB offer three significant advantages: (i) the potential for higher overall PHA yields, (ii) the elimination of the need for aeration systems, resulting in

energy savings, and (iii) the rapid enrichment of PHA-accumulating cultures in wastewater through infrared illumination (Capson-Tojo et al., 2020).

Although organic acids are the preferred source of carbon and electrons for PNSB, agro-industrial waste often contains complex sugars, cellulose, hemicellulose, and lignin that cannot be used directly by PNSB and require pre-treatment. Physical and chemical pretreatments are effective, but expensive, energy-intensive, and sometimes involve hazardous substances. DF, on the other hand, is a sustainable, biological approach that enriches substrates with organic acids (Ghosh et al., 2017). In addition, DF can produce bio-H_2 depending on the microorganisms involved in the process. Its effluents, rich in organic acids, can be further converted by PNSB to generate additional bio-H_2 or PHB. Consequently, coupling the two processes enhances overall resource valorization (Mishra et al., 2019). However, the most recalcitrant substrates, such as cellulose, hemicellulose, and lignin, still require additional pre-treatment to increase their microbial digestibility (Ghosh et al., 2017).

Tab. 1 and Tab.2 show the main studies concerning, respectively, the production of bio-H_2 and PHB from agro-industrial waste using PNSB. As can be seen, a wide range of substrates has been tested over the years, including agro-industrial liquid waste, vegetable and food waste, and other complex waste such as residual biomass with a high lignocellulosic content.

Two critical aspects emerge from the analysis of the studies reported in the tables. The first relates to the scale of the experiments: most of the work is still limited to small-volume cultures of less than 500 mL. While this allows for accurate control of operating parameters, it does not permit evaluation of the process's actual scalability, which requires a gradual transition from laboratory to pilot to industrial scale. The second critical aspect is light, which is one of the key parameters for the effective use of PNSB as microbial factories. Most studies have used non-selective light sources, which emit wavelengths that are not absorbed by photosynthetic pigments. This results in energy inefficiency. Using lighting systems calibrated to the specific absorption bands of PNSB could significantly increase bio-H_2 and PHB yields (Craven et al., 2019).

The following subsections will analyze the most relevant parameters for obtaining significant yields of bio-H_2 and PHB from PNSB. As the two processes share many metabolic and operational features, they will be discussed together, with the specific characteristics of each process highlighted where necessary.

4.3.1 Effect of Substrate Carbon-to-Nitrogen (C/N) Ratio

The optimum C/N ratio of the substrate is fundamental for promoting both bio-H_2 and PHB production in PNSB. In general, a high C/N ratio favors both processes. This is because the elevated carbon content of the substrate generates a surplus of reducing equivalents that cannot be dissipated through biomass formation due to the limited nitrogen availability, which is essential for amino acid and nucleic acid biosynthesis. As a result, metabolic fluxes are redirected toward bio-H_2 evolution and PHB accumulation, which serve to consume the excess reducing power. In addition, high concentrations of NH_4^+ exert an inhibitory effect on nitrogenase, further reinforcing the importance of maintaining an adequate C/N balance. However, an excessively high C/N ratio can be counterproductive, as it stimulates excessive microbial growth with consequent cell self-shading phenomena, which reduce light capture efficiency in photobioreactors (Ghosh et al., 2017; Monroy & Buitrón, 2020).

Many experimental studies have attempted to identify an optimal C/N ratio for each process; however, the heterogeneity of substrates and microbial species makes it difficult to establish a universally valid range. Optimizing the C/N ratio, therefore, requires case-by-case calibration, considering both substrate composition and the physiological characteristics of the bacterial strain. For bio-H_2, Androga et al. (2011) reported an optimal C/N ratio of 25, while Pattanamanee et al. (2012) found a significantly higher value (65 w/w) for *R. sphaeroides* S10 grown on oil palm empty fruit bunches. Yetis et al. (2000) identified an optimal C/N ratio of 35 mol/mol (≈ 30 w/w) for *R. sphaeroides* O.U. 001 using sugar refinery wastewater. For PHB, literature reports indicate that C/N ratios above 30 are favorable for enhancing polymer accumulation in PNSB (Monroy & Buitrón, 2020).

4.3.2 Influence of Nutrient Availability

Bio-H_2 and PHB production is strongly regulated by the availability of trace metals and nutrients, which act as cofactors in key enzymatic processes and influence the distribution of reducing equivalents. In the case of bio-H_2 production, several micronutrients are indispensable (Ghosh et al., 2017). Iron (Fe) and magnesium (Mg) are among the most critical, as they activate essential metabolic pathways and sustain photosynthetic function (Kars et al., 2006). Supplementation of dark-fermented bread waste with iron citrate and magnesium sulfate significantly increased H_2 yields, reaching 3.1 mol H_2 per mol of glucose (Adessi et al., 2018). Mg is also an essential structural component of bacteriochlorophyll (BChl) (Solov'ev & Erokhin, 2013). Molybdenum

(Mo) is another essential nutrient because it forms the catalytic core of nitrogenase with Fe, thereby ensuring high enzymatic activity (Hu & Ribbe, 2013).

In contrast, for PHB biosynthesis, nutrient limitation rather than supplementation is beneficial. As previously mentioned, nitrogen scarcity promotes PHB production by limiting cell growth (Capson-Tojo et al., 2020). Limitations of other macronutrients, including phosphorus (P), sulfur, and magnesium, can further enhance polymer accumulation. Moreover, excessive concentrations of trace metals such as Fe, Cu, Mn, and Zn may negatively affect PHB yields, underlining the need for precise regulation (Monroy & Buitrón, 2020).

4.3.3 Temperature and pH

Temperature and pH are among the most critical environmental factors regulating bio-H_2 and PHB production in PNSB. For bio-H_2, temperature influences microbial growth and enzymatic activity, and the optimal range is generally reported between 25 °C and 35 °C, although strain-specific variations exist (Eroglu et al., 2010; Gupta et al., 2024). Similarly, pH plays a fundamental role by affecting cell metabolism, the activity of hydrogenase and nitrogenase, nutrient solubility, and the availability of protons (H^+), which act as direct substrates in the nitrogenase-catalyzed reaction. Proper pH regulation is therefore essential, with optimal values between 6.8 and 7.5 (Al-Mohammedawi, Zanad, & Eroglu, 2018; Gupta et al., 2024).

In parallel, pH also exerts a decisive effect on PHA production. Neutral to slightly alkaline conditions generally favor both microbial growth and polymer accumulation, likely due to the reduced bio-H_2 production observed under more alkaline environments (Sali & Mackey, 2021). However, the optimum varies with bacterial strain and carbon source. For instance, *R. sphaeroides* was reported to reach a PHA content of 40 % of cell dry weight (CDW) at pH 10 with pyruvate, whereas other studies indicate optimal values in the range of 6.5-7.0 (Ghimire et al., 2016; Khatipov et al., 1998; Kumar et al., 2019). Temperature is equally crucial for PHA accumulation, with optimal values typically between 24 °C and 30 °C (Monroy & Buitrón, 2020), though some strains exhibit maxima at 35 °C (Sangkharak & Prasertsan, 2007).

4.3.4 Light-Related Issues

Light is the key parameter that regulates the photoheterotrophic metabolism of PNSB. Its intensity and spectral quality primarily influence the production of bio-H_2 and PHB. Spectroscopically, PNSB absorb light over a wide range of wavelengths: carotenoids

absorb between 450 and 550 nm and play a photoprotective role, while bacteriochlorophylls (BChls) are primary photosynthetic pigments with absorption peaks at 590, 800, 850, and 880 nm, as well as an Soret band around 390 nm in the near UV (Adessi & De Philippis, 2014; Yu et al., 2018).

Light intensity represents the first crucial parameter. For bio-H_2, maximum light conversion efficiency (LCE) is achieved only at low irradiances, which, however, restrict productivity. In contrast, higher intensities enhance hydrogen output but reduce efficiency (Nath & Das, 2009; Adessi & De Philippis, 2014). PHB production follows a similar trend; elevated intensities promote PHB accumulation, since PNSB dissipate excess reducing power into polymer synthesis as a protective mechanism against photo-oxidative stress (Imam et al., 2015; Licht et al., 2020; Muzziotti et al., 2017). For instance, Fradinho et al. (2016) reported that moderate illumination (127 W m^{-2}) maximized biomass yield, while a higher intensity (227 W m^{-2}) decreased growth but increased PHA accumulation up to 60 % of CDW.

The choice of light source is crucial for optimizing both processes. Artificial lighting provides stability and spectral control, enabling customization of the wavelength to improve energy conversion into bio-H_2 (Santos et al., 2025). Tungsten lamps have historically been the most widely used due to their spectral similarity to sunlight. However, they are characterized by high energy consumption (Adessi & De Philippis, 2012). Light-emitting diodes (LEDs) are a more sustainable alternative, reducing energy costs by up to 98% and lasting up to 17 times longer (Kawagoshi et al., 2010). However, their narrow emission spectra do not fully cover the optimal absorption range of PNSB. Nevertheless, infrared LEDs have proven effective for hydrogen production in *R. palustris* (Bosman, Pott & Bradshaw, 2023).

Although studies on the effect of wavelength on PHA and bio-H_2 production are limited, recent findings suggest that the spectral composition of the light source can significantly influence production outcomes, particularly when using selected wavelengths (Sali, McKay, & Mackey, 2025). However, systematic investigations are still scarce, highlighting a critical knowledge gap that needs to be filled to optimize light-driven processes in PNSB.

Finally, another non-negligible factor that significantly influences the LCE of photobiological systems is the color of the substrate. Highly colored wastewaters absorb and scatter incoming radiation, thereby reducing light penetration into photobioreactors and consequently lowering bio-H_2 and PHB yields (Ghosh et al., 2017; Adessi & De

Philippis, 2014). Wastewater color is closely related to the amount and degradation state of the organic matter present and is mainly associated with polyphenols, pigments, melanoidins, and, in the case of food industry effluents, artificial dyes (Arimi, Zhang, & Geißen, 2015; Ghosh et al., 2017). Strategies such as dilution, clay adsorption, or treatment with manganese oxides have proven effective in improving medium transparency, thereby increasing light availability and enhancing bio-H_2 yields (Arimi, Zhang, & Geißen, 2015; Eroğlu et al., 2008; Keskin & Hallenbeck, 2012; Seifert, Waligórska, & Łaniecki, 2010a).

4.3.5 Competing Metabolic Pathways

Under conditions of a high C/N ratio, bio-H_2 production can compete with PHB synthesis for reducing equivalents (e^-), which result from the oxidation of organic substrates, mainly through glycolysis and the TCA cycle (Ghosh et al., 2017; Montiel-Corona & Buitrón, 2021). Indeed, both nitrogenase and the enzymes involved in PHB synthesis are highly reducing metabolic pathways that require large amounts of e^-. Furthermore, these reducing equivalents can be diverted to other metabolic processes, such as CO_2 fixation or the synthesis of new cellular biomass. Consequently, various metabolic trade-offs arise, whereby favoring one metabolic pathway necessarily disadvantages others (Hädicke, Grammel, & Klamt, 2011; McKinlay & Harwood, 2011; Montiel-Corona & Buitrón, 2021). Another obstacle is uptake hydrogenase (Hup), a membrane-bound nickel-iron enzyme that re-oxidizes the H_2 produced by nitrogenase to recover its reducing equivalents. This process consumes some of the bio-H_2, thereby lowering overall yields (Rey, Oda, & Harwood, 2006).

Several strategies have been proposed in the literature to enhance either bio-H_2 or PHB production by inhibiting metabolic trade-offs. One of the simplest and most effective strategies for increasing PHB accumulation is to add NH_4^+ as a nitrogen source while maintaining a high C/N ratio in the substrate. Indeed, NH_4^+ inhibits nitrogenase without hindering polymer synthesis. Furthermore, the selective limitation of other nutrients directs reducing power towards PHB (see Section 4.3.2) (Capson-Tojo et al., 2020).

The use of light/dark cycles has also proven effective in boosting PHA production. Montiel-Corona *et al*. (2017) observed that applying 30:30-minute light/dark cycles to *R. capsulatus* cultures led to a threefold increase in PHB content (308 ± 2 mg PHB/g CDW) compared to continuous illumination, along with a 20 % reduction in cumulative bio-H_2 production.

Beyond nutritional and light-based strategies, numerous metabolic engineering approaches have been explored. For example, deleting the *phbC* gene, which encodes PHB synthase, has been shown to enhance H_2 production. Kim et al. (2011) reported that an *R. sphaeroides phbC*$^-$ mutant produced approximately twice as much H_2 as the wild type when grown on acetate and butyrate.

Further improvements were achieved by deactivating the carbon fixation and oxygen-sensing pathways. Wang et al. (2014) demonstrated that simultaneous elimination of the *cbbP* and *ccoNOQP* genes in *R. capsulatus* SB1003 significantly increases nitrogenase activity and bio-H_2 yield. The *cbbP* gene encodes phosphoribulokinase and is essential for the functioning of the CBB cycle; its removal abolishes CO_2 fixation and increases the availability of e^- for nitrogenase. The *ccoNOQP* gene encodes cytochrome cbb_3 oxidase, which is responsible for O_2 reduction and repression of nitrogenase expression via the RegB/RegA system.

Finally, disabling the Hup enzyme is still one of the most well-established ways of increasing bio-H_2 yields. For example, Uyar et al. (2015) showed that an *R. capsulatus hup*$^-$ mutant produced the same or greater amounts of hydrogen than the wild-type strain when dark-fermented molasses waste was used in batch and continuous systems.

4.3.6 Photobioreactors Design and Fermentation Strategies

Photobioreactors constitute the reactive environment in which PF and PHB production occur, and their correct design and management are fundamental to the system's overall efficiency. They must be closed systems capable of maintaining stable anaerobic conditions (Adessi & De Philippis, 2014). The presence of O_2 directly inhibits nitrogenase activity and suppresses the expression of photosynthetic genes via the PpsR transcriptional regulator (Elsen et al., 2025). Anaerobiosis is also crucial for PHB accumulation, as it enhances the activity of isocitrate dehydrogenase (IDH), a key enzyme of the TCA cycle, thereby increasing NADPH availability and driving the reduction steps of PHB biosynthesis (Higuchi-Takeuchi & Numata, 2019). Finally, a closed system is necessary for efficiently collecting bio-H_2, which usually occurs in the upper or lateral part of the photobioreactor (Adessi & De Philippis, 2014).

Another crucial aspect is the presence of an adequate agitation system, which is usually mechanical. In PF, agitation ensures the rapid removal of bio-H_2 from the culture medium. This prevents re-oxidation by Hup-equipped strains, thereby improving net yields. At the same time, agitation promotes uniform light distribution throughout the culture, which is important for both bio-H_2 and PHB production. A constant and homogeneous light

intensity prevents self-shading and photo-inhibition, while ensuring stable photosynthetic activity (Adessi & De Philippis, 2014)

In terms of photobioreactor geometry, a high surface-to-volume ratio (s/v) is essential to maximize light availability per unit volume, limit self-shading of the cells, and facilitate better temperature control (Adessi & De Philippis, 2014). To date, most available studies have focused on photobioreactors developed for producing biohydrogen from PNSB or for microalgal cultures. However, much of the knowledge gained from these systems can be applied to PHA production, given the strong similarities between the processes (Sali & Mackey, 2021). Various photobioreactor geometries have been proposed over the years, but the main ones are tubular and flat panels (Zarei et al., 2024).

Tubular photobioreactors consist of cylindrical tubes that can be arranged horizontally or vertically; their length must be limited to minimize the residence time of H_2 bubbles and avoid re-oxidation by Hup (Adessi & De Philippis, 2014; Zarei et al., 2024). Flat-panel systems, in contrast, are transparent rectangular containers that can be positioned vertically or at different inclinations. They offer advantages such as ease of construction, modularity, and the possibility of being arranged in series to enhance productivity per unit area, although their application remains largely confined to small-scale and research contexts (Adessi & De Philippis, 2014). More recently, increasing attention has been given to immobilized-cell photobioreactors, which provide higher cell stability, greater resistance to mechanical stress, higher biomass densities, and improved nutrient management, ultimately resulting in greater yields and faster bio-H_2 production (Touloupakis et al., 2022). Among these, fluidized-bed configurations coupled with immobilized cells have proven particularly effective (Ross & Pott, 2021).

Regarding fermentation strategies, several configurations have been proposed in the literature. Among these, the single-stage process is the most applied, both for photofermentative bio-H_2 production and PHB accumulation, particularly when agro-industrial wastewater is used as the substrate. In this approach, the feedstock can be pre-enriched in short-chain organic acids through DF and subsequently subjected to fermentation with PNSB (Sali & Mackey, 2021).

Two-stage strategies are mainly employed to maximize PHB production in mixed cultures. Here, fermentation is conducted in two consecutive phases: an initial phase with high nutrient availability to select PHB-producing cells, followed by a second phase under carbon excess, which stimulates intracellular polymer accumulation (Pagliano et al., 2017).

More advanced three-stage configurations are designed to decouple the competing metabolic pathways of bio-H_2 and PHB. This scheme involves an initial nutrient-rich phase to maximize biomass growth, a second nitrogen-deprivation phase to stimulate nitrogenase activity and bio-H_2 production, and a final sulfur-deprivation phase. The latter inhibits nitrogenase and de novo amino acid biosynthesis, thereby halting cell proliferation and redirecting metabolic fluxes towards PHB accumulation (Carlozzi et al., 2019).

Table 1. Overview of the most relevant studies on bio-H_2 production by PNSB using agro-industrial waste as substrate. The table summarizes the PNSB strains, substrates, production strategy, operational mode (OM), reactor type, culture volume (CV), light source (LS), light intensity (LI), bio-H_2 yield (Y), and references (Ref.). NA: not available; NS: not specified.

PNSB strain	Substrate	Production strategy	OM	Reactor type	CV (L)	LS	LI	Y	Ref.
R. palustris 42OL	Bread waste	DF+PF	Batch	Glass bottle	0.250	Artificial (NS)	40 W m^{-2}	3.1 mol H_2/mol glucose	Adessi *et al*., 2018
Rhodopseudomonas BHU 01	Cheese whey	DF+PF	Batch	Glass bottle	0.100	Artificial (NS)	8 W m^{-2}	3.40 mol H_2/mol lactose	Rai *et al*., 2012
R. sphaeroides DSM 158	Pretreated Mixed effluents (restaurant and brewery)	PF	Batch	Clear glass photobioreactor	0.120	Artificial (halogen lamps)	126 W m^{-2}	0.95 mL H_2 mL^{-1}	Znad *et al*., 2021
R. sphaeroides S10	Oil palm waste hydrolysate.	PF	Batch	Cylindrical bioreactor	0.500	Artificial (tungsten lamps)	14.6 W m^{-2}	22.4 mL H_2 L^{-1} h^{-1}	Pattanamanee *et al*., 2012
R. sphaeroides NCIMB8253	Pulp and paper mill effluent	PF	Batch	Glass bottle	0.100	Artificial (NS)	7 klux	9.62 mL H_2 mL^{-1}	Hay *et al*., 2016
Rhodobacter sphaeroides O.U.001	Olive mill wastewater	PF	Batch	Glass bottle	0.055	Artificial (tungsten lamps)	NS	31.5 mL H_2 mL^{-1}	Eroğlu *et al*., 2008
R.palustris AV33	Vegetable residues	DF+PF	Batch	Glass bottle	0.250	Artificial (Incandescent lamp)	150 µmol (photons) m^{-2} s^{-1}	16.4 ± 2.3 mL H_2 L^{-1} h^{-1}	Bianchi *et al*., 2010

PNSB strain	Substrate	Production strategy	OM	Reactor type	CV (L)	LS	LI	Y	Ref.
R. sphaeroides S10	Oil palm empty fruit bunch hydrolysate	PF	Continuous	Tubular	2 (recirculating system: photoreactor + culture vessel)	Artificial (tungsten lamps)	10 klux	0.52 mL H_2 mL^{-1}	Palamae *et al*., 2018
R. sphaeroides S10	Oil palm empty fruit bunch hydrolysate	PF	Continuous	Tubular	2 (recirculating system: photoreactor + culture vessel)	Natural (sunlight)	0.15-66 klux (diurnal cycle)	0.43 mL H_2 mL^{-1}	Palamae *et al*., 2018
R. palustris CGA676	Ensiled wheat bran	DF+PF	Batch	Glass bottle	0.100	Artificial (Incandescent lamp)	200 µmol (photons) m^{-2} s^{-1}	0.65 mL H_2 mL^{-1}	Corneli *et al*., 2016
R. palustris CGA676	Ensiled maize	DF+PF	Batch	Glass bottle	0.100	Artificial (incandescent lamp)	200 µmol (photons) m^{-2} s^{-1}	0.32 mL H_2 mL^{-1}	Corneli *et al*., 2016
Bacterial consortium (*Rhodobium marinum* dominant strain)	Soy sauce wastewater	PF	Batch	Glass bottle	0.075	Artificial (NS)	60 W m^{-2}	2.67 mL H_2 mL^{-1}	Anam *et al*., 2012
Bacterial consortium (*R.* m*marinum* dominant strain)	Bagasse	PF	Batch	Glass bottle	0.075	Artificial (NS)	60 W m^{-2}	0.55 mL H_2 mL^{-1}	Anam *et al*., 2012
Mixed PNSB consortia	Winery wastewar	PF	Batch	NA	0.400	Artificial (LED strips)	4 klux	0.47 mL H_2 mL^{-1}	Policastro *et al*., 2020
R. sphaeroides DSM 158	Pretreated brewery wastewater	PF	Batch	Glass bottle	0.120	Artificial (halogen lamp)	NS	0.41 mL H_2 mL^{-1}	Al-Mohammedawi et al., 2019
R. palustris 42OL	Water lettuce effluent	DF+PF	Batch	Glass bottle	0.100	Artificial (incandescent lamp)	200 µmol (photons) m^{-2} s^{-1}	1.22 mL H_2 mL^{-1}	Corneli *et al*., 2017
R. palustris CGA676	Water lettuce effluent	DF+PF	Batch	Glass bottle	0.100	Artificial (incandescent lamp)	200 µmol (photons) m^{-2} s^{-1}	0.72 mL H_2 mL^{-1}	Corneli *et al*., 2017

PNSB strain	Substrate	Production strategy	OM	Reactor type	CV (L)	LS	LI	Y	Ref.
Rhodobacter sphaeroides O.U.001	Cheese whey	DF+PF	Batch	Cylindrical bioreactor	2	Artificial (CFL and LED)	15 W m^{-2}	6.65 mol H_2/mol lattosio*	Rao & Basak, 2022
Bacterial consortium (enriched with *Rhodopseudomonas* sp. Strain BR0Y6)	Cheese whey	PF	Semi-continuous	Tubular	3.34	Artificial (LED strips)	4 klux	0.61 mL H_2 mL^{-1}	Policastro *et al*., 2023
Rhodobacter capsulatus YO3 (hup^- mutant)	Sugar beet thick juice	DF+PF	Batch	Glass bottle	0.050	Artificial (Incandescent lamps)	2 klux	1.07 mL H_2 mL^{-1}	Uyar *et al*., 2015
R. capsulatus YO3 (hup^- mutant)	Sugar beet thick juice	DF+PF	Continuous	Flat panel	4	Artificial (Incandescent lamps)	2 klux	1.01 mL H_2 mL^{-1}	Uyar *et al*., 2015
R. sphaeroides O.U.001	Potato waste	DF+PF	Batch	Cylindrical bioreactor	2	Artificial (LED strips)	10 klx	0.8 mL H_2 mL^{-1}	Das & Basak, 2025
Rhodopseudomonas pseudopalustris MCC 3029	Distillery biowaste effluents	PF	Batch	Glass bottle	0.1	Artificial (NS)	190-310 $\mu E \cdot m^{-2} \cdot s^{-1}$	0.2 mL H_2 mL^{-1}	Jacob *et al*., 2025
R. sphaeroides O.U. 001	Dairy wastewater	PF	Batch	Glass bottle	0.025	Artificial (mercury-tungsten lamp)	9 klx	8.6 mL H_2 mL^{-1}	Seifert *et al*., 2010b
Bacterial consortium (predominant *R. palustris*)	Starch wastewater	DF+PF	Continuous	Vertical tubular bioreactor	1.625	Artificial (tungsten lamps)	190 W m^{-2}	3050 mL H_2 d^{-1}	Tawfik *et al*., 2014
R. sphaeroides NCIMB8253	Palm oil mill together with pulp and paper mill effluent	PF	Batch	Glass bottle	0.1	Artificial (fluorescent lamps)	4 klux	4.670 mL H_2 mL^{-1}	Budiman *et al*., 2015
R. capsulatus YO3 (hup^- mutant)	Molasses	PF	Continuous	Stacked U-tube bioreactor	9	Natural (sunlight)	228 W m^{-2}	0.31 mol H_2 m^{-3} h^{-1}	Kayahan *et al*., 2017

PNSB strain	Substrate	Production strategy	OM	Reactor type	CV (L)	LS	LI	Y	Ref.
R. sphaeroides TJ-0803 (glutamine auxotrophic mutant)	Tofu wastewater	PF	Batch	Glass bottle	0.150	Artificial (NS)	6-7 klux	14.2 ml L^{-1} h^{-1}	Zheng *et al*., 2010

Table 2. Overview of recent studies on PHB production by PNSB using agro-industrial waste as substrate. The table summarizes the PNSB strains, substrates, production strategy, operational mode (OM), reactor type, culture volume (CV), light source (LS), light intensity (LI), PHB yield (Y, expressed as % wPHB/wCDW), and references (Ref.). NA: not available.

PNSB strain	Substrate	Production strategy	OM	Reactor type	CV (L)	LS	LI	Y	Ref.
R. sphaeroides AV1b	Food waste	DF+PF	Batch	Glass bottle	400 mL	Artificial (Fluorescent lamps)	4000 lx	32.5 %	Ghimire *et al*., 2016
R. capsulatus	Fruit and vegetable wastes	DF+PF	Batch	Glass bottle	120 mL	Artificial (LED and halogen lamps)	3000 lx	24 %	Montiel-Corona *et al*., 2017
R. capsulatus	Fruit and vegetable wastes	DF+PF	Batch	Glass bottle	120 mL	Natural (sunlight)	3000 lx	29 %	Montiel-Corona *et al*., 2015
Mixed photosynthetic culture	Cheese whey	DF+PF	Batch	NA	450 mL	Artificial (Halogen lamps)	19 klx	20 %	Fradinho, Oehmen, & Reis, 2019
Mixed photosynthetic culture	Pre-treated food waste	PF	Batch	Glass bottle	100 mL	Artificial (Infrared lamps)	45 W m^{-2}	19 %	Allegue, Puyol, & Melero, 2020
Mixed photosynthetic culture	Domestic wastewater	DF+PF	Batch	Glass bottle	500 mL	Artificial (Halogen lamps)	6.17 W L^{-1}	30.8 %	Almeida *et al*., 2021
R. sphaeroides AV1b	Municipal organic waste	DF+PF	Batch	NA	400 mL	Artificial (Fluorescent lamps)	4000 lx	83 %	Luongo *et al*., 2017
Mixed culture of enriched PNSB	Winery wastewater	PF	Batch	NA	400 mL	Artificial (LED strips)	4000 lx	12-14 %	Policastro *et al*., 2020
Rhodopseudomonas sp. S16- VOGS3	Molasses	DF+PF	Semicontinuous	Bioreactor	NA	Artificial (Halogen-quartz-iodide)	74 W m^{-2}	30-42 %	Carlozzi *et al*., 2019b

PNSB strain	Substrate	Production strategy	OM	Reactor type	CV (L)	LS	LI	Y	Ref.
Rhodopseudomonas sp. S16-VOGS3	Solid fraction of digested sludge	PF	Batch	Cylindrical glass bioreactor	220 mL	Artificial (Halogen-quartz-iodide)	80 W m^{-2}	5 %	Touloupakis *et al*., 2023

Chapter V

Exploring PNSB Metabolism through Metabolic Modelling

5.1 From GENREs to GEMs: Concepts and Functional Insights

PNSB are characterized by high metabolic versatility and are naturally capable of producing high-value-added molecules, such as biofuels, bioplastics, and fine chemicals. In addition, they can be exploited in wastewater treatment, allowing the valorization of residual biomass into fertilizers and animal feed (Morrison & Bose, 2025). However, over the years, their evolution has been geared towards survival in the natural environments they colonize rather than industrial production. As a result, metabolic engineering strategies are often needed to increase the yield of molecules of interest (McKinlay, 2014).

The physiology of phototrophs, including PNSB, is less well understood than that of the heterotrophic microorganisms that are commonly used in industry. Consequently, metabolic engineering in these organisms is less advanced due to limited genetic tools (e.g., synthetic promoters or transformation methods), low transformation efficiencies, and the instability of engineered strains (Gudmundsson, Agudo & Nogales, 2017; Stephens, Mahadevan & Allen, 2021). To overcome these limitations, the metabolic specificities of PNSB must be investigated in greater depth, with approaches that avoid reliance on heterotrophic models.

In this context, systems biology offers powerful tools to accelerate understanding of PNSB metabolism and promote its biotechnological use (O'Brien, Monk, & Palsson, 2015). Among the most powerful tools in systems biology are genome-scale network reconstructions (GENREs), which are fundamental for linking an organism's genotype to its phenotype. GENREs are structured, curated representations of a microorganism's metabolic capabilities, based on annotated genomic sequences and integrated with biochemical and physiological knowledge (Haggart et al., 2011). In practice, a GENRE is a set of stoichiometrically balanced reactions associated with metabolites, enzymes, cellular compartments, and gene-protein-reaction (GPR) relationships (Gudmundsson, Agudo, & Nogales, 2017).

Once constructed, a GENRE can be converted into a genome-scale metabolic model (GEM): a quantitative computational model that describes cellular metabolism on a genomic scale. GEMs enable the *in-silico* simulation of an organism's metabolic behavior under specific conditions by integrating reactions with mathematical constraints, such as

flux limits, objective functions, and biomass reactions. GEMs can also be used to interpret omic data (Gudmundsson, Agudo, & Nogales, 2017).

Although the development of GENREs and GEMs in PNSBs is slower than in model organisms such as *E. coli* and *S. cerevisiae*, interest is growing, and an increasing number of reconstructions are becoming available. This chapter will present methods for constructing and analyzing models and discuss their applications in PNSB.

5.2 Construction and analysis of GENREs and GEMs

The construction of a GENRE and, subsequently, a GEM is divided into several stages, which in practice represent an iterative process of continuous revisions and refinements. Numerous protocols have been developed to guide the creation of high-quality metabolic reconstructions; among these, the most widely used is that proposed by Thiele and Palsson (2010). In summary, the process comprises four steps: 1) generation of a preliminary model; 2) manual refinement; 3) conversion into a mathematical format (the GEM); 4) evaluation and analysis of the metabolic network (Gudmundsson, Agudo & Nogales, 2017).

The first step is genomic annotation of the organism of interest. High-quality annotation is essential, as errors at this stage can compromise the reliability of the model. Based on the annotation, a preliminary model can be automatically generated using bioinformatic tools such as ModelSEED, CarveMe, and KBase (Arkin et al., 2018; Devoid et al., 2013; Machado et al., 2018). The result is a draft GENRE containing biochemical reactions associated with the annotated genes. However, this draft requires manual curation to correct errors, integrate missing reactions, and balance the network in terms of stoichiometry (Gudmundsson, Agudo & Nogales, 2017).

The model can be manually revised by consulting various databases, primarily KEGG, BRENDA, MetaCyc, ModelSEED, BiGG Models, and MetaNetX (Ganter et al., 2013; Gudmundsson, Agudo, & Nogales, 2017). At this stage, reactions must be verified in terms of mass and charge balance, directionality, gene-reaction association, and cellular compartmentalization. New reactions can be added based on information from the databases or biochemical data found in literature. Although essential for accuracy, this phase is very time-consuming, requiring up to years of work (Thiele & Palsson, 2010).

Once the GENRE has been completed, it is transformed into a GEM by mathematically representing the reactions in a stoichiometric matrix (S). This is an m × n matrix, where m represents the metabolites and n represents the reactions in the model. The elements S_{ij}

of the matrix contain the stoichiometric coefficients of metabolite *i* in reaction *j*; if the metabolite is consumed in the reaction, its stoichiometric coefficient will be negative, and if it is produced, it will be positive. If the metabolite does not participate in the reaction, the value will be zero (Haggart et al., 2011).

Once the stoichiometric matrix S has been constructed, GEM can only be performed by imposing constraints on the metabolic network. This is necessary because kinetic data for all individual metabolic reactions are not available, making it impossible to describe the system's behavior over time (Orth, Thiele & Palsson, 2010).

The first constraint imposed is the assumption of a steady state. This hypothesis posits that intracellular metabolite concentrations remain constant over time, i.e., that their production and consumption rates are balanced. This leads to a system of equations of the form $Sv = 0$, where S is the stoichiometric matrix and v is a vector representing the metabolic flows, or the rates at which individual reactions occur. These flows are the model's main variables, as they describe the metabolic network's functional behavior (Haggart et al., 2011; Orth, Thiele, & Palsson, 2010).

However, the resulting system of equations is indeterminate and cannot be treated without further constraints, since in large-scale models the number of reactions (n) exceeds that of metabolites (m), generating more unknowns than equations. As a result, there are infinite flow vectors compatible with the mass balance. To narrow down the solution space, the flows v are limited by lower (v_{min}) and upper (v_{max}) constraints; in irreversible reactions, v_{min} is equal to zero. These constraints define the admissible space of metabolic flows (Haggart et al., 2011; Orth, Thiele & Palsson, 2010).

Once the constraints have been defined, the GEM can be analyzed. The most widely used method is FBA, which requires the identification of a biologically relevant objective function, such as biomass maximization or the production of a metabolite of interest (e.g., bio-H_2 or PHB) (Gudmundsson, Agudo & Nogales, 2017). If the objective is growth, biomass is represented as an artificial reaction whose coefficients reflect the cell composition normalized to 1 g of dry biomass. In the model, this means that a unit flow through the biomass reaction corresponds to the production of one gram of new biomass for each gram of existing biomass per unit of time (Chan et al., 2017).

Once the objective function (or functions) has been defined, optimization can begin. In this phase, the distribution of the metabolic flux vector v that maximizes the objective function is identified, respecting the constraints imposed on the model. Mathematically, optimization is expressed as (Eq. 11):

$$Z = c^T \times v \quad (11)$$

where Z represents the objective function, v the flux vector, and c a vector that assigns a weight to each reaction based on its relevance. For example, to maximize cell growth, the value of c is equal to 1 for the biomass reaction and 0 for all others. This type of problem is solved using linear programming (Haggart et al., 2011).

Even once the GEM has been obtained, the resulting model is often still incomplete. Some metabolic pathways may be interrupted, which can prevent the production of essential metabolites or hinder the growth of the organism under certain conditions. Consequently, a gap-filling phase is necessary to identify and add the missing reactions to the model in a controlled manner. After each modification, FBA is rerun to verify whether the problem has been resolved. This process is repeated until the model exhibits behavior consistent with the available experimental data, such as the ability to grow on specific carbon sources or produce certain metabolites (Thiele & Palsson, 2010).

Various experimental techniques are employed to validate and enhance the model. These include growth tests on different carbon sources (e.g., Biolog plates), analysis of extracellular metabolites via high-performance liquid chromatography (HPLC), and mutagenesis studies involving gene knockouts. In silico simulations can also be compared with real metabolic fluxes obtained using isotopic tracers (e.g., ^{13}C) and enzyme mapping with fluorescent substrates (Haggart et al., 2011).

Numerous open-source software programs that implement these algorithms are now available for various programming languages, including MATLAB, Python, and R, and can be used to iteratively correct and improve GEM models (Fang, Lloyd, & Palsson, 2020).

5.3 An Overview of Existing PNSB GEMs and Their Applications in Biotechnology

Over the last ten years, PNSB have emerged as key microorganisms for numerous biotechnological applications thanks to their metabolic versatility and ability to adapt to different environments. In this context, GEMs are essential tools for understanding the complexity of their metabolism and directing its exploitation for productive purposes. Although the number of models available is still low compared to those developed for other phototrophs, such as cyanobacteria and microalgae, interest in obtaining GEMs in

PNSB has grown significantly in recent years. This has led to the development of increasingly comprehensive and accurate models.

The first significant contribution to constructing a GEM for PNSB was the pioneering study by Golomysova et al. (2010). This study modelled the photoheterotrophic metabolism of *R. sphaeroides* for the first time, to support metabolic engineering for bio-H_2 production. Consisting of 314 reactions and 287 metabolites, the model introduces an innovative aspect compared to traditional approaches by simultaneously optimizing two cellular objectives: biomass production and the removal of reducing equivalents. This reflects a unique characteristic of PNSB: the need to dispose of excess electrons resulting from the oxidation of organic substrates. The model showed good consistency with the available experimental data, paving the way for subsequent reconstructions.

In a subsequent study, Hädicke, Grammel, and Klamt (2011) reconstructed three distinct GEMs representing the central metabolism of *R. sphaeroides*, *R. rubrum,* and *R. palustris*. Using Flux Variability Analysis (FVA), a method that determines the possible flux range for each reaction while preserving the optimal value of the objective function, the study quantitatively elucidated the unexpected role of the Calvin cycle. Notably, the cycle was found to be active under conditions where it is not usually expected to operate, such as when CO_2 is released. This highlights its primary role in maintaining redox balance rather than carbon fixation. This function makes the Calvin cycle essential for the metabolism of many organic substrates. Additionally, the models differentiated alternative acetate assimilation pathways in *R. sphaeroides* and *R. rubrum*, both of which lack isocitrate lyase. Finally, the study demonstrated the potential of the models in biotechnology by simulating theoretical photoheterotrophic bio-H_2 production and identifying possible genetic interventions to enhance hydrogen yield.

Further progress was made in the construction of the iRsp1095 model for the *R. sphaeroides* 2.4.1 strain by Imam et al. (2011). This model incorporates 1095 genes, 796 metabolites, and 1158 reactions. It has enabled the identification of additional metabolic pathways that the microorganism can use to dissipate excess reducing power, alongside those already recognized, including CO_2 fixation, PHB synthesis, and bio-H_2 production. These alternative pathways include H_2S production via sulphite reductase, reductive carbon assimilation via ethylmalonyl-CoA, and secretion of metabolites such as lactate and formate. Additionally, the model identified a set of reactions whose elimination would result in a hydrogen yield nearly equivalent to the theoretical maximum, providing valuable insights for metabolic engineering.

Imam, Noguera, and Donohue (2013) developed an improved version of the iRsp1095 model, iRsp1140, by integrating phenotypic, transcriptomic, and genetic data. This update improved the accuracy with which key metabolic processes were simulated, particularly under photosynthetic conditions. The study concentrated on NADPH metabolism and the pivotal function of PntAB transhydrogenase, an enzyme that is vital for photosynthetic growth when different organic electron donors are present. Constraint-based simulations and gene expression analysis identified alternative NADPH synthesis pathways that are activated in the ΔpntAB mutant to compensate for the absence of the enzyme. These changes involve a redistribution of metabolic fluxes to maintain redox balance, particularly under photoheterotrophic conditions.

Burger et al. (2017) took a further step forward in achieving a systemic understanding of the metabolism of *R. sphaeroides* by adopting an innovative approach based on generating a library of mutants through transposon insertion and analyzing it using the Tn-seq technique. This method enabled the identification of numerous genes that are essential for aerobic growth in both rich and minimal media, as well as genes that are indispensable for photosynthetic growth. The resulting data were subsequently integrated into an existing genome-scale metabolic model, thereby refining the model and enhancing its predictive capabilities.

Recently, interest has focused on *R. palustris*, a species of PNSB with a wide range of environmental and industrial biotechnological applications. Alsiyabi, Immethun, and Saha (2019) obtained the iRpa940 model of the *R. palustris* CGA009 strain, which comprises 940 genes, 1393 reactions, and 1491 metabolites. They validated the model using a parsimonious flux balance analysis (pFBA) approach, an extension of flux balance analysis (FBA) that minimizes non-essential fluxes, in conjunction with experimental data from metabolic flux analysis (MFA). MFA is a technique that quantifies actual metabolic fluxes using isotopic tracers. The study revealed the need for an unidentified quinol oxidation reaction and demonstrated that the redox state of the quinone pool directly controls CO_2 fixation via the CBB cycle. This provides new insights into the regulation of photosynthetic metabolism and opens up prospects for biotechnological applications.

Further work by Navid et al. (2019) shed additional light on the metabolism of R. palustris under photoheterotrophic conditions. A multi-objective analysis showed that the metabolism of the species is primarily limited by light rather than carbon availability. Under these conditions, *R. palustris* prioritizes carbon use efficiency, followed by ATP

production and growth, and can divert energy from biomass to CO_2 fixation. The study also revealed that, while of biotechnological interest, hydrogen production comes at the expense of cell growth.

Chowdhury, Alsiyabi, and Saha (2022) recently developed the first ME (Metabolism and Expression) model of *R. palustris* CGA009. This model integrates transcription, translation, and macromolecular synthesis, thereby overcoming the limitations of classical metabolic models. The model has enabled ferredoxin to be identified as a key regulator of electron distribution, and malate dehydrogenase and glycerol-3-phosphate dehydrogenase to be recognized as potential alternative "sinks" that can consume excess electrons and maintain cellular redox balance. This provides new insights into redox balance bottlenecks and has biotechnological implications to produce bio-H_2 and bioplastic precursors.

Finally, Tec-Campos et al. (2023) developed the iDT1294 model for the *R. palustris* Bis A53 strain. This model consists of 2721 reactions, 2123 metabolites, and 1294 genes. The model was validated using phenotypic, physiological, and kinetic data obtained from over 350 growth conditions. Compared to previous models, it significantly expands metabolic coverage, enabling accurate analysis of aromatic compound degradation and transitions between photoheterotrophic and photoautotrophic modes.

Although GEMs developed for PNSB are less widespread than those available for other photosynthetic microorganisms, there has been a gradual development of increasingly accurate and mature models in recent years. These models are ready to guide targeted metabolic engineering interventions and fully exploit the potential of PNSBs in biotechnological processes.

References

Munir, M. T., Mansouri, S. S., Udugama, I. A., Baroutian, S., Gernaey, K. V., & Young, B. R. (2018). Resource recovery from organic solid waste using hydrothermal processing: Opportunities and challenges. *Renewable and Sustainable Energy Reviews, 96*, 64–75. https://doi.org/10.1016/j.rser.2018.07.039.

Shah, A. V., Singh, A., Mohanty, S. S., Srivastava, V. K., & Varjani, S. (2022). Organic solid waste: Biorefinery approach as a sustainable strategy in circular bioeconomy. *Bioresource Technology, 349,* 126835. https://doi.org/10.1016/j.biortech.2022.126835.

Pengadeth, D., Basak, N., Bernabò, L., & Adessi, A. (2024). Recent advances in dark fermentative hydrogen production from vegetable waste: Role of inoculum, consolidated bioprocessing, and machine learning. *Environmental Science and Pollution Research, 31,* 66537–66550. https://doi.org/10.1007/s11356-024-35668-7.

Freitas, L. C., Barbosa, J. R., da Costa, A. L. C., Bezerra, F. W. F., Pinto, R. H. H., & de Carvalho Junior, R. N. (2021). From waste to sustainable industry: How can agro-industrial wastes help in the development of new products? *Resources, Conservation and Recycling, 169,* 105466. https://doi.org/10.1016/j.resconrec.2021.105466.

Ragini, Y. P., Karishma, S., Kamalesh, R., Saravanan, A., TajSabreen, B., & Eswaar, D. K. (2025). Sustainable biorefinery approaches in the valorization of agro-food industrial residues for biofuel production: Economic and future perspectives. *Sustainable Energy Technologies and Assessments, 75,* 104239. https://doi.org/10.1016/j.seta.2025.104239.

Baral, B., Akhgari, A., & Metsä-Ketelä, M. (2018). Activation of microbial secondary metabolic pathways: Avenues and challenges. *Synthetic and Systems Biotechnology, 3*(3), 163–178. https://doi.org/10.1016/j.synbio.2018.09.001.

Paes, B. G., & Almeida, J. R. (2014). Genetic improvement of microorganisms for applications in biorefineries. *Chemical and Biological Technologies in Agriculture, 1,* 21. https://doi.org/10.1186/s40538-014-0021-1.

Decker, S. R., Brunecky, R., Yarbrough, J. M., & Subramanian, V. (2023). Perspectives on biorefineries in microbial production of fuels and chemicals. *Frontiers in Industrial Microbiology, 1,* 1202269. https://doi.org/10.3389/finmi.2023.1202269.

Saini, P., & Mishra, P. (2024). Microbial bioprospecting for biorefinery application: An overview of a sustainable and renewable source of energy. In *Bioprospecting of microbial resources for agriculture, environment and bio-chemical industry*. Springer. https://doi.org/10.1007/978-3-031-63844-2_6.

Gaur, S., Kaur, M., Kalra, R., Rene, E. R., & Goel, M. (2024). Application of microbial resources in biorefineries: Current trend and future prospects. *Heliyon, 10*(8), e28615. https://doi.org/10.1016/j.heliyon.2024.e28615.

Thapa, S., Mishra, J., Arora, N., Mishra, P., Li, H., O'Hair, J., Bhatti, S., & Zhou, S. (2020). Microbial cellulolytic enzymes: diversity and biotechnology with reference to lignocellulosic biomass degradation. *Reviews in Environmental Science and Bio/Technology, 19*(3), 621–648. https://doi.org/10.1007/s11157-020-09536-y.

Trivedi, A., & Joshi, S. (2025). Biofuels as energy for tomorrow. In A. Kuila & D. Kumar (Eds.), *Optimizing biofuel production with artificial intelligence* (Chapter 3). Wiley. https://doi.org/10.1002/9781394301287.ch3.

Melin, K., Nieminen, H., Klüh, D., Laari, A., Koiranen, T., & Gaderer, M. (2022). Techno-economic evaluation of novel hybrid biomass and electricity-based ethanol fuel production. *Frontiers in Energy Research, 10,* 796104. https://doi.org/10.3389/fenrg.2022.796104.

Pandey, A., Larroche, C., Gnansounou, E., Khanal, S. K., Dussap, C. G., & Ricke, S. (Eds.). (2019). *Biomass, biofuels, biochemicals: Biofuels: Alternative feedstocks and conversion processes for the production of liquid and gaseous biofuels* (2nd ed.). Academic Press. ISBN 978-0-12-816856-1.

Antoni, D., Zverlov, V. V., & Schwarz, W. H. (2007). Biofuels from microbes. *Applied Microbiology and Biotechnology, 77*(1), 23–35. https://doi.org/10.1007/s00253-007-1163-x.

Daggubati, L., Sobhani, Z., Carbery, M., Ramadass, K., & Palanisami, T. (2025). Fingerprinting risk from recycled plastic products using physical and chemical properties. *Journal of Hazardous Materials, 488,* 137507. https://doi.org/10.1016/j.jhazmat.2025.137507.

Walker, T. R., & Fequet, L. (2023). Current trends of unsustainable plastic production and micro(nano)plastic pollution. *TrAC Trends in Analytical Chemistry, 160,* 116984. https://doi.org/10.1016/j.trac.2023.116984.

Schmaltz, E., Melvin, E. C., Diana, Z., Gunady, E. F., Rittschof, D., Somarelli, J. A., Virdin, J., & Dunphy-Daly, M. M. (2020). Plastic pollution solutions: Emerging technologies to prevent and collect marine plastic pollution. *Environment International, 144,* 106067. https://doi.org/10.1016/j.envint.2020.106067.

Xuyang, W., Khalil, K., Zhuo, T., Keyan, C., Nazir, M. Y. M., Aqma, W. S., & Hong, N. Q. (2025). Addressing the plastisphere: Sustainable approaches to combat plastic pollution. *Science of The Total Environment, 959,* 178105. https://doi.org/10.1016/j.scitotenv.2024.178105.

Hale, R. C., Seeley, M. E., La Guardia, M. J., Mai, L., & Zeng, E. Y. (2020). A global perspective on microplastics. *Journal of Geophysical Research: Oceans, 125*(2), e2018JC014719. https://doi.org/10.1029/2018JC014719.

Tirkey, A., & Upadhyay, L. S. B. (2021). Microplastics: An overview on separation, identification and characterization of microplastics. *Marine Pollution Bulletin, 170,* 112604. https://doi.org/10.1016/j.marpolbul.2021.112604.

Alias, N. H., Abdullah, N., Othman, N. H., Marpani, F., Zainol, M. M., & Shayuti, M. S. M. (2022). Sustainability challenges and future perspectives of biopolymer. In A. K. Nadda, S. Sharma, & R. Bhat (Eds.), *Biopolymers* (pp. 373–389). Springer. https://doi.org/10.1007/978-3-030-98392-5_17.

Chaudry, S., Hurtado-McCormick, V., Cheng, K. Y., Willis, A., Speight, R., & Kaksonen, A. H. (2025). Microalgae to bioplastics - Routes and challenges. *Cleaner Engineering and Technology, 25,* 100922. https://doi.org/10.1016/j.clet.2025.100922.

Montiel-Corona, V., & Buitrón, G. (2021). Polyhydroxyalkanoates from organic waste streams using purple non-sulfur bacteria. *Bioresource Technology, 323,* 124610. https://doi.org/10.1016/j.biortech.2020.124610.

Martínez-Burgos, W. J., Pozzan, R., Pacheco Quintero, A. R., de Souza Vandenberghe, L. P., & Soccol, C. R. (2023). Production of bioplastics through microorganisms. In *Encyclopedia of green materials* (pp. 1-10). Singapore: Springer Nature Singapore.

Kawaguchi, H., Ogino, C., & Kondo, A. (2017). Microbial conversion of biomass into bio-based polymers. *Bioresource Technology, 245*(Part B), 1664–1673. https://doi.org/10.1016/j.biortech.2017.06.135.

Lee, J. W., Kim, H. U., Choi, S., Yi, J., & Lee, S. Y. (2011). Microbial production of building block chemicals and polymers. *Current Opinion in Biotechnology, 22*(6), 758–767. https://doi.org/10.1016/j.copbio.2011.02.011.

Nambiar, K., Saravana Kumari, P., Devaraj, D., & Sevanan, M. (2024). Development of biopolymers from microbes and their environmental applications. *Physical Sciences Reviews, 9*(4), 1903–1929. https://doi.org/10.1515/psr-2022-0219.

Reshmy, R., Thomas, D., Philip, E., Paul, S. A., Madhavan, A., Sindhu, R., & Binod, P. (2021). Bioplastic production from renewable lignocellulosic feedstocks: A review. *Reviews in Environmental Science and Bio/Technology, 20*(1), 167–187. https://doi.org/10.1007/s11157-021-09565-1.

Sharma, M., Tellili, N., Kacem, I., & Rouissi, T. (2024). Microbial biopolymers: From production to environmental applications-A review. *Applied Sciences, 14*(12), 5081. https://doi.org/10.3390/app14125081.

Monclaro, A. V., Gomes, H. A. R., Duarte, G. C., de Souza Moreira, L. R., & Filho, E. X. F. (2024). Unveiling the biomass valorization: The microbial diversity in promoting a sustainable socio-economy. *BioEnergy Research, 17*(3), 1355–1374. https://doi.org/10.1007/s12155-024-10743-6.

Mankar, A. R., Pandey, A., Modak, A., & Pant, K. K. (2021). Pretreatment of lignocellulosic biomass: A review on recent advances. *Bioresource Technology, 334,* 125235. https://doi.org/10.1016/j.biortech.2021.125235.

Sharma, H. K., Xu, C., & Qin, W. (2019). Biological pretreatment of lignocellulosic biomass for biofuels and bioproducts: An overview. *Waste and Biomass Valorization, 10*(2), 235–251. https://doi.org/10.1007/s12649-017-0059-y.

Dahiya, S., Kumar, A. N., Sravan, J. S., Chatterjee, S., Sarkar, O., & Mohan, S. V. (2018). Food waste biorefinery: Sustainable strategy for circular bioeconomy. *Bioresource Technology, 248*(Part A), 2–12. https://doi.org/10.1016/j.biortech.2017.07.176.

Nazzaro, F., Fratianni, F., Ombra, M. N., d'Acierno, A., & Coppola, R. (2018). Recovery of biomolecules of high benefit from food waste. *Current Opinion in Food Science, 22,* 43–54. https://doi.org/10.1016/j.cofs.2018.01.012.

Gu, C., Kim, G. B., Kim, W. J., Kim, H. U., & Lee, S. Y. (2019). Current status and applications of genome-scale metabolic models. *Genome Biology, 20*(1), 121. https://doi.org/10.1186/s13059-019-1730-3.

Van der Hauwaert, L., Regueira, A., & Mauricio-Iglesias, M. (2024). Advancing biorefinery design through the integration of metabolic models. *Journal of Cleaner Production, 465,* 142793. https://doi.org/10.1016/j.jclepro.2024.142793.

Abdin, Z., Zafaranloo, A., Rafiee, A., Mérida, W., Lipiński, W., & Khalilpour, K. R. (2020). Hydrogen as an energy vector. Renewable and Sustainable Energy Reviews, 120, 109620. https://doi.org/10.1016/j.rser.2019.109620.

Milkov, A. V. (2022). Molecular hydrogen in surface and subsurface natural gases: Abundance, origins and ideas for deliberate exploration. Earth-Science Reviews, 230, 104063. https://doi.org/10.1016/j.earscirev.2022.104063.

Nikolaidis, P., & Poullikkas, A. (2017). A comparative overview of hydrogen production processes. Renewable and Sustainable Energy Reviews, 67, 597–611. https://doi.org/10.1016/j.rser.2016.09.044.

Xu, X., Zhou, Q., & Yu, D. (2022). The future of hydrogen energy: Bio-hydrogen production technology. International Journal of Hydrogen Energy, 47(79), 33677–33698. https://doi.org/10.1016/j.ijhydene.2022.07.261.

Cavaliere, P. (2025). Hydrogen: Energy vector and fuel. In Hydrogen embrittlement in metals and alloys (pp. 1–155). Springer. https://doi.org/10.1007/978-3-031-83681-7_1.

Aba, M. M., Sauer, I. L., & Amado, N. B. (2024). Comparative review of hydrogen and electricity as energy carriers for the energy transition. International Journal of Hydrogen Energy, 57, 660–678. https://doi.org/10.1016/j.ijhydene.2024.01.034.

Matias, J. C. de O., & Devezas, T. C. (2007). Consumption dynamics of primary-energy sources: The century of alternative energies. Applied Energy, 84(7–8), 763–770. https://doi.org/10.1016/j.apenergy.2007.01.007.

Arsad, A. Z., Hannan, M. A., Al-Shetwi, A. Q., Mansur, M., Muttaqi, K. M., Dong, Z. Y., & Blaabjerg, F. (2022). Hydrogen energy storage integrated hybrid renewable energy systems: A review analysis for future research directions. International Journal of Hydrogen Energy, 47(39), 17285–17312. https://doi.org/10.1016/j.ijhydene.2022.03.208.

Schrotenboer, A. H., Veenstra, A. A. T., uit het Broek, M. A. J., & Ursavas, E. (2022). A green hydrogen energy system: Optimal control strategies for integrated hydrogen storage and power generation with wind energy. Renewable and Sustainable Energy Reviews, 168, 112744. https://doi.org/10.1016/j.rser.2022.112744.

Calabrese, M., Portarapillo, M., Di Nardo, A., Venezia, V., Turco, M., Luciani, G., & Di Benedetto, A. (2024). Hydrogen safety challenges: A comprehensive review on production, storage, transport, utilization, and CFD-based consequence and risk assessment. Energies, 17(6), 1350. https://doi.org/10.3390/en17061350.

Dincer, I., & Acar, C. (2015). Review and evaluation of hydrogen production methods for better sustainability. International Journal of Hydrogen Energy, 40(34), 11094–11111. https://doi.org/10.1016/j.ijhydene.2014.12.035.

Longden, T., Beck, F. J., Jotzo, F., Andrews, R., & Prasad, M. (2022). 'Clean' hydrogen? – Comparing the emissions and costs of fossil fuel versus renewable electricity-based hydrogen. Applied Energy, 306(Part B), 118145. https://doi.org/10.1016/j.apenergy.2021.118145.

Akhlaghi, N., & Najafpour-Darzi, G. (2020). A comprehensive review on biological hydrogen production. *International Journal of Hydrogen Energy, 45*(43), 22492–22512. https://doi.org/10.1016/j.ijhydene.2020.06.182.

Sinha, P., & Pandey, A. (2011). An evaluative report and challenges for fermentative biohydrogen production. *International Journal of Hydrogen Energy, 36*(13), 7460–7478. https://doi.org/10.1016/j.ijhydene.2011.03.077.

Hallenbeck, P. C. (2014). Bioenergy from microorganisms: An overview. In D. Zannoni & R. De Philippis (Eds.), Microbial BioEnergy: Hydrogen production (Vol. 38, pp. 1–20). Springer. https://doi.org/10.1007/978-94-017-8554-9_1.

Manish, S., & Banerjee, R. (2008). Comparison of biohydrogen production processes. International Journal of Hydrogen Energy, 33(1), 279–286. https://doi.org/10.1016/j.ijhydene.2007.07.026.

Rai, P. K., & Singh, S. P. (2016). Integrated dark- and photo-fermentation: Recent advances and provisions for improvement. International Journal of Hydrogen Energy, 41(44), 19957–19971. https://doi.org/10.1016/j.ijhydene.2016.08.084.

Nagarajan, D., Lee, D.-J., Kondo, A., & Chang, J.-S. (2017). Recent insights into biohydrogen production by microalgae – From biophotolysis to dark fermentation. Bioresource Technology, 227, 373–387. https://doi.org/10.1016/j.biortech.2016.12.104.

Melis, A., Zhang, L., Forestier, M., Ghirardi, M. L., & Seibert, M. (2000). Sustained photobiological hydrogen gas production upon reversible inactivation of oxygen evolution in the green alga Chlamydomonas reinhardtii. Plant Physiology, 122(1), 127–136. https://doi.org/10.1104/pp.122.1.127.

Saravanan, S., Kumar, P. S., Khoo, K. S., Show, P.-L., Carolin, C. F., Jackulin, C. F., Jeevanantham, S., Karishma, S., Show, K.-Y., Lee, D.-J., & Chang, J.-S. (2021). Biohydrogen from organic wastes as a clean and environment-friendly energy source: Production pathways, feedstock types, and future prospects. Bioresource Technology, 342, 126021. https://doi.org/10.1016/j.biortech.2021.126021.

McKinlay, J. B. (2014). Systems biology of photobiological hydrogen production by purple non-sulfur bacteria. In D. Zannoni & R. De Philippis (Eds.), Microbial BioEnergy: Hydrogen production (Vol. 38, pp. 155–176). Springer. https://doi.org/10.1007/978-94-017-8554-9_7.

Adessi, L., La Cava, E., & De Philippis, R. (2021). Photosynthesis | Purple bacteria: Electron acceptors and donors. In J. Jez (Ed.), Encyclopedia of Biological Chemistry III (3rd ed., pp. 305–314). Elsevier. https://doi.org/10.1016/B978-0-12-819460-7.00016-5.

Corneli, E., Adessi, A., Olguín, E. J., Ragaglini, G., García-López, D. A., & De Philippis, R. (2017). Biotransformation of water lettuce (Pistia stratiotes) to biohydrogen by Rhodopseudomonas palustris. Journal of Applied Microbiology, 123(6), 1438–1446. https://doi.org/10.1111/jam.13599.

Ghosh, S., Dairkee, U. K., Chowdhury, R., & Bhattacharya, P. (2017). Hydrogen from food processing wastes via photofermentation using purple non-sulfur bacteria (PNSB) – A review. Energy Conversion and Management, 141, 299–314. https://doi.org/10.1016/j.enconman.2016.09.001.

Anjum, A., Zuber, M., Zia, K. M., Noreen, A., Anjum, M. N., & Tabasum, S. (2016). Microbial production of polyhydroxyalkanoates (PHAs) and its copolymers: A review of recent advancements. International Journal of Biological Macromolecules, 89, 161–174. https://doi.org/10.1016/j.ijbiomac.2016.04.069.

Jayakumar, A., Radoor, S., Siengchin, S., Shin, G. H., & Kim, J. T. (2023). Recent progress of bioplastics in their properties, standards, certifications and regulations: A review. Science of The Total Environment, 878, 163156. https://doi.org/10.1016/j.scitotenv.2023.163156.

Lackner, M., Mukherjee, A., & Koller, M. (2023). What are “bioplastics”? Defining renewability, biosynthesis, biodegradability, and biocompatibility. Polymers, 15(24), 4695. https://doi.org/10.3390/polym15244695.

European Bioplastics. (n.d.). Bioplastics. Retrieved June 17, 2025, from https://www.european-bioplastics.org/bioplastics/.

Narayan, R. (2017). Biodegradable and biobased plastics: An overview. In M. Malinconico (Ed.), Soil degradable bioplastics for a sustainable modern agriculture (pp. 13–31). Springer. https://doi.org/10.1007/978-3-662-54130-2_2.

Koller, M., Gasser, I., Schmid, F., & Berg, G. (2011). Linking ecology with economy: Insights into polyhydroxyalkanoate-producing microorganisms. Engineering in Life Sciences, 11(3), 222–237. https://doi.org/10.1002/elsc.201000190.

Sali, S., & Mackey, H. R. (2021). The application of purple non-sulfur bacteria for microbial mixed culture polyhydroxyalkanoates production. Reviews in Environmental Science and Bio/Technology, 20, 959–983. https://doi.org/10.1007/s11157-021-09597-7.

Lim, J., You, M., Li, J., & Li, Z. (2017). Emerging bone tissue engineering via Polyhydroxyalkanoate (PHA)-based scaffolds. Materials Science and Engineering: C, 79, 917–929. https://doi.org/10.1016/j.msec.2017.05.132.

Sharma, V., Sehgal, R., & Gupta, R. (2021). Polyhydroxyalkanoate (PHA): Properties and modifications. Polymer, 212, 123161. https://doi.org/10.1016/j.polymer.2020.123161.

Tan, G.-Y. A., Chen, C.-L., Li, L., Ge, L., Wang, L., Razaad, I. M. N., Li, Y., Zhao, L., Mo, Y., & Wang, J.-Y. (2014). Start a research on biopolymer polyhydroxyalkanoate (PHA): A review. Polymers, 6(3), 706–754. https://doi.org/10.3390/polym6030706.

Caputo, M. R., Tang, X., Westlie, A. H., Sardon, H., Chen, E. Y. X., & Müller, A. J. (2022). Effect of chain stereoconfiguration on poly(3-hydroxybutyrate) crystallization kinetics. Biomacromolecules, 23(9), 3847–3859. https://doi.org/10.1021/acs.biomac.2c00682.

Lenz, R. W., & Marchessault, R. H. (2005). Bacterial polyesters: biosynthesis, biodegradable plastics and biotechnology. Biomacromolecules, 6(1), 1-8. https://doi.org/10.1021/bm049700c.

Turco, R., Santagata, G., Corrado, I., Pezzella, C., & Di Serio, M. (2021). In vivo and post-synthesis strategies to enhance the properties of PHB-based materials: A review.

Frontiers in Bioengineering and Biotechnology, 8, 619266. https://doi.org/10.3389/fbioe.2020.619266.

Sudesh, K., Abe, H., & Doi, Y. (2000). Synthesis, structure and properties of polyhydroxyalkanoates: Biological polyesters. Progress in Polymer Science, 25(10), 1503–1555. https://doi.org/10.1016/S0079-6700(00)00035-6.

Numata, K., Abe, H., & Iwata, T. (2009). Biodegradability of poly(hydroxyalkanoate) materials. Materials, 2(3), 1104–1126. https://doi.org/10.3390/ma2031104.

Yanti, N. A., Sembiring, L., Margino, S., & Ahmad, S. W. (2021). Bacterial production of poly β hydroxybutyrate (PHB): Converting starch into bioplastics. In M. Kuddus & Roohi (Eds.), Bioplastics for sustainable development (pp. 259–276). Springer. https://doi.org/10.1007/978-981-16-1823-9_9.

dos Santos, A. J., Oliveira Dalla Valentina, L. V., Hidalgo Schulz, A. A., & Tomaz Duarte, M. A. (2017). From obtaining to degradation of PHB: Material properties. Part I. Ingeniería y Ciencia, 13(26), 269–298. https://doi.org/10.17230/ingciencia.13.26.10.

Paduvari, R., & Somashekara, D. M. (2025). Advancements in genetic engineering for enhanced polyhydroxyalkanoates (PHA) production: A comprehensive review of metabolic pathway manipulation and gene deletion strategies. Bioengineered, 16(1), 2458363. https://doi.org/10.1080/21655979.2025.2458363.

Yañez, L., Conejeros, R., Vergara-Fernández, A., & Scott, F. (2020). Beyond intracellular accumulation of polyhydroxyalkanoates: Chiral hydroxyalkanoic acids and polymer secretion. Frontiers in Bioengineering and Biotechnology, 8, 248. https://doi.org/10.3389/fbioe.2020.00248.

Sharma, V., Sehgal, R., & Gupta, R. (2021). Polyhydroxyalkanoate (PHA): Properties and modifications. Polymer, 212, 123161. https://doi.org/10.1016/j.polymer.2020.123161.

Ghasemlou, M., Barrow, C. J., & Adhikari, B. (2024). The future of bioplastics in food packaging: An industrial perspective. Food Packaging and Shelf Life, 43, 101279. https://doi.org/10.1016/j.fpsl.2024.101279.

Zytner, P., Kumar, D., Elsayed, A., Mohanty, A., Ramarao, B. V., & Misra, M. (2023). A review on polyhydroxyalkanoate (PHA) production through the use of lignocellulosic biomass. RSC Sustainability, 1(2120–2134). https://doi.org/10.1039/D3SU00126A.

Gundlapalli, M., & Ganesan, S. (2025). Polyhydroxyalkanoates (PHAs): Key challenges in production and sustainable strategies for cost reduction within a circular economy framework. Results in Engineering, 26, 105345. https://doi.org/10.1016/j.rineng.2025.105345.

Getino, L., Martín, J. L., & Chamizo-Ampudia, A. (2024). A review of polyhydroxyalkanoates: Characterization, production, and application from waste. Microorganisms, 12(10), 2028. https://doi.org/10.3390/microorganisms12102028.

Adessi, A., Venturi, M., Candeliere, F., Galli, V., Granchi, L., & De Philippis, R. (2018). Bread wastes to energy: Sequential lactic and photo-fermentation for hydrogen production. International Journal of Hydrogen Energy, 43(20), 9569–9576. https://doi.org/10.1016/j.ijhydene.2018.04.053.

Povolo, S., Toffano, P., Basaglia, M., & Casella, S. (2010). Polyhydroxyalkanoates production by engineered Cupriavidus necator from waste material containing lactose. Bioresource Technology, 101(20), 7902–7907. https://doi.org/10.1016/j.biortech.2010.05.029.

Chen, G.-Q., & Jiang, X.-R. (2018). Engineering microorganisms for improving polyhydroxyalkanoate biosynthesis. Current Opinion in Biotechnology, 53, 20–25. https://doi.org/10.1016/j.copbio.2017.10.008.

Monroy, I., & Buitrón, G. (2020). Production of polyhydroxybutyrate by pure and mixed cultures of purple non-sulfur bacteria: A review. *Journal of Biotechnology, 317,* 39–47. https://doi.org/10.1016/j.jbiotec.2020.04.012.

Srirangan, K., Liu, X., Tran, T. T., Charles, T. C., Moo-Young, M., & Chou, C. P. (2016). Engineering of *Escherichia coli* for direct and modulated biosynthesis of poly(3-hydroxybutyrate-co-3-hydroxyvalerate) copolymer using unrelated carbon sources. Scientific Reports, 6, 36470. https://doi.org/10.1038/srep36470.

Brown, B., Immethun, C., Alsiyabi, A., Long, D., Wilkins, M., & Saha, R. (2022). Heterologous phasin expression in *Rhodopseudomonas palustris* CGA009 for bioplastic production from lignocellulosic biomass. Metabolic Engineering Communications, 14, e00191. https://doi.org/10.1016/j.mec.2021.e00191.

Gao, Q., Yang, H., Wang, C., Xie, X.-Y., Liu, K.-X., Lin, Y., Han, S.-Y., Zhu, M., Neureiter, M., Lin, Y., & Ye, J.-W. (2022). Advances and trends in microbial production of polyhydroxyalkanoates and their building blocks. Frontiers in Bioengineering and Biotechnology, 10, Article 966598. https://doi.org/10.3389/fbioe.2022.966598.

Jiang, X.-R., Wang, H., Shen, R., & Chen, G.-Q. (2015). Engineering the bacterial shapes for enhanced inclusion bodies accumulation. Metabolic Engineering, 29, 227–237. https://doi.org/10.1016/j.ymben.2015.03.017.

Simeonidis, E., & Price, N. D. (2015). Genome-scale modeling for metabolic engineering. Journal of Industrial Microbiology and Biotechnology, 42(3), 327–338. https://doi.org/10.1007/s10295-014-1576-3.

Madigan, M. T., & Jung, D. O. (2009). An overview of purple bacteria: systematics, physiology, and habitats. The purple phototrophic bacteria, 1-15. https://doi.org/10.1007/978-1-4020-8815-5.

Cohen-Bazire, G., Sistrom, W. R., & Stanier, R. Y. (1957). Kinetic studies of pigment synthesis by non-sulfur purple bacteria. Journal of Cellular and Comparative Physiology, 49(1), 25–68. https://doi.org/10.1002/jcp.1030490104.

Capson-Tojo, G., Batstone, D. J., Grassino, M., Vlaeminck, S. E., Puyol, D., Verstraete, W., Kleerebezem, R., Oehmen, A., Ghimire, A., Pikaar, I., Lema, J. M., & Hülsen, T. (2020). Purple phototrophic bacteria for resource recovery: Challenges and opportunities. Biotechnology Advances, 43, 107567. https://doi.org/10.1016/j.biotechadv.2020.107567.

Schmidt, T. M., Zahn, J. A., Boyd, E. S., de la Mora, A., & DiSpirito, A. A. (2003). Role of Rhodobacter sp. strain PS9, a purple non-sulfur photosynthetic bacterium isolated from an anaerobic swine waste lagoon, in odor remediation. Applied and Environmental Microbiology, 69(3), 1710–1720. https://doi.org/10.1128/AEM.69.3.1710-1720.2003.

Morrison, H. M., & Bose, A. (2024). Purple non-sulfur bacteria for biotechnological applications. Journal of Industrial Microbiology and Biotechnology, 52, kuae052. https://doi.org/10.1093/jimb/kuae052.

Petushkova, E., Mayorova, E., & Tsygankov, A. (2021). TCA cycle replenishing pathways in photosynthetic purple non-sulfur bacteria growing with acetate. Life, 11(7), 711. https://doi.org/10.3390/life11070711.

Martinez-Burgos, W. J., Sydney, E. B., Medeiros, A. B. P., Magalhães, A. I., de Carvalho, J. C., Karp, S. G., Vandenberghe, L. P. S., Letti, L. A. J., Soccol, V. T., Pereira, G. V. de M., Rodrigues, C., Woiciechowski, A. L., & Soccol, C. R. (2021). Agro-industrial wastewater in a circular economy: Characteristics, impacts and applications for bioenergy and biochemicals. Bioresource Technology, 341, 125795. https://doi.org/10.1016/j.biortech.2021.125795.

Seifert, K., Waligorska, M., & Laniecki, M. (2010a). Brewery wastewaters in photobiological hydrogen generation in presence of Rhodobacter sphaeroides O.U. 001.

International Journal of Hydrogen Energy, 35(9), 4085–4091. https://doi.org/10.1016/j.ijhydene.2010.01.126.

Zhang, T., Quijano, G., & Wang, M. (2024). Fast development of purple nonsulfur bacteria (PNSB) in a bubble column photobioreactor: Influence of carbon source and dissolved O_2 availability on wastewater treatment performance. Journal of Water Process Engineering, 65, 105885. https://doi.org/10.1016/j.jwpe.2024.105885.

Zhang, L., Jiang, Z., Tsui, T.-H., Loh, K.-C., Dai, Y., & Tong, Y. W. (2022). A review on enhancing *Cupriavidus necator* fermentation for poly(3-hydroxybutyrate) (PHB) production from low-cost carbon sources. Frontiers in Bioengineering and Biotechnology, 10, 946085. https://doi.org/10.3389/fbioe.2022.946085.

Mishra, P., Krishnan, S., Rana, S., Singh, L., Sakinah, M., & Ab Wahid, Z. (2019). Outlook of fermentative hydrogen production techniques: An overview of dark, photo and integrated dark-photo fermentative approach to biomass. *Energy Strategy Reviews, 24,* 27–37. https://doi.org/10.1016/j.esr.2019.01.001.

Craven, J., Sultan, M. A., Sarma, R., Wilson, S., Meeks, N., Kim, D. Y., Hastings, J. T., & Bhattacharyya, D. (2019). *Rhodopseudomonas palustris*-based conversion of organic acids to hydrogen using plasmonic nanoparticles and near-infrared light. *RSC Advances, 9*(71), 41218–41227. https://doi.org/10.1039/C9RA08747H.

Androga, D. D., Özgür, E., Eroglu, I., Gündüz, U., Yücel, M. (2011). Significance of carbon to nitrogen ratio on the long-term stability of continuous photofermentative hydrogen production. International Journal of Hydrogen Energy, 36(24), 15583–15594. https://doi.org/10.1016/j.ijhydene.2011.09.043.

Pattanamanee, W., Choorit, W., Deesan, C., Sirisansaneeyakul, S., & Chisti, Y. (2012). Photofermentive production of biohydrogen from oil palm waste hydrolysate. International Journal of Hydrogen Energy, 37(5), 4077–4087. https://doi.org/10.1016/j.ijhydene.2011.12.002.

Yetis, M., Gündüz, U., Eroglu, I., Yücel, M., & Türker, L. (2000). Photoproduction of hydrogen from sugar refinery wastewater by *Rhodobacter sphaeroides* O.U. 001. International Journal of Hydrogen Energy, 25(11), 1035–1041. https://doi.org/10.1016/S0360-3199(00)00027-6.

Kars, G., Gündüz, U., Yücel, M., Türker, L., & Eroglu, İ. (2006). Hydrogen production and transcriptional analysis of nifD, nifK and hupS genes in Rhodobacter sphaeroides O.U.001 grown in media with different concentrations of molybdenum and iron. International Journal of Hydrogen Energy, 31(11), 1536–1544. https://doi.org/10.1016/j.ijhydene.2006.06.021.

Solov'ev, A. A., & Erokhin, Y. E. (2013). Role of bacteriochlorophyll in stabilization of the structure of the core and peripheral light-harvesting complexes from purple photosynthetic bacteria. Microbiology, 82(5), 554–561. https://doi.org/10.1134/S0026261713050123.

Hu, Y., & Ribbe, M. W. (2013). Biosynthesis of the iron-molybdenum cofactor of nitrogenase. Journal of Biological Chemistry, 288(19), 13173–13177. https://doi.org/10.1074/jbc.R113.454041.

Eroglu, I.; Sevinç, P.; Gündüz, U.; Grube, T.; Stolten, D.; Yücel, M. The Effect of Temperature and Light Intensity on Hydrogen Production by *Rhodobacter capsulatus*. In Proceedings of the 18th World Hydrogen Energy Conference 2010: WHEC 2010 Proceedings Forschungszentrum Jülich, Essen, Germany, 16-21 May 2010.

Gupta, S., Fernandes, A., Lopes, A., Grasa, L., & Salafranca, J. (2024). Photo-fermentative bacteria used for hydrogen production. Applied Sciences, 14(3), 1191. https://doi.org/10.3390/app14031191.

Al-Mohammedawi, H. H., Znad, H., & Eroglu, E. (2018). Synergistic effects and optimization of photo-fermentative hydrogen production of Rhodobacter sphaeroides

DSM 158. International Journal of Hydrogen Energy, 43(33), 15823-15834. https://doi.org/10.1016/j.ijhydene.2018.06.140.

Ghimire, A., Valentino, S., Frunzo, L., Pirozzi, L., Lens, P. N. L., & Esposito, G. (2016). Concomitant biohydrogen and poly-β-hydroxybutyrate production from dark fermentation effluents by adapted Rhodobacter sphaeroides and mixed photofermentative cultures. Bioresource Technology, 217, 157–164. https://doi.org/10.1016/j.biortech.2016.03.017.

Khatipov, E., Miyake, M., Miyake, J., & Asada, Y. (1998). Accumulation of poly-β-hydroxybutyrate by *Rhodobacter sphaeroides* on various carbon and nitrogen substrates. FEMS Microbiology Letters, 162(1), 39–45. https://doi.org/10.1111/j.1574-6968.1998.tb12976.x.

Kumar, G., Kumar Ponnusamy, V., Bhosale, R. R., Shobana, S., Yoon, J.-J., Bhatia, S. K., Banu, J. R., & Kim, S.-H. (2019). A review on the conversion of volatile fatty acids to polyhydroxyalkanoates using dark fermentative effluents from hydrogen production. Bioresource Technology Reports, 287, 121427. https://doi.org/10.1016/j.biortech.2019.121427.

Sangkharak, K., & Prasertsan, P. (2007). Optimization of polyhydroxybutyrate production from a wild type and two mutant strains of Rhodobacter sphaeroides using statistical method. Journal of Biotechnology, 132(3), 331–340. https://doi.org/10.1016/j.jbiotec.2007.07.721.

Adessi, A., & De Philippis, R. (2014). Photobioreactor design and illumination systems for H_2 production with anoxygenic photosynthetic bacteria: A review. International Journal of Hydrogen Energy, 39(7), 3127-3141. https://doi.org/10.1016/j.ijhydene.2013.12.084.

Yu, J., Tan, L.-M., Kawakami, T., Wang, P., Fu, L.-M., Wang-Otomo, Z.-Y., & Zhang, J.-P. (2018). Cooperative photoprotection by multicompositional carotenoids in the LH1 antenna from a mutant strain of Rhodobacter sphaeroides. The Journal of Physical Chemistry B, 122(33), 8028–8036. https://doi.org/10.1021/acs.jpcb.8b06080.

Nath, A., & Das, D. (2009). Effect of light intensity and initial pH during hydrogen production by an integrated dark and photofermentation process. International Journal of Hydrogen Energy, 34(17), 7497–7501. https://doi.org/10.1016/j.ijhydene.2008.11.065.

Imam, S., Fitzgerald, C. M., Cook, E. M., Donohue, T. J., & Noguera, D. R. (2015). Quantifying the effects of light intensity on bioproduction and maintenance energy during photosynthetic growth of *Rhodobacter sphaeroides*. Photosynthesis Research, 123(2), 167–182. https://doi.org/10.1007/s11120-014-0061-1.

Licht, M. K., Nuss, A. M., Volk, M., Konzer, A., Beckstette, M., Berghoff, B. A., & Klug, G. (2020). Adaptation to photooxidative stress: Common and special strategies of the Alphaproteobacteria *Rhodobacter sphaeroides* and *Rhodobacter capsulatus*. Microorganisms, 8(2), 283. https://doi.org/10.3390/microorganisms8020283.

Muzziotti, D., Adessi, A., Faraloni, C., Torzillo, G., & De Philippis, R. (2017). Acclimation strategy of Rhodopseudomonas palustris to high light irradiance. Microbiological Research, 197, 49–55. https://doi.org/10.1016/j.micres.2017.01.007.

Fradinho, J. C., Reis, M. A. M., & Oehmen, A. (2016). Beyond feast and famine: Selecting a PHA accumulating photosynthetic mixed culture in a permanent feast regime. Water Research, 105, 421–428. https://doi.org/10.1016/j.watres.2016.09.022.

Santos, G. A., Bortoli, L. D., Santos, D. A., Lobato, F. S., Cardoso, V. L., & Batista, F. R. X. (2025). Insights of light spectra on biohydrogen production by photo-fermentation. International Journal of Hydrogen Energy, 149, 150088. https://doi.org/10.1016/j.ijhydene.2025.150088.

Adessi, A., & De Philippis, R. (2012). Hydrogen production: Photofermentation. In P. C. Hallenbeck (Ed.), Microbial technologies in advanced biofuels production (pp. 53-75). Springer. https://doi.org/10.1007/978-1-4614-1208-3_4.

Kawagoshi, Y., Oki, Y., Nakano, I., Fujimoto, A., & Takahashi, H. (2010). Biohydrogen production by isolated halotolerant photosynthetic bacteria using long-wavelength light-emitting diode (LW-LED). International Journal of Hydrogen Energy, 35(24), 13365–13369. https://doi.org/10.1016/j.ijhydene.2009.11.121.

Bosman, C. E., Pott, R. W. M., & Bradshaw, S. M. (2023). The effect of light emission spectrum on biohydrogen production by *Rhodopseudomonas palustris*. Bioprocess and Biosystems Engineering, 46(6), 913–919. https://doi.org/10.1007/s00449-023-02863-8.

Sali, S., McKay, G., & Mackey, H. R. (2025). Exploring the influence of light wavelength ranges and nutrients reduced availability's impacts on polyhydroxyalkanoates accumulation in purple phototrophic bacteria. Fermentation, 11(4), 216. https://doi.org/10.3390/fermentation11040216.

Arimi, M. M., Zhang, Y., & Geißen, S.-U. (2015). Color removal of melanoidin-rich industrial effluent by natural manganese oxides. Separation and Purification Technology, 150, 286–291. https://doi.org/10.1016/j.seppur.2015.07.013.

Eroğlu, E., Eroğlu, İ., Gündüz, U., & Yücel, M. (2008). Effect of clay pretreatment on photofermentative hydrogen production from olive mill wastewater. Bioresource Technology, 99(15), 6799–6808. https://doi.org/10.1016/j.biortech.2008.01.076.

Keskin, T., & Hallenbeck, P. C. (2012). Hydrogen production from sugar industry wastes using single-stage photofermentation. Bioresource Technology, 112, 131–136. https://doi.org/10.1016/j.biortech.2012.02.077.

Hädicke, O., Grammel, H., & Klamt, S. (2011). Metabolic network modeling of redox balancing and biohydrogen production in purple nonsulfur bacteria. BMC Systems Biology, 5, 150. https://doi.org/10.1186/1752-0509-5-150.

McKinlay, J. B., & Harwood, C. S. (2011). Calvin cycle flux, pathway constraints, and substrate oxidation state together determine the H_2 biofuel yield in photoheterotrophic bacteria. mBio, 2(1), e00323-10. https://doi.org/10.1128/mBio.00323-10.

Rey, F. E., Oda, Y., & Harwood, C. S. (2006). Regulation of uptake hydrogenase and effects of hydrogen utilization on gene expression in *Rhodopseudomonas palustris*. Journal of Bacteriology, 188(17), 6143–6152. https://doi.org/10.1128/JB.00381-06.

Montiel Corona, V., Le Borgne, S., Revah, S., & Morales, M. (2017). Effect of light-dark cycles on hydrogen and poly-β-hydroxybutyrate production by a photoheterotrophic culture and Rhodobacter capsulatus using a dark fermentation effluent as substrate. Bioresource Technology, 226, 238–246. https://doi.org/10.1016/j.biortech.2016.12.021.

Kim, M.-S., Kim, D.-H., Son, H.-N., Ten, L. N., & Lee, J. K. (2011). Enhancing photo-fermentative hydrogen production by *Rhodobacter sphaeroides* KD131 and its PHB synthase deleted-mutant from acetate and butyrate. International Journal of Hydrogen Energy, 36(21), 13964–13971. https://doi.org/10.1016/j.ijhydene.2011.03.099.

Wang, X., Yang, H., Ma, C., & Guo, L. (2014). Enhanced photosynthetic hydrogen production performance of Rhodobacter capsulatus by deactivating CBB cycle and cytochrome c oxidase. International Journal of Hydrogen Energy, 39(7), 3176–3184. https://doi.org/10.1016/j.ijhydene.2013.12.098.

Uyar, B., Gürgan, M., Özgür, E., & Eroğlu, İ. (2015). Hydrogen production by hup^- mutant and wild-type strains of Rhodobacter capsulatus from dark fermentation effluent of sugar beet thick juice in batch and continuous photobioreactors. Bioprocess and Biosystems Engineering, 38, 1935–1942. https://doi.org/10.1007/s00449-015-1435-2.

Elsen, S., Jaubert, M., Pignol, D., & Giraud, E. (2005). PpsR: A multifaceted regulator of photosynthesis gene expression in purple bacteria. Molecular Microbiology, 57(1), 17–26. https://doi.org/10.1111/j.1365-2958.2005.04655.x.

Higuchi-Takeuchi, M., & Numata, K. (2019). Acetate-inducing metabolic states enhance polyhydroxyalkanoate production in marine purple non-sulfur bacteria under aerobic conditions. Frontiers in Bioengineering and Biotechnology, 7, 118. https://doi.org/10.3389/fbioe.2019.00118.

Zarei, Z., Malekshahi, P., Morowvat, M. H., & Trzcinski, A. P. (2024). A review of bioreactor configurations for hydrogen production by cyanobacteria and microalgae. International Journal of Hydrogen Energy, 49(Part A), 472–495. https://doi.org/10.1016/j.ijhydene.2023.09.108.

Touloupakis, E., Chatziathanasiou, A., Ghanotakis, D. F., Carlozzi, P., & Pecorini, I. (2022). Hydrogen production by immobilized *Rhodopseudomonas sp*. cells in calcium alginate beads. Energies, 15(22), 8355. https://doi.org/10.3390/en15228355.

Ross, B. S., & Pott, R. W. M. (2021). Hydrogen production by immobilized *Rhodopseudomonas palustris* in packed or fluidized bed photobioreactor systems. International Journal of Hydrogen Energy, 46(2), 1715–1727. https://doi.org/10.1016/j.ijhydene.2020.10.061.

Pagliano, G., Ventorino, V., Panico, A., & Pepe, O. (2017). Integrated systems for biopolymers and bioenergy production from organic waste and by-products: A review of microbial processes. Biotechnology for Biofuels, 10, 113. https://doi.org/10.1186/s13068-017-0802-4.

Carlozzi, P., Giovannelli, A., Traversi, M. L., Touloupakis, E., & Di Lorenzo, T. (2019). Poly-3-hydroxybutyrate and H_2 production by Rhodopseudomonas sp. S16-VOGS3 grown in a new generation photobioreactor under single or combined nutrient deficiency. International Journal of Biological Macromolecules, 135, 821–828. https://doi.org/10.1016/j.ijbiomac.2019.05.220.

Gudmundsson, S., Agudo, L., & Nogales, J. (2017). Applications of genome-scale metabolic models of microalgae and cyanobacteria in biotechnology. In C. Gonzalez-Fernandez & R. Muñoz (Eds.), Microalgae-based biofuels and bioproducts (Woodhead Publishing Series in Energy, pp. 93–111). Woodhead Publishing. https://doi.org/10.1016/B978-0-08-101023-5.00004-2.

Stephens, S., Mahadevan, R., & Allen, D. G. (2021). Engineering photosynthetic bioprocesses for sustainable chemical production: A review. Frontiers in Bioengineering and Biotechnology, 8, 610723. https://doi.org/10.3389/fbioe.2020.610723.

O'Brien, E. J., Monk, J. M., & Palsson, B. O. (2015). Using genome-scale models to predict biological capabilities. Cell, 161(5), 971–987. https://doi.org/10.1016/j.cell.2015.05.019.

Haggart, C. R., Bartell, J. A., Saucerman, J. J., & Papin, J. A. (2011). Whole-genome metabolic network reconstruction and constraint-based modeling. In D. Jameson, M. Verma, & H. V. Westerhoff (Eds.), Methods in enzymology (Vol. 500, pp. 411–433). Academic Press. https://doi.org/10.1016/B978-0-12-385118-5.00021-9.

Thiele, I., & Palsson, B. Ø. (2010). A protocol for generating a high-quality genome-scale metabolic reconstruction. Nature Protocols, 5(1), 93–121. https://doi.org/10.1038/nprot.2009.203.

Arkin, A., Cottingham, R., Henry, C., et al. (2018). KBase: The United States Department of Energy Systems Biology Knowledgebase. Nature Biotechnology, 36(7), 566–569. https://doi.org/10.1038/nbt.4163.

Devoid, S., Overbeek, R., DeJongh, M., Vonstein, V., Best, A.A., Henry, C. (2013). Automated Genome Annotation and Metabolic Model Reconstruction in the SEED and Model SEED. In: Alper, H. (eds) Systems Metabolic Engineering. Methods in Molecular Biology, vol 985. Humana Press, Totowa, NJ. https://doi.org/10.1007/978-1-62703-299-5_2.

Machado, D., Andrejev, S., Tramontano, M., & Patil, K. R. (2018). Fast automated reconstruction of genome-scale metabolic models for microbial species and communities. Nucleic Acids Research, 46(15), 7542–7553. https://doi.org/10.1093/nar/gky537.

Ganter, M., Bernard, T., Moretti, S., Stelling, J., & Pagni, M. (2013). MetaNetX.org: A website and repository for accessing, analysing and manipulating metabolic networks. Bioinformatics, 29(6), 815–816. https://doi.org/10.1093/bioinformatics/btt036.

Orth, J. D., Thiele, I., & Palsson, B. Ø. (2010). What is flux balance analysis? Nature Biotechnology, 28(3), 245–248. https://doi.org/10.1038/nbt.1614.

Chan, S. H. J., Cai, J., Wang, L., Simons-Senftle, M. N., & Maranas, C. D. (2017). Standardizing biomass reactions and ensuring complete mass balance in genome-scale metabolic models. Bioinformatics, 33(22), 3603–3609. https://doi.org/10.1093/bioinformatics/btx453.

Fang, X., Lloyd, C. J., & Palsson, B. O. (2020). Reconstructing organisms in silico: Genome-scale models and their emerging applications. Nature Reviews Microbiology, 18(12), 731–743. https://doi.org/10.1038/s41579-020-00440-4.

Golomysova, A., Gomelsky, M., & Ivanov, P. S. (2010). Flux balance analysis of photoheterotrophic growth of purple nonsulfur bacteria relevant to biohydrogen production. International Journal of Hydrogen Energy, 35(23), 12751–12760. https://doi.org/10.1016/j.ijhydene.2010.08.133.

Hädicke, O., Grammel, H., & Klamt, S. (2011). Metabolic network modeling of redox balancing and biohydrogen production in purple nonsulfur bacteria. BMC Systems Biology, 5, 150. https://doi.org/10.1186/1752-0509-5-150.

Imam, S., Yilmaz, S., Sohmen, U., Gorzalski, A. S., Reed, J. L., Noguera, D. R., & Donohue, T. J. (2011). iRsp1095: A genome-scale reconstruction of the Rhodobacter sphaeroides metabolic network. BMC Systems Biology, 5(1), 116. https://doi.org/10.1186/1752-0509-5-116.

Imam, S., Noguera, D. R., & Donohue, T. J. (2013). Global insights into energetic and metabolic networks in Rhodobacter sphaeroides. BMC Systems Biology, 7, 89. https://doi.org/10.1186/1752-0509-7-89.

Burger, B. T., Imam, S., Scarborough, M. J., Noguera, D. R., & Donohue, T. J. (2017). Combining genome-scale experimental and computational methods to identify essential genes in Rhodobacter sphaeroides. mSystems, 2(3), e00015-17. https://doi.org/10.1128/mSystems.00015-17.

Alsiyabi, A., Immethun, C. M., & Saha, R. (2019). Modeling the interplay between photosynthesis, CO_2 fixation, and the quinone pool in a purple non-sulfur bacterium. Scientific Reports, 9, 12638. https://doi.org/10.1038/s41598-019-49079-z.

Navid, A., Jiao, Y., Wong, S. E., & Pett-Ridge, J. (2019). System-level analysis of metabolic trade-offs during anaerobic photoheterotrophic growth in Rhodopseudomonas palustris. BMC Bioinformatics, 20(1), 233. https://doi.org/10.1186/s12859-019-2844-z.

Chowdhury, N. B., Alsiyabi, A., & Saha, R. (2022). Characterizing the interplay of Rubisco and nitrogenase enzymes in anaerobic-photoheterotrophically grown Rhodopseudomonas palustris CGA009 through a genome-scale metabolic and expression model. Microbiology Spectrum, 10(6), e01463-22. https://doi.org/10.1128/spectrum.01463-22.

Tec-Campos, D., Posadas, C., Tibocha-Bonilla, J. D., Thiruppathy, D., Glonek, N., Zuñiga, C., Zepeda, A., & Zengler, K. (2023). The genome-scale metabolic model for the purple non-sulfur bacterium Rhodopseudomonas palustris Bis A53 accurately predicts phenotypes under chemoheterotrophic, chemoautotrophic, photoheterotrophic, and photoautotrophic growth conditions. PLoS Computational Biology, 19(8), e1011371. https://doi.org/10.1371/journal.pcbi.1011371.

PART II

Aim of the Thesis

This thesis aims to demonstrate the feasibility of utilizing various agro-industrial effluents to produce biohydrogen (bio-H_2) and poly-β-hydroxybutyrate (PHB) using purple non-sulfur bacteria (PNSB). The purpose is to develop a sustainable biotechnological process that converts waste streams into valuable bio-based products, in line with circular economy principles. Often considered expensive to treat and environmentally problematic, agro-industrial effluents have been reimagined as valuable resources that can be used as feedstocks for producing fine chemicals through a biorefinery process based on microbial metabolism. To achieve this goal, the valorization strategy adopted in this thesis integrated dark fermentation (DF) and photofermentation (PF), thereby reducing the need for both chemical and physical pretreatments of the substrates, while minimizing energy consumption and the use of potentially hazardous compounds. During DF, heterotrophic bacteria enriched the effluents with organic acids, which PNSB subsequently utilized during PF to produce PHB and bio-H_2.

This thesis also initiates the development of a genome-scale metabolic model (GEM) for *R. palustris* 42OL, as a first step towards enabling future metabolic engineering strategies aimed at improving the strain's efficiency in converting agro-industrial effluents into industrially relevant molecules.

In conclusion, this research contributes to the transition towards a circular economy by promoting a shift from the current linear "take, make, consume and dispose" system to a more sustainable paradigm based on the principles of "reduce, reuse, recycle". This approach aims to minimize waste and extend the value of resources over time.

To achieve the general objectives described above, this thesis is structured into three research lines, each addressing a specific goal and presented in the chapters of Part III (Results).

The first research line, presented in Chapter I, focuses on developing a process for the valorization of bread waste, one of the main household food residues in Italy, to produce PHB, scaling up the process from small volumes to a semi-pilot scale. Bread waste was preliminarily subjected to DF to enrich its organic acid content and make it suitable for subsequent utilization by PNSB during the PF phase. To this end, the ability of six different PNSB strains to grow and accumulate PHB using fermented bread waste as a substrate was evaluated. Based on this screening, the strain exhibiting the highest growth rate and PHB yield was selected for the subsequent scale-up of the process. This involved transitioning from 95-mL batch glass bottles sealed with rubber stoppers to a 5-L photobioreactor operated under artificial illumination. To optimize PHB biosynthesis, the

reactor was equipped with selected LED sources (SL) emitting in the yellow (λ = 593 nm) and near-infrared (λ = 860 nm) regions of the spectrum, corresponding to the main absorption peaks of bacteriochlorophyll a (BChl*a*) in PNSB.

The second research line, presented in Chapter II, focuses on the valorization of a dairy by-product, the second cheese whey (SCW), a waste stream generated during ricotta cheese production, using *R. palustris* 42OL. The objective of this chapter is twofold: first, to demonstrate the feasibility of valorizing SCW to produce bio-H_2 and PHB; and second, to investigate the effect of light quality, particularly wavelength, on the growth of *R. palustris* 42OL and its production of bacteriochlorophyll a (BChl*a*), bio-H_2, and PHB. A two-stage process was again applied, in which a DF step (lactic fermentation) enriched the effluent with lactic acid, followed by a PF stage carried out in a 5-L photobioreactor operated under two different LED illumination systems: white LEDs (WL) and selected LEDs (SL).

The third research line, presented in Chapter III, shifts the focus from process optimization to a systems-level metabolic analysis of *R. palustris* 42OL, one of the most efficient bio-H_2-producing strains reported in the literature. The aim is to initiate the construction of a genome-scale metabolic model (GEM), thereby laying the foundation for future metabolic engineering strategies to enhance the strain's waste-to-resource conversion capabilities, particularly towards PHB and bio-H_2 production. In this context, the development and validation of a GEM for *R. palustris* 42OL were undertaken to quantitatively describe its metabolic network using flux balance analysis (FBA). In parallel, a phenotypic screening was performed using the Biolog® Phenotype Microarray (PM) platform to assess the strain's ability to utilize different carbon and nitrogen sources under distinct metabolic conditions. This analysis provided valuable information for evaluating and resolving metabolic gaps during model reconstruction.

Finally, in Part V of this thesis (Appendix), complementary studies carried out during this doctoral research are presented, all sharing the common objective of valorizing agro-industrial and food residues to produce bio-H_2 and PHB.

Chapter I aims to provide a comprehensive review of the advantages and limitations associated with the use of vegetable waste as a feedstock for hydrogen production via DF, with particular attention to process-enhancement strategies such as the use of extremophilic microorganisms, bioaugmentation, single-pot conversion, and mixed-culture.

Chapter II focuses on the valorization of a specific by-product of the olive oil industry, the ingested pâté olive cake (IPOC), using PNSB for PHB production. The experimental plan is organized in two phases. In the first phase, the molecular identification and physiological characterization of six PNSB strains are performed using a synthetic growth medium containing different single carbon sources (acetic, lactic, and malic acid), evaluating their growth and PHB accumulation. In the second phase, the growth performance and PHB production of the six selected strains are investigated using IPOC as substrate.

These studies offer further insights into the valorization potential of agro-industrial residues and underscore the importance of PNSB-based processes within the context of the circular bioeconomy.

PART III

Results

Chapter I

Poly-β-hydroxybutyrate Production from Bread Waste via Sequential Dark Fermentation and Photofermentation

Luca Bernabò [1], Giulia Daly [1], Gianmarco Mugnai [1,2], Viola Galli [3], Elisa Corneli [1], Lisa Granchi [1], and Alessandra Adessi [1,*].

[1] Department of Agriculture, Food, Environment and Forestry (DAGRI), University of Florence, Piazzale delle Cascine, 18, 50144 Florence, Italy.

[2] Department of Agronomy, Food, Natural Resources, Animals and Environment, Viale dell'Università 16, 35020 Legnaro, Italy.

[3] FoodMicroTeam s.r.l., Academic Spin-Off of University of Florence, Via Santo Spirito 14, 50125 Florence, Italy.

[*] Correspondence: alessandra.adessi@unifi.it; Tel.: +39-0552755534

Manuscript published in **Foods** (8 May 2025)

https://doi.org/10.3390/foods14101659

Abstract

This study explores the valorization of bread waste for poly-β-hydroxybutyrate (PHB) production through a combined dark fermentation (DF) and photofermentation (PF) process. DF, performed using *Lactobacillus amylovorus* DSM 20532, efficiently converted bread waste into a lactate- and acetate-rich substrate within 120 h. The resulting fermented bread broth (FBB) was enriched with essential nutrients by adding digestate from anaerobic digestion, replacing the need for chemical supplements. Six purple non-sulfur bacteria (PNSB) strains were screened for PHB production in the FBB. *Cereibacter johrii* Pisa7 demonstrated the highest PHB accumulation (50.73% w PHB/w cells), and biomass increase (+1.26 g L^{-1}) over 336 h, leading to its selection for scale-up. Scale-up experiments were conducted in a 5 L photobioreactor with LED lights optimized for PNSB growth. *C. johrii* Pisa7 accumulated PHB at 15.17% and 11.51% w PHB/w cells in two independent trials, corresponding to productivities of 2.03 and 0.89 mg PHB L^{-1} h^{-1}. These results confirm the scalability of the process while maintaining competitive PHB yields. This study highlights the potential of bread waste as a low-cost carbon source for bioplastic production, contributing to a circular bioeconomy by converting food waste into sustainable materials.

Keywords

Lactic acid fermentation; *Cereibacter johrii* Pisa7; fermented bread broth; LED-optimized photobioreactor; purple non-sulfur bacteria.

1. Introduction

Since the 1950s, plastic consumption has increased significantly, driven by demographic and economic growth and favored by its unique properties, including lightness, durability, versatility, and low production costs [1,2]. However, the widespread use of petroleum-based plastics has led to severe environmental issues due to their persistence and disposal challenges, particularly in low-income countries [3,4]. Growing awareness of their ecological impact and the need to reduce reliance on fossil fuels has accelerated the search for sustainable alternatives.

In this context, bioplastics derived from renewable biomass, such as biopolymers, are emerging as innovative materials that offer properties comparable to conventional plastics but with a lower environmental footprint [5,6].

Among biopolymers, polyhydroxyalkanoates (PHAs) have garnered increasing interest. They are valued for their biodegradability, biocompatibility, water insolubility, UV resistance, and thermoplastic properties, making them promising substitutes for conventional plastics [7].

PHAs are polyesters synthesized by bacteria, archaea, and yeasts as energy reserves, especially under nutrient-deficient conditions (e.g., high C/N ratios or limited phosphorus, sulfur, or magnesium) [8-12].

Currently, most biopolymers are produced from first- and second-generation feedstocks. First-generation sources, such as maize and sugar beet, compete with food and feed production, requiring arable land, fertilizers, and water, thus contributing to environmental impacts. Second-generation feedstocks, including lignocellulosic biomass and organic waste, mitigate this competition but require costly chemical and enzymatic treatments for processing [13]. To address these limitations, third-generation feedstocks, such as microbes, are gaining attention as a more sustainable alternative. They do not compete for arable land or freshwater resources and facilitate biomass conversion into biopolymers, reducing costs and environmental impact [13].

Poly-β-hydroxybutyrate (PHB), a short-chain-length PHA (Scl-PHA) that is the most extensively studied member of this family [14,15], is synthesized by various microorganisms, including photosynthetic bacteria, using simple feedstocks such as carbohydrates, organic acids, alcohols, and glycerol [14].

Purple non-sulfur bacteria (PNSB) have the capability to accumulate PHB [7,16-18]. Under anaerobic conditions, PNSB can perform photofermentation (PF), converting organic acids into PHB while utilizing light as an energy source [7,19]. These bacteria

can also synthesize biohydrogen (bio-H_2) via nitrogenase enzyme, although PHB biosynthesis competes with bio-H_2 production for reductants [20]. The most studied PNSB species for PHB production include *Cereibacter sphaeroides* (formerly *Rhodobacter shpaeroides*), *Rhodopseudomonas palustris*, *Rhodobacter capsulatus*, *Rhodobacter sulfidophilus*, and *Rhodospirillum rubrum* [16,21,22].

Despite its potential, the industrial-scale production of PHAs faces economic barriers, with costs of USD 3-5/kg compared to USD 1-1.50/kg for conventional plastics [23]. A significant portion (30-50%) of PHA production costs stem from the carbon source used in microbial growth media. To address this, utilizing low-cost, abundant carbon sources derived from food waste, combined with metabolically versatile microorganisms, offers a promising strategy to reduce costs [19,24,25].

Integrating PF with dark fermentation (DF) offers an efficient way to utilize food waste for PHA production. During DF, heterotrophic bacteria first convert sugars contained in food waste into organic acids, which PNSB subsequently transform into PHB and/or bio-H2 during PF.

Bread waste, which constitutes a significant contributor to household food waste in Europe, is a promising substrate for microbial fermentation due to its high carbohydrate content, primarily in the form of starch (~70%), [26]. In the European Union, 88 million tons of food waste are generated annually, with bread comprising approximately 19% of household waste in Italy [26,27]. The utilization of bread waste in fermentation can lead to the production of value-added products, thereby enhancing resource efficiency and contributing to circular economy initiatives. Therefore, amylolytic lactic acid bacteria (LAB) can efficiently convert starch-rich bread waste into lactate through DF, avoiding the need for added amylolytic enzymes. One of these amylolytic LAB is *Lactobacillus amylovorus*, which has been shown to produce lactate from starch-based substrates [26,28–32]. The lactate produced can then be converted into PHB or bio-H2 through PNSB-driven PF.

Despite the promising potential of bread waste as a substrate for PHB production, comprehensive research in this area remains limited. Critical factors influencing the fermentation process (such as the impact of light quality on PNSB) have not been extensively explored. Since the efficiency of PHB and bio-H2 production in PNSB is highly dependent on light quality, with bacteriochlorophylls (BChls) absorbing light at 590 nm and in the near-infrared range (800-880 nm) [33], the incident light spectrum can be designed to enhance PF.

The present study aimed to evaluate six PNSB strains for their ability to grow and produce PHB using bread waste as a substrate. A combined system was implemented, consisting of an initial DF stage to enrich the waste stream with organic acids, followed by a PF stage, minimizing the need for extensive pretreatment of the waste stream. The PNSB strain demonstrating the highest growth and PHB production was then selected for scale-up in a 5 L photobioreactor equipped with LED lights emitting in the yellow (λ = 593 nm) and infrared (λ = 860 nm) spectra.

2. Materials and Methods

2.1. Bacterial Strains

L. amylovorus DSM 20532 was obtained from the German Collection of Microorganisms and Cell Cultures GmbH, Leibniz Institute DSMZ, Braunschweig, Germany [34]. Six previously identified PNSB strains [35] were selected to assess their capability to produce PHB via PF using bread waste. Salient information on the PNSB strains used in this study is listed in Tab. 1. The microorganisms were stored in sealed agar tubes at the Department of Agricultural, Food, Environment and Forestry (DAGRI) of the University of Florence, Italy.

Table 1. List of used strains and details about their origin.

Species	Origin	Reference
Rhodopseudomonas palustris strain 42OL	Sugar refinery waste treatment pond; Castiglion Fiorentino (AR), Italy.	[36]
Rhodopseudomonas palustris strain AV33	Trophic lake; Pozzuoli (NA), Italy.	[37]
Rhodopseudomonas palustris strain CGA009	Chloramphenicol-resistant derivative of *R. palustris* CGA001; courtesy of Prof. C. S. Harwood, University of Washington.	[38]
Cereibacter johrii strain 9Cis	Dairy effluent; Bologna (BO), Italy.	[35]
Cereibacter johrii strain Pisa7	Lake; San Rossore (PI), Italy.	[35]
Cereibacter sphaeroides strain F17	Sewage treatment pond; Florence (FI), Italy.	[35]

2.2. Inoculum and Dark Fermentation Assay Using Bread Waste

L. amylovorus DSM 20532 was cultured for 24 h in MR3i medium containing peptone 5 g L^{-1}; tryptone 5 g L^{-1}; lab-lemco 5 g L^{-1}; yeast extract 12 g L^{-1}; maltose 20 mg L^{-1};

glucose 6 g L^{-1}; fructose 6 g L^{-1}; sodium gluconate 2 g L^{-1}; sodium acetate 2 g L^{-1}; ammonium citrate 2 g L^{-1}; dipotassium hydrogen phosphate 2 g L^{-1}; magnesium sulfate 7·H_2O 0.2 g L^{-1}; manganese sulfate 10·H_2O 0.05 g L^{-1}; cysteine 0.5 g L^{-1}; vitamin mix 1000 × 1 mL L^{-1}; Tween 80 1 mL L^{-1}; fresh yeast extract 15 mL L^{-1}; and distilled water. The pH of the medium was adjusted to 5.6. Stationary phase cells were collected by centrifugation at 1500 × g for 15 minutes (min) at 22 °C using a Sigma centrifuge model 3-16KL (Sigma Laborzentrifugen GmbH, Osterode am Harz, Germany) and resuspended in bread effluent for the DF phase.

To obtain the fermented bread broth (FBB) for the PF tests, bread waste was oven-dried overnight at 60 °C and then ground with a mixer to a particle size of 500-1000 µm. *L. amylovorus* DSM 20532 was inoculated at a final concentration of 1 × 10^9 CFU mL^{-1} into a substrate consisting of 7.5% bread/water (w/v).

To optimize the duration of the DF process, triplicate fermentation tests were conducted using the inoculated bread substrate, in 100 mL Erlenmeyer flasks. The flasks were incubated at 37 °C and subjected to horizontal shaking at 100 rpm for 168 hours (h). Throughout the experiment, the concentrations of organic acids were monitored at 24 h intervals using high-performance liquid chromatography (HPLC) analysis to track their variations over time. Additionally, pH changes in the substrate were recorded every 24 h.

The DF to produce FBB for subsequent PF tests was carried out in 3 L Erlenmeyer flasks under the same conditions described above and lasted for 120 h. The FBB was obtained by filtering the dark fermented bread waste with a metal sieve, followed by centrifugation at 3800 × g for 15 min at 22 °C using a Beckman centrifuge model J2-21 (Beckman Coulter, Brea, CA, USA). The resulting effluent was supplemented with: (1) 10 mL L^{-1} of digestate from an anaerobic digestion (AD) plant of Società Agricola Lomas s.r.l., Collesalvetti (LI), Italy, and (2) 10 mL L^{-1} of a phosphate buffer (K_2HPO_4, 50 g L^{-1}; KH_2PO_4, 30 g L^{-1}). The digestate had been pre-filtered using 1.2 µm mixed cellulose ester (MCE) membranes (Fisher Scientific International, Inc., Pittsburgh, PA, USA). Finally, the FBB was sterilized at 121 °C for 15 min using a Vapormatic autoclave model 770 (Carlo Erba Reagents s.r.l., Cornaredo, MI, Italy) to prevent residual lactic acid bacteria metabolic activity, which could lower the pH, and to maintain it within the optimal range (6.5-7.0) for PHB production [7]. The pH of the substrate was adjusted to 6.8 before and after autoclaving.

2.3. Inoculum and Batch Photofermentation Assays Using Fermented Bread Broth

Preliminary batch PF screening tests were conducted using pure cultures of each PNSB strain to identify the most effective PHB-producing candidate. Before the experiments, the PNSB strains were activated in 250 mL bottles containing RPN medium supplemented with DL-lactic acid (1.8 g L^{-1}) as the carbon source. Cultures were incubated at 25 °C under continuous illumination at 150 µmol photons m^{-2} s^{-1}.

The RPN medium consisted of NH_4Cl 0.5 g L^{-1}, K_2HPO_4 0.5 g L^{-1}, KH_2PO_4 0.3 g L^{-1}, $MgSO_4 \cdot 7H_2O$ 0.4 g L^{-1}, NaCl 0.4 g L^{-1}, $CaCl_2 \cdot 2H_2O$ 0.075 g L^{-1}, ferric citrate 0.005 g L^{-1}, and yeast extract 0.4 g L^{-1}. Trace elements were added at 10 mL per liter from a stock solution containing $ZnSO_4 \cdot 7H_2O$ 10 mg L^{-1}, $MnCl_2 \cdot 4H_2O$ 3 mg L^{-1}, H_3BO_3 30 mg L^{-1}, $CoCl_2 \cdot 6H_2O$ 20 mg L^{-1}, $CuCl_2 \cdot 2H_2O$ 1 mg L^{-1}, $NiCl_2 \cdot 6H_2O$ 2 mg L^{-1}, and $Na_2MoO_4 \cdot 2H_2O$ 30 mg L^{-1}. The medium pH was adjusted to 6.8 using NaOH prior to autoclaving.

For the PF batch tests, each PNSB strain was harvested by centrifugation at 3000 × g for 20 min at 22 °C using a Beckman J2-21 centrifuge (Beckman Coulter, Brea, CA, USA). The cell pellets were then resuspended in FBB, which served as the test substrate. Each culture was inoculated to reach a final biomass concentration of 100 mg L^{-1}.

PF assays were carried out in sealed 100 mL serum bottles equipped with rubber stoppers and clamps. To allow biohydrogen (bio-H2) release while preventing microbial contamination, each bottle was fitted with a needle equipped with a 0.2 µm syringe filter (Lab Logistics Group GmbH, Meckenheim, Germany).

Before the PF trials, the FBB medium was analyzed for macro- and micronutrients, organic acids, and ammonium content. The bottles were incubated under batch conditions at 25 °C with continuous white LED light (150 µmol photons m^{-2} s^{-1}). All experiments were performed in triplicate and lasted 336 h.

Cell dry weight (CDW) was measured at both the beginning (T0, 0 h) and the end (T14, 336 h) of the experiment. PHB accumulation and transmission electron microscopy (TEM) observations were carried out at the end of the test (T14) to assess the presence of intracellular PHB granules. Further details on the analytical procedures are provided in Section 2.5 (Analytical Methods).

2.4. Photobioreactor Design and Scale-Up of PHB Production

The scale-up PF tests were set up in a tubular photobioreactor designed by Biosyntex s.r.l. (Bologna, BO, Italy) and constructed by Tecnocom s.r.l. (Prato, PO, Italy). The system consisted of a skid of dimensions 515 mm × 400 mm, comprising (1) a

thermostated DURAN glass tube, measuring H 700 mm × D 140 mm and equipped with an internal chamber of D 110 mm; (2) a pH control instrument (B&C Electronics s.r.l., Carnate, MB, Italy); (3) a temperature control instrument (Gefran S.p.a., Provaglio d'Iseo, BS, Italy); (4) a mechanical stirrer model AM20-D 50 (Argolab, Carpi, MO, Italy) with manual speed control and a polypropylene (PP) rod (H 800 mm × D 8 mm); (5) two 150W dimmable LED lamps, measuring 600 × 70 × 40 mm (Ambra Elettronica s.r.l., Bolzano Vicentino, VI, Italy); (6) an ON/OFF electric valve for thermostatic control; (7) an electrical control and command panel. Each LED lamp consists of 32 LEDs with an emission spectrum in the yellow region (λ = 593 nm) and 8 LEDs with an emission spectrum in the infrared region (λ = 860 nm).

The 5 L photobioreactor was used for the scale-up of the PHB production process, employing *Cereibacter johrii* Pisa7, the strain selected during the preliminary PF screening. Before inoculation, the strain was pre-activated in an RPN medium supplemented with DL-lactic acid, as described in Section 2.3 (Inoculum and Batch Photofermentation Assays using Fermented Bread Broth). The culture was then harvested by centrifugation and resuspended in fermented bread broth (FBB), following the same procedure outlined in Section 2.3. Inoculation into the photobioreactor was performed to reach a final optical density at 660 nm (OD_{660}) of 0.2. Before inoculation, the substrate was reanalyzed to determine its organic acid and ammonium content. The experiment was conducted twice as independent trials (named Run_1 and Run_2).

Before each experiment, the 5 L photobioreactor was disinfected through the following steps: (1) initial cleaning and rinsing of the column with non-sterile deionized water; (2) filling of the column with non-sterile deionized water and addition of 0.5 mL L^{-1} of a commercial 15% NaClO solution (150 g L^{-1} of active chlorine), followed by continuous stirring at 60 rpm for 12 h; (3) addition of 1 ppm $Na_2S_2O_3 \cdot 5H_2O$ for each ppm of active chlorine and continuous stirring at 60 rpm for 30 min; (4) double rinsing with sterile deionized water.

The scale-up experiments lasted a total of 336 h. Each day, the culture was kept static except for a 30 min period during which it was agitated at 170 rpm. Microbial growth was monitored by quantifying bacteriochlorophyll a (BChl*a*) every 48 h and by determining CDW at T0 (0 h), T7 (168 h), and T14 (336 h). Organic compounds and ammonium concentrations were assessed at T0, T7, and T14 h using HPLC and the Nessler method, respectively. PHB content was measured at T0, T7, and T14. Further details on the analytical methods used are provided in Section 2.5 (Analytical Methods).

Throughout the experiment, light intensity was increased stepwise. During the first 24 h, it was set at 150 µmol photons m^{-2} s^{-1}. Between 24 and 120 h, it was raised to 250 µmol photons m^{-2} s^{-1}, and from 120 h onward, it was stabilized at 400 µmol photons m^{-2} s^{-1} until the end of the experiment.

2.5. Analytical Methods

2.5.1. FBB Chemical Characterization

The concentration of metals and other inorganic compounds of the FBB was determined through an inductively coupled plasma–optical emission spectrometry ICP-OES analyzer (Thermo Scientific™ iCAP™ 7400, Waltham, MA, USA), using IRSA 3010 (conventional acid mineralization) and IRSA A-3020 (determination of chemical elements by spectroscopy emission with plasma source) methods.

The organic compounds content of the FBB was determined using a Varian Pro Star HPLC system equipped with an Aminex 87H column maintained at 65 °C. The system utilized a 20 µL injection loop, a UV detector (λ = 210 nm), and a refractive index (RI) detector. The eluent was 0.01 N H_2SO_4, at a flow rate of 0.6 mL min^{-1}.

The ammonium concentration was determined using the HI93764B-25 Ammonia HR reagents set (Hanna Instruments, Woonsocket, RI, USA), based on the Nessler method, and quantified spectrophotometrically using a Varian Cary50 UV-visible spectrophotometer (Varian, Mulgrave, Australia).

2.5.2. C/N Ratio and Organic Acids Yield Calculation

The C/N ratio of the substrates was calculated by dividing the sum of the moles of carbon contained in lactate and acetate by the moles of nitrogen in ammonium.

The fermentation efficiency in terms of organic acid yield was calculated as the ratio between the sum of lactic and acetic acid concentrations (g L^{-1}), produced during dark fermentation, and the total carbohydrate content present in the diluted substrate (7.5% w/v). The carbohydrate content per 100 g of bread was derived from Adessi et al. [26], as the same substrate was used in the present study.

2.5.3. Monitoring of PNSB Growth

CDW was determined in triplicate on a 3 mL culture sample, through a filtration with 0.45 µm mixed cellulose ester (MCE) membranes (Fisher Scientific International, Inc., Pittsburgh, PA, USA). The membranes had been previously activated with 5 mL of distilled water. After filtration, the cells were washed twice with distilled water, oven-

dried at 105 °C for 3 h, and weighed on an analytical balance (Sartorius AG, Gottingen, Germany).

BChl*a* content was determined according to Carlozzi and Sacchi [39]. Briefly, a 2 mL sample was centrifuged at 4000 × g for 10 min with a Hermle Z 167 M centrifuge (Hermle Labortechnik GmbH, Wehingen, Germany), and the supernatant was removed. BChl*a* was extracted from the cell pellet, resuspending it with a 2 mL acetone/methanol 7:2 v/v ratio solution. The sample was incubated at 4 °C for 30 min and centrifuged at 4000 × g for 10 min. The BChl*a* content was determined by measuring the absorbance (A) at 775 nm (ε = 75 mM^{-1} cm^{-1}) with a Varian Cary50 UV-visible spectrophotometer (Varian, Mulgrave, Australia).

The optical density was determined in triplicate on 2 mL samples at a wavelength of 660 nm (OD_{660}) using a Varian Cary50 UV-visible spectrophotometer (Varian, Mulgrave, Australia). The RPN medium was used as a blank.

2.5.4. Transmission Electron Microscopy (TEM) Analysis

TEM observations were conducted at the end of the preliminary screening test (336 h) on the FBB substrate, using a Philips CM12 TEM (Philips Electronics, Amsterdam, The Netherlands) equipped with CRYO-GATAN UHRST 3500 technology and a digital camera. Before image acquisition, bacterial cells were prepared as follows: the cells were treated with 2.5% (w/v) glutaraldehyde at 4 °C and then washed twice in 0.1 M phosphate buffer (PBS), pH 7.0, for 15 min each. Subsequently, the cells were fixed with 1% osmium tetroxide, pH 7, for 1 h. The samples were then suspended in PBS and air-dried. Next, the samples were gradually rehydrated in an ethanol series (25%, 50%, 70%, 80%, 90%, and 100%) for 10 min at each concentration. Spurr's epoxy resin was used for infiltration and embedding of the samples. The epoxy resin was first incubated in propylene oxide for 10 min in a 2:1 mixture of propylene oxide/resin, followed by a 1:1 mixture for at least 1 h, and finally in a 1:2 mixture of propylene oxide/resin for 1 h to overnight. The samples were cut and post-stained with uranyl acetate and lead citrate.

2.5.5. PHB Quantification

PHB production was measured following the method described by De Philippis et al. [40] through acid cellular hydrolysis. It was quantified as crotonic acid using a Varian Pro Star HPLC system, equipped with an Aminex 87H column maintained at 65 °C. The system employed a 20 μL injection loop, a UV detector (λ = 210 nm), and a refractive

index (RI) detector. The eluent was 0.01 N H_2SO_4 (Carlo Erba, Milan, Italy) at a flow rate of 0.6 mL min^{-1}.

2.6. Statistical Analysis

All the analyses were conducted in experimental triplicates (N = 3); a minimum number of three instrumental replicates was always used for each measurement (n = 3).

To determine whether the results were significantly different, data were analyzed using independent t-tests and one-way analysis of variance (ANOVA) at 95% of the significance, followed by Tukey's honest significance difference (HSD) post hoc test. Results were considered statistically significant at $p < 0.05$. Before the t-test, all data were checked for normality using the Shapiro-Wilk test. Before ANOVA, normality was assessed with the Shapiro-Wilk test, and homogeneity of variance was evaluated using Bartlett's test. Statistical analysis was performed using R software version 4.4.1.

3. Results

3.1. Dark Fermentation (DF) Optimization

The DF process of bread waste using *Lactobacillus amylovorus* DSM 20532 was optimized to determine the optimal fermentation duration and maximize lactate yield, as shown in Fig. 1. The highest lactate concentration was recorded after 120 h, reaching 2.72 (± 0.04) g L^{-1}. Acetate production followed a similar trend, peaking at 0.53 (± 0.04) g L^{-1} at the same time point. This pattern was further supported by the pH values, which reflect the accumulation of these organic acids. Based on these findings, the optimal fermentation time was established at 120 h, and all subsequent bread waste fermentations were conducted for this duration.

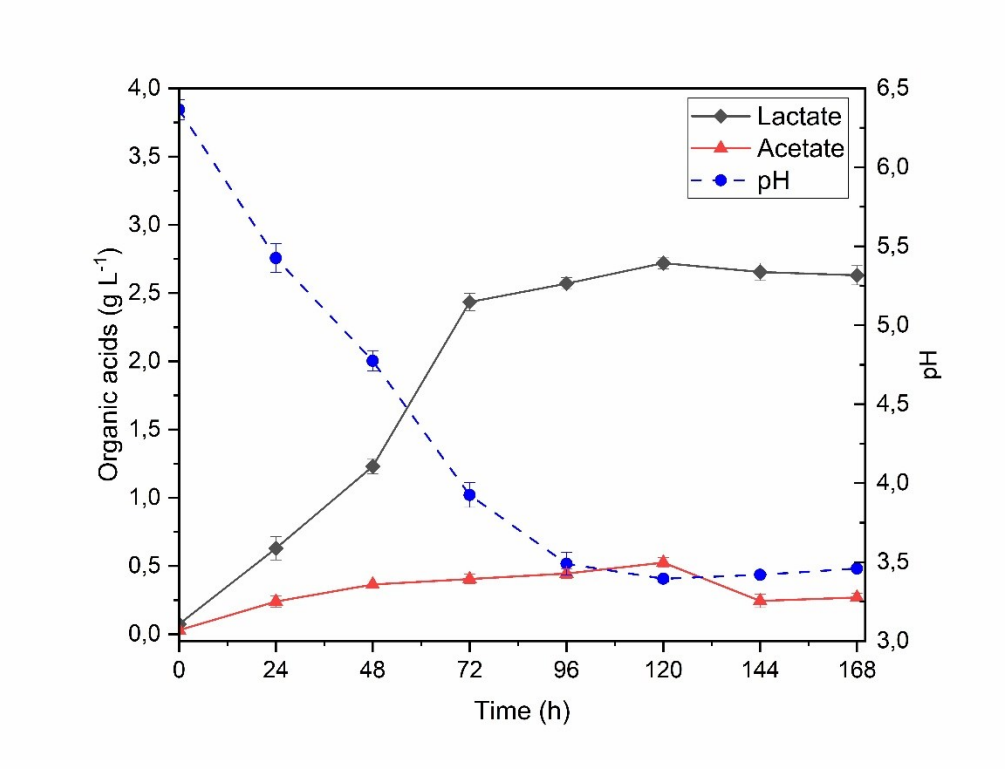

Figure 1. Time-course profiles of lactate, acetate, and pH during the optimization process of DF.

3.2. FBB Chemical Composition

The metal and inorganic element composition of the FBB, after the digestate addition, used in the PF experiments is reported in Tab. 2.

Table 2. Composition in Metal and Other Inorganic Elements of the FBB. Data are expressed as mean ± standard deviation (n = 3). *nd* = not detected.

Compounds	**Concentration (g L^{-1})**
B	nd
Ca	1.27 (± 0.53)
Cd	nd
Co	nd
Cr	nd
Cu	nd
Fe	nd
K	2.74 (± 0.24)
Mg	0.66 (± 0.012)
Mn	nd
Mo	nd
Na	8.76 (± 2.14)
Ni	nd
S	0.14 (± 0.007)
Si	0.042 (± 0.003)
Zn	nd

The lactate, acetate, and ammonium content, the C/N ratio, and the organic acids yield in the FBB substrates used for the three PF trials are reported in Tab. 3. One-way ANOVA revealed no statistically significant differences among the substrates for lactate, acetate, ammonium, the C/N ratio, and the organic acids yield.

Table 3. Composition of substrates used in the photofermentation tests, including lactate, acetate, ammonium, the C/N ratio, and organic acids yield. Values are presented as mean ± standard deviation (n = 3). Different lowercase letters indicate significant differences ($p < 0.05$) according to one-way ANOVA followed by Tukey's post hoc test. As no significant differences were found, all values within each parameter share the same letter (a).

Compounds	FBB for the screening test	FBB for Run_1	FBB for Run_2
Lactate (g L^{-1})	2.64 (±0.06) [a]	3.12 (± 0.30) [a]	2.96 (± 0.01) [a]
Acetate (g L^{-1})	0.20 (±0.04) [a]	0.19 (± 0.05) [a]	0.20 (± 0.05) [a]
Ammonium (mg L^{-1})	25.32 (± 1.95) [a]	25.66 (± 2.90) [a]	27.90 (± 4.96) [a]
C/N ratio	67.27 (± 2.52) [a]	77.50 (± 6.70) [a]	67.95 (± 1.37) [a]
Organic acids yield (%)	5.89 (± 0.22)[a]	6.91 (± 0.57) [a]	6.56 (± 0.13) [a]

3.3. Screening of PNSB Strains for Growth and PHB Production on FBB

The first PF test aimed to assess the growth and PHB synthesis capabilities of six different PNSB strains cultivated on FBB by using batch setups. Fig. 2 illustrates the variation in CDW over time and the PHB accumulation measured at the end of the trial.

In Fig. 2A, cellular growth, expressed as CDW (g L^{-1}), is compared between the initial time point (T0, white bars) and after 14 days of cultivation (T14, black bars). A paired t-test revealed significant differences ($p < 0.05$, *) in four out of six strains. Notably, *R. palustris* 42OL, *R. palustris* CGA009, and *C. johrii* Pisa7 exhibited a significant increase in CDW over the cultivation period, with *C. johrii* Pisa7 showing the highest increase (+ 1.26 g L^{-1} ± 0.15). In contrast, *C. johrii* 9Cis displayed a marked decrease in CDW (- 0.54 g L^{-1} ± 0.10). Meanwhile, *R. palustris* AV33 and *C. sphaeroides* F17 showed no significant variation in CDW over the tested period.

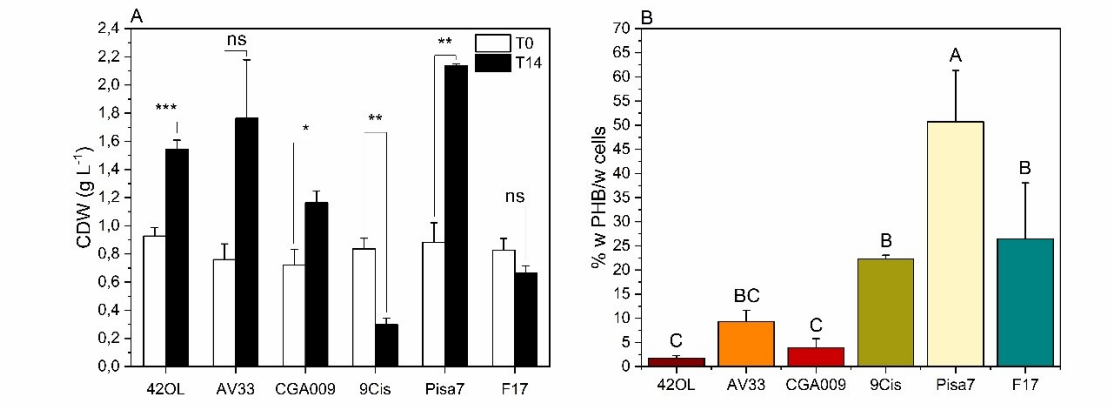

Figure 2. Growth and PHB production in six PNSB strains (*R. palustris* 42OL, *R. palustris* AV33, *R. palustris* CGA009, *C. johrii* 9Cis, *C. johrii* Pisa7, and *C. sphaeroides* F17) during the preliminary screening test. (A) CDW (g L−1) at the start (T0) and end (T14) of the trial. Statistical significance between time points was assessed for each strain using a paired t-test, with significant differences indicated by asterisks (* $p < 0.05$, ** $p < 0.01$, *** $p < 0.001$) and "ns" for not significant. Error bars represent standard deviations (n = 3). (B) PHB content (w PHB/w cells) measured at T14. Differences among strains were analyzed using one-way ANOVA, followed by Tukey's HSD post hoc test, with significance indicated by uppercase letters (A, B, C). Error bars represent standard deviations (n = 3).

Figure 2B illustrates the accumulation of PHB (% w PHB/w cells) in the six tested strains, quantified at the end of the experiment (T14). *C. johrii* Pisa7 significantly exhibited the highest PHB accumulation (50.73% w PHB/w cells ± 10.60), followed by *C. sphaeroides* F17 (26.47% w PHB/w cells ± 11.58) and *C. johrii* 9Cis (22.31% w PHB/w cells ± 0.77). In contrast, *R. palustris* strains (42OL, AV33, and CGA009) displayed no significant differences in PHB accumulation levels, which were below 10% w PHB/w cells.

The volumetric production of PHB at T14, together with hourly and daily productivity, is presented in Tab. 4. *C. johrii* Pisa7 showed the highest volumetric production of PHB, reaching 1083.76 ± 220.05 mg PHB L^{-1}, with a daily productivity of 77.41 ± 15.72 mg PHB L^{-1} d^{-1}. This was followed by *C. sphaeroides* F17 (179.47 ± 92.29 mg PHB L^{-1}, 12.82 ± 6.59 mg PHB L^{-1} d^{-1}) and *R. palustris* AV33 (159.68 ± 42.02 mg PHB L^{-1}, 11.41 ± 3.00 mg PHB L^{-1} d^{-1}). The remaining strains showed significantly lower PHB production, with values below 100 mg PHB L^{-1} and daily productions below 10 mg PHB L^{-1} d^{-1}.

At the end of the screening test (T14), TEM observations confirmed the presence of cytoplasmic PHB inclusions in all the analyzed samples (Figure 3). Among the *R. palustris* strains, *R. palustris* 42OL (Figure 3a) exhibited the largest cell length (L), with an average of 1.42 ± 0.11 µm, followed by *R. palustris* CGA009 (1.34 ± 0.08 µm) and *R.*

palustris AV33 (1.14 ± 0.09 µm), respectively, in Figures 3b and 3c. In terms of cell width (W), *R. palustris* 42OL also ranked highest, averaging 0.84 ± 0.04 µm, slightly exceeding *R. palustris* CGA009 (0.82 ± 0.03 µm) and *R. palustris* AV33 (0.80 ± 0.07 µm). Regarding PHB inclusions, *R. palustris* CGA009 stood out with the largest inclusion dimensions, displaying an average W of 0.49 ± 0.17 µm and L of 0.65 ± 0.18 µm, compared to *R. palustris* 42OL (W: 0.22 ± 0.04 µm; L: 0.21 ± 0.04 µm) and *R. palustris* AV33 (W: 0.17 ± 0.01 µm; L: 0.25 ± 0.02 µm).

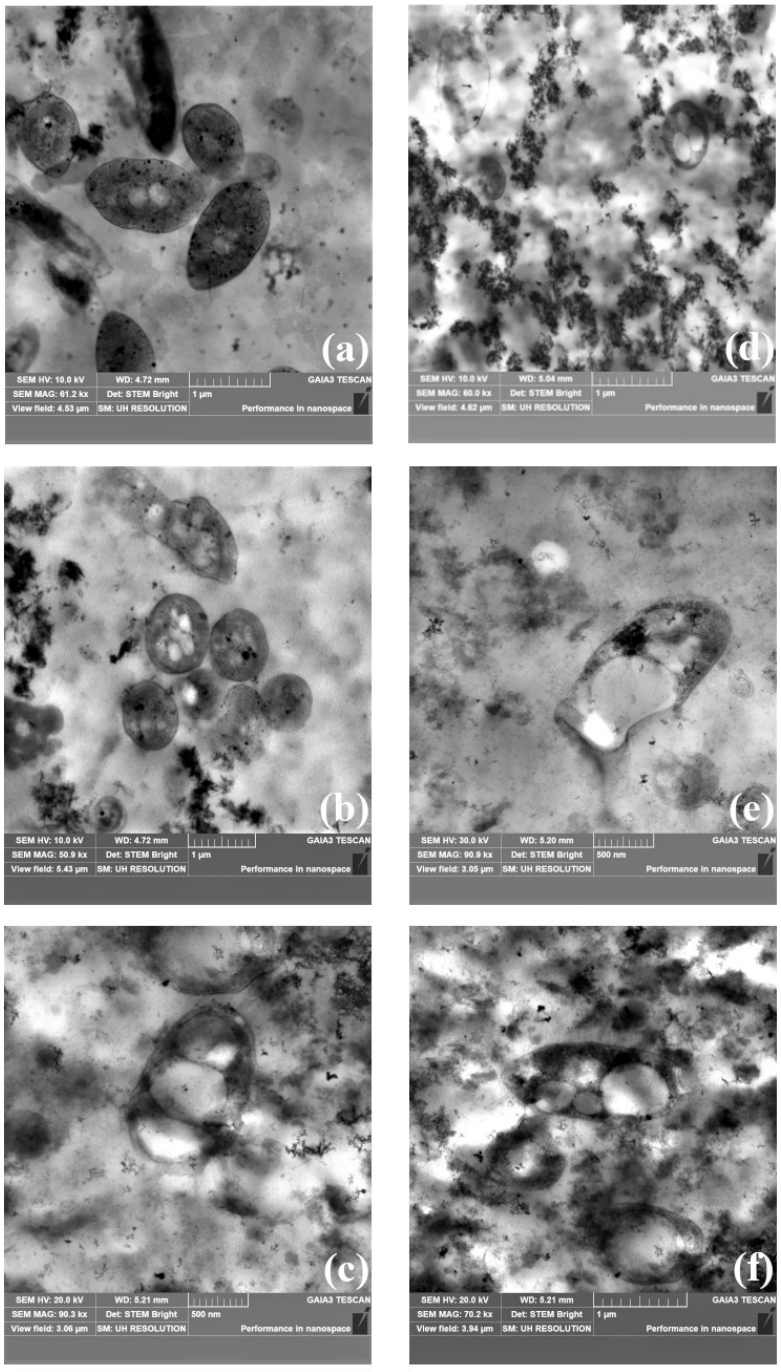

Figure 3. Transmission electron microscopy (TEM) images of the inclusion bodies from screening tests conducted using *R. palustris* strain 42OL (**a**), *R. palustris* strain AV33 (**b**), *R. palustris* strain CGA009 (**c**), C. *johrii* strain Pisa7 (**d**), *C. johrii* strain 9Cis (**e**), and *C. sphaeroides* strain F17 (**f**) growth on FBB at the end of the photofermentation experiment (T14).

Table 4. Volumetric PHB production at T14 (mg PHB L_{cult}^{-1}), PHB productivity per hour (mg PHB L_{cult}^{-1} h^{-1}), and PHB productivity per day (mg PHB L_{cult}^{-1} d^{-1}) across different strains in the screening batch experiment and experimental runs in the photobioreactor. Values are presented as mean ± standard deviation (n = 3). Statistical significance was assessed using one-way ANOVA (95% confidence level) followed by Tukey's HSD post hoc test. Different lowercase letters (a, b) indicate significant differences among strains in the screening experiment, while different uppercase letters (A, B) indicate significant differences between photobioreactor runs ($p < 0.05$).

Strain/Run	mg PHB L_{cult}^{-1}	mg PHB L_{cult}^{-1} h^{-1}	mg PHB L_{cult}^{-1} d^{-1}
R. palustris 42OL	27.11 (± 8.36) ^{b}	0.08 (± 0.02) ^{b}	1.94 (± 0.60) ^{b}
R. palustris AV33	159.68 (± 42.02) ^{b}	0.48 (± 0.13) ^{b}	11.41 (± 3.00) ^{b}
R. palustris CGA009	44.66 (± 17.66) ^{b}	0.13 (± 0.05) ^{b}	3.19 (± 1.26) ^{b}
C. johrii 9Cis	66.13 (± 8.51) ^{b}	0.20 (± 0.03) ^{b}	4.72 (± 0.61) ^{b}
C. johrii Pisa7	1083.76 (± 220.05) ^{a}	3.23 (± 0.65) ^{a}	77.41 (± 15.72) ^{a}
C. sphaeroides F17	179.47 (± 92.29) ^{b}	0.53 (± 0.27) ^{b}	12.82 (± 6.59) ^{b}
Run_1	744.22 (± 61.22) ^{A}	2.03 (± 0.18) ^{A}	48.82 (± 4.34) ^{A}
Run_2	352.01 (± 57.78) ^{B}	0.89 (± 0.19) ^{B}	21.33 (± 4.55) ^{B}

For the *Cereibacter* genus, *C. sphaeroides* F17 (Figure 3f) displayed the largest cell dimensions, with an average length (L) of 1.73 ± 0.24 µm and width (W) of 0.81 ± 0.07 µm, followed by *C. johrii* 9Cis (L: 1.16 ± 0.37 µm, W: 0.78 ± 0.04 µm) and *C. johrii* Pisa7 (L: 0.86 ± 0.01 µm, W: 0.56 ± 0.04 µm), respectively, in Figures 3d and 3e. Similarly, PHB inclusion size reflected these trends. *C. sphaeroides* F17 showed the largest inclusions, with an average W of 0.50 ± 0.05 µm and L of 0.61 ± 0.10 µm. *C. johrii* 9Cis followed with inclusion dimensions of 0.48 ± 0.12 µm (W) and 0.59 ± 0.12 µm (L), while *C. johrii* Pisa7 displayed the smallest inclusions, with a W of 0.17 ± 0.05 µm and L of 0.30 ± 0.11 µm.

3.4. Scale-Up of PHB Production in a 5 L Photobioreactor

Based on the results presented in Section 3.3 (*Screening of PNSB Strains for Growth and PHB Production on FBB*), *C. johrii* Pisa7 was selected for the subsequent scale-up of the process in a 5 L photobioreactor. The photobioreactor was equipped with LED lamps emitting light at two specific wavelengths, 593 nm and 860 nm. *C. johrii* Pisa7 was

cultivated on FBB for 14 days (336 h), and the experiment was conducted twice as independent trials. These trials are referred to as Run_1 and Run_2 in the following text.

Fig. 4A shows the progression of cell growth in *C. johrii* Pisa7, measured as CDW (g L^{-1}) at T0, T7, and T14 from the start of the experiment. In both replicates (Run_1 and Run_2), Tukey's HSD post hoc test revealed a statistically significant increase in CDW during the first 168 h (T0-T7). However, in both runs, CDW stabilized over the subsequent 168 h (T7-T14), with no significant further increase. The highest CDW values were recorded at T14, with 4.90 g L^{-1} (± 0.26) in Run_1 and 3.05 g L^{-1} (± 0.09) in Run_2, the latter being significantly lower than Run_1.

The growth of *C. johrii* Pisa7 in FBB was also assessed by monitoring changes in BChl*a* content over time (Fig. 4B). The most significant increase in BChl*a* occurred during the first 168 h (T0-T7) of inoculation for both runs, with Run_2 showing significantly higher values than Run_1 after the first 48 h (T2). Between 168 h (T7) and 336 h (T14), the BChl*a* content in Run_1 stabilized, with no significant variations. In contrast, Run_2 exhibited a statistically significant reduction in BChl*a* between 216 h (T9) and 264 h (T12), followed by a subsequent increase in the next interval. The maximum BChl*a* levels were observed at the end of the incubation period (T14), reaching 25.92 µg mL^{-1} (± 2.41) and 28.98 µg mL^{-1} (± 0.90) in Run_1 and Run_2, respectively, with no significant differences between the two runs.

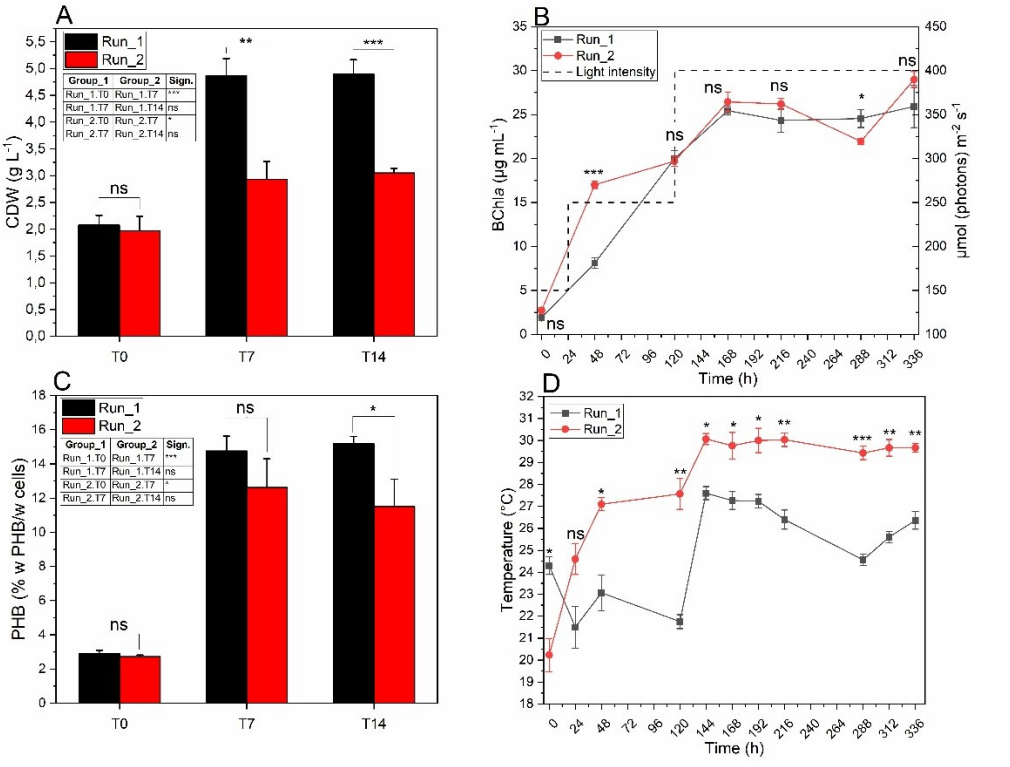

Figure 4. Profiles of CDW, BChl*a*, PHB, and temperature during the experiments. (A) Cell dry weight (CDW, g L^{-1}) at T0 (0 h), T7 (168 h), and T14 (336 h). (B) Time course of BChl*a* synthesis. (C) PHB content (% w PHB / w Cells) at T0, T7, and T14. (D) Temperature profile (°C). Statistical differences between Runs at the same time point were assessed using independent t-tests, while differences between time points within the same Run were analyzed via one-way ANOVA (95% significance) followed by Tukey's HSD post-hoc tests. Error bars represent standard deviations (n = 3). Significant differences are indicated by asterisks ($p < 0.05$*, $p < 0.01$**, $p < 0.001$***); ns = not significant.

The accumulation of PHB (% w PHB/w cells) was evaluated at T0, T7, and T14 for both runs (Fig. 4C). The most substantial increase in PHB was observed during the first 168 h of inoculation (T0–T7), with increments of +11.85% w PHB/w cells (± 1.03) and +9.90% w PHB/w cells (± 0.93) in Run_1 and Run_2, respectively. Over the subsequent 168 h (T7–T14), no significant changes in PHB content were detected in either run. At T14 (336 h), comparing the two trials, the first experiment (Run_1) reached significantly higher PHB levels compared to Run_2 ($p < 0.05$, *), with final values of 15.17% w PHB/w cells (±0.43) and 11.51% w PHB/w cells for Run_1 and Run_2, respectively.

The PHB accumulation trends described above align with volumetric production and the hourly and daily productivities presented in Tab. 4. Run_1 achieved an average productivity of 744.22 ± 61.22 mg PHB L^{-1}, corresponding to a daily productivity of 48.82 ± 4.34 mg PHB L^{-1} d^{-1}, while Run_2 recorded lower values, with 352.01 ± 57.78 mg PHB L^{-1} and 21.33 ± 4.55 mg PHB L^{-1} d^{-1}.

Fig. 4D shows the temperature profiles recorded during the two experiments, which were conducted under uncontrolled room temperature conditions to minimize energy input. Starting 24 h after inoculation (T1), Run_2 showed significantly higher temperatures than Run_1. Starting 144 h after inoculation (T6), the temperatures of Run_2 stabilized, with minimum fluctuations between 30.1 °C (± 0.25) and 29.4 °C (± 0.31) until the end of the experiment. In contrast, the temperatures of Run_1 showed more pronounced variations during the same period, fluctuating from a maximum of 27.6 °C (± 0.30) to a minimum of 24.6 °C (± 0.25).

Tab. 5 summarizes the variation in the concentration of key compounds (carbohydrates, organic acids, ethanol, and ammonium) during the photofermentative process at different time points (T0, T7, and T14) for both experimental trials (Run_1 and Run_2).

Table 5. Variation in the concentration of key compounds during PF at different time points (T0, T7, T14) for Run_1 and Run_2. Values represent the mean ± standard deviation ($n = 3$). *nd* = not detected. Statistical differences between runs at the same time point were assessed using independent *t*-tests, while differences

between time points within the same run were analyzed via one-way ANOVA (95% significance) followed by Tukey's HSD post hoc tests. Statistically significant differences ($p < 0.05$) between time points within the same run are indicated by lowercase letters (*a, b, c*), while differences between runs at the same time point are denoted by uppercase letters (*A, B*).

Compound	Run	T0 (0 h)	T7 (168 h)	T14 (336 h)
Maltotriose (g L^{-1})	Run_1	0.73 (± 0.17) $^{a, A}$	0.16 (± 0.04) $^{b, A}$	nd
	Run_2	0.67 (± 0.11) $^{a, A}$	0.09 (±0.05) $^{b, A}$	0.02 (± 0.01) ^{b}
Maltose (g L^{-1})	Run_1	0.28 (± 0.07) $^{a, A}$	0.17 (± 0.02) $^{b, A}$	nd
	Run_2	0.24 (± 0.10) $^{a, A}$	0.04 (±0.02) $^{b, B}$	nd
Lactate (g L^{-1})	Run_1	3.12 (± 0.30) $^{a, A}$	2.15 (± 0.03) $^{b, A}$	1.98 (± 0.06) $^{b, A}$
	Run_2	2.96 (± 0.01) $^{a, A}$	1.99 (± 0.41) $^{b, A}$	2.27 (± 0.53) $^{b, A}$
Acetate (g L^{-1})	Run_1	0.19 (± 0.05) $^{a, A}$	0.31 (± 0.02) $^{b, A}$	0.75 (± 0.03) $^{c, A}$
	Run_2	0.20 (± 0.05) $^{a, A}$	0.36 (± 0.09) $^{b, A}$	0.97 (± 0.25) $^{c, A}$
Ethanol (g L^{-1})	Run_1	1.21 (± 0.12) $^{a, A}$	1.24 (± 0.12) $^{ab, A}$	1.58 (± 0.00) $^{b, A}$
	Run_2	0.95 (± 0.11) $^{a, A}$	1.29 (± 0.28) $^{ab, A}$	2.21 (± 0.52) $^{b, A}$
Ammonium (mg L^{-1})	Run_1	25.66 (± 2.90) $^{a, A}$	25.33 (± 2.65) $^{a, A}$	15.53 (± 0.32) $^{b, A}$
	Run_2	27.90 (± 4.96) $^{a, A}$	27.63 (± 0.76) $^{a, A}$	11.60 (± 2.18) $^{b, A}$

The concentrations of maltotriose and maltose decreased significantly over time in both runs. In Run_1, maltotriose was completely consumed by T14, whereas a small residual amount of 0.02 g L^{-1} (±0.01) remained in Run_2. A similar trend was observed for maltose, which was fully consumed by T14 in both runs. However, the reduction in maltose concentration between T0 (0 h) and T14 (168 h) was significantly greater in Run_2 compared to Run_1.

The lactate concentration decreased significantly between T0 and T7 in both runs. In contrast, no statistically significant change was observed between T7 and T14, although a slight increase was noted in Run_2 during this period. The acetate concentration, on the other hand, increased significantly over time in both runs, reaching final concentrations of 0.75 g L^{-1} (± 0.03) in Run_1 and 0.97 g L^{-1} (± 0.25) in Run_2 at T14. No significant differences in acetate levels were observed between the runs at any time point.

The ethanol concentration remained relatively stable between T0 and T7 in both runs. However, a significant increase was observed between T7 and T14 in Run_1, with ethanol levels reaching a peak of 1.58 g L^{-1} (± 0.00). In contrast, although ethanol in Run_2 also peaked at 2.21 g L^{-1} (± 0.52) during the same period, the increase between T7 and T14 was not statistically significant.

Ammonium levels remained relatively constant between T0 and T7 in both runs but showed a significant reduction by T14, reaching 15.53 mg L^{-1} (± 0.32) in Run_1 and 11.60 mg L^{-1} (± 2.18) in Run_2. No significant differences in ammonium concentrations were detected between the runs at any time point.

4. Discussion

The DF of bread waste aimed to maximize the yield of lactic acid, making the waste suitable for the subsequent PF step. Indeed, PNSB can oxidize lactic acid into pyruvate, which can be further converted into acetyl-CoA, a key precursor for PHB accumulation [41]. The DF was conducted at 37 °C by inoculating bread waste with *L. amylovorus* DSM 20532 (1×10^9 CFU mL^{-1}), applying the methodology described by Adessi et al. [26]. In their study, Adessi et al. [26] reported a peak lactic acid production of 4.93 ± 0.29 g L^{-1} after 18 h. In contrast, our optimization trials in 100 mL flasks yielded a maximum lactate concentration of 2.72 ± 0.04 g L^{-1} at 120 h (Fig. 1), after which it declined, likely due to lactic acid-consuming microbes. These differences in yield and duration may be attributed to the higher dilution (7.5% vs. 10% w/v used by Adessi et al. [26]) in this study, as well as the inherent variability of food waste composition.

Unlike the findings of Adessi et al. [26], our study observed an unexpected production of acetic acid during DF (Fig. 1). This production peaked after 120 h of incubation before declining. Acetate production cannot be attributed to *L. amylovorus* DSM 20532, which belongs to obligately homofermentative LAB [42], but could be due to the presence of other microorganisms already present in the bread wastes, which were not sterilized before use. The decision not to sterilize the bread waste reflects the aim of simulating more realistic, scalable conditions, as dark fermentation was primarily intended to enrich the substrate with organic acids, especially lactic acid, rather than to ensure strict axenic conditions.

The simultaneous production of lactate and acetate is noteworthy, as acetate can be efficiently assimilated in the metabolic pathway for acetyl-CoA synthesis, as extensively documented [43-45]. Once the duration of DF was optimized, FBB production was carried out in 3 L Erlenmeyer flasks.

At the end of the DF process, the FBB was supplemented with digestate, obtained from an AD process, and a phosphate buffer. The addition of digestate enriches bread waste with essential macro- and micronutrients required for PNSB growth, eliminating the need for chemical supplements that would increase process costs. Indeed, during anaerobic

digestion, macronutrients (N, P, K, S, Mg, Ca) and micronutrients (B, Cl, Cu, Fe, Mn, Mo, Ni, Zn) concentrate in the digestate [46].

The macro- and micronutrient composition of FBB after digestate addition (Tab. 2) shows higher concentrations of Ca, K, Mg, Na, and S compared to the synthetic RPN medium. However, the lower or undetectable levels of trace elements (B, Co, Cu, Fe, Mn, Mo, Ni, Zn) in FBB compared to RPN may help mitigate the adverse effects of macronutrient excess and favor PHB synthesis [47,48]. The absence of Fe, Mo, and Ni inhibits nitrogenase and hydrogenase, reducing bio-H_2 production, which competes for reducing power with PHB synthesis, potentially increasing PHB yield [18,19]. The digestate proved optimal for supplying essential nutrients while maintaining ideal conditions for PHB production.

Scaling-up from 100 mL to 3 L did not reduce acetate and lactate production efficiency (Tab. 3). The lactate content of the FBB substrates was higher than that of the synthetic RPN lactate medium (1.8 g L^{-1}) and consistent with levels reported in other studies on PHB production by PNSB using synthetic media with lactate as a carbon source, confirming its adequacy [49,50]. Conversely, the acetate content was lower than the minimum recommended level (2.15 g L^{-1}) to ensure sufficient PHB accumulation [7]. However, the low ammonium content of the FBB medium significantly enhances its C/N ratio, making it highly favorable for PHB production. In all three PF tests, the FBB C/N ratio was more than twice the minimum recommended value of 30 [7].

The preliminary screening on FBB aimed to identify the strain with the highest potential for PHB production, to be scaled up in a 5 L photobioreactor. Six different strains were tested, three belonging to *R. palustris* (42OL, AV33, CGA009), recognized for their metabolic versatility on various substrates, and three others including two species of *C. johrii* (Pisa7, 9Cis) and one of *C. sphaeroides* (F17). These latter strains were chosen for their distinct ecological origins (Tab. 1), which shaped their unique metabolic traits and ability to thrive under nutrient-limited conditions. All six strains had previously been assessed by Mugnai et al. [35] for their ability to produce PHB on both synthetic media and olive oil effluents.

R. palustris strains (42OL, AV33, CGA009) exhibited a metabolism more oriented towards biomass growth than PHB accumulation (Fig. 2). Specifically, *R. palustris* 42OL and *R. palustris* CGA009 showed a significant increase in CDW over 336 h, whereas *R. palustris* AV33 exhibited an increase in CDW that was not statistically significant. In all cases, the PHB concentration did not exceed 10% w PHB/w cells at T14. These results

are consistent with previous studies reporting the generally low PHB accumulation ability of *R. palustris* strains compared to other purple non-sulfur bacteria. In particular, Mugnai et al. [35] observed that *R. palustris* accumulated significantly lower amounts of PHB than both *C. sphaeroides* and *C. johrii* when cultivated in synthetic media and in agroindustrial waste-based substrates. Conversely, *Cereibacter* strains demonstrated higher PHB accumulation, with *C. johrii* Pisa7 achieving the highest value at 50.73% (±10.60) w PHB/w cells, significantly outperforming *C. sphaeroides* F17 (26.47% ± 11.58) and *C. johrii* 9Cis (22.31% ± 0.77) (Figure 2). *C. johrii* Pisa7 also exhibited the highest absolute growth, with a CDW increase of +1.26 g L^{-1} (±0.15). This dual capacity for high biomass and PHB yield makes *C. johrii* Pisa7 particularly promising for industrial PHB production.

From the TEM analysis (Fig. 3), *C. johrii* Pisa7 shows a notable difference compared to the other *Cereibacter* strains. Despite its high PHB accumulation percentage, *C. johrii* Pisa7 exhibits the smallest cell and PHB inclusion sizes. The literature suggests that smaller, more abundant PHB granules can optimize intracellular space utilization, ultimately enhancing overall PHB production efficiency [51]. Based on these results, *C. johrii* was selected for scale-up in a 5 L photobioreactor, highlighting its promising potential for efficient biopolymer production on an industrial scale.

Process scale-up was conducted in a 5 L photobioreactor equipped with selected LED lights capable of emitting light in the yellow (λ = 593 nm) and near-infrared (λ = 860 nm) regions. The light intensity was increased stepwise. Initially set at 150 µmol photons m^{-2} s^{-1} to allow *C. johrii* Pisa7 to adapt to the substrate FBB, it was raised to 250 µmol photons m^{-2} s^{-1} after 24 h and to 400 µmol photons m^{-2} s^{-1} after 120 h. This adjustment ensured sufficient light penetration, preventing productivity loss caused by cell growth.

In both experiments (Run_1 and Run_2), *C. johrii* Pisa7 showed a significant increase in CDW between T0 and T7, stabilizing from T7 to T14 (Fig. 4A). Run_1 had a higher CDW than Run_2 at both T7 and T14. Lactic acid consumption (Tab. 5) reflected this trend, with significant utilization between T0 and T7 to support growth and PHB synthesis, followed by stabilization. Growth stabilized after T7 may be due to depletion of essential macro- or micronutrients, explaining the residual lactic acid at the end of the tests.

The reactor temperature was not actively controlled, as the ambient room temperature remained stable and consistently within or close to the optimal range for PHB production (24-30 °C) [7] (Fig. 4D). Despite the lower temperature in Run_1, its CDW was

significantly higher than that of Run_2 at both T7 and T14 (Fig. 4A). This can be attributed to a greater accumulation of PHB in Run_1 compared to Run_2. The lower initial temperatures (20-24 °C) in Run_1 may have induced metabolic stress, promoting the accumulation of storage compounds such as PHB at the expense of active cell growth. As shown in Fig. 4C, PHB accumulation was higher in Run_1 than in Run_2 at both T7 and T14. However, a statistically significant difference was observed only at T14 ($p < 0.05$, *). The absence of significant differences at T7 suggests that the temperature effect becomes more pronounced over time. Indeed, during the early phase (T0-T7), PHB accumulation followed a similar trend in both conditions.

The growth of *C. johrii* Pisa7 was also assessed by monitoring BChl*a* content over time (Fig. 4B), which mirrored the general growth trend. A significant increase in BChl*a* was observed in both experiments during the first 168 h, followed by stabilization. However, no statistically significant differences in BChl*a* were observed between Run_1 and Run_2 at T7 and T14, indicating that the increase in CDW did not correlate with a proportional rise in BChl*a*. This discrepancy can be attributed to the fact that BChl*a* synthesis is primarily influenced by light intensity and quality, which was the same in both runs. Although BChl*a* content provides a reliable indication of growth tendency, it is not directly related to CDW, which is influenced by other factors, such as PHB accumulation.

The consumption of lactate (Tab. 5) reflects the growth of *C. johrii* Pisa7, showing a significant decrease during the first 168 h (T0-T7), followed by stabilization with no significant variations. This indicates that lactate is utilized as the main carbon source to support both growth and PHB accumulation. In contrast, ammonium (Tab. 5) remains stable during the first 168 h but decreases in the subsequent phase (T7-T14). The lack of ammonium consumption in the initial phase may be explained by the microorganism relying on internal nitrogen reserves accumulated during its growth on the synthetic RPN medium during inoculum preparation. Nitrogen is subsequently consumed between T7 and T14 to sustain metabolic processes related to maintenance and adaptation, even in the absence of further cell growth.

The concentrations of maltose, maltotriose, acetic acid, and ethanol (Tab. 5) were monitored during PF. A reduction in complex sugars (maltose and maltotriose) and a consistent increase in acetic acid and ethanol suggested possible contamination. The potential contamination observed in the photobioreactor could mainly be attributed to the fact that the system was not sterilized but only subjected to a disinfection procedure. This

choice was dictated by the large size of the reactor, which made autoclave sterilization technically impractical. However, this approach better reflects industrial-scale operations, where complete sterilization is often not feasible.

At the end of the PF trials, *C. johrii* Pisa7 accumulated PHB at levels of 15.17% (± 0.43) w PHB/w cells and 11.51% (± 1.60) w PHB/w cells in Run_1 and Run_2, respectively. These percentages are over 70% lower than those observed during screening experiments. However, the screening experiments were conducted at a working volume of 100 mL, approximately 50 times smaller than the bioreactor volume, a difference that likely contributed to the observed loss of efficiency.

The results of this study appear promising when compared to those reported in the literature, as extensively reviewed by Sali and Mackey [41] and by Montiel-Corona and Buitrón [19]. A comparison with relevant studies is summarized in Table 6, which reports PHB production by different pure or mixed PNSB cultures, grown on dark-fermented organic waste.

Notably, most literature data refer to small-scale systems (≤ 400 mL), while the present study was conducted in a 5 L photobioreactor. Our results are in line with those reported by *Rhodopseudomonas* sp. S16-VOGS3, which was cultivated in a 4 L photobioreactor on dark-fermented cheese whey, reaching 18% PHB/CDW [52]. In contrast, higher PHB contents (up to 83% PHB/CDW) were achieved with *Rhodobacter sphaeroides* AV1b grown on dark-fermented municipal or food waste [53,54], but these results were obtained in 400 mL batch systems under highly controlled conditions, making them less directly comparable to this scale-up trial.

Moreover, when comparing the PHB production of *C. johrii* Pisa7 cultivated in 100 mL obtained in this study during preliminary photofermentation tests with other studies conducted at similar volumes [55-57], its PHB content was found to be significantly higher. This highlights the strain's strong potential for efficient PHB accumulation.

Overall, these comparisons confirm the robustness and scalability of the process developed in this work. Furthermore, no bio-H_2 production was detected in any tested strains, either during screening experiments or in photobioreactor tests, confirming that FBB supports selective PHB production by reducing competition between metabolic pathways. This may also be due to the composition of the medium used in this study.

While Adessi et al. [26] enhanced hydrogen production by adding ferric citrate and magnesium sulfate (key elements for nitrogenase activity), we only supplemented the FBB with digestate from AD and a phosphate buffer. The lack of supplementation with

iron and sulfate, and their possible deficiency in the digestate, may have limited bio-H_2 production and instead promoted PHB accumulation, highlighting the advantage of using FBB to increase PHB yield.

Table 6. PHB production by pure or mixed PNSB cultures grown on dark-fermented organic waste. The table includes the type of inoculum and substrate, PHB content (% of CDW), volumetric PHB production (mg L^{-1}), working volume (WV), light source used during photofermentation, and reference (Ref.).

Inoculum	**Substrate**	**Light**	**PHB (or PHA) (%** CDW**)**	**PHB** (mg L_{cult}^{-1})	**WV** (mL)	**Ref.**
Rhodopseudomonas capsulatus	DF fruit and vegetable waste	White	24	-	76	[52]
Rhodopseudomonas capsulatus	DF fruit and vegetable waste	White	5	-	76	[53]
Rhodobacter sphaeroides AV1b	DF food waste	White	80	800	400	[54]
Rhodobacter sphaeroides AV1b	DF municipal organic waste	White	83	882	400	[55]
Rhodopseudomonas sp. S16- VOGS3	DF cheese whey	White	18	232	4000	[56]
Mixed photosynthetic culture	DF food waste	Infrared	19 (PHA)	-	100	[57]
C. johrii Pisa7	DF bread waste (FBB)	White	50.73	1083.76	100	This study
C. johrii Pisa7 (Run_1)	DF bread waste (FBB)	Selected (593 and 860 nm)	15.17	744.22	5000	This study

In the literature, most studies reporting higher PHA concentrations rely on synthetic substrates, which, while effective, are costly and less environmentally sustainable. By contrast, this study employed a real, complex substrate derived from bread waste, with minimal medium modifications, demonstrating the technical feasibility of PHB production at the larger scale and under conditions more closely aligned with potential industrial applications. However, the transition to an industrial-scale process still faces significant limitations, particularly the need for a detailed quantification of the energy inputs associated with the two-stage system, including both dark fermentation and photofermentation. It is essential to assess the energy costs related to light management, temperature control, and substrate pre-treatment, as well as those required for PHB extraction, which remains one of the most economically demanding steps. Additionally, harvesting biomass from low-density phototrophic cultures poses major efficiency and cost challenges. Further research is therefore needed to overcome these technical barriers,

improve process efficiency, and validate the system's performance over time under realistic, non-sterile conditions representative of the industrial sector.

5. Conclusions

This study demonstrated the feasibility of using bread waste as a substrate for PHB production via a combined DF and PF process. During DF, *L. amylovorus* DSM 20532 enriched bread waste effluent with lactate and acetate in 120 h, generating a substrate suitable for PF. The addition of digestate supplied essential macro- and micronutrients, eliminating the need for chemical additives and enhancing process sustainability.

Among the six tested PNSB strains in small-scale experiments (100 mL bottles), *C. johrii* Pisa7 showed the highest PHB accumulation and biomass increase, highlighting its potential as the most promising strain for industrial applications. Consequently, *C. johrii* Pisa7 was selected for scale-up experiments conducted in a 5 L photobioreactor equipped with LED lights tuned to the absorption peaks of PNSB bacteriochlorophylls. In these trials, *C. johrii* Pisa7 accumulated PHB up to 15.17% ± 0.43 w PHB/w cells. While reduced efficiency was observed compared to small-scale tests, PHB yields remained comparable to those reported in similar studies, validating the scalability of the process.

From an environmental perspective, further research is needed to assess the overall energy consumption of the process, including light management, temperature control, and sterilization. It is also important to explore integration with renewable energy sources. In particular, a thorough evaluation of these energy inputs through a life cycle assessment (LCA) will be essential to establish a sustainable and scalable model for the industrial valorization of agro-industrial waste into bioplastics.

In conclusion, this study contributes to advancing a circular bioeconomy by transforming waste streams into sustainable materials. Addressing technical, economic, and policy challenges will require interdisciplinary collaboration to unlock its full potential.

Acknowledgements

The authors would like to acknowledge Dr. Maria Cristina Salvatici at CE.M.E., CNR, Florence, Italy, for the electron micrographs.

Author contributions

Conceptualization, L.B., G.D., G.M., V.G., and A.A.; methodology, L.B., G.D., G.M., V.G., and A.A.; formal analysis, L.B., G.D., G.M., V.G.; investigation, L.B., E.C., A.A.; resources, L.G. and A.A.; data curation, L.B., G.D., G.M., and V.G.; writing-original draft preparation, L.B.; writing-review and editing, L.B., G.D., G.M., V.G., E.C., L.G., and A.A.; supervision, L.G. and A.A. All authors have read and agreed to the published version of the manuscript.

References

[1] He, Y., Deng, X., Jiang, L., Hao, L., Shi, Y., Lyu, M., ... & Wang, S. (2024). Current advances, challenges and strategies for enhancing the biodegradation of plastic waste. *Science of The Total Environment*, 906, 167850. https://doi.org/10.1016/j.scitotenv.2023.167850.

[2] Singh, N., & Walker, T. R. (2024). Plastic recycling: A panacea or environmental pollution problem. *Npj Materials Sustainability*, 2(1), 17. https://doi.org/10.1038/s44296-024-00024-w.

[3] Luengo, J. M., García, B., Sandoval, A., Naharro, G., & Olivera, E. R. (2003). Bioplastics from microorganisms. *Current opinion in microbiology*, 6(3), 251-260. https://doi.org/10.1016/S1369-5274(03)00040-7.

[4] Singh, N., Ogunseitan, O. A., Wong, M. H., & Tang, Y. (2022). Sustainable materials alternative to petrochemical plastics pollution: A review analysis. *Sustainable horizons*, 2, 100016. https://doi.org/10.1016/j.horiz.2022.100016.

[5] Bishop, G., Styles, D., & Lens, P. N. (2021). Environmental performance comparison of bioplastics and petrochemical plastics: A review of life cycle assessment (LCA) methodological decisions. *Resources, Conservation and Recycling*, 168, 105451. https://doi.org/10.1016/j.resconrec.2021.105451.

[6] Kumar, R., Lalnundiki, V., Shelare, S. D., Abhishek, G. J., Sharma, S., Sharma, D., ... & Abbas, M. (2024). An investigation of the environmental implications of bioplastics: Recent advancements on the development of environmentally friendly bioplastics solutions. *Environmental Research*, 244, 117707. https://doi.org/10.1016/j.envres.2023.117707.

[7] Monroy, I., & Buitrón, G. (2020). Production of polyhydroxybutyrate by pure and mixed cultures of purple non-sulfur bacteria: A review. *Journal of biotechnology*, 317, 39-47. https://doi.org/10.1016/j.jbiotec.2020.04.012.

[8] Corneli, E., Adessi, A., Dragoni, F., Ragaglini, G., Bonari, E., & De Philippis, R. (2016). Agroindustrial residues and energy crops for the production of hydrogen and poly-β-hydroxybutyrate via photofermentation. *Bioresource technology*, 216, 941-947. https://doi.org/10.1016/j.biortech.2016.06.046.

[9] Moradali, M. F., & Rehm, B. H. (2020). Bacterial biopolymers: from pathogenesis to advanced materials. *Nature Reviews Microbiology*, 18(4), 195-210. https://doi.org/10.1038/s41579-019-0313-3.

[10] Obruca, S., Sedlacek, P., Slaninova, E., Fritz, I., Daffert, C., Meixner, K., ... & Koller, M. (2020). Novel unexpected functions of PHA granules. *Applied microbiology and biotechnology*, 104, 4795-4810. https://doi.org/10.1007/s00253-020-10568-1.

[11] Poli, A., Di Donato, P., Abbamondi, G. R., & Nicolaus, B. (2011). Synthesis, production, and biotechnological applications of exopolysaccharides and polyhydroxyalkanoates by archaea. *Archaea*, 2011(1), 693253. https://doi.org/10.1155/2011/693253.

[12] Thu, N. T. T., Hoang, L. H., Cuong, P. K., Viet-Linh, N., Nga, T. T. H., Kim, D. D., ... & Nhi-Cong, L. T. (2023). Evaluation of polyhydroxyalkanoate (PHA) synthesis by Pichia sp. TSLS24 yeast isolated in Vietnam. *Scientific Reports*, 13(1), 3137. https://doi.org/10.1038/s41598-023-28220-z.

[13] Amadu, A. A., Qiu, S., Ge, S., Addico, G. N. D., Ameka, G. K., Yu, Z., ... & Wang, S. (2021). A review of biopolymer (Poly-β-hydroxybutyrate) synthesis in microbes cultivated on wastewater. *Science of the Total Environment*, 756, 143729. https://doi.org/10.1016/j.scitotenv.2020.143729.

[14] Koller, M., & Mukherjee, A. (2022). A new wave of industrialization of PHA biopolyesters. *Bioengineering*, 9(2), 74. https://doi.org/10.3390/bioengineering9020074.

[15] Muneer, F., Rasul, I., Azeem, F., Siddique, M.H., Zubair, M., Nadeem, H., 2020. Microbial Polyhydroxyalkanoates (PHAs): Efficient Replacement of Synthetic Polymers. *J Polym Environ* 28 (9), 2301–2323. https://doi.org/10.1007/s10924-020-01772-1.

[16] Adessi, A., Corneli, E., De Philippis, R. (2017). Photosynthetic Purple Non Sulfur Bacteria in Hydrogen Producing Systems: New Approaches in the Use of Well Known and Innovative Substrates. In*: Hallenbeck, P. (eds) Modern Topics in the Phototrophic Prokaryotes*. Springer, Cham. https://doi.org/10.1007/978-3-319-46261-5_10.

[17] Alsiyabi, A., Immethun, C.M., Saha, R., 2019. Modeling the Interplay between Photosynthesis, CO2 Fixation, and the Quinone Pool in a Purple Non-Sulfur Bacterium. *Sci Rep* 9 (1). https://doi.org/10.1038/s41598-019-49079-z.

[18] McKinlay, J. B. (2014). Systems biology of photobiological hydrogen production by purple non-sulfur bacteria. In *Microbial bioenergy: hydrogen production* (pp. 155-176). Dordrecht: Springer Netherlands. https://doi.org/10.1007/978-94-017-8554-9_7.

[19] Montiel-Corona, V., & Buitrón, G. (2021). Polyhydroxyalkanoates from organic waste streams using purple non-sulfur bacteria. *Bioresource Technology*, 323, 124610. https://doi.org/10.1016/j.biortech.2020.124610.

[20] Wu, S. C., Liou, S. Z., & Lee, C. M. (2012). Correlation between bio-hydrogen production and polyhydroxybutyrate (PHB) synthesis by *Rhodopseudomonas palustris* WP3-5. *Bioresource technology*, 113, 44-50. https://doi.org/10.1016/j.biortech.2012.01.090.

[21] Argun, H., & Kargi, F. (2011). Bio-hydrogen production by different operational modes of dark and photo-fermentation: an overview. *International Journal of Hydrogen Energy*, 36(13), 7443-7459. https://doi.org/10.1016/j.ijhydene.2011.03.116.

[22] Hördt, A., López, M. G., Meier-Kolthoff, J. P., Schleuning, M., Weinhold, L. M., Tindall, B. J., ... & Göker, M. (2020). Analysis of 1,000+ type-strain genomes substantially improves taxonomic classification of Alphaproteobacteria. *Frontiers in microbiology*, 11, 468. https://doi.org/10.3389/fmicb.2020.00468.

[23] Gahlawat, G., Kumari, P., & Bhagat, N. R. (2020). Technological advances in the production of polyhydroxyalkanoate biopolymers. *Current Sustainable/Renewable Energy Reports*, 7, 73-83. https://doi.org/10.1007/s40518-020-00154-4.

[24] Gowda, V., & Shivakumar, S. (2014). Agrowaste-based Polyhydroxyalkanoate (PHA) production using hydrolytic potential of *Bacillus thuringiensis* IAM 12077. *Brazilian Archives of Biology and Technology*, 57, 55-61. https://doi.org/10.1590/S1516-89132014000100009.

[25] Sirohi, R., Pandey, J. P., Gaur, V. K., Gnansounou, E., & Sindhu, R. (2020). Critical overview of biomass feedstocks as sustainable substrates for the production of polyhydroxybutyrate (PHB). *Bioresource Technology*, 311, 123536. https://doi.org/10.1016/j.biortech.2020.123536.

[26] Adessi, A., Venturi, M., Candeliere, F., Galli, V., Granchi, L., & De Philippis, R. (2018). Bread wastes to energy: sequential lactic and photo-fermentation for hydrogen

production. *International Journal of Hydrogen Energy*, 43(20), 9569-9576. https://doi.org/10.1016/j.ijhydene.2018.04.053.

[27] Verni, M., Minisci, A., Convertino, S., Nionelli, L., & Rizzello, C. G. (2020). Wasted bread as substrate for the cultivation of starters for the food industry. *Frontiers in Microbiology*, 11, 293. https://doi.org/10.3389/fmicb.2020.00293.

[28] Ike, A., Toda, N., Tsuji, N., Hirata, K., & Miyamoto, K. (1997). Hydrogen photoproduction from CO_2-fixing microalgal biomass: application of halotolerant photosynthetic bacteria. *Journal of fermentation and bioengineering*, 84(6), 606-609. https://doi.org/10.1016/S0922-338X(97)81921-6.

[29] Oda, Y., Park, B. S., Moon, K. H., & Tonomura, K. (1997). Recycling of bakery wastes using an amylolytic lactic acid bacterium. *Bioresource Technology*, 60(2), 101-106. https://doi.org/10.1016/S0960-8524(97)00008-4.

[30] Kapdan, I. K., & Kargi, F. (2006). Bio-hydrogen production from waste materials. *Enzyme and microbial technology*, 38(5), 569-582. https://doi.org/10.1016/j.enzmictec.2005.09.015.

[31] Kawaguchi, H., Hashimoto, K., Hirata, K., & Miyamoto, K. (2001). H_2 production from algal biomass by a mixed culture of *Rhodobium marinum* A-501 and *Lactobacillus amylovorus*. *Journal of bioscience and bioengineering*, 91(3), 277-282. https://doi.org/10.1016/S1389-1723(01)80134-1.

[32] Trontel, A., Baršić, V., Slavica, A., Šantek, B., & Novak, S. (2010). Modelling the effect of different substrates and temperature on the growth and lactic acid production by *Lactobacillus amylovorus* DSM 20531T in batch process. *Food Technology and Biotechnology*, 48(3), 352-361. https://urn.nsk.hr/urn:nbn:hr:159:642072.

[33] Adessi, A., & De Philippis, R. (2014). Photobioreactor design and illumination systems for H_2 production with anoxygenic photosynthetic bacteria: a review. *International Journal of Hydrogen Energy*, 39(7), 3127-3141. https://doi.org/10.1016/j.ijhydene.2013.12.084.

[34] Leibniz Institute DSMZ German Collection of Microorganisms and Cell Cultures GmbH. Available online: https://www.dsmz.de/ (accessed on 25 March 2025).

[35] Mugnai, G., Bernabò, L., Daly, G., Corneli, E., & Adessi, A. (2025). Photofermentative production of poly-β-hydroxybutyrate (PHB) by purple non-sulfur bacteria using olive oil by-products. *Bioresources and Bioprocessing*, *12*(1), 1-15. https://doi.org/10.1186/s40643-025-00856-x.

[36] Adessi, A., Spini, G., Presta, L., Mengoni, A., Viti, C., Giovannetti, L., ... & De Philippis, R. (2016). Draft genome sequence and overview of the purple non sulfur bacterium *Rhodopseudomonas palustris* 42OL. *Standards in genomic sciences*, 11, 1-7. https://doi.org/10.1186/s40793-016-0145-y.

[37] Bianchi, L., Mannelli, F., Viti, C., Adessi, A., & De Philippis, R. (2010). Hydrogen-producing purple non-sulfur bacteria isolated from the trophic lake Averno (Naples, Italy). *International journal of hydrogen energy*, 35(22), 12216-12223. https://doi.org/10.1016/j.ijhydene.2010.08.038.

[38] Kim, M. K., & Harwood, C. S. (1991). Regulation of benzoate-CoA ligase *in Rhodopseudomonas palustris*. *FEMS microbiology letters*, 83(2), 199-203. https://doi.org/10.1111/j.1574-6968.1991.tb04440.x-i1.

[39] Carlozzi, P., & Sacchi, A. (2001). Biomass production and studies on *Rhodopseudomonas palustris* grown in an outdoor, temperature controlled, underwater tubular photobioreactor. *Journal of Biotechnology*, 88(3), 239-249. https://doi.org/10.1016/S0168-1656(01)00280-2.

[40] De Philippis, R., Sili, C., & Vincenzini, M. (1992). Glycogen and poly-β-hydroxybutyrate synthesis in *Spirulina maxima*. Microbiology, 138(8), 1623-1628. https://doi.org/10.1099/00221287-138-8-1623.

[41] Sali, S., & Mackey, H. R. (2021). The application of purple non-sulfur bacteria for microbial mixed culture polyhydroxyalkanoates production. *Reviews in Environmental Science and Bio/Technology*, 20(4), 959-983. https://doi.org/10.1007/s11157-021-09597-7.

[42] Zheng, J., Wittouck, S., Salvetti, E., Franz, C. M., Harris, H. M., Mattarelli, P., ... & Lebeer, S. (2020). A taxonomic note on the genus Lactobacillus: Description of 23 novel genera, emended description of the genus Lactobacillus Beijerinck 1901, and union of Lactobacillaceae and Leuconostocaceae. *International journal of systematic and evolutionary microbiology*, 70(4), 2782-2858. https://doi.org/10.1099/ijsem.0.004107.

[43] Brandl, H., Gross, R. A., Lenz, R. W., Lloyd, R., & Fuller, R. C. (1991). The accumulation of poly (3-hydroxyalkanoates) in *Rhodobacter sphaeroides*. *Archives of microbiology*, 155, 337-340. https://doi.org/10.1007/BF00243452.

[44] Fradinho, J. C., Oehmen, A., & Reis, M. A. M. (2014). Photosynthetic mixed culture polyhydroxyalkanoate (PHA) production from individual and mixed volatile fatty acids (VFAs): Substrate preferences and co-substrate uptake. Journal of Biotechnology, 185, 19-27. https://doi.org/10.1016/j.jbiotec.2014.05.035.

[45] Liebergesell, M., Hustede, E., Timm, A., Steinbüchel, A., Fuller, R. C., Lenz, R. W., & Schlegel, H. G. (1991). Formation of poly (3-hydroxyalkanoates) by phototrophic and chemolithotrophic bacteria. *Archives of Microbiology*, 155, 415-421. https://doi.org/10.1007/BF00244955.

[46] Häfner, F., Hartung, J., & Möller, K. (2022). Digestate composition affecting N fertiliser value and C mineralisation. *Waste and biomass valorization*, 13(8), 3445-3462. https://doi.org/10.1007/s12649-022-01723-y.

[47] Demiriz, B. Ö., Kars, G., Yücel, M., Eroğlu, İ., & Gündüz, U. (2019). Hydrogen and poly-β-hydroxybutyric acid production at various acetate concentrations using *Rhodobacter capsulatus* DSM 1710. *International Journal of Hydrogen Energy*, 44(32), 17269-17277. https://doi.org/10.1016/j.ijhydene.2019.02.036.

[48] Alsafadi, D., & Al-Mashaqbeh, O. (2017). A one-stage cultivation process for the production of poly-3-(hydroxybutyrate-co-hydroxyvalerate) from olive mill wastewater by *Haloferax mediterranei*. *New biotechnology*, 34, 47-53. https://doi.org/10.1016/j.nbt.2016.05.003.

[49] Carlozzi, P., Seggiani, M., Cinelli, P., Mallegni, N., & Lazzeri, A. (2018). Photofermentative poly-3-hydroxybutyrate production by *Rhodopseudomonas* sp. S16-VOGS3 in a novel outdoor 70-L photobioreactor. *Sustainability*, 10(9), 3133. https://doi.org/10.3390/su10093133.

[50] Khatipov, E., Miyake, M., Miyake, J., & Asada, Y. (1998). Accumulation of poly-β-hydroxybutyrate by *Rhodobacter sphaeroides* on various carbon and nitrogen substrates. *FEMS Microbiology Letters*, 162(1), 39-45. https://doi.org/10.1111/j.1574-6968.1998.tb12976.x.

[51] Brown, B., Immethun, C., Alsiyabi, A., Long, D., Wilkins, M., & Saha, R. (2022). Heterologous phasin expression in *Rhodopseudomonas palustris* CGA009 for bioplastic production from lignocellulosic biomass. Metabolic Engineering Communications, 14, e00191. https://doi.org/10.1016/j.mec.2021.e00191.

[52] Corona, V. M., Le Borgne, S., Revah, S., & Morales, M. (2017). Effect of light-dark cycles on hydrogen and poly-β-hydroxybutyrate production by a photoheterotrophic culture and Rhodobacter capsulatus using a dark fermentation effluent as substrate. *Bioresource technology*, 226, 238-246. https://doi.org/10.1016/j.biortech.2016.12.021.

[53] Montiel-Corona, V., Revah, S., & Morales, M. (2015). Hydrogen production by an enriched photoheterotrophic culture using dark fermentation effluent as substrate: Effect of flushing method, bicarbonate addition, and outdoor–indoor conditions.

International journal of hydrogen energy, 40(30), 9096-9105. https://doi.org/10.1016/j.ijhydene.2015.05.067.

[54] Ghimire, A., Valentino, S., Frunzo, L., Pirozzi, F., Lens, P. N., & Esposito, G. (2016). Concomitant biohydrogen and poly-β-hydroxybutyrate production from dark fermentation effluents by adapted *Rhodobacter sphaeroides* and mixed photofermentative cultures. *Bioresource technology*, 217, 157-164. https://doi.org/10.1016/j.biortech.2016.03.017.

[55] Luongo, V., Ghimire, A., Frunzo, L., Fabbricino, M., d'Antonio, G., Pirozzi, F., & Esposito, G. (2017). Photofermentative production of hydrogen and poly-β-hydroxybutyrate from dark fermentation products. Bioresource technology, 228, 171-175. https://doi.org/10.1016/j.biortech.2016.12.079.

[56] Carlozzi, P., Touloupakis, E., Di Lorenzo, T., Giovannelli, A., Seggiani, M., Cinelli, P., & Lazzeri, A. (2019). Whey and molasses as inexpensive raw materials for parallel production of biohydrogen and polyesters via a two-stage bioprocess: new routes towards a circular bioeconomy. *Journal of Biotechnology*, *303*, 37-45. https://doi.org/10.1016/j.jbiotec.2019.07.008.

[57] Allegue, L. D., Puyol, D., & Melero, J. A. (2020). Food waste valorization by purple phototrophic bacteria and anaerobic digestion after thermal hydrolysis. *Biomass and Bioenergy*, 142, 105803. https://doi.org/10.1016/j.biombioe.2020.105803.

Chapter II

Selected-Wavelength Illumination for Enhanced Hydrogen and Poly-β-hydroxybutyrate Production from Second Cheese Whey by *Rhodopseudomonas palustris*

Luca Bernabò[1], Giulia Daly[1], Viola Galli[2], Simona Guerrini[1], Carlo Viti[1], Lisa Granchi[1], and Alessandra Adessi[1]*

[1]Department of Agriculture, Food, Environment and Forestry (DAGRI), University of Florence, Piazzale delle Cascine, 18, Florence, 50144, Italy.

[2]FoodMicroTeam s.r.l, Academic Spin-Off of University of Florence, Via Santo Spirito 14, Florence, 50125, Italy

*Correspondence: alessandra.adessi@unifi.it; Tel.: +39-0552755534

Manuscript published in **Microorganisms** (22 December 2025)

https://doi.org/10.3390/microorganisms14010032

Abstract

Second cheese whey (SCW), a major by-product of ricotta cheese production, poses significant environmental challenges due to its high lactose content. Biohydrogen (Bio-H_2) and poly-β-hydroxybutyrate (PHB) production offer a sustainable reuse of SCW, that could provide ideal nutrients for microbial growth. This study aimed to convert SCW into Bio-H_2 and PHB using a 5-liter tubular bioreactor in a sequential lactic fermentation and photofermentation system. Two lighting conditions were tested: white LED (WL) and selected LED (SL). Optimal results were achieved with a co-inoculum of *Lactococcus lactis* MK L84 and *Lacticaseibacillus paracasei* MK L49 at pH 4.5-5.5, followed by photofermentation with *Rhodopseudomonas palustris* 42OL under SL condition. The process yielded an average of 0.47 L of H_2 per liter of substrate and 1.66% wPHB/wCDW. This approach successfully transformed dairy waste into high-value products, promoting circular economy principles.

Keywords

Rhodopseudomonas palustris 42OL; lactic acid bacteria, second cheese whey; hydrogen production; poly-β-hydroxybutyrate; light quality; energy recovery.

Abbreviations

CW, cheese whey; DW, dairy wastewater; SCW, second cheese whey; Bio-H_2, biohydrogen; PNSB, purple non-sulfur bacteria; CDW, cellular dry weight; BChls, bacteriochlorophylls; Bchl*a*, bacteriochlorophylls *a*; OD_{660nm}, optical density at 660nm; VHPR, volumetric hydrogen production rate; SHPR, specific hydrogen production rate; SCE, substrate conversion efficiency; LCE, light conversion efficiency; H_{max}, maximum cumulative hydrogen; R_{max,H_2}, maximum rate of hydrogen production.

1. Introduction

Currently, most energy comes from non-renewable fossil fuels, driving climate change [1]. The EU targets a 90% reduction in greenhouse gas emissions by 2040 and climate neutrality by 2050 [2]. Hydrogen (H_2), with zero emissions and high energy density, is a promising alternative to fossil fuels [3]. H_2 can find applications across sectors like transportation, electricity, and industry [4]. However, fossil-fuel-based H_2 production releases ~830 million tons of CO_2 annually [5].

In this scenario, microbiological H_2 production (Bio-H_2) using agro-industrial waste offers a sustainable alternative, by producing H_2 independently of fossil fuels and converting waste into valuable resources, in line with circular economy principles [6,7]. Bio-H_2 can be produced *via* bio-photolysis, dark fermentation, and photofermentation using microorganisms such as microalgae, non-photosynthetic bacteria, and photosynthetic bacteria (PSB) [8].

Integrating dark fermentation and photofermentation optimizes Bio-H_2 production showing potential for future industrial applications [9,10]. Dark fermentation, driven by anaerobic bacteria, generates Bio-H_2, organic acids, volatile fatty acids (VFAs), and CO_2 without light [10]. The organic acids serve as substrates for photofermentation by purple non-sulfur bacteria (PNSB), which generates Bio-H_2 *via* nitrogenase enzyme under nitrogen-limited conditions [11,12]. During photofermentation, PNSB grow photoheterotrophically under anaerobic conditions, using organic acids as carbon and electron sources while harnessing light as their energy source [12].

Agro-industrial wastewater is often rich in ammoniacal nitrogen, which inhibits nitrogenase activity and thus hampers Bio-H_2 production [13]. Substrate dilution is a common strategy to mitigate this issue, although this approach may increase substrate volumes and process costs [14,15].

Rhodopseudomonas palustris is a highly versatile PNSB for Bio-H_2 production, as it efficiently utilizes various organic substrates, including industrial waste [16,17]. Its versatility is also linked to three nitrogenase isoforms (molybdenum, vanadium, and iron), each varying based on the metal in the enzyme's active site, allowing Bio-H_2 production under different environmental conditions [18,19].

PNSB can produce and accumulate poly-β-hydroxybutyrate (PHB), a biodegradable polymer from the polyhydroxyalkanoates (PHA) family, suitable for bioplastics production [9]. PHB acts as an energy reserve and stress protector, synthesized under high carbon-nitrogen (C/N) ratios and nutrient-limited conditions (e.g., sulfate, phosphate,

magnesium) [20]. While PHB biosynthesis competes with Bio-H_2 production as a reductive pathway, both can be simultaneously generated [21].

Dairy production plays a crucial role in human nutrition but generates millions of tons of waste per year, including cheese whey (CW) and second cheese whey (SCW), both with high environmental impact if not correctly managed [22-24]. SCW, produced by heating CW during ricotta cheese production, is rich in lactose (35–50 g L^{-1}) and has high COD (50 g L^{-1}) and BOD (80 g L^{-1}) levels [24]. In Italy, 15% of CW is used to obtain ricotta cheese, producing about 1 million tons of SCW per year. Though often reused as animal feed, SCW contains valuable compounds like proteins, peptides, and lactose, making it an excellent resource for biotechnological valorization [24,25]. Integrating dark fermentation and photofermentation, with *R. palustris*, offers a sustainable method to treat SCW, reducing COD and producing Bio-H_2 and/or PHB as valuable by-products.

Lactic acid bacteria (LAB) are widely used in the fermentation of dairy products due to their ability to metabolize carbohydrates into organic acids, exopolysaccharides, and other compounds, depending on the type of fermentation they perform (homo- or heterofermentative). LAB can be used to convert residual lactose present SCW into lactate, which is the preferred carbon source for *R. palustris* in the photobiological production of Bio-H_2 [26,27].

The efficiency of Bio-H_2 and PHB production in PNSB depends on the quality of light, as bacteriochlorophylls (BChls) absorb light at 590 nm and in the near-infrared range (800–880 nm) [28]. Studies show that LEDs matched to BChl absorption significantly enhance Bio-H_2 production [29]. For instance, *R. palustris* achieved higher H_2 yields under 590 nm light compared to other wavelengths [30], while filtering light above 760 nm reduced H_2 production in *Rhodobacter sphaeroides* [31].

This study evaluates the potential for producing Bio-H_2 and PHB from SCW using *Rhodopseudomonas palustris* strain 42OL in a two-stage process within a 5L bioreactor. The first step involves lactic fermentation to enrich the substrate with lactic acid, followed by photofermentation under two types of LED lighting: white LEDs (WL) and selected LEDs (SL) emitting in the yellow (593 nm) and infrared (860 nm) ranges. The aim is to assess the feasibility of SCW valorization while analyzing the effects of light on *R. palustris* growth, BChl production, Bio-H_2 generation, and PHB synthesis.

2. Materials and methods

2.1. Bacterial Strains

For the dark fermentation tests, a microbial consortium consisting of two different species of lactic acid bacteria (LAB) was used: *Lactococcus lactis* MK L84 and *Lacticaseibacillus paracasei* MK L49, both belonging to the collection of Department of Agriculture, Food, Environment and Forestry (DAGRI) of the University of Florence (Italy) and previously isolated from spontaneous raw milk fermentations [32]. The selected LAB strains were chosen for their proven fermentative efficiency, robustness, and ability to produce lactic acid from complex substrates, as reported by Galli et al. [32].

For the photofermentation tests, *Rhodopseudomonas palustris* 42OL was employed, a microorganism from the DAGRI collection isolated in 1973 from a waste treatment pond of a sugar refinery. This strain was selected due to its adaptability to different types of substrates and because it has been reported in the literature to achieve high Bio-H_2 production yields [33]. The draft genome sequence of *R. palustris* 42OL is available in the NCBI database under BioProject accession number PRJNA283573 (assembly accession GCA_001020905.1).

2.2. Cultivation Media

Before being used in the dark fermentation tests, the lactic acid bacteria (LAB) were cultured for 48 hours in M17 broth (Oxoid, Basingstoke, UK) with the following composition: Tryptone 5.0 g L^{-1}; Soy Peptone 5.0 g L^{-1}; Yeast Extract 2.5 g L^{-1}; Meat Extract 5.0 g L^{-1}; Sodium Glycerophosphate 19.0 g L^{-1}; Magnesium Sulphate 0.25 g L^{-1}; Ascorbic Acid 0.5 g L^{-1}; Lactose 5.0 g L^{-1}; deionized water. The pH of the medium was 6.69 ± 0.2 at 25°C. The strains were maintained at 30°C under constant agitation (80 rpm). Stationary phase cells were harvested, centrifugated at 3700 rpm for 15 min (Sigma Laborzentrifugen GmbH, Osterode am Harz, Germany), and resuspended in the SCW for tests. The dark fermentation process of SCW will be explored in detail in paragraph 2.4.

The culture of *R. palustris* 42OL was maintained at 30°C, under a light intensity of 150 µmol (photons) m^{-2} s^{-1}, in an RPN medium, containing DL-malic acid as the primary carbon source [34]. The medium had the following composition: DL-malic acid 2.0 g L^{-1}; NH_4Cl 0.5 g L^{-1}; K_2HPO_4 0.5 g L^{-1}; KH_2PO_4 0.3 g L^{-1}; $MgSO_4$.7H2O 0.4 g L^{-1}; NaCl 0.4 g L^{-1}; $CaCl_2 \cdot 2H_2O$ 0.075 g L^{-1}; Ferric citrate 0.005 g L^{-1}; Yeast Extract 0.4 g L^{-1}. Trace elements were provided by adding 10 mL per liter of a solution containing: $ZnSO_4 \cdot 7H_2O$ 10 mg L^{-1}; $MnCl_2 \cdot 4H_2O$ 3 mg L^{-1}; H_3BO_3 30 mg L^{-1}; $CoCl_2 \cdot 6H_2O$ 20 mg L^{-1}; $CuCl_2 \cdot 2H_2O$ 1 mg L^{-1}; $NiCl_2 \cdot 6H_2O$ 2 mg L^{-1}; $Na_2MoO_4 \cdot 2H_2O$ 30 mg L^{-1}. The pH of the medium was adjusted to 6.8 with NaOH before autoclaving.

For Bio-H_2 production tests, *R. palustris* 42OL was activated in RPP medium for 10 days, as described by Bianchi et al. [34]. The strain was maintained at 30°C, under a light intensity of 150 µmol (photons) m^{-2} s^{-1}. The medium had the following composition: DL-lactic acid 3.6 g L^{-1}; Na glutamate 1 g L^{-1}; K_2HPO_4 0.5 g L^{-1}; KH_2PO_4 0.3 g L^{-1}; $MgSO_4 \cdot 7H_2O$ 0.4 g L^{-1}; NaCl 0.4 g L^{-1}; $CaCl_2 \cdot 2H_2O$ 0.075 g L^{-1}; Ferric citrate 0.005 g L^{-1}. The trace elements were added as reported above. To promote microbial growth, 1 mL per liter of medium of a solution containing 20 mg per 100 mL of p-aminobenzoic acid (PABA) was added after autoclave. The pH of the medium was adjusted to 6.8 with NaOH before autoclaving. Activated cells were then centrifuged for 20 minutes at 5000 rpm (Beckman Coulter, Brea, CA, USA) and resuspended in the SCW for the photofermentation tests.

2.3 Bioreactor Design

The photofermentation test was set up in a tubular photobioreactor designed by Biosyntex S.r.l. (Bologna, BO, Italy) and constructed by Tecnocom S.r.l. (Prato, PO, Italy). The layout of the bioreactor used in this study is reported in Fig.1. The system consists of a skid of dimensions 515 mm × 400 mm, comprising: (1) a thermostated DURAN glass tube, measuring H 700 mm × D 140 mm and equipped with an internal chamber of D 110 mm; (2) a pH control instrument (B&C Electronics S.r.l., Carnate, MB, Italy); (3) a temperature control instrument (Gefran S.p.a., Provaglio d'Iseo, BS, Italy); (4) a mechanical stirrer model AM20-D 50 (Argolab, Carpi, MO, Italy) with manual speed control and a polypropylene (PP) rod (H 800 mm × D 8 mm); (5) two 150W dimmable LED lamps, measuring 600 mm × 70 mm × 40 mm (Ambra Elettronica S.r.l., Bolzano Vicentino, VI, Italy); (6) an ON/OFF electric valve for thermostatic control; (7) an electrical control and command panel.

The bioreactor makes it possible to replace white LED lamps (WL) with selected LED lamps (SL). The WL emitted light across different wavelengths with the following distribution: 19.66% in the blue region (λ = 450 nm), 15.20% in the green region (λ = 520 nm), 64.19% in the red region (λ = 660 nm), and 0.96% in the far-red region (λ = 730 nm). The SL emitted in the yellow region (λ = 593 nm) and the infrared region (λ = 860 nm), with distributions of 80% and 20%, respectively.

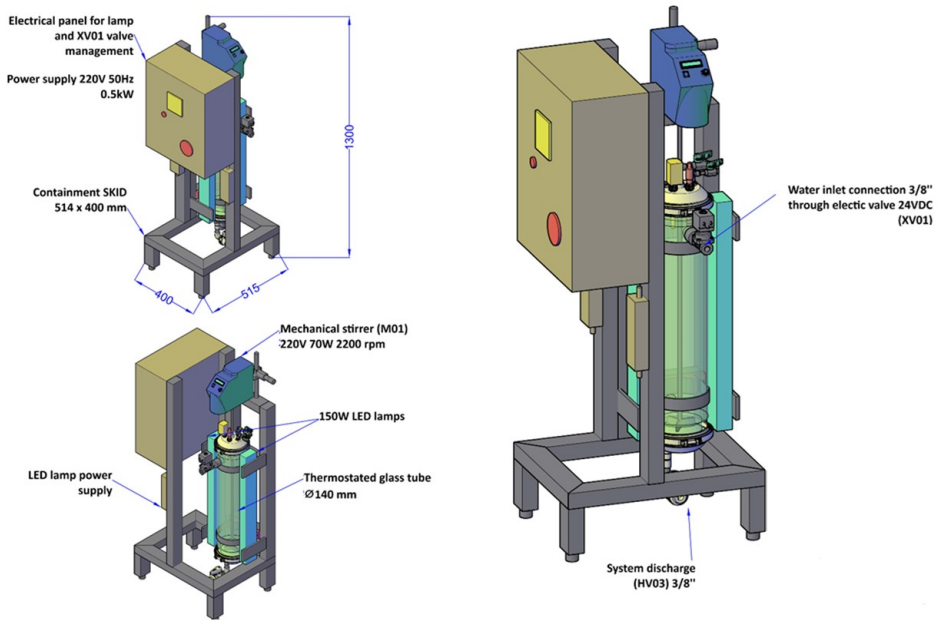

Figure 1. Layout of the bioreactor used in this study.

2.4. Dark Fermentation of SCW

This study used a SCW obtained from ricotta cheese production. The effluent was provided by the cheese factory "I Formaggi del Dottore", located in Castelfiorentino (FI), Italy. The effluent was stored at -20°C until use. The SCW was initially analyzed for its macro- and microelement content, as well as its ammonium, lactose, and lactic acid content. Further details on the analytical methods employed will be provided in Section 2.6.

The SCW was initially tested to evaluate potential lactic acid production through self-fermentation, using its indigenous microflora. The tests were conducted in triplicate. Briefly, 40 mL of SCW, diluted at 25% v/v with non-sterile deionized water, were incubated at 30°C for 96 hours under constant agitation at 80 rpm in tightly sealed 50 mL Falcon® tubes. Lactic acid production was quantified at the end of the experiment using High-Performance Liquid Chromatography (HPLC) analysis (see Section 2.6)

To test the SCW as a substrate for lactic acid production, a co-inoculation was performed using the LAB microbial consortium described in section 2.1. The inocula of the two LAB species were prepared as outlined in Section 2.2 and co-resuspended in 40 mL of defrosted SCW, diluted at 25% v/v with non-sterile deionized water, to a final concentration of 1×10^8 CFU mL^{-1} for each strain. The test was conducted in triplicate, using tightly sealed 50 mL Falcon® tubes, and incubated under the same conditions

described above. Lactic acid production was quantified at the end of the experiment through HPLC analysis (see section 2.6).

After the preliminary tests in tightly sealed 50 mL Falcon® tubes, the dark fermentation experiments were continued inside the 5-litre bioreactor, as described below.

The SCW was diluted at 25% v/v with non-sterile deionized water. During the dilution, 10 mL L^{-1} of a phosphate buffer solution was added, with the following composition: K_2HPO_4 50 g L^{-1}; KH_2PO_4 30 g L^{-1}. The LAB strains were co-inoculated into the effluent at a final concentration of 1×10^8 CFU mL^{-1} each.

Dark fermentation was conducted at 30°C, with continuous stirring at 60 rpm, and lasted for 96 hours. Three different pH conditions were evaluated to identify the optimal conditions for achieving the highest lactic acid yields: without pH control, pH maintained between 3.5 and 4.5, and pH maintained between 4.5 and 5.5. The pH was corrected using NaOH 4M. The experiments were performed in duplicate for each pH condition. The lactic acid content was monitored every 24 h.

2.5. Photofermentation tests

For the photofermentation trials conducted with *R. palustris* 42OL, the dark-fermented SCW obtained with controlled pH (maintained between 3.5 and 4.5, and between 4.5 and 5.5) was combined, homogenized, and used as a culture medium. The effluent was further diluted with non-sterile deionized water at a final concentration of 18% v/v (compared to undiluted SCW) and supplemented with 10 mL L^{-1} of the following solutions: phosphate buffer (K_2HPO_4, 50 g L^{-1}; KH_2PO_4, 30 g L^{-1}), ferric citrate (0.5 g L^{-1}), and $MgSO_4\cdot7H_2O$ (40 g L^{-1}), as described by Adessi et al. [26]. The culture medium was autoclaved twice at 121°C for 15 minutes, with a 48-h interval between the two cycles, to ensure the complete elimination of LAB. The pH was adjusted to 6.8 with 2M NaOH before and after each autoclaving. Between the two autoclaving cycles, the culture medium was centrifuged under sterile conditions at 5000 rpm for 15 minutes (Beckman Coulter, Brea, CA, USA). This was followed by sterile filtration through filter paper under a horizontal laminar flow hood.

R. palustris 42OL, previously grown in RPP medium (described in Section 2.2) was inoculated into the culture medium, in a final volume of 5.2 L. The initial cell concentration was equal to $OD_{660nm} = 0.4$ for each test.

Two distinct lighting conditions were tested for the culture: white LED lights (hereafter referred to as WL) and selected LED lights (hereafter referred to as SL). Detailed information about the lights used in these tests is provided in Section 2.3.

The experiments were conducted in duplicate for each type of light, with a total duration of 336 h for each test. The culture was initially exposed to a light intensity of 150 µmol photons m^{-2} s^{-1} for the first 24 h to allow the microorganism to adapt to the bioreactor environment. This intensity was then increased to 300 µmol photons m^{-2} s^{-1} until 168 h after the start of the experiment and finally increased to 400 µmol photons m^{-2} s^{-1} for the remainder of the experiment. The adjustment in light intensity was necessary to ensure optimal photosynthetic activity. Indeed, the growth of the microorganism, with the consequent increase in the medium's turbidity, limited light penetration in the bioreactor.

Bacterial growth was assessed by measuring bacteriochlorophyll *a* (BChl*a*), optical density at 660 nm (OD_{660nm}) every 48 h, and cellular dry weight (CDW) at 0, 168, and 336 h from the start of the experiment. Lactic acid consumption was measured every 48 hours from the start of the experiment, while ammonium (NH_4^+) concentration was determined at 0, 168, and 336 h from the beginning of the experiment. PHB production was determined at the end of the experiment (336 h). Further details on the analytical methods used are provided in Section 2.6.

The Bio-H_2 gas produced was collected on a calibrated column and measured by the water displacement method [26]. The calibrated column was submerged in a CO_2-absorber solution (1.0 M NaOH, 3.4 M NaCl), as reported by Touloupakis *et al*. [35].

2.6. Analytical Methods

The lactic acid concentration was determined by High-Performance Liquid Chromatography (HPLC) analysis (Varian Inc, Palo Alto, CA, USA). Before injection, each sample was centrifuged at 14000 rpm for 10 min to ensure the complete separation of solid particles from the supernatant. Separation was obtained with a Rezex ROA organic acid H^+ column (300 mm x 7.8 mm; Phenomenex, Castel Maggiore, Bologna, Italy), connected to a refractive index detector (Knauer K-2301, GmbH, Berlin, Germany) and UV detector (λ=210). Elution was performed at 65 °C with 0.013 N H_2SO_4 eluent at a flow rate of 0.6 mL/min. Data were collected and analyzed by using the Galaxie software version 1.8.4.1 (Varian Inc, Palo Alto, CA, USA). Quantitative analysis was carried out by standard curve designed for lactic acid.

The concentration of metals and other inorganic compounds was determined through an inductively coupled plasma-optical emission spectrometry ICP-OES analyzer (Thermo Scientific™ iCAP™ 7400, Waltham, MA, USA), using IRSA 3010 (conventional acid mineralization) and IRSA A-3020 (determination of chemical elements by spectroscopy emission with plasma source) methods.

CDW was determined in triplicate on a 3 mL culture sample, through a filtration with 0.45 μm Mixed Cellulose Esters (MCE) membranes (Fisher Scientific International, Inc., Pittsburgh, PA, USA). Membranes were previously activated with 5 mL of distilled water. After filtration the cells were washed twice with distilled water, oven-dried at 105°C for 3h, and weighed on an analytical balance (Sartorius AG, Göttingen, Germany).

BChl*a* content was determined according to Carlozzi and Sacchi [36]. Briefly, a 2 mL sample was centrifugated at 7000 rpm for 10 min with a Hermle Z 167 M centrifuge (Hermle Labortechnik GmbH, Wehingen, Germany), and the supernatant was removed. BChl*a* was extracted from the cell pellet, resuspending it with a 2 mL acetone/methanol 7:2 v/v ratio solution. The sample was incubated at 4°C for 30 min and centrifugated at 7000 rpm for 10 min. BChl*a* content was determined by measuring the absorbance (A) at 775 nm ($\varepsilon = 75\ mM^{-1}\ cm^{-1}$) with a Varian Cary50 UV-visible spectrophotometer (Varian, Mulgrave, Australia).

The optical density was determined in triplicate on 2 mL samples at a wavelength of 660 nm (OD_{660nm}) using a Varian Cary50 UV-visible spectrophotometer (Varian, Mulgrave, Australia). In the spectrophotometric measurement, the DF-SCW was used as the blank.

The cellular concentration of lactic acid bacteria (LAB) for determining the inoculum in dairy wastewater was measured using cell counting with a Neubauer improved counting chamber (Paul Marienfeld GmbH & Co. KG, Lauda-Königshofen, Germany) with a depth of 0.01 mm.

The ammonium concentration was determined using the HI93764B-25 Ammonia HR reagents set (Hanna Instruments, Woonsocket, RI, USA), based on the Nessler method, and quantified spectrophotometrically using a Varian Cary50 UV-visible spectrophotometer (Varian, Mulgrave, Australia), as reported by Rice et al. [37].

The intensity of the light reaching the culture surface was measured with a quantum/radiometer/photometer model DO9721 equipped with a quantum sensor model LP9021 (Delta Ohm, Italy).

Bio-H_2 was collected and quantified volumetrically using the water displacement method, as described in section 2.5, and subsequently analyzed by gas chromatography, as reported by Adessi et al. [38].

Poly-β-hydroxybutyrate (PHB) production was determined at the end of the experiment (336 h), according to the method described by De Philippis et al. [39].

2.7. Calculation and Statistical Analysis

The substrate conversion efficiency (SCE) was determined according to Eq. 1 [28], as the percentage ratio between the moles of hydrogen produced and the theoretical moles of hydrogen obtainable from the complete conversion of the substrate into hydrogen (Eq. 2) [26].

$$\text{SCE (\%)} = \frac{molH_2\ obtained}{molH_2\ theoretical} \times 100 \quad (1)$$

$$C_3H_6O_3 + 3H_2O \rightarrow 6H_2 + 3CO_2 \quad (2)$$

The moles of hydrogen produced were calculated based on the hydrogen collected, applying the ideal gas law under ambient conditions (T = 25°C, P = 1 atm).

The efficiency of light energy conversion to hydrogen (LCE) during the hydrogen production period was calculated according to Eq. 3, as Adessi *et al*. [26] reported, assuming that the culture absorbed all the incident light.

$$\text{LCE (\%)} = \frac{Combustion\ enthalpy\ of\ H_2 \times H_2\ production\ rate}{Absorbed\ light\ energy} \times 100 \quad (3)$$

All analyses were conducted in experimental triplicates (*N*=3); a minimum number of three instrumental replicates was always used for each measurement (*n*=3). To determine whether the results were significantly different, the data were analyzed using one-way analysis of variance (ANOVA) at the 95% level of significance, followed by Tukey's post-hoc test of honest difference in significance (HSD). The results were considered statistically significant at $p \leq 0.05$. Before the ANOVA, all data were checked for assumptions of normality using the D'Agostino-Pearson normality test and for homogeneity of variance using Bartlett's test. To check for statistical differences between the mean values of the two lighting conditions, independent t-tests were performed. All analyses were conducted using R software version 4.4.1.

3. Results

3.1. Chemical composition of SCW

The chemical composition of SCW used in this study (before dilution) is reported in Tab.1. The effluent had an initial pH of 6.30 (± 0.02).

The analysis revealed that lactose was the most abundant compound, with a concentration of 43.73 g L^{-1} (± 1.72). Lactic acid was detected in lower amounts, at 0.31 g L^{-1} (±0.08). Regarding the nitrogen content, ammonium (NH_4^+) was present at a significant concentration of 504.53 mg L^{-1} (±7.47).

Among the macronutrients, sodium (Na), phosphorus (P), and potassium (K) were present in the highest concentrations, with values of 0.88 g L^{-1} (± 0.06), 0.31 g L^{-1} (± 0.03), and 1.66 g L^{-1} (± 0.15), respectively. Additionally, calcium (Ca), magnesium (Mg), and sulfur (S) were present in measurable concentrations, with values of 0.23 g L^{-1} (± 0.02), 0.16 g L^{-1} (± 0.015), and 7.83 mg L^{-1} (± 1.37), respectively.

As regards the micronutrients, boron (B) was present at the highest concentration, 0.26 (±0.02) mg L^{-1}, followed by iron (Fe) and zinc (Zn), with concentrations of 0.25 (±0.11) and 0.13 (±0.05) mg L^{-1}, respectively. Finally, trace elements including cobalt (Co), copper (Cu), manganese (Mn), molybdenum (Mo), nickel (Ni), and vanadium (V) were detected at microgram-per-liter levels.

Table 1. Chemical composition of raw SCW used in this study (before dilution). The standard deviation is indicated in brackets.

Compounds	**Concentration**
Lactose (g L^{-1})	43.73 (±1.72)
Lactic acid (g L^{-1})	0.31 (±0.08)
NH_4^+ (mg L^{-1})	504.53 (±7.47)
B (mg L^{-1})	0.26 (±0.02)
Ca (g L^{-1})	0.23 (±0.02)
Co (µg L^{-1})	0.92 (±0.32)
Cu (µg L^{-1})	19.97 (±4.97)
Fe (mg L^{-1})	0.25 (±0.11)
K (g L^{-1})	1.66 (±0.15)
Mg (g L^{-1})	0.16 (±0.015)
Mn (µg L^{-1})	11.64 (±2.45)
Mo (µg L^{-1})	13.37 (±1.53)
Na (g L^{-1})	0.88 (±0.06)
Ni (µg L^{-1})	1.23 (±0.66)
P (g L^{-1})	0.31 (±0.03)
S (mg L^{-1})	7.83 (±1.37)
V (µg L^{-1})	11.79 (±3.01)
Zn (mg L^{-1})	0.13 (±0.05)

3.2. Lactic Acid Production during Dark Fermentation of SCW

The first step assessed whether the indigenous microflora in the defrosted and diluted SCW could produce significant amounts of lactic acid. After 96 h of testing, the lactic acid concentration reached 0.74 g L^{-1} (±0.07), with a final substrate pH of 4.91 (± 0.07). To maximize lactic acid production, fermentation was evaluated by co-inoculating two LAB species (see section 2.1 for further details on the species used). In this case, after 96 hours, the lactic acid concentration reached 2.06 g L^{-1} (± 0.09), with a final pH of 3.37 (±0.11). An independent t-test revealed a statistically significant difference in lactic acid production between the two conditions (without inoculum and with co-inoculum) ($p < 0.001$, ***), confirming that the inoculated samples produced significantly more lactic acid compared to the non-inoculated ones.

Subsequent efforts focused on optimizing the dark fermentation process in a 5-litre bioreactor, to maximize lactic acid yield from the co-inoculation of LAB. Three different pH conditions were tested in duplicate: (1) without pH control; (2) $3.5 \leq pH < 4.5$; and (3) $4.5 \leq pH < 5.5$.

In the tests without pH control, the pH dropped to 3.53 (± 0.05) in the first 24 h, reaching a final value of 3.14 (±0.04) at the end of the experiment. Fig. 2 shows the lactic acid yield (g L^{-1}) after 96 h post-inoculation for the three conditions tested, with statistically significant differences ($P < 0.001$, ***). Lactic acid production remained very low in dark fermentation (DF) trials DF_1 and DF_2 without pH control, reaching an average concentration of 1.75 g L^{-1} (± 0.00). Lactic acid production increased significantly to an average value of 5.53 g L^{-1} (± 0.09) under controlled pH $3.5 \leq pH < 4.5$ in DF_3 and DF_4 tests. The highest production was achieved in the pH range of $4.5 \leq pH < 5.5$ (DF_5 and DF_6), with an average lactic acid concentration of 9.35 g L^{-1} (± 0.11).

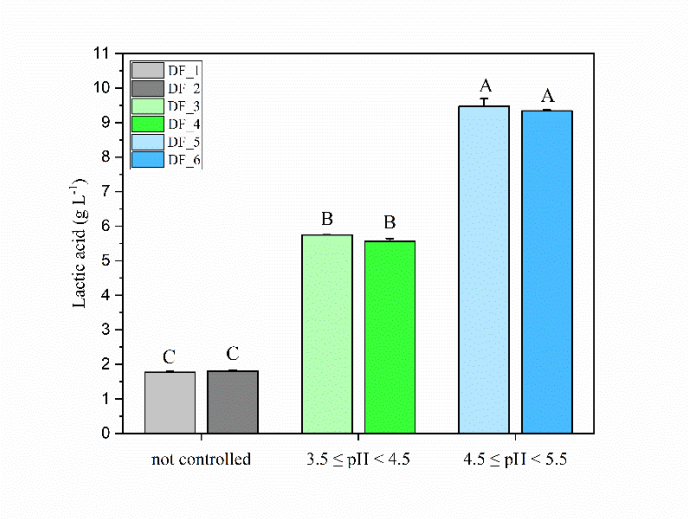

Figure 2. Lactic acid yield (g L^{-1}) after 96 h of dark fermentation using the co-inoculation of *L. lactis* MK L84 and *L. paracasei* MK L49 under different pH conditions. Trials were conducted without pH control (DF_1 and DF_2), at pH 3.5 ≤ pH < 4.5 (DF_3 and DF_4), and at pH 4.5 ≤ pH < 5.5 (DF_5 and DF_6). Error bars indicate the standard deviation of 3 technical replicates. Different letters above the bars indicate statistically significant differences according to one-way ANOVA (95% significance level) followed by Tukey's HSD post-hoc test.

Table 2. Concentrations of ammonium and lactic acid of the diluted dark-fermented SCW at the beginning of the four photofermentation tests under WL and SL conditions. The C/N ratio of each substrate in each test is also provided. Data are presented as mean values with standard deviations in brackets.

Parameter	WL_1	WL_2	SL_1	SL_2
NH_4^+ (mg L^{-1})	90.50 (±2.20)	91.60 (±1.90)	103.27 (±8.76)	75.73 (±2.23)
Lactic acid (g L^{-1})	3.74 (± 0.05)	3.78 (± 0.04)	3.80 (± 0.04)	3.71(± 0.06)
C/N	41.6	41.1	38	46.4

3.3. Photofermentation Results

Tab. 2 presents the substrate's initial ammonium and lactic acid concentrations for each photofermentation test. C/N ratios are also reported.

Concerning the initial ammonium content, variability was observed among different photofermentation runs. The WL_1 and WL_2 runs showed similar ammonium levels, with no statistically significant differences, and mean concentrations of 90.50 mg L^{-1} (± 2.20) and 91.60 mg L^{-1} (± 1.90), respectively. In contrast, the SL_1 run had a significantly higher initial ammonium content ($p < 0.01$, **) compared to SL_2, with concentrations of 103.27 mg L^{-1} (± 8.76) and 75.73 mg L^{-1} (± 2.23), respectively. No statistically significant differences were observed among the four photofermentation runs concerning lactic acid content ($p = 0.203$).

The growth of *R. palustris* 42OL in each of the four photofermentation runs was monitored by measuring the CDW at 0, 168, and 336 hours (Fig. 3C), as well as every 48 hours by assessing the OD_{660nm} (Fig. 3A) and quantifying BChl*a* concentration (Fig. 3B). The light intensity was managed in three steps during the experiment. It was initially set to 150 µmol m^{-2} s^{-1} for the first 24 h, then increased to 300 µmol m^{-2} s^{-1} for the following 144 h, and finally raised to 400 µmol m^{-2} s^{-1} for the remaining 168 h.

In all four runs, a progressive increase in CDW (Fig. 3C) was observed over time, with the highest values recorded at the end of the experiment in the two tests conducted under SL conditions. Across all conditions, the most substantial increases occurred between 168

and 336 h, coinciding with an increase in light intensity from 300 to 400 µmol m^{-2} s^{-1}, except for WL_2, where a slightly larger increase was observed between 0 and 168 hours. The greatest overall increase in CDW was observed in the SL_2 test, with a rise of +0.68 g L^{-1} between 168 and 336 hours. After 336 hours post-inoculation, statistically significant differences in CDW were observed between the WL and SL runs.

Fig. 3A illustrates the variation of OD_{660nm} during the 336-hour test period for the four runs. Up to 216 h, all tests showed a progressive and comparable growth of OD_{660nm}. After this point, OD_{660nm} stabilized in the two WL runs, reaching final values of 2.38 (± 0.06) for WL_1 and 2.19 (± 0.06) for WL_2. In contrast, the SL runs showed a continuous growth of OD_{660nm}, with final values of 4.72 (± 0.09) for SL_1 and 4.76 (± 0.04) for SL_2. Notably, as with the CDW measurements, the divergence between the WL and SL curves became evident after the second increase in light intensity, from 300 µmol m^{-2} s^{-1} to 400 µmol m^{-2} s^{-1}.

Fig. 3B presents the accumulation of BChl*a* over time for the four photofermentation runs. The trend closely mirrors OD_{660nm}, with a pronounced increase in BChl*a* concentration in the SL tests after 216 h, following the second increase in light intensity. During the first 216 hours, BChl*a* levels remained consistently higher in the SL trials than in the WL trials. At 336 hours BChl*a* levels in SL_1 and SL_2 peaked respectively at 32.45 µg mL^{-1} (±2.29) and 31.84 µg mL^{-1} (±4.84), significantly higher than WL_1 (12.32 µg mL^{-1} ±0.26) and WL_2 (11.85 µg mL^{-1} ±0.13) ($p < 0.001$, ***).

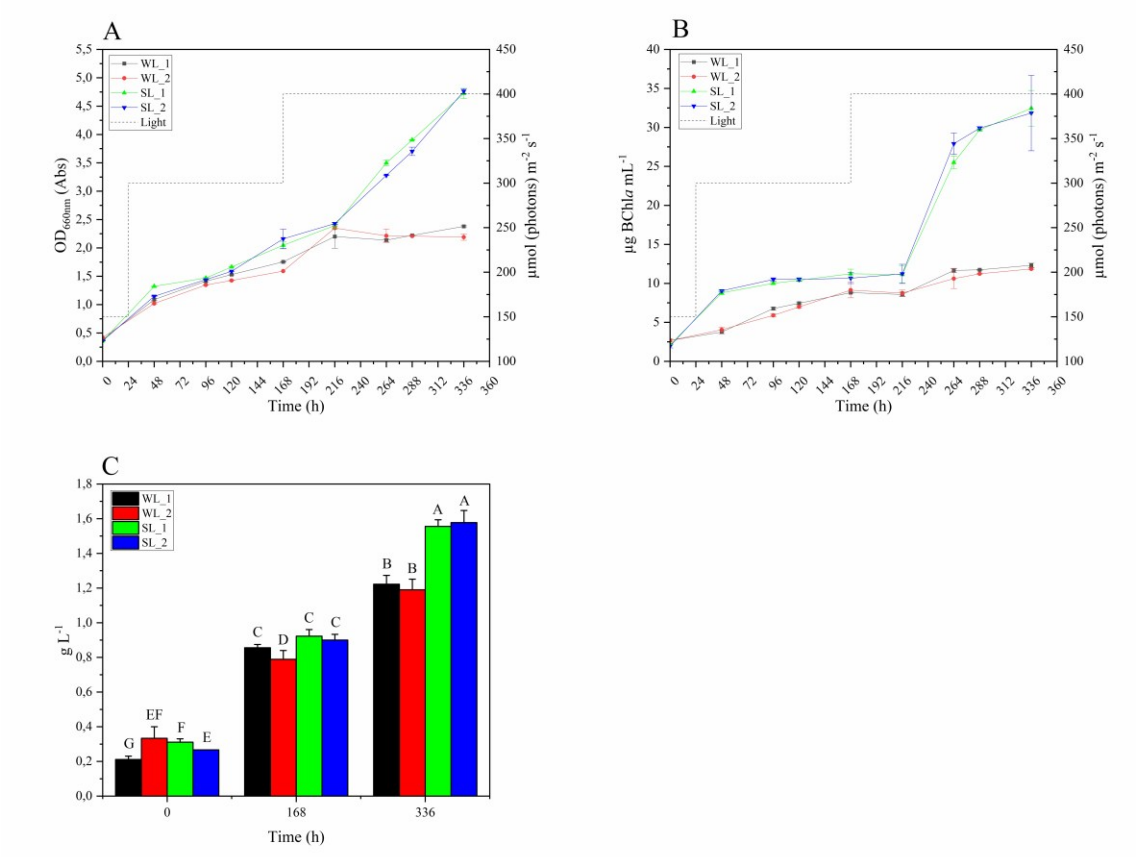

Figure 3. (A) Growth of *R. palustris* 42OL, represented as OD_{660nm}, under WL and SL conditions during photofermentation. (B) BChl*a* accumulation, under WL and SL conditions over 336 hours. (C) Variation in the CDW of *R. palustris* 42OL over time under WL and SL conditions. The light intensity is reported as a dashed line (---). Error bars indicate the standard deviation of 3 technical replicates. Different letters above the bars indicate statistically significant differences according to one-way ANOVA (95% significance level) followed by Tukey's HSD post-hoc test.

Fig. 4A shows the progression of lactic acid concentration during 336 h for the four photofermentation tests. In all tests, the lactic acid concentration reaches values close to zero at the end of the experiment. However, in the SL tests, consumption was significantly faster in the first two days after the start of the experiment. Specifically, the percentage consumption in the first 48 hours was -40.53% in SL_1 and -46.05% in SL_2, whereas in WL_1 and WL_2 it was only -4.01% and -3.27%, respectively.

Fig. 4B illustrates the progression of NH_4^+ concentration over time for the four runs. During the first 168 h, all runs showed significant reductions in NH_4^+ levels, with rates varying between conditions. More specifically, the WL runs showed the greatest reductions, with WL_1 showing a reduction of 67.90% and WL_2 the highest at 70.47%. In contrast, the SL runs showed smaller decreases, with SL_1 reducing by 61.18% and SL_2 by 51.56%. After 168 hours, the NH_4^+ consumption slowed across all runs,

coinciding with the increase in light intensity from 300 to 400 µmol photons m^{-2} s^{-1}, reaching similar levels by the end of the experiment.

The final Bio-H_2 production obtained at the end of the experiment, for the four runs, is shown in Tab. 3, and the time course of Bio-H_2 production is reported in Fig. 4C. The time course of Bio-H_2 production varied significantly across the four runs. In the WL_1 and WL_2 conditions, Bio-H_2 production began only after 48 hours, with WL_1 stabilizing at 1860 mL by 168 h, and WL_2 reaching 1700 mL by 192 h, with no significant increases afterwards. In contrast, the SL_1 condition started Bio-H_2 production at 24 h, reaching a maximum value of 2420 mL at 336 h. The SL_2 condition showed the most rapid onset, with production starting immediately at the beginning of the experiment and reaching 2400 mL by 288 h, when it stabilized. At the end of the runs, the SL condition showed a significantly higher total Bio-H_2 production ($p < 0.05$, *) than the WL condition.

Regarding the VHPR and the specific hydrogen production rate (SHPR), shown in Tab. 3, no statistical difference was observed between the two types of illumination.

Tab. 3 also shows data on light utilization efficiency (LCE) and substrate (lactic acid) to H_2 conversion efficiency (SCE). While no statistically significant differences were recorded for the first parameter between the two lighting types, the SCE was significantly higher ($p < 0.05$, *) in the SL tests.

Tab. 3 reports the PHB production at the end of the experiment for the four photofermentation runs. *R. palustris* 42OL accumulated significantly higher levels of PHB (% w/w) in the trials conducted under selected light (SL) compared to those under white light (WL) ($p < 0.001$, ***). In the SL trials, PHB levels reached 1.65% (± 0.03) and 1.67% (± 0.03) for SL_1 and SL_2, respectively.

Table 3. Total Bio-H_2 production, derived parameters, final PHB production, and their statistical analysis (independent two-sample t-test). Significance: * ($p < 0.05$), *** ($p < 0.001$), ns: not significant. SCE = substrate conversion efficiency; VHPR = volumetric hydrogen production rate; SHPR = specific hydrogen production rate; LCE = light conversion efficiency; H_{max} = maximum cumulative H_2 l/l_{medium}; $\boldsymbol{R_{max,H_2}}$ = maximum rate of H_2 production, l/l/h.

Parameter	WL_1	WL_2	SL_1	SL_2	t-test (WL vs. SL)
SCE (%)	5.87	5.31	7.52	7.63	*
VHPR (mL L^{-1} h^{-1})	1.24	1.14	1.49	1.37	ns
SHPR (mL mg^{-1} h^{-1})	0.0064	0.0069	0.0062	0.0055	ns
Total H_2 (mL)	1860	1700	2420	2400	*
H_{max} (L L^{-1})	0.36	0.33	0.47	0.46	*

Parameter	WL_1	WL_2	SL_1	SL_2	t-test (WL vs. SL)
R_{max,H_2} (L L^{-1} h^{-1})	0.004	0.003	0.004	0.004	ns
LCE (%)	0.14	0.13	0.11	0.12	ns
PHB (% w_{PHB}/w_{CDW})	0.60 (±0.09)	0.57 (±0.05)	1.65 (±0.03)	1.67 (±0.03)	***

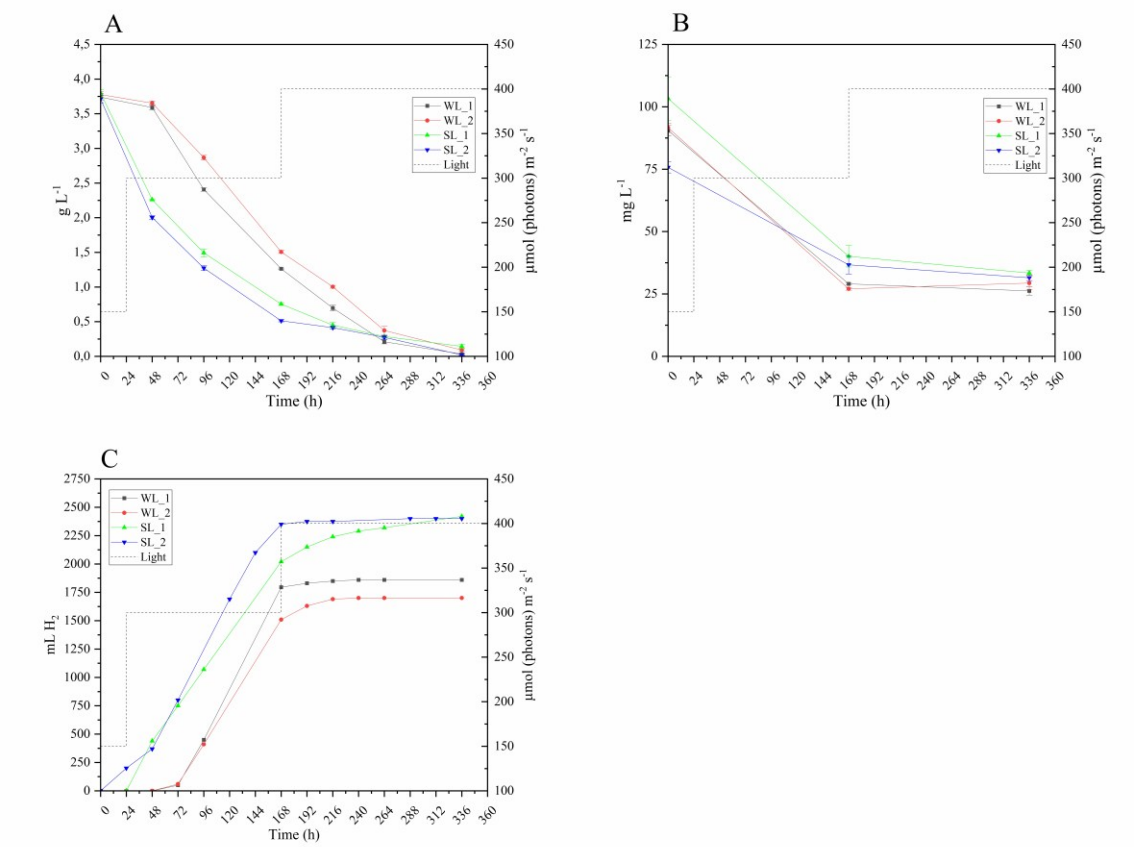

Figure 4. (A). Lactic acid concentration (g L^{-1}) under WL and SL conditions during 336 h of photofermentation. (B) Ammonium consumption (mg L^{-1}) over 336 h under WL and SL conditions. (C) Time course of Bio-H_2 production (mL) under WL and SL conditions during 336 h of photofermentation. The light intensity is reported as a dashed line (- - -). Error bars indicate the standard deviation of 3 biological replicates.

4. Discussion

The dairy industry produces organic-rich wastewater that, if discharged untreated into water bodies, causes acidification and eutrophication, harming ecosystems. Using PNSB to convert this wastewater into Bio-H_2 and PHB offers a solution, reducing organic load while generating valuable compounds.

The analysis of the raw composition of SCW used in this study revealed a high NH_4^+ concentration (504.53 mg L^{-1} ± 7.47). The literature widely documents that an excess of

ammoniacal nitrogen inhibits Bio-H_2 production by PNSB, as it interferes with the regulatory mechanisms of the nitrogenase enzyme [40,41]. For this reason, the effluent was initially diluted at 25% v/v with non-sterile deionized water to significantly reduce ammonium content while retaining enough lactose for the subsequent dark fermentation step. Although dilution increases substrate volume and management costs, it enhances light penetration in the photofermentation phase, thus shortening the Bio-H_2 accumulation lag phase [14,15].

Lactate is the preferred carbon source for *R. palustris* 42OL to maximize Bio-H_2 yield [42]. The lactate content in the raw SCW (0.31 g L^{-1} ± 0.08) was approximately one order of magnitude lower than in the synthetic RPP medium (3.6 g L^{-1}). The subsequent dilution of the effluent further reduced the lactose concentration, necessitating a dark fermentation step to achieve lactate enrichment.

To select the best conditions to produce lactate with a minimum number of treatments, we initially considered using the effluent's indigenous microflora to ferment lactose into lactate. However, trials yielded only a minimal increase in lactate, reaching a final concentration of 0.74 g L^{-1} (±0.07), still substantially below the level in the RPP synthetic medium. This limited lactic acid production was probably due to the freezing process applied to the effluent, which may have altered and reduced the indigenous microflora. Therefore, we investigated the effect of a LAB co-inoculum, which resulted in a significantly higher lactic acid yield of 2.06 g L^{-1} (±0.09), nearly tripling the yield obtained by the indigenous microflora. However, this lactate concentration was still insufficient for photofermentation, remaining below that of the synthetic RPP medium. At the end of the LAB co-inoculation tests, the pH reached 3.37 (±0.11), likely limiting lactate yield, as its production is minimal in acidic conditions [43]. Therefore, our focus shifted towards identifying the optimal substrate pH to maximize lactate production by LAB co-inoculum in a 5 L photobioreactor. To prevent the pH from dropping too quickly and complicating manual control, a phosphate buffer was added to the substrate (see Section 2.4). The highest yields were achieved at pH between 4.5 and 5.5 (Fig. 2), with an average lactate concentration of 9.40 g L^{-1} (±0.09), which was 1.7 and 5.2 times higher than the results obtained at pH levels between 3.5 and 4.5 and with uncontrolled pH, respectively. This result is supported by studies showing that the optimal pH for lactic acid production lies between 5 and 6, where LAB activity peaks, enabling efficient fermentation [43-45]. Moradi et al. [46] produced 14.2 g L^{-1} lactic acid using *Lactobacillus delbrueckii* subsp. *lactis* (PTCC: 1743) on a substrate consisting of DW

and glucose, with a fermentation time of 41.41 h at 37 °C and an enzymatic hydrolysis step. Our co-inoculum produced approximately 34% less lactic acid, but with significant advantages that simplify the process and reduce overall costs: reduced production time, a lower temperature (30 °C), and the absence of expensive carbon sources or additional enzymatic treatments.

Prior to each Bio-H_2 production experiment, the photofermentation substrate was supplemented, as nutrient levels were insufficient due to prior dilution. For this purpose, iron citrate and magnesium sulfate were added, based on Adessi et al. [26], who showed these nutrients enhance Bio-H_2 production by *R. palustris* 42OL grown on fermented bread effluent. Iron and sulfate are essential for nitrogenase synthesis [38], while magnesium is involved in BChls synthesis [47].

Growth, Bio-H_2, and PHB production in *R. palustris* 42OL were then evaluated on the dark-fermented SCW, comparing white light (WL) LEDs with specific wavelength LEDs (SL, 593 nm, and 860 nm) matching the absorption peaks of BChls in *R. palustris* 42OL. This approach clarified how specific wavelengths enhance photofermentative efficiency and high-value molecule yields.

Light intensity was gradually raised throughout the experiment to maintain adequate light penetration as cell density increased. Initially, it was set to 150 µmol photons m^{-2} s^{-1} for the first 24 h to minimize cellular stress and support cell adaptation. It was then increased to 300 µmol photons m^{-2} s^{-1} for the following 144 h and finally elevated to 400 µmol photons m^{-2} s^{-1} until the end of the experiment.

The first Bio-H_2 production experiment in the 5 L photobioreactor under white light (WL), using substrate diluted at 25% (v/v), showed no gas accumulation during the first 168 h post-inoculation. This result was attributed to the presence of ammonium at concentrations exceeding inhibitory levels for *R. palustris* 42OL.

The presence of ammonium ions above a threshold concentration of approximately 2 mM (corresponding to approximately 36 mg L^{-1} NH_4^+) has been reported to inhibit Bio-H_2 production by PNSB. However, this inhibitory threshold may vary depending on the specific PNSB strain and operating conditions [48]. Consequently, to reduce ammonium inhibition while simultaneously limiting substrate dilution and water consumption, the dark-fermented substrate was diluted to achieve an ammonium concentration below 100 mg L^{-1}.

The substrate diluted to this level (18% v/v relative to the raw wastewater) was used in the subsequent four photofermentation experiments. The initial lactate and ammonium concentrations for each photofermentation test are reported in Table 2.

The cumulative Bio-H_2 production trends under WL and SL conditions are shown in Figure 4C. In the WL runs, Bio-H_2 production began 48 h after inoculation. On the contrary, the SL runs showed a reduced lag phase; in SL_1, Bio-H_2 production started after 24 h, while in SL_2, it began immediately. The difference in lag phases between the two SL trials is likely connected to the lower ammonium concentration in SL_2 compared to SL_1, due to the heterogeneity of the substrate.

Table 3 shows the total Bio-H_2 and PHB production at the end of the experiment. On average, the SL condition produced 35.5% more H_2 than the WL condition. Similarly, PHB production increased significantly in the SL condition, almost tripling the values obtained with WL.

The higher production of H_2 and PHB under selected light wavelengths is likely due to higher light utilization efficiency. BChl*a*, in PNSB, has absorption peaks around 590-600 nm and 850-870 nm [28], making selected wavelengths more effective than broad-spectrum WL. Targeted light absorption enhances photophosphorylation, generating ATP and reducing power (NADPH) essential for PHB and H_2 biosynthesis [21]. In contrast, exposure to broad-spectrum light may increase energy dispersion and photo-oxidative stress due to inefficiently absorbed wavelengths.

The higher efficiency of the SL compared to WL is evident also in the growth profiles of *R. palustris* 42OL (Fig. 3). During the first 168 h, growth proceeds similarly in both lighting conditions, with a steady increase in CDW, OD_{660nm}, and BChl*a* levels over time. Under SL conditions, a higher lactic acid consumption is observed (Fig. 4A), mainly due to the higher biomass concentration achieved under SL, since the specific H_2 production rates are the same (not significantly different) under SL and WL conditions (Tab. 3). After 168 h, the increase in light intensity from 300 to 400 µmol photons m^{-2} s^{-1} marked a critical point: Bio-H_2 production decreased drastically (Fig. 4C), and ammonium consumption stabilized (Fig. 4B). This is followed by a 48 h phase in which both lighting conditions show a steady and comparable increase in OD_{660nm}, along with stabilization in BChl*a* synthesis, likely as an adaptation to the new light conditions. From 216 h onwards, the conditions diverge markedly; under SL, a significant increase in BChl*a* and OD_{660nm} is observed, likely due to greater efficiency in photon utilization under this condition. In contrast, WL leads to high energy dissipation and photooxidative stress, halting growth

and limiting BChl*a* accumulation. Despite sustained cellular growth under SL, ammonium consumption stabilization appears contradictory, as nitrogen is essential for building cellular biomass. However, the Nessler method used for its quantification (see Section 2.6) detects only free ammonium, not nitrogen in amino groups of amino acids [49]. Dairy wastewater contains protein and amino acid residues that *R. palustris* 42OL can use as a nitrogen and carbon source [17,24]. The increase in light intensity, with the consequent greater availability of energy, may have favored the use of amino acids, which provide a combined source of nitrogen and carbon, advantageous under high-energy conditions. Indeed, amino acid degradation requires additional metabolic pathways and specialized enzyme systems that consume substantial amounts of ATP, helping to stabilize the cell's energy balance. However, further studies will be needed to demonstrate the higher utilization of amino acids as a source of carbon and nitrogen under high light conditions com-pared to ammoniacal nitrogen.

The maximum cumulative hydrogen (H_{max}) obtained under both lighting conditions (Tab. 3) was significantly lower than the value reported by Seifert et al. [50], who obtained an H_{max} of 3.23 L H_2 L^{-1} of substrate by cultivating *Rhodobacter sphaeroides* O.U. 001 on diluted dairy wastewater with a modified Biebel and Pfennig medium lacking a carbon source (malic acid). Optimum results were achieved at a dilution of 40% (v/v) and a light intensity of 9 klx.

It should be noted that, in the study by Seifert et al. [50], the raw dairy wastewater contained 40 mg dm^{-3} of ammonium nitrogen ($N\text{-}NH_4^+$), corresponding to approximately 51.4 mg L^{-1} of NH_4^+. This concentration was further reduced by dilution, as photofermentation was carried out at 40% (v/v) wastewater. Moreover, the dairy wastewater was filtered before photofermentation, which likely reduced the particulate fraction and the contribution of protein-associated nitrogen, thereby limiting ammonium availability in the photofermentation medium. Therefore, the effective ammonium concentration in their system was substantially lower than that in the present study, which employed a dark fermentation effluent.

This substantial difference in hydrogen production can be attributed not only to differences in substrate characteristics, including ammonium availability, but also to the different experimental scales, as efficiency generally decreases with process scale-up. Indeed, while Seifert et al. [50] conducted their experiments in small 25 mL vials filled to 12.5 mL, this study involved a 416-fold larger working volume (5200 mL). Furthermore, in the present study, the substrate was diluted with deionized water rather

than with a synthetic medium, supplemented only with the minimal essential compounds required for hydrogen production.

Regarding PHB production, an important factor for optimizing its accumulation is the C/N ratio of the growth medium; ratios above 30 are generally recommended for optimal PHB synthesis [21]. In our study, the substrate showed an average C/N ratio of 41.8 (±3.47) (Tab. 2), indicating favorable conditions for PHB accumulation. However, lactate is not the preferred carbon source for PHB synthesis in PNSB; acetate and butyrate are more efficient substrates [21], but neither was detected in our substrate. Unlike lactate, which must first be oxidized to pyruvate and subsequently converted to acetyl-CoA (the key precursor for PHB synthesis), acetate and butyrate can be directly converted to acetyl-CoA with lower energetic costs. Consequently, lactate is often directed toward metabolic pathways favoring hydrogen production rather than PHB synthesis [21].

In agreement with this metabolic framework, Wu et al. [50] reported that *R. palustris* WP3-5 produced the highest cumulative H_2 volume when grown on lactate (131.3 mL over 114 h). However, acetate exhibited the highest SCE (14.2%), indicating a more efficient conversion of the substrate into hydrogen. When lactate was used, the SCE was lower (approximately 9.3%) and remained nearly constant regardless of PHB accumulation, suggesting limited competition between PHB synthesis and H_2 production under lactate-fed conditions.

Wu et al. [51] also reported a PHB accumulation of 1.4% (w/w) in *R. palustris* WP3-5 when grown on lactate, which is comparable to the values obtained in our study under SL conditions. In our experiments, higher PHB production was observed under SL conditions, which also exhibited a faster lactate consumption. This accelerated lactate utilization may also be attributed to the enhanced PHB synthesis observed under these conditions. However, since PHB was quantified only at the end of the experimental runs, it is not possible to assess its accumulation dynamics or potential intracellular reutilization over time.

Future experiments should therefore include measurements of PHB at different cultivation times to better elucidate its role in the distribution of reducing equivalents and its interaction with hydrogen production. This interpretation is consistent with the observations of Wu et al. [51], who suggested that PHB does not merely compete with hydrogen production for reducing power, but rather plays a more complex metabolic role, particularly under stress conditions.

5. Conclusions

In this study, we demonstrated the feasibility of using second cheese whey (SCW) for H_2 and PHB production with *Rhodopseudomonas palustris* strain 42OL in a 5 L tubular photobioreactor within an integrated dark-fermentation/photofermentation system. During the dark fermentation phase, a co-inoculum of lactic acid bacteria (LAB) comprising *Lactococcus lactis* MK L84 and *Lacticaseibacillus paracasei* MK L49 proved optimal for obtaining high concentrations of lactic acid from properly diluted wastewater when maintained at 30 °C and a pH of 4.5 to 5.5 for 96 h. In the subsequent photofermentation phase, the quality of light significantly influenced the H_2 and PHB yields. The highest yields were achieved with selected light (SL) at wavelengths corresponding to the absorption peaks of the PNSB BChls, with an average yield of 0.47 L of H_2 per liter of substrate (±0.007) and 1.66% wPHB/wCDW (±0.01). Under SL conditions, a light intensity of 400 µmol photons m^{-2} s^{-1} appeared to favor biomass growth and BChl*a* synthesis over H_2 production.

Dairy wastewater composition is naturally variable, mainly due to the origin of the whey and the specific production processes used to obtain it. Processes for the valorization of these effluents must be adapted accordingly. The development of strategies for the transformation of dairy waste into resources for energy and biopolymers production is crucial to converting waste streams into inputs for subsequent processes, thus supporting the transition from a linear to a circular economic model.

Future studies will focus on providing a detailed assessment of SCW conversion efficiency under the operating conditions that demonstrated the most promising performance in this study, particularly those obtained using selected lighting (SL). In addition, a comprehensive assessment of the technical and economic feasibility of the process will be necessary to determine its potential for combining biohydrogen and PHB production in the sustainable valorization of dairy wastewater. Such analyses are essential to compare this approach with alternative treatment and valorization technologies and to support its potential industrial implementation.

Acknowledgements

The authors would like to thank Biosyntex S.r.l. for the technical support provided during the experimental tests. We are also grateful for their permission to share the technical specifications of the bioreactor used in this study.

Author contributions

L.B., G.D., A.A. and L.G. Conceptualization; L.B., G.D., V.G. and A.A. Data curation; L.B. and G.D. Formal analysis; L.B., G.D., V.G. and S.G. Methodology; A.A., L.G. and C.V. Supervision; A.A. Funding Acquisition; L.B. Writing-original draft; L.B., G.D., V.G., S.G., C.V., L.G. and A.A. Writing-review and editing. All authors have read and agreed to the published version of the manuscript.

References

[1] Wang, X., Lu, Y., Chen, C., Yi, X., & Cui, H. (2024). Total-factor energy efficiency of ten major global energy-consuming countries. *Journal of Environmental Sciences*, *137*, 41-52. https://doi.org/10.1016/j.jes.2023.02.031

[2] Koponen, K., Braun, J., Gutiérrez, S. C., Evatt, A., Golmen, L., Guillén-Gosálbez, G., ... & Werner, C. (2024). Responsible carbon dioxide removals and the EU's 2040 climate target. *Environmental Research Letters*, *19*(9), 091006. DOI 10.1088/1748-9326/ad6d83

[3] Kapdan, I. K., & Kargi, F. (2006). Bio-hydrogen production from waste materials. *Enzyme and microbial technology*, *38*(5), 569-582. https://doi.org/10.1016/j.enzmictec.2005.09.015

[4] Halder, P., Babaie, M., Salek, F., Haque, N., Savage, R., Stevanovic, S., ... & Zare, A. (2024). Advancements in hydrogen production, storage, distribution and refuelling for a sustainable transport sector: Hydrogen fuel cell vehicles. *International Journal of Hydrogen Energy*, *52*, 973-1004. https://doi.org/10.1016/j.ijhydene.2023.07.204

[5] Qureshi, F., Yusuf, M., Kamyab, H., Vo, D. V. N., Chelliapan, S., Joo, S. W., & Vasseghian, Y. (2022). Latest eco-friendly avenues on hydrogen production towards a circular bioeconomy: Currents challenges, innovative insights, and future perspectives. *Renewable and Sustainable Energy Reviews*, *168*, 112916. DOI: 10.1016/j.rser.2022.112916

[6] Chandrasekhar, K., Kumar, S., Lee, B. D., & Kim, S. H. (2020). Waste based hydrogen production for circular bioeconomy: Current status and future directions. *Bioresource technology*, 302, 122920. https://doi.org/10.1016/j.biortech.2020.122920

[7] Bartocci, A., Cantelmo, A., Cova, P., Notarpietro, A., & Pisani, M. (2024). Monetary and fiscal policy responses to fossil fuel price shocks. *Energy Economics*, *136*, 107737. https://doi.org/10.1016/j.eneco.2024.107737

[8] Sali, S., & Mackey, H. R. (2021). The application of purple non-sulfur bacteria for microbial mixed culture polyhydroxyalkanoates production. *Reviews in Environmental Science and Bio/Technology*, *20*(4), 959-983. https://doi.org/10.1007/s11157-021-09597-7

[9] Corneli, E., Adessi, A., Dragoni, F., Ragaglini, G., Bonari, E., & De Philippis, R. (2016). Agroindustrial residues and energy crops for the production of hydrogen and poly-β-hydroxybutyrate via photofermentation. *Bioresource technology*, *216*, 941-947. https://doi.org/10.1016/j.biortech.2016.06.046

[10] Rai, P. K., & Singh, S. P. (2016). Integrated dark-and photo-fermentation: Recent advances and provisions for improvement. *International journal of hydrogen energy*, *41*(44), 19957-19971. https://doi.org/10.1016/j.ijhydene.2016.08.084

[11] McKinlay, J. B. (2014a). Systems biology of photobiological hydrogen production by purple non-sulfur bacteria. In *Microbial bioenergy: hydrogen production* (pp. 155-176). Dordrecht: Springer Netherlands. https://doi.org/10.1007/978-94-017-8554-9_7

[12] Gupta, S., Fernandes, A., Lopes, A., Grasa, L., & Salafranca, J. (2024). Photo-Fermentative Bacteria Used for Hydrogen Production. *Applied Sciences*, *14*(3), 1191. https://doi.org/10.3390/app14031191

[13] Gómez, X., Fernández, C., Fierro, J., Sánchez, M. E., Escapa, A., & Morán, A. (2011). Hydrogen production: two stage processes for waste degradation. *Bioresource Technology*, *102*(18), 8621-8627. https://doi.org/10.1016/j.biortech.2011.03.055

[14] Keskin, T., Abo-Hashesh, M., & Hallenbeck, P. C. (2011). Photofermentative hydrogen production from wastes. *Bioresource Technology*, *102*(18), 8557-8568. https://doi.org/10.1016/j.biortech.2011.04.004

[15] Corneli, E., Adessi, A., Olguín, E. J., Ragaglini, G., García-López, D. A., & De Philippis, R. (2017). Biotransformation of water lettuce (Pistia stratiotes) to biohydrogen by *Rhodopseudomonas palustris*. *Journal of applied microbiology*, *123*(6), 1438-1446. https://doi.org/10.1111/jam.13599

[16] Brown, B., Wilkins, M., & Saha, R. (2022). *Rhodopseudomonas palustris*: A biotechnology chassis. *Biotechnology Advances*, *60*, 108001. https://doi.org/10.1016/j.biotechadv.2022.108001

[17] Li, M., Ning, P., Sun, Y., Luo, J., & Yang, J. (2022). Characteristics and application of *Rhodopseudomonas palustris* as a microbial cell factory. *Frontiers in bioengineering and biotechnology*, *10*, 897003. https://doi.org/10.3389/fbioe.2022.897003

[18] Oda, Y., Samanta, S. K., Rey, F. E., Wu, L., Liu, X., Yan, T., ... & Harwood, C. S. (2005). Functional genomic analysis of three nitrogenase isozymes in the photosynthetic bacterium *Rhodopseudomonas palustris*. *Journal of bacteriology*, *187*(22), 7784-7794. https://doi.org/10.1128/jb.187.22.7784-7794.2005

[19] McKinlay, J. B., Oda, Y., Rühl, M., Posto, A. L., Sauer, U., & Harwood, C. S. (2014b). Non-growing *Rhodopseudomonas palustris* increases the hydrogen gas yield from acetate by shifting from the glyoxylate shunt to the tricarboxylic acid cycle. *Journal of Biological Chemistry*, *289*(4), 1960-1970. https://doi.org/10.1074/jbc.M113.527515

[20] Montiel-Corona, V., & Buitrón, G. (2021). Polyhydroxyalkanoates from organic waste streams using purple non-sulfur bacteria. *Bioresource Technology*, *323*, 124610. https://doi.org/10.1016/j.biortech.2020.124610

[21] Monroy, I., & Buitrón, G. (2020). Production of polyhydroxybutyrate by pure and mixed cultures of purple non-sulfur bacteria: A review. *Journal of biotechnology*, *317*, 39-47. https://doi.org/10.1016/j.jbiotec.2020.04.012

[22] Thorning, T. K., Raben, A., Tholstrup, T., Soedamah-Muthu, S. S., Givens, I., & Astrup, A. (2016). Milk and dairy products: good or bad for human health? An assessment of the totality of scientific evidence. *Food & nutrition research*, *60*(1), 32527. https://doi.org/10.3402/fnr.v60.32527

[23] Miglietta, P. P., De Leo, F., Coluccia, B., Vecchio, Y., & Capitanio, F. (2021). Evaluation of virtual water and water sustainability of dairy production in trentino alto Adige (North-eastern Italy). *Animals*, *11*(4), 1047. https://doi.org/10.3390/ani11041047

[24] Pires, A. F., Marnotes, N. G., Rubio, O. D., Garcia, A. C., & Pereira, C. D. (2021). Dairy by-products: A review on the valorization of whey and second cheese whey. *Foods*, *10*(5), 1067. https://doi.org/10.3390/foods10051067

[25] Demirel, B., Yenigun, O., & Onay, T. T. (2005). Anaerobic treatment of dairy wastewaters: a review. *Process biochemistry*, *40*(8), 2583-2595. https://doi.org/10.1016/j.procbio.2004.12.015

[26] Adessi, A., Venturi, M., Candeliere, F., Galli, V., Granchi, L., & De Philippis, R. (2018). Bread wastes to energy: sequential lactic and photo-fermentation for hydrogen production. *International Journal of Hydrogen Energy*, *43*(20), 9569-9576. https://doi.org/10.1016/j.ijhydene.2018.04.053

[27] Yang, X., Hong, J., Wang, L., Cai, C., Mo, H., Wang, J., ... & Liao, Z. (2024). Effect of Lactic Acid Bacteria Fermentation on Plant-Based Products. *Fermentation*, 10(1), 48. https://doi.org/10.3390/fermentation10010048

[28] Adessi, A., & De Philippis, R. (2014). Photobioreactor design and illumination systems for H_2 production with anoxygenic photosynthetic bacteria: a review. *International Journal of Hydrogen Energy*, *39*(7), 3127-3141. https://doi.org/10.1016/j.ijhydene.2013.12.084

[29] Craven, J., Sultan, M. A., Sarma, R., Wilson, S., Meeks, N., Kim, D. Y., ... & Bhattacharyya, D. (2019). *Rhodopseudomonas palustris*-based conversion of organic acids to hydrogen using plasmonic nanoparticles and near-infrared light. *RSC advances*, *9*(70), 41218-41227. https://doi.org/10.1039/C9RA08747H

[30] Liao, Q., Wang, Y. J., Wang, Y. Z., Zhu, X., Tian, X., & Li, J. (2010). Formation and hydrogen production of photosynthetic bacterial biofilm under various illumination conditions. *Bioresource technology*, *101*(14), 5315-5324. https://doi.org/10.1016/j.biortech.2010.02.019

[31] Uyar, B., Eroglu, I., Yücel, M., Gündüz, U., & Türker, L. (2007). Effect of light intensity, wavelength and illumination protocol on hydrogen production in photobioreactors. *International Journal of Hydrogen Energy*, *32*(18), 4670-4677. https://doi.org/10.1016/j.ijhydene.2007.07.002

[32] Galli, V., Venturi, M., Mari, E., Guerrini, S., & Granchi, L. (2022). Selection of yeast and lactic acid bacteria strains, isolated from spontaneous raw milk fermentation, for the production of a potential probiotic fermented milk. *Fermentation*, *8*(8), 407. https://doi.org/10.3390/fermentation8080407

[33] Adessi, A., Spini, G., Presta, L., Mengoni, A., Viti, C., Giovannetti, L., ... & De Philippis, R. (2016). Draft genome sequence and overview of the purple non-sulfur bacterium *Rhodopseudomonas palustris* 42OL. *Standards in genomic sciences*, *11*, 1-7. https://doi.org/10.1186/s40793-016-0145-y

[34] Bianchi, L., Mannelli, F., Viti, C., Adessi, A., & De Philippis, R. (2010). Hydrogen-producing purple non-sulfur bacteria isolated from the trophic lake Averno (Naples, Italy). *International journal of hydrogen energy*, *35*(22), 12216-12223. https://doi.org/10.1016/j.ijhydene.2010.08.038

[35] Touloupakis, E., Chatziathanasiou, A., Ghanotakis, D. F., Carlozzi, P., & Pecorini, I. (2022). Hydrogen production by immobilized *Rhodopseudomonas* sp. cells in calcium alginate beads. *Energies*, *15*(22), 8355. https://doi.org/10.3390/en15228355

[36] Carlozzi, P., & Sacchi, A. (2001). Biomass production and studies on *Rhodopseudomonas palustris* grown in an outdoor, temperature controlled, underwater tubular photobioreactor. *Journal of Biotechnology*, 88(3), 239-249. https://doi.org/10.1016/S0168-1656(01)00280-2

[37] Rice, E. W., Bridgewater, L., & American Public Health Association (Eds.). (2012). *Standard methods for the examination of water and wastewater* (Vol. 10). Washington, DC: American public health association.

[38] Adessi, A., McKinlay, J. B., Harwood, C. S., & De Philippis, R. (2012). A *Rhodopseudomonas palustris* nifA* mutant produces H_2 from NH_4^+-containing vegetable wastes. *International journal of hydrogen energy*, *37*(21), 15893-15900. https://doi.org/10.1016/j.ijhydene.2012.08.009

[39] De Philippis, R., Sili, C., & Vincenzini, M. (1992). Glycogen and poly-β-hydroxybutyrate synthesis in *Spirulina maxima*. *Microbiology*, *138*(8), 1623-1628. https://doi.org/10.1099/00221287-138-8-1623

[40] Kim, E. J., Lee, M. K., Kim, M. S., & Lee, J. K. (2008). Molecular hydrogen production by nitrogenase of *Rhodobacter sphaeroides* and by Fe-only hydrogenase of

Rhodospirillum rubrum. *International Journal of Hydrogen Energy*, *33*(5), 1516-1521. https://doi.org/10.1016/j.ijhydene.2007.09.044

[41] Heiniger, E. K., Oda, Y., Samanta, S. K., & Harwood, C. S. (2012). How posttranslational modification of nitrogenase is circumvented in *Rhodopseudomonas palustris* strains that produce hydrogen gas constitutively. *Applied and environmental microbiology*, *78*(4), 1023-1032. https://doi.org/10.1128/AEM.07254-11

[42] Dipasquale, L., Adessi, A., d'Ippolito, G., Rossi, F., Fontana, A., & De Philippis, R. (2015). Introducing capnophilic lactic fermentation in a combined dark-photo fermentation process: a route to unparalleled H_2 yields. *Applied microbiology and biotechnology*, *99*, 1001-1010. https://doi.org/10.1007/s00253-014-6231-4

[43] Komesu, A., de Oliveira, J. A. R., da Silva Martins, L. H., Maciel, M. W., & Maciel Filho, R. (2017). Lactic acid production to purification: a review. *BioResources*, *12*(2), 4364-4383. DOI: 10.15376/biores.12.2.Komesu

[44] Adamberg, K., Kask, S., Laht, T. M., & Paalme, T. (2003). The effect of temperature and pH on the growth of lactic acid bacteria: a pH-auxostat study. *International journal of food microbiology*, 85(1-2), 171-183. https://doi.org/10.1016/S0168-1605(02)00537-8

[45] Hofvendahl, K., and Hahn-Hägerdal, B. (2000). "Factors affecting the fermentative lactic acid production from renewable resources," *Enzyme Microb. Tech*. 26(2-4), 87-107. https://doi.org/10.1016/S0141-0229(99)00155-6

[46] Moradi, S., Zeraatpisheh, F., & Tabatabaee-Yazdi, F. (2023). Investigation of lactic acid production in optimized dairy wastewater culture medium. *Biomass Conversion and Biorefinery*, *13*(16), 14837-14848. https://doi.org/10.1007/s13399-022-03230-5

[47] Willows, R.D., Kriegel, A.M. (2009). Biosynthesis of Bacteriochlorophylls in Purple Bacteria. In: Hunter, C.N., Daldal, F., Thurnauer, M.C., Beatty, J.T. (eds) The Purple Phototrophic Bacteria. Advances in Photosynthesis and Respiration, vol 28. Springer, Dordrecht. https://doi.org/10.1007/978-1-4020-8815-5_4

[48] Ghosh, S.; Dairkee, U.K.; Chowdhury, R.; Bhattacharya, P. Hydrogen from food processing wastes via photofermentation using purple non-sulfur bacteria (PNSB): A review. *Energy Convers. Manag*. 2017, 141, 299–314. https://doi.org/10.1016/j.enconman.2016.09.001

[49] Wang, J., Wang, X., Chen, J., & Fei, Z. (2019). Experimental exploration for measurement of ammonia nitrogen in water by Nessler's reagent colorimetry. *Civil Environ. Res.*, *11*(1), 08. DOI: 10.7176/CER/11-1-08

[50] Seifert, K., Waligorska, M., & Laniecki, M. (2010). Hydrogen generation in photobiological process from dairy wastewater. *International Journal of Hydrogen Energy*, *35*(18), 9624-9629. https://doi.org/10.1016/j.ijhydene.2010.07.015

[51] Wu, S. C., Liou, S. Z., & Lee, C. M. (2012). Correlation between bio-hydrogen production and polyhydroxybutyrate (PHB) synthesis by *Rhodopseudomonas palustris* WP3-5. *Bioresource technology*, *113*, 44-50. https://doi.org/10.1016/j.biortech.2012.01.090

Chapter III

Towards a Genome-Scale Metabolic Model of *Rhodopseudomonas palustris* 42OL: Reconstruction Strategies and Phenotypic Characterization

Luca Bernabò[1], Michele Giovannini[2], Giulia Daly[1], Francesca Decorosi[1], Carlo Viti[1], Sergio Bordel Velasco[3], Marco Fondi[2], Lisa Granchi[1] and Alessandra Adessi[1]*

[1]Department of Agriculture, Food, Environment and Forestry (DAGRI), University of Florence, Piazzale delle Cascine 18, 50144 Florence, Italy.

[2]Department of Biology (DBIO), University of Florence, via Madonna del Piano 10, 50019 Sesto Fiorentino, Italy.

[3]Department of Chemical Engineering and Environmental Technology, School of Industrial Engineering, University of Valladolid, Dr. Mergelina, s/n, 47011, Valladolid, Spain.

* Correspondence: alessandra.adessi@unifi.it; Tel.: +39-0552755534

Manuscript in preparation for submission to **PLOS Computational Biology**

https://journals.plos.org/ploscompbiol/

Abstract

Rhodopseudomonas palustris 42OL is a metabolically versatile bacterium with strong potential for the sustainable production of high-value molecules, such as biohydrogen (bio-H_2) and poly-β-hydroxybutyrate (PHB), using agro-industrial effluents as feedstock. However, many mechanisms involved in the degradation and assimilation of diverse carbon and nitrogen sources remain poorly understood, as do the metabolic trade-offs that can reduce yields in products of biotechnological interest.

Systems biology approaches, particularly genome-scale metabolic models (GEMs), emerge as key tools as they enable the study of metabolic flexibility, allow quantitative evaluation of flux distributions, and support the design of biotechnological strategies. In this work, we initiated the reconstruction of a GEM for *R. palustris* 42OL using two complementary strategies. The first employed an automated pipeline to generate a draft model, subsequently refined through manual curation; the second involved a fully manual reconstruction following gold-standard protocols. The automated model, although rapidly obtained, exhibited structural inconsistencies and unrealistic predictions. The manual reconstruction, still ongoing, has required greater effort but has already produced a curated database suitable as a template for related microorganisms, currently comprising 967 cytosolic reactions, 43 transport reactions, 1138 metabolites, and 158 artificial reactions.

Phenotypic profiling with Biolog® microarrays confirmed the broad metabolic versatility of *R. palustris* 42OL and revealed significant differences in substrate utilization under distinct growth modes, particularly under anaerobic light (AnL) conditions, which are most relevant for high-value product biosynthesis. Overall, this work has contributed to the establishment of a curated reaction database that, once completed, will give rise to a high-quality GEM of *R. palustris* 42OL.

Keywords

Rhodopseudomonas palustris 42OL; Genome-scale metabolic model (GEM) reconstruction; Biolog® phenotype microarrays; Biolog® PM1, PM2A, and PM3B plates; Systems biology.

Abbreviations

PNSBs, purple non-sulfur bacteria; bio-H_2, biohydrogen; PHB, poly-β-hydroxybutyrate; GEMs, genome-scale metabolic models; PM, phenotype microarray; GPR, gene-protein-

reaction; KEGG, Kyoto Encyclopedia of Genes and Genomes; BChl*a*, bacteriochlorophyll *a*; BOF, biomass objective function; KO, KEGG orthologs; RC, reaction center; FBA, flux balance analysis;

1. Introduction

Rhodopseudomonas palustris is a metabolically versatile, Gram-negative, purple non-sulfur bacterium (PNSB) that belongs to the class Alphaproteobacteria. It has been isolated from a variety of environments, including eutrophic lagoons, freshwater ponds, marshy soils, and marine sediments [1]. This highlights the ability of PNSBs to thrive under both illuminated and dark conditions across diverse ecological niches by employing distinct metabolic modules [2-4].

In the absence of light, *R. palustris* grows under aerobic or anaerobic conditions. Anaerobic respiration involves the use of different terminal electron acceptors, which vary across species and even among strains. Commonly utilized acceptors include nitrate (NO_3^-), nitrous oxide (N_2O), dimethylsulfide, and trimethylammonium oxide [3,4].

Under illuminated conditions, *R. palustris* can adopt either a photoautotrophic or a photoheterotrophic lifestyle. In photoautotrophy, it relies on inorganic electron donors such as hydrogen (H_2), thiosulfate ($S_2O_3^{2-}$), or ferrous iron (Fe^{2+}), with carbon dioxide (CO_2) as the sole carbon source. Alternatively, in photoheterotrophy, it utilizes organic compounds as both carbon and electron sources [3,4].

In addition, *R. palustris* is a diazotrophic organism that can fix molecular nitrogen (N_2) through three distinct nitrogenases [3-5]. These nitrogenases differ in the type of metal cofactor they employ: iron, vanadium, or molybdenum. The activity of these nitrogenases is highly sensitive to mineral availability and the concentration of molecular oxygen (O_2); consequently, their expression is tightly regulated according to O_2 levels [4,5].

Like other PNSB, *R. palustris* performs anoxygenic photosynthesis via a single photosystem homologous to photosystem II but lacking the capacity to oxidize water. As a result, unlike oxygenic phototrophs such as plants, algae, and cyanobacteria, it does not produce molecular oxygen as a by-product [6].

R. palustris is predominantly studied under photoheterotrophic conditions, as it is under these circumstances that it can catabolize a wide variety of feedstocks and convert them into high-value products, including biohydrogen (bio-H_2) and poly-β-hydroxybutyrate (PHB), which represent, respectively, a biofuel and a polyester suitable to produce bioplastics [7,8].

Bio-H_2 is primarily produced as a by-product of nitrogenase activity. This process can also occur in the absence of nitrogen (N_2) and requires a high C/N ratio and low ammonium (NH_4^+) availability. The uptake hydrogenase enzyme can also generate

hydrogen; however, since this reversible enzyme typically favors hydrogen consumption to recover electrons, its activity generally reduces the overall yield of hydrogen [7].

PHB, by contrast, is accumulated intracellularly in the form of granules as an energy-storage compound under imbalanced nutritional conditions, typically characterized by an excess of carbon and a limitation of other essential nutrients such as nitrogen, phosphorus, or sulfur [8].

Strain *R. palustris* 42OL has previously been investigated for its ability to produce bio-H_2 and PHB under various experimental conditions, including different substrates, culture conditions (natural or artificial light), and growth modes (suspended or immobilized cells) [9-12]. The relationship between PHB accumulation and bio-H_2 production has also been explored. While many of *R. palustris* 42OL's metabolic strategies have been elucidated, important features and mechanisms remain unknown, particularly concerning the utilization of different carbon and nitrogen sources under the diverse metabolic conditions that this bacterium can adopt [13]. The application of genome-scale metabolic models (GEMs) can further clarify these aspects by providing a global view of microbial metabolic networks, integrating experimental data, and enabling in silico simulation of different growth scenarios. This allows metabolic fluxes to be predicted, metabolic bottlenecks to be identified, and future biotechnological strategies to be guided [14].

Previous studies have developed GEMs of *R. palustris*, contributing to our understanding of its metabolism and clarifying the mechanisms and flux distributions underlying growth under illuminated and anoxic conditions. However, most of these studies have focused exclusively on the photoheterotrophic phenotype, overlooking the wide range of possible lifestyles of this microorganism [13,15,16].

The present study aims to initiate a pathway for the reconstruction and validation of a GEM for *R. palustris* 42OL. This was achieved using two distinct approaches: an automated reconstruction method, which enabled the rapid generation of a preliminary model but was affected by structural inconsistencies that proved difficult to resolve through manual curation; and a fully manual approach, aimed at obtaining a highly curated reaction database that can serve as a foundation for the reconstruction of a GEM not only for *R. palustris* 42OL but also for phylogenetically related microorganisms.

Model validation and identification of potential metabolic gaps were undertaken by integrating experimental data obtained using a Biolog® Phenotype Microarray (PM) [14]. This allowed carbon and nitrogen source utilization to be assessed under variable metabolic conditions, including anaerobiosis and aerobiosis, in both the presence and

absence of light (plates PM1, PM2A, and PM3B). While a fully functional model has yet to be achieved, this work has revealed the limitations of conventional approaches and provided an opportunity to explore the potential of new reconstruction paradigms, paving the way for future progress.

2. Materials and Methods.

2.1. Microorganism used in this study.

For the construction of the metabolic model and the phenotypic microarray tests, *R. palustris* 42OL was employed. This microorganism was originally isolated in 1973 from an effluent catchment basin of a sugar refinery waste treatment pond in Castiglion Fiorentino (AR), Italy [1]. The strain is part of the culture collection maintained by the Department of Agricultural, Food, Environmental, and Forestry Sciences and Technologies (DAGRI) at the University of Florence (Florence, FI, Italy). It is preserved under anaerobic-light conditions at 25 °C in sealed agar tubes containing solid RPN medium (detailed composition reported in section 2.4) [17].

The genome of *R. palustris* 42OL was previously sequenced by Adessi et al. [1]. Project information is available in the Genomes OnLine Database (GOLD) under study ID Gs0114708. The whole genome shotgun (WGS) sequence is deposited in GenBank under accession number LCZM00000000.

2.2. Automated Reconstruction of the Draft Genome-Scale Metabolic Model via KBase.

The draft genome-scale metabolic model of *R. palustris* 42OL was generated through an automated reconstruction process, as described below. The genome of *R. palustris* 42OL (available under accession number GCA_001020905.1) was first re-annotated using the KBase Annotation App (RASTtk version 1.073), which utilizes components of the RAST (Rapid Annotations using Subsystems Technology) toolkit to annotate prokaryotic genomes [18]. The re-annotated genome was then used as input for the KBase ModelSEED2 application (MS2, Build Prokaryotic Metabolic Models, version 2.0.0) [19]. The resulting model was gap-filled in complete medium to enforce a minimum flux of 0.1 through the bio1 reaction, which represents the biomass synthesis (growth objective) reaction commonly used in genome-scale metabolic models. This application allowed the automatic generation of a preliminary gene-protein-reaction (GPR) association within the metabolic network. At the end of this phase, an initial metabolic network, linking gene sequences, enzymes, metabolites, reactions, and biochemical pathways, was generated, culminating in the draft metabolic model of *R. palustris* 42OL.

2.2.1. Refinement of the Draft Model Through Manual Curation.

A manual refinement of the draft model was subsequently performed, involving a detailed revision of the model's metabolic pathways and the addition of missing reactions

to improve its completeness and accuracy. For this purpose, the public database KEGG (Kyoto Encyclopedia of Genes and Genomes) was utilized, providing manually curated and detailed information on metabolic pathways, associated reactions, and gene products (enzymes) [20]. Seven strains of *R. palustris* (CGA009, HaA2, BisB18, BisB5, BisA53, TIE-1, DX-1) were selected from KEGG, as they are phylogenetically related to *R. palustris* 42OL. Their metabolic pathways were compared against those in the automatically generated draft model, allowing the identification and incorporation of missing reactions.

For each reaction added to the model, a corresponding GPR association was defined, linking one or more genes to the reaction. The type of enzymatic relationship, either AND or OR, was also defined. An AND relationship indicates cooperation between subunits in protein complexes, whereas an OR relationship reflects the presence of isoenzymes. The enzymatic relationships were assigned based on information from the KEGG database for the seven selected *R. palustris* strains. Specifically, when multiple genes were associated with the same enzymatic activity (same EC number) but encoded different isoforms or classes of the enzyme, an OR relationship was applied, indicating that any of the genes could catalyze the reaction. Conversely, when multiple genes were required to form a functional protein complex, an AND relationship was assigned.

To identify the protein sequence of *R. palustris* 42OL associated with a specific reaction, candidate genes from its proteome were analyzed using BLASTp, comparing them against proteins linked to the corresponding reactions in other *R. palustris* strains available in the KEGG database. In cases where the reaction was not present in KEGG but physiological evidence supported its existence, protein sequences from other microorganisms were retrieved from the UniProt or BiGG databases [21,22]. The physiological evidence included reports from the scientific literature and experimental observations obtained through Biolog® PM analyses. Selection criteria for BLASTp analysis were set as follows: E-value $\leq 1e^{-10}$, query coverage $\geq 80\%$, and sequence identity $\geq 40\%$ [13]. The best match meeting these criteria was assigned to the corresponding reaction. In instances where no matches fulfilled the predefined thresholds, the top-scoring match was further evaluated through protein domain analysis using the Pfam database (The Protein Families Database) [23]. Proteins were retained only if they exhibited conserved domains consistent with the expected enzymatic function. In cases where no gene could be annotated through homology but physiological evidence supported the presence of the reaction, the reaction was nevertheless retained in the

model, albeit without a gene association. At the end of the manual curation process, the refined and biologically consistent model of *R. palustris* 42OL was obtained.

2.2.2 Incorporation of Anoxygenic Photosynthesis Reactions into the Metabolic Model.

Anoxygenic photosynthesis in *R. palustris* 42OL was modelled based on the framework proposed by Adessi, La Cava, and De Philippis [24]. Initially, the photon metabolite (cpd11632_e0) was added to the extracellular compartment (e0), along with its corresponding exchange reaction (EX_cpd11632_e0). In the context of GEMs, exchange reactions represent the interface between the model and its external environment. They are used to define which metabolites can enter or leave the system boundaries. In this case, the exchange reaction enables the model to import photons from the external environment as the energy source for the photosynthetic process. After that, transport reaction (rxn31154_c0) was introduced to allow the transfer of photons from the extracellular space into the intracellular compartment (cpd11632_c0). Transport reactions connect different cellular compartments, enabling the movement of metabolites between them (e.g., from extracellular to cytosolic space, or between cytoplasm and periplasm).

Subsequently, a light-capture reaction (rxnPHOTO001_c0) was incorporated to simulate the activity of light-harvesting (LH1/LH2) complexes. In this reaction, an intracellular photon interacts with a bacteriochlorophyll *a* (Bchl*a*) molecule (cpd08107_c0), promoting it from its ground state to an excited state (BChla_E_c0).

An electron transfer reaction (rxnPHOTO002_c0) was then added to represent the process occurring in the reaction center (RC), whereby the excited bacteriochlorophyll *a* transfers an electron to an oxidized quinone (cpd11669_c0). Once the quinone is fully reduced (cpd11665_c0), for instance, following the absorption of a second photon, it is reoxidized by the cytochrome bc_1 complex (rxn06106_c0). In this step, two molecules of cytochrome c^{3+} (cpd00109_c0) are reduced to cytochrome c^{2+} (cpd00110_c0). The reduced cytochrome c^{2+} molecules subsequently donate electrons to the oxidized bacteriochlorophyll *a*, restoring it to its neutral ground state. During this process, two protons are translocated to the extracellular compartment (cpd00067_e0) and subsequently utilized by ATP synthase (rxn08173_c0) to generate ATP.

2.2.3 Biomass Objective Function (BOF) Construction.

Since no data on the biomass composition of *R. palustris* 42OL were available, the biomass stoichiometry defined by Tec-Campos et al. [13] was adopted.

The metabolites involved in biomass production were grouped into nine principal categories: amino acids, cell wall components, pigments, cofactors, RNA, DNA, carbohydrates, minerals, and miscellaneous compounds. The final biomass objective function for the *R. palustris* 42OL model contained 98 constituents. The BOF was used as the primary optimization objective to predict growth and internal metabolic fluxes across the different metabolic modes of *R. palustris* 42OL.

2.3 Manual Genome-Scale Metabolic Model Reconstruction

In addition to the automated reconstruction, a manual approach was carried out following the protocol proposed by Thiele & Palsson [25]. This protocol divides the process into four main phases: i) creation of the draft reconstruction, ii) refinement, iii) conversion into a mathematical model, and iv) validation and integration of the network.

In this context, KEGG was used as the reference database, with particular emphasis on the KEGG Orthologs (KO) system. Each KO represents an evolutionarily conserved enzymatic function and can be associated with multiple orthologous genes in different organisms, as well as with several biochemical reactions when the corresponding enzyme catalyzes different transformations [20].

The functional annotation of the *R. palustris* 42OL genome was obtained using eggNOG-mapper v2, which assigns each protein-coding gene to its corresponding KO based on evolutionary orthology relationships [26]. The output provides, for each protein, the most probable ortholog, the KO identifier, the functional description, and the associated KEGG pathways.

During the manual reconstruction, each annotated protein was examined: starting from the KO or the enzymatic function identified, the corresponding reaction was retrieved from KEGG. This reaction was then transcribed and standardized in BiGG format within a dedicated spreadsheet, where it was linked to the corresponding ortholog(s). In this way, every reaction included in the draft model was supported by at least one annotated gene ortholog, allowing the formulation of the related GPRs rules and ensuring consistency between the genomic content of the strain and its potential metabolic capabilities.

2.3.1 Compilation of the Draft Reconstruction

The draft model was progressively compiled within a spreadsheet organized into multiple worksheets, dedicated to cytoplasmic reactions (R), transport reactions (T, involving metabolites in the extracellular compartment), and metabolites (M). Cytoplasmic reactions were defined as transformations occurring exclusively within the

cytoplasm, with metabolites indicated by the suffix "_c". In contrast, transport reactions involved metabolites located in different compartments and followed the internal convention of using the suffixes "_c" and "_e" to denote cytoplasmic and extracellular localization, respectively.

The introduction of new reactions followed strict rules to ensure biochemical consistency and process traceability. Reactions were systematically added on a pathway-by-pathway basis, starting from canonical pathways and progressively extending to those more specific to the strain under study. Each reaction was verified for mass and charge balance (at physiological pH) and connected to pre-existing metabolites included in the corresponding worksheet, thereby preventing the creation of isolated reactions or dead-end pathways.

Reactions are identified using BiGG IDs or, when not available, with custom identifiers that comply with BiGG nomenclature conventions. For each reaction, the extended name is also reported, together with the corresponding KEGG Reaction ID, to maintain consistency with the reference database. In addition, every reaction is associated with one or more KOs through universal GPRs, expressed in Boolean logic (AND/OR), to represent either multisubunit enzyme complexes or isoenzymes.

The directionality (reversible or irreversible) of cytoplasmic reactions was assigned according to the information reported in KEGG maps. Additionally, all reactions involving quinones or the transfer of a phosphate group to an acceptor molecule were categorized as irreversible, except for ATP synthase, which operates in the reverse direction.

Transport reactions between the extracellular compartment and the cytoplasm were handled in two distinct ways, depending on the available information about the specific transporter. When no evidence was available regarding the transport system of a metabolite, generic reactions were introduced, linking the extracellular and cytoplasmic forms through a facilitated diffusion process across the membrane, and annotated as "orphan". Conversely, when the nature of the transporter was known from KO assignments or bibliographic evidence, the transport mechanism was modelled explicitly. In these cases, ABC transporters were represented as ATP-dependent and irreversible reactions, while symport and antiport systems were defined according to the ions or metabolites co-transported.

Metabolites were added to the worksheet M using a BiGG identifier, the corresponding KEGG Compound ID, the molecular formula, the charge, the name, and the associated

cellular compartment. For each reaction included in the model, the metabolites involved were entered into the corresponding worksheet, consistently with their subcellular localization. In this way, every reaction was directly linked to its substrates and products, ensuring structural consistency and full traceability between reactions and metabolites.

2.3.2 Modelling of Hydrogen Production via Nitrogenases

Bio-H_2 production was modelled by including the three known nitrogenase isoforms (Mo-, V-, and Fe-nitrogenase), which are distinguished by their respective metal cofactors. Two types of reactions were implemented for each isoform: i) assembly reactions, describing the activation of apo-nitrogenase (aponit_c) through the incorporation of the specific cofactor (Mo, V or Fe), leading to the formation of the respective active holo-nitrogenase (olonitmo_c, olonitv_c or olonitfe_c); and ii) catalytic reactions, representing the reduction of molecular nitrogen with concomitant H_2 production.

Catalytic reactions were defined based on stoichiometric equations available in KEGG and in the literature [4]. For Mo-nitrogenase, in addition to the canonical reaction that reduces N_2 to NH_4^+ with concomitant production of H_2 (NIT1b), an alternative reaction (NIT1bNON) was also included, which describes the condition of N_2 absence, in which the entire reducing flow is directed towards hydrogen production. Similarly, catalytic reactions were modelled for V-nitrogenase (NITV) and Fe-nitrogenase (NITFE), characterized by specific stoichiometric consumption of ATP and reducing equivalents, as well as different H_2/NH_4^+ production ratios. The regeneration of aponit_c was also included in all catalytic reactions to allow for the cyclic repetition of the enzymatic process.

2.3.3 Modeling of Anoxygenic Photosynthesis

In accordance with the approach described by Adessi, La Cava, and De Philippis [24], modelling of anoxygenic photosynthesis was initiated by introducing the BChl*a* excitation reaction (BCHPHEXC) as a transport reaction. This reaction marks the initial stage of the process, whereby a BChl*a* molecule in its ground state (bchphya_c) absorbs a photon (photon870_e) from the extracellular environment and transitions to the excited state (bchphya_exc_c).

The RC_PNSB1 reaction was then introduced to describe the transfer of energy from the excited BChl*a* to the reaction center. The reaction center then transitions from the

ground state (rc_pnsb_c) to the excited state (rc_pnsb_exc_c), while the BChl*a* returns to its ground state.

The next step was represented by the RC_PNSB2 reaction, which models the primary charge separation event in the reaction center. During this process, the reaction center becomes oxidized, while ubiquinone (q8_c) acts as the primary electron acceptor. Following two sequential photoexcitation events, ubiquinone is reduced to ubiquinol (q8h2_c) with the concomitant uptake of two protons from the cytoplasm. As a result, the reaction yields the reduced ubiquinol together with the oxidized form of the reaction center, denoted as rc_pnsb_sep_c.

The ubiquinol produced is subsequently reoxidized to ubiquinone via the CYTBC1 reaction, which involves the reduction of two molecules of oxidized cytochrome c_2 (cytc2ox_c) to reduced cytochrome c_2 (cytc2red_c). This process is coupled with the release of protons (h_e) into the periplasmic space, contributing to the formation of the transmembrane proton gradient, which is essential for ATP synthesis via ATP synthase.

Finally, the recharge phase of the reaction center was modelled using the RC_PNSB3 reaction. In this step, reduced cytochrome c_2 donates an electron to the oxidized reaction center (rc_pnsb_sep_c), returning it to the ground state (rc_pnsb_c) and regenerating the oxidized cytochrome (cytc2ox_c). This reaction closes the cyclic electron flow and allows the photosynthetic process to continue.

2.3.4 BOF Construction.

The BOF was implemented as an artificial reaction that consumes the main precursors required for macromolecule synthesis and produces a pseudo-metabolite called biomass. The flux through this reaction was used as the objective function in FBA simulations, representing the model's growth potential. As described in subsection 2.2.3, the biomass composition and stoichiometry were adopted from Tec-Campos et al. [13] due to the absence of strain-specific data for *R. palustris* 42OL.

2.3.5 Conversion of the Reconstruction into Mathematical Model and Gap-Filling Procedures.

Once the manual reconstruction process was complete, the spreadsheet was converted into a mathematical model using COBRApy [27]. A Python script analyzed the spreadsheets and transformed each record into a COBRApy object (*Metabolite*, *Reaction*, or *Gene*). Specifically, each row of sheet M was converted into a metabolite, with a BiGG identifier, extended name, chemical formula, charge, and compartment of belonging; the

rows of sheets R and T were converted into reactions, characterized by a BiGG identifier, extended name, pathway annotation, and flow limits that define their directionality. Reactants, products, and their stoichiometric coefficients were parsed from the reaction string (rstring) and mapped to the corresponding imported metabolites. Reaction directionality was inferred from the arrow symbol in the rstring: "-->" (irreversible forward) was assigned lower_bound = 0 and upper_bound = 1000, whereas "<=>" (reversible) was assigned lower_bound = -1000 and upper_bound = 1000.

GPR rules, stored in the spreadsheet as Boolean expressions, were imported and associated with reactions through *Gene* objects, thereby linking each reaction to its corresponding set of orthologs. The assembled model was then exported in SBML (.xml) format for subsequent analyses.

Model performance was evaluated by flux balance analysis (FBA) to test its ability to synthesize biomass precursors. The feasibility of producing individual biomass components was assessed in two modified M9 minimal media: (i) M9 supplemented with D-malic acid as the sole carbon source, and (ii) M9photo, configured with D-malic acid as the carbon source, no O_2 exchange, N_2 as the nitrogen source, and photons enabled to simulate light. This evaluation highlighted gaps that prevented *in silico* growth; consequently, only the minimal set of reactions required to restore network functionality (i.e., to enable biomass precursor synthesis) was added.

During gap filling, blocked reactions were also identified. These are defined as reactions that cannot carry flux under any simulated condition and that are directly or indirectly associated with dead-end metabolites, namely metabolites that are produced but not consumed, or vice versa. To address these dead ends, in addition to adding biochemically supported reactions, artificial boundary reactions were introduced where appropriate: sink reactions, which allow non-specific import and/or export of a metabolite when the physiological direction is uncertain, and demand reactions, which act as irreversible drains permitting the accumulation or removal of a terminal metabolite as a final product. These modelling strategies improved network connectivity and facilitated the identification of missing pathways.

2.4 Assessment of Metabolic Capabilities of *R. palustris* 42OL Using Phenotype Microarrays

R. palustris 42OL was previously grown anaerobically on Petri dishes for 15 days under a light intensity of 40 µmol (photons) m^{-2} s^{-1} at 26 °C. The culture was carried out

in an RPN agar medium that consisted of: DL-malic acid 2.0 g L^{-1}, NH_4Cl 0.5 g L^{-1}, K_2HPO_4 0.5 g L^{-1}, KH_2PO_4 0.3 g L^{-1}, $MgSO_4 \cdot 7H_2O$ 0.4 g L^{-1}, NaCl 0.4 g L^{-1}, $CaCl_2 \cdot 2H_2O$ 0.075 g L^{-1}, ferric citrate 0.005 g L^{-1}, yeast extract 0.4 g L^{-1} and bacteriological agar 15 g L^{-1}. Trace elements were added at 10 mL per liter from a stock solution containing: $ZnSO_4 \cdot 7H_2O$ 10 mg L^{-1}, $MnCl_2 \cdot 4H_2O$ 3 mg L^{-1}, H_3BO_3 30 mg L^{-1}, $CoCl_2 \cdot 6H_2O$ 20 mg L-1, $CuCl_2 \cdot 2H_2O$ 1 mg L^{-1}, $NiCl_2 \cdot 6H_2O$ 2 mg L^{-1}, and $Na_2MoO_4 \cdot 2H_2O$ 30 mg L^{-1}. The pH was adjusted to 6.8 using NaOH before autoclaving.

Bacterial suspensions were tested for growth on plates PM1 and PM2A (carbon sources) and PM 3B (nitrogen sources) from Biolog, Inc. (Hayward, California, USA) under four metabolic conditions: i) anaerobiosis in the dark (AnD); ii) aerobiosis in the dark (AeD); iii) anaerobiosis in the light (AnL); iv) aerobiosis in the light (AeL). Tests were performed in duplicate. Briefly, 15-day-old colonies were collected from the Petri dishes using a sterile cotton swab and suspended in a sterile saline solution (0.9 % NaCl) until an OD_{600} of 0.5 was reached, using a Biolog® turbidimeter (Biolog Inc., Hayward, California, USA).

For the PM1 and PM2A plates, each well was inoculated with 100 µL of a solution containing: (i) a *R. palustris* 42OL cell suspension adjusted to an OD_{600} of 0.01; (ii) RPN medium without carbon source and yeast extract, supplemented with 1 mL L^{-1} of p-aminobenzoic acid (prepared as a 20 mg per 100 mL stock solution); and (iii) dye G (Biolog Inc., Hayward, California, USA) at a final concentration of 1×, obtained by adding 1 µL of a 100× stock solution per 100 µL of the inoculum. For PM3B plates, the 100 µL inoculum solution was modified using the same RPN medium but deprived of the nitrogen source (NH_4Cl) and added with the carbon source (DL-Malic acid), in a concentration equal to the RPN agar medium previously described.

To evaluate growth under anaerobic conditions, plates were sealed inside PM gas bags (Biolog Inc., Hayward, California, USA) in the presence of oxygen-absorbing AnaeroGen Compact packs (Thermo Fisher Scientific Inc., Waltham, Massachusetts) with an anaerobic indicator (Thermo Fisher Scientific Inc., Waltham, Massachusetts). For the aerobic conditions, plates were sealed with a double-sided adhesive film placed between the plate and the lid to minimize condensation and prevent liquid evaporation.

To assess growth in the dark, plates were incubated at 30 °C in an Omnilog® PM system (Biolog Inc., Hayward, California, USA). The reduction of tetrazolium dye results in the formation of a purple color that is recorded by a Charge-Coupled Device (CCD) camera every 15 min. Instead, to assess growth in the light, plates were incubated under

a light intensity of 40 µmol (photons) m^{-2} s^{-1} at 30 °C, inside a Binder incubator (BINDER GmbH, Tuttlingen, Germany) equipped with LED lights. Dye reduction was read daily using the Omnilog PM system. The trial lasted a total of 15 days and was interrupted when microbial growth reached a plateau. Substrate utilization was considered positive when the maximum OD_{600} reached in the presence of the substrate exceeded that of the negative control by at least 20 % after 360 hours of incubation.

3. Results and Discussion

3.1 GEM reconstruction of *R. palustris* 42OL

The first attempt at reconstructing a GEM for *R. palustris* 42OL relied on an automated reconstruction tool available on the KBase platform, MS2. The decision to use an automated reconstruction tool was motivated by the fact that these pipelines enable the rapid generation of draft models (within seconds to a few hours), which drastically reduces the amount of manual effort required for data collection and network assembly [19].

MS2 is a widely used and up-to-date tool for automated GEM reconstruction. It introduces control procedures to ensure the energetic consistency of metabolism, producing biologically realistic models from the outset [19]. Its biochemistry database is constantly updated and integrates information from authoritative sources, such as KEGG, MetaCyc [28], BiGG, and published models. MS2 also employs machine-learning classifiers to automatically select the most appropriate template, i.e. a predefined set of metabolic reactions and GPR associations specific to taxonomic groups such as bacteria, archaea, and eukaryotes [19]. Overall, MS2 produces more accurate draft models than earlier pipelines, typically including a greater number of genes and fewer gap-filled reactions [19].

Following the automatic reconstruction, MS2 produced a model comprising two compartments (cytosolic and extracellular), incorporating 1189 reactions, 1226 metabolites, and 1094 genes. A total of 31 gap-filled reactions were added automatically to enable growth via the universal biomass function (bio1). Growth was tested by default on two reference media: *RefGlucoseMinimal* (a minimal medium with glucose as the sole carbon source) and *Complete Medium* (a rich medium). This ensured that the resulting draft model was computationally functional.

Although this model provided a starting point, it was inevitably incomplete and not representative of the physiology of *R. palustris* 42OL, as many reactions were absent or lacked association with specific genes. This incompleteness became evident when testing growth on synthetic media reported in the literature for *R. palustris* 42OL (RPN malate and RPP malate) [17], where the model predicted no growth (flux = 0).

To overcome these limitations, a process of manual curation was undertaken to improve metabolic coverage and GPR associations. Overall, 721 reactions and 521 metabolites were added, while GPRs were integrated for 530 reactions that were not

previously linked to genes. Several metabolic pathways were curated, with particular focus on carbohydrate metabolism (including the butanoate metabolism pathway, relevant for PHB synthesis), amino acid metabolism, lipid metabolism, and cofactor/vitamin biosynthesis. Furthermore, nitrogen metabolism (including nitrogenase-catalyzed reactions), sulfur metabolism, the CBB cycle, and oxidative phosphorylation were extensively revised. Notably, anoxygenic photosynthesis reactions were added, since universal templates used in automated reconstructions, including MS2, typically neglect highly specialized pathways such as phototrophy, while favoring central metabolism. Genes encoding photosynthetic complexes and pigments are not always correctly annotated or mapped to biochemical reactions in the database, resulting in their systematic exclusion from automatic models.

During this phase, a new biomass function (bio2) was also integrated. The bio1 function introduced by MS2 is a universal biomass formulation common to the major taxonomic groups of Bacteria and Archaea, rather than being specific to *R. palustris* 42OL. To improve accuracy, bio2 was imported from a published model of *R. palustris* BisA53, which is a closely related organism [13]. The model's ability to synthesize each biomass precursor was verified through demand reactions, each of which was optimized as the objective function in FBA simulations. An optimal flux greater than zero was interpreted as evidence that the model could autonomously produce the metabolite. Where this was not the case, gap-filling was applied to introduce the required synthesis reactions. This strategy improved biological consistency by replacing the universal biomass function with one calibrated on a phylogenetically close organism.

After integrating bio2, the model was retested on synthetic media. In this new configuration, the model predicted growth with a biomass flux of 0.164. However, when all carbon sources (both organic and inorganic) were removed, the model continued to predict growth at the same rate, highlighting inconsistent behavior. From a biological point of view, *R. palustris* cannot proliferate in the absence of carbon sources, which are essential for the synthesis of cellular precursors and growth.

The first limitation is related to one of the main disadvantages of automated reconstruction tools, namely their tendency to assign non-specific directionality to many reactions, which are often considered reversible in the absence of thermodynamic data. These overly permissive constraints can generate futile cycles or energetically unfeasible pathways, leading to growth predictions that do not reflect biologically feasible conditions [25].

A second limitation relates to the reaction and metabolite identification system adopted by ModelSEED. This system is based on numerical IDs that cannot be read by humans. For instance, pyruvate is encoded as “cpd00020” and phosphoenolpyruvate kinase as “rxn00148”. These identifiers are difficult to recognize, which significantly increases the time required for manual curation and increases the likelihood of errors. They also complicate the integration of knowledge drawn from literature [29].

These limitations motivated the adoption of a second strategy: a fully manual reconstruction of the metabolic network of *R. palustris* 42OL, aimed at producing a curated “reaction database” in accordance with the gold standards defined by Thiele & Palsson [25]. This database employs BiGG identifiers, which have the advantage of being human-readable: for example, pyruvate is denoted as “pyr” and phosphoenolpyruvate kinase as “PYK”. Each reaction is mass- and charge-balanced and assigned a specific directionality.

Furthermore, the association of each reaction with its KO identifier allows this database to be used as a template for GEM reconstruction of other PNSB strains. With eggNOG annotations, proteins can be mapped to their KO, enabling curated reactions to be automatically reassigned to genes in the new strain. In this way, the curation effort performed here becomes reusable and transferable to related organisms [26,29].

At present, the curated database comprises 967 cytosolic reactions (either gene-associated or spontaneous), 43 transport reactions, 1138 metabolites, and 158 artificial reactions (including sinks, demands, exchanges, and the biomass function). Overall, the database covers 64% of the KOs identified by eggNOG annotation. Compared with the automatic reconstruction, the curated database improves nitrogenase representation by including alternative isoforms and their metal cofactors, thereby accounting for different catalytic stoichiometries and kinetics.

The enrichment of the database to further refine the representation of *R. palustris* metabolism is ongoing and will continue as part of future work, with the ultimate aim of obtaining a curated model suitable for reliable *in silico* simulations.

3.2 Phenotypic profiling of *R. palustris* 42OL through phenotype microarrays

The metabolic versatility of *R. palustris* 42OL is a distinctive trait that not only explains its ecological success in various natural environments but also its numerous potential biotechnological applications. This makes it an ideal candidate for producing high-value molecules from agro-industrial waste [1-4,30]. The phenotype microarray

technique is an effective tool for systematically evaluating a microorganism's metabolic activity on a wide range of substrates and metabolic configurations. This provides a physiological profile that integrates and complements genomic predictions [14,31].

In this study, the ability of the *R. palustris* 42OL strain to utilize different carbon and nitrogen sources was analyzed under four metabolic conditions (AnL, AnD, AeL, and AeD). This analysis revealed significant differences in substrate utilization relating to the experimental conditions, while also generating useful data for validating metabolic models, filling in gaps, and correcting discrepancies between *in silico* predictions and the observed phenotype. The results obtained for carbon and nitrogen sources are presented and discussed in the following subsections.

3.2.1 Carbon Sources Utilization Profile

Fig. 1 shows the results of the phenotypic screening of *R. palustris* 42OL using Biolog PM1 and PM2A microplates (carbon sources), divided into seven categories: carbohydrates (Fig. 1A), carboxylic acids (Fig. 1B), amino acids (Fig. 1C), amines/amides (Fig. 1D), alcohols (Fig. 1E), polymers (Fig. 1F), esters and fatty acids (Fig. 1G). Overall, the microorganism showed the ability to utilize a wide range of substrates, although with a clear preference for organic acids and with significant differences related to metabolic conditions.

The AnL condition (photoheterotrophy) is the most favorable for *R. palustris* 42OL, which uses light as its primary energy source and organic acids as sources of carbon and electrons (Fig. 1B). In this mode, the carbon in the substrates is used almost entirely to produce new biomass [3]. The CBB cycle can also be activated, which has the role of dissipating excess reducing power through CO_2 fixation. The latter derives from the catabolism of substrates that are more oxidized than biomass (such as succinate and malate), which require an increase in their degree of reduction to be assimilated. This occurs through the release of CO_2, which increases the H/C ratio of the substrates, allowing them to be assimilated in the biomass [32].

Organic acids are also used significantly under AeD and AeL conditions. In the presence of oxygen, anoxygenic photosynthesis is inhibited and metabolism becomes chemoheterotrophic, whereby organic substrates are fully oxidized to CO_2 via the TCA cycle and aerobic respiration. Under these conditions, however, only a small proportion of the carbon in the substrates is incorporated into the biomass compared to photoheterotrophy [3,4,33].

In AnD, however, organic acids are poorly utilized and only certain carbohydrates, such as glycerol, fructose-6-phosphate and rhamnose, permit minimal metabolic activity (Fig. 1A). The most plausible hypothesis is that, in the absence of oxygen and light, cells are unable to obtain sufficient reducing power, and therefore energy, from using organic acids as these are already partially oxidized substrates. Moreover, anaerobic respiration is presumably blocked due to the lack of alternative electron acceptors in the growth medium, such as nitrate, dimethyl sulfoxide, or trimethylamine N-oxide. Under these conditions, only certain carbohydrates can support growth, probably via fermentation pathways that provide limited energy, but sufficient to sustain minimal metabolic activity [3,4,34].

*R. palustri*s 42OL showed high metabolic activity even in the presence of esters and fatty acids as substrates (Fig. 1G), under AnL conditions. Esters are presumably hydrolyzed by non-specific hydrolases (esterases/lipases) [35,36]. In the case of lipid esters, hydrolysis releases fatty acids that are activated to acyl-CoA and subsequently degraded via β-oxidation, producing acetyl-CoA, which enters the TCA cycle and supports growth [37]. In the case of methylpyruvate and D-lactic acid methyl ester, hydrolysis releases pyruvate and D-lactate, respectively, both of which are central metabolites that can be immediately channelled into the cell's main catabolic and anabolic pathways [35-38]. The phenotypic results also appear consistent with the genome of *R. palustris* 42OL, which contains multiple genes encoding putative esterases (e.g., *tesA*, EC 3.1.1.1) and lipases/phospholipases (e.g., *pldB*, EC 3.1.1.5), confirming that this microorganism possesses the enzymatic tools for the hydrolysis of ester substrates.

Regarding other substrates categories, such as alcohols, amino acids, polymers, amines and amides, their use as a carbon source has been only marginal and mainly under AnL conditions.

Among the alcohols (Fig. 1E), *R. palustris* 42OL showed a clear ability to grow on 2,3-butanedione (diacetyl) and 3-hydroxy-2-butanone (acetoin) under AnL conditions, but to a lesser extent also under the two aerobic conditions. Genomic evidence from the microorganism confirms the findings revealed by PM. Acetoin can be converted to acetyl-CoA through the action of the acetoin dehydrogenase complex (EC 2.3.1.190). The acetyl-CoA thus produced enters the TCA cycle, providing energy and biosynthetic precursors and supporting the metabolic activity of the microorganism. The genome of *R. palustris* 42OL contains two genes, acoA_1 and acoA_2 (EC 1.1.1.-), annotated as α subunits of an acetoin oxidoreductase, which could allow the utilization of acetoin.

Diacetyl can be used in a similar way after preliminary conversion to acetoin. Genomic evidence also confirms this conversion capacity with the presence of genes that enable this transformation, such as diacetyl reductase (EC 1.1.1.304) and acetoin reductase (EC 1.1.1.303) [39].

As regards polymers (Fig. 1F), in *R. palustris* 42OL, the use of dextrins as a carbon source can be explained by the presence of specific enzymes for the metabolism of maltodextrins, both linear and branched. In particular, the following have been identified in the genome: maltodextrin phosphorylase (*malP*, EC 2.4.1.1), which progressively degrades α-1,4 chains, releasing glucose-1-phosphate; α-glucosidase (*palH*, EC 3.2.1.20), which hydrolyses terminal oligosaccharides to produce free glucose; and glycogen debranching enzyme (*glgX*_2, EC 3.2.1.68), which breaks the α-1,6-glycosidic bonds of the branches. In addition to these, *glgE1* (EC 2.4.99.16) is involved in the reprocessing of α-glucans and maltose-1-phosphate, linking dextrin metabolism with central metabolic pathways [20].

Finally, although the genome of *R. palustris* 42OL contains numerous ABC transporters for amino acids and specific systems for polyamines, these compounds are used very rarely as a carbon source. This is probably because amino acids, amines, and amides are primarily used as a nitrogen source, and the carbon skeleton is not effectively channeled into central metabolism due to incomplete or poorly active catabolic pathways [40]. Only a few compounds, such as histidine, methionine, glucuronamide, and octopamine, have supported measurable growth under AnL conditions, where light energy compensates for the unprofitability of their catabolism.

3.2.2 Nitrogen Sources Utilization Profile

Fig. 2 shows the utilization of different nitrogen sources by *R. palustris* 42OL under three different conditions: AeL, AeD, and AnD, using the Biolog® PM3B plate. In this case, the AnL condition was not included, as in this metabolic strategy the microorganism can fix molecular nitrogen, making it impossible to discriminate the contribution of individual nitrogen substrates [3,4]. The nitrogen sources tested were divided into four categories: amino acids (Fig. 2A), peptides (Fig. 2B), inorganic compounds (Fig. 2C) and other compounds (Fig. 2D).

Regarding amino acids (Fig. 2A), phenotypic analysis shows that the microorganism can use only a limited number of substrates as a source of nitrogen, with marked differences depending on the metabolic condition. In aerobic conditions (AeL and AeD), high activity is observed towards L-alanine, L-asparagine, L-glutamine, L-leucine, D-

alanine, D-asparagine and L-pyroglutamic acid, while D-asparagine and L-leucine are also metabolized in AnD. Particularly interesting is the case of L-histidine, which is used exclusively in AeL but not in AeD, although both conditions share the absence of photosynthesis. This result suggests that light may promote the activation of specific pathways for the transport and/or assimilation of histidine, modulating its use as a source of nitrogen; however, this hypothesis requires further verification. In AnD, in addition to the amino acids common to aerobic conditions, L-isoleucine, L-phenylalanine, D-glutamic acid and L-lysine are also metabolized.

Among the peptides tested as a source of nitrogen (Fig. 2B), Ala-Leu was the only one to be stably metabolized under all conditions, although with very low consumption in AeD. Ala-Gly is used consistently only in aerobic conditions (AeL and AeD), while Ala-Thr and Gly-Glu are metabolized exclusively in AnD. Gly-Gln also shows high consumption in AnD, accompanied by significant activity in AeD, while dipeptides such as Ala-Gln, Gly-Asn, Gly-Met, and Met-Ala show selective metabolism in AeD and are little or not at all used in other conditions. The differences observed between AeD and AeL cannot be attributed to photosynthetic activity, which is repressed by the presence of oxygen, but may depend on several factors. It is possible, for example, that light acts as an environmental signal triggering transcriptional and post-transcriptional regulatory mechanisms that modulate the expression of genes involved in nitrogen metabolism [41,42]. Furthermore, the concomitant presence of light and oxygen could promote the formation of reactive oxygen species (ROS), responsible for oxidative stress and specific cellular responses that could influence peptide transport and catabolism [43]. Finally, secondary physical effects cannot be ruled out, such as a slight increase in temperature due to light or local variations in the availability of dissolved oxygen, which could alter the physiological state of the cells.

Within the inorganic compounds (Fig. 2C), NH_4^+ represents the preferred nitrogen source, showing high and similar metabolic activities in all conditions analyzed. Nitrite (NO_2^-) is only used in AeL and AeD, while nitrate (NO_3^-) is not metabolized in any condition. The use of NH_4^+ in AnD, compared to the lack of use of nitrite and nitrate, although these compounds are known as potential sources of nitrogen, can be explained by considering the different chemical nature of the molecules. In fact, NH_4^+, being already in reduced form, is directly assimilated by the microorganism through the GS/GOGAT enzyme system, without the need for further reduction processes. On the contrary, the metabolism of nitrite and nitrate requires their preliminary conversion into ammonium, a

process that involves considerable consumption of reducing equivalents [44]. Under AnD conditions, where cellular metabolism does not have sufficient reducing power, these processes do not occur and, as a result, nitrite and nitrate are not utilized. This behavior highlights how the availability of energy and reducing power is a determining factor in the choice and exploitation of different nitrogen sources by *R. palustris* 42OL.

Finally, the category of other compounds (Fig. 2D) includes a heterogeneous set of nitrogenous organic molecules not included in the previous categories. In general, the utilization pattern appears similar in the two aerobic conditions, with some exceptions: histamine (aromatic biogenic amine) and xanthine (purine base) are metabolized only in AeL, while guanosine (purine nucleoside) and formamide (simple primary amide) are metabolized exclusively in AeD. In aerobiosis, *R. palustris* 42OL also shows a high capacity to metabolize various ureide derivatives (urea, allantoin, parabenic acid and alloxan) and amide derivatives (acetamide, glucuronamide and DL-lactamide), while biuret (another ureide derivative) is used only in AnD.

As regards amino sugars, under aerobic conditions, strong metabolic activity is observed towards D-galactosamine and D-mannosamine, weaker towards D-glucosamine, while N-acetylated forms are not used. Among the amines, in addition to histidine, activity is observed in AnD with methylamine and N-amylamine. Nucleosides and nitrogenous bases also exhibit selective behavior: xanthine is used only in AeL, guanosine weakly under aerobic conditions, guanine shows limited consumption in aerobiosis, while uracil is metabolized significantly in AnD.

None of the non-proteinogenic amino acids are used in AnD. In aerobiosis, however, γ-aminobutyric acid (GABA) emerges as the most efficiently metabolised substrate, together with ε-aminocaproic acid. Also notable is δ-amino-N-valeric acid, which is used significantly in both aerobic conditions, with greater activity in AeD than in AeL.

A particularly relevant aspect concerns the AnD condition in the nitrogen source utilization tests. In this case, the carbon source supplied was malic acid which, as shown by the specific tests on organic acids (Fig. 1B), is not metabolized under this condition. The growth observed with several organic nitrogen sources in AnD can therefore be explained by the fact that these compounds provide the microorganism with not only nitrogen but also carbon, thereby enabling a certain level of metabolic activity independent of malate [40]. The activity detected in the presence of NH_4^+ under the same condition could instead be attributed, in addition to its direct assimilation, to the

utilization of intracellular carbon reserves, such as PHB, which would have supported cellular metabolism.

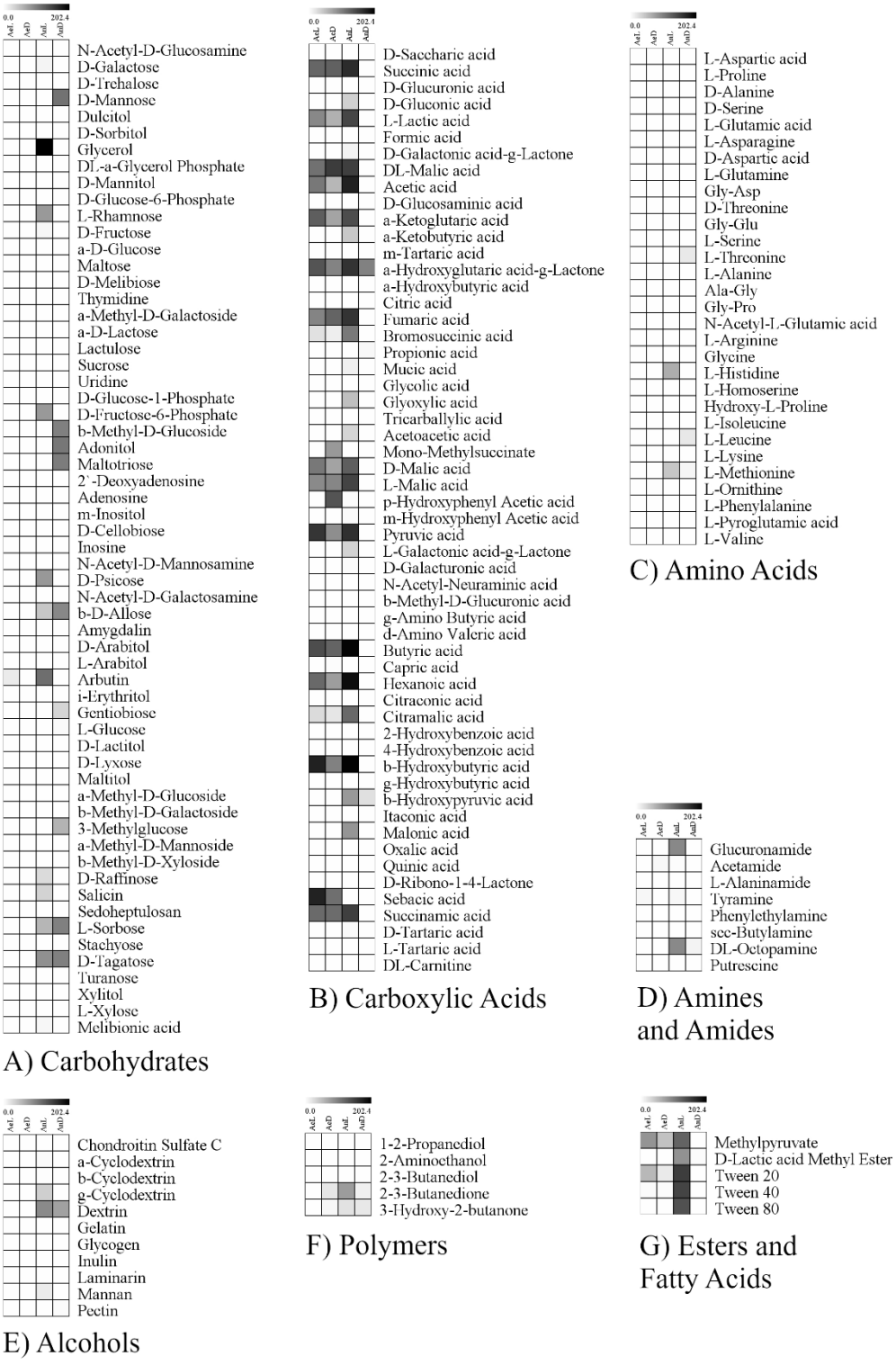

Figure 1. Carbon source utilization profile of *R. palustris* 42OL. Substrate utilization was tested under four metabolic conditions: anaerobiosis in the light (AnL), anaerobiosis in the dark (AnD), aerobiosis in the light (AeL), and aerobiosis in the dark (AeD). Carbon sources are grouped into seven categories: A) Carbohydrates, B) Carboxylic acids, C) Amino acids, D) Amines and amides, E) Alcohols, F) Polymers,

and G) Esters and fatty acids. The intensity of color indicates the level of substrate utilization, as measured by the reduction of tetrazolium dye during the assay.

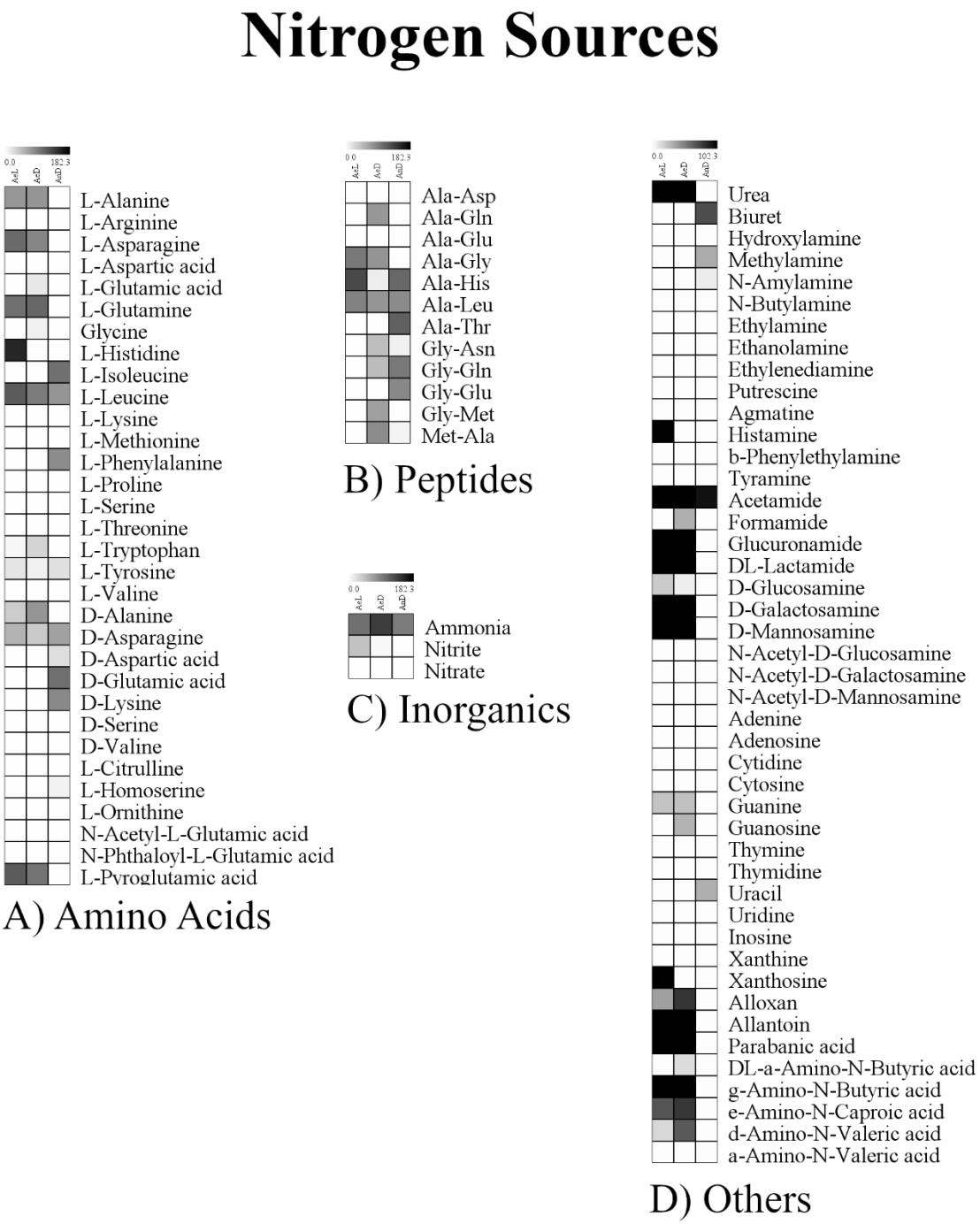

Figure 2. Nitrogen source utilization profile. Substrate utilization was tested under three metabolic conditions: anaerobiosis in the dark (AnD), aerobiosis in the light (AeL), and aerobiosis in the dark (AeD). Nitrogen sources are grouped into four categories: A) Amino acids, B) Peptides, C) Inorganics, and D) Others. The category Others comprises a heterogeneous set of nitrogenous organic molecules not included in the previous categories. The intensity of color indicates the level of substrate utilization, as measured by the reduction of tetrazolium dye during the assay.

4 Final Considerations and Future Developments

GEMs are fundamental tools in systems biology. They enable the large-scale description of a specific microbial strain's metabolism under investigation and allow for the exploration of its metabolic flexibility under different nutritional conditions. GEMs also provide a predictive framework for flux distributions. This framework is extremely valuable for guiding metabolic engineering strategies that aim to maximize the production of valuable industrial molecules.

This study tested two different approaches to initiating the reconstruction of a GEM for *R. palustris* 42OL. The automated approach enabled a fast generation of a draft model, but the subsequent manual curation phase proved challenging. The need to integrate and adjust a large number of automatically generated reactions may have introduced inconsistencies and biases, resulting in model outcomes that diverged from experimental growth behavior. In contrast, the fully manual approach was more time-consuming but ensured greater accuracy in the formulation of reactions, which were all correctly balanced for mass and charge and associated with reliable GPRs, which can also be used to develop GEM models of biologically related microorganisms. This approach produced a highly curated database of reactions and metabolites. Although this database is still incomplete, it provides a solid basis for describing the metabolic functions that *R. palustris* 42OL can perform. This database will subsequently be converted into a functional computational model. Furthermore, the use of BiGG identifiers instead of SEED numerical identifiers ensured human readability, facilitating curation and reducing interpretation time and errors.

The phenotypic profile obtained using Biolog® microplates confirmed the high metabolic versatility of R. palustris 42OL, highlighting differences in the assimilation of carbon and nitrogen sources in different metabolic regimes. The experimental data obtained from this profiling will be fundamental during the model validation phase. In particular, the results will be interpreted in binary form (0: no growth; 1: growth), and the model will be tested to verify its ability to reproduce growth *in silico* on simulated culture media designed to contain the specific carbon and nitrogen sources to be tested. Any discrepancies between the *in silico* predictions and the observed phenotype will be corrected through an iterative refinement process.

Once validated, the GEM will provide a versatile platform to simulate gene knockouts and identify metabolic bottlenecks, to optimize the production of biotechnologically relevant compounds, such as PHB and bio-H_2.

5 References

[1] Adessi, A., Spini, G., Presta, L., Mengoni, A., Viti, C., Giovannetti, L., Fani, R., & De Philippis, R. (2016). *Draft genome sequence and overview of the purple non-sulfur bacterium Rhodopseudomonas palustris 42OL*. Standards in Genomic Sciences, 11, 24. https://doi.org/10.1186/s40793-016-0145-y

[2] Li, M., Ning, P., Sun, Y., Luo, J., & Yang, J. (2022). *Characteristics and application of Rhodopseudomonas palustris as a microbial cell factory*. Frontiers in Bioengineering and Biotechnology, 10, 897003. https://doi.org/10.3389/fbioe.2022.897003

[3] Morrison, H. M., & Bose, A. (2025). *Purple non-sulfur bacteria for biotechnological applications*. Journal of Industrial Microbiology and Biotechnology, 52, kuae052. https://doi.org/10.1093/jimb/kuae052

[4] McKinlay, J. B. (2014). *Systems biology of photobiological hydrogen production by purple non-sulfur bacteria.* In D. Zannoni & R. De Philippis (Eds.), *Microbial bioenergy: Hydrogen production* (Advances in Photosynthesis and Respiration, Vol. 38, pp. 117–135). Springer. https://doi.org/10.1007/978-94-017-8554-9_7

[5] Harwood, C. S. (2020). *Iron-only and vanadium nitrogenases: Fail-safe enzymes or something more?* Annual Review of Microbiology, 74, 247–266. https://doi.org/10.1146/annurev-micro-022620-014338

[6] Adessi, A., & De Philippis, R. (2014). *Photosynthesis and hydrogen production in purple non-sulfur bacteria: Fundamental and applied aspects.* In D. Zannoni & R. De Philippis (Eds.), *Microbial bioenergy: Hydrogen production* (Advances in Photosynthesis and Respiration, Vol. 38, pp. 241–265). Springer. https://doi.org/10.1007/978-94-017-8554-9_12

[7] Ghosh, S., Dairkee, U. K., Chowdhury, R., & Bhattacharya, P. (2017). *Hydrogen from food processing wastes via photofermentation using purple non-sulfur bacteria (PNSB) – A review.* Energy Conversion and Management, 141, 299–314. https://doi.org/10.1016/j.enconman.2016.09.001

[8] Montiel-Corona, V., & Buitrón, G. (2021). *Polyhydroxyalkanoates from organic waste streams using purple non-sulfur bacteria.* Bioresource Technology, 323, 124610. https://doi.org/10.1016/j.biortech.2020.124610

[9] Adessi, A., Corneli, E., & De Philippis, R. (2017). *Photosynthetic purple non-sulfur bacteria in hydrogen producing systems: New approaches in the use of well-known and innovative substrates.* In P. Hallenbeck (Ed.), *Modern topics in the phototrophic prokaryotes* (pp. 217–239). Springer. https://doi.org/10.1007/978-3-319-46261-5_10

[10] Adessi, A., & De Philippis, R. (2014). *Photobioreactor design and illumination systems for H_2 production with anoxygenic photosynthetic bacteria: A review.* International Journal of Hydrogen Energy, 39(7), 3127–3141. https://doi.org/10.1016/j.ijhydene.2013.12.084

[11] Keskin Gundogdu, T., Akboncuk, M. B., & Azbar, N. (2014). *Biohydrogen production via a novel immobilized cell bioreactor.* Biofuels, 5(6), 595–603. https://doi.org/10.4155/bfs.13.48

[12] Monroy, I., & Buitrón, G. (2020). *Production of polyhydroxybutyrate by pure and mixed cultures of purple non-sulfur bacteria: A review.* Journal of Biotechnology, 317, 39–47. https://doi.org/10.1016/j.jbiotec.2020.04.012

[13] Tec-Campos, D., Posadas, C., Tibocha-Bonilla, J. D., Thiruppathy, D., Glonek, N., Zuñiga, C., Zepeda, A., & Zengler, K. (2023). *The genome-scale metabolic model for the purple non-sulfur bacterium Rhodopseudomonas palustris Bis A53 accurately predicts phenotypes under chemoheterotrophic, chemoautotrophic, photoheterotrophic, and photoautotrophic growth conditions.* PLOS Computational Biology, 19(8), e1011371. https://doi.org/10.1371/journal.pcbi.1011371

[14] Haggart, C. R., Bartell, J. A., Saucerman, J. J., & Papin, J. A. (2011). *Whole-genome metabolic network reconstruction and constraint-based modeling.* In D. Jameson, M. Verma, & H. V. Westerhoff (Eds.), *Methods in enzymology* (Vol. 500, pp. 411–433). Academic Press. https://doi.org/10.1016/B978-0-12-385118-5.00021-9

[15] Navid, A., Jiao, Y., Wong, S. E., & Pett-Ridge, J. (2019). *System-level analysis of metabolic trade-offs during anaerobic photoheterotrophic growth in Rhodopseudomonas palustris.* BMC Bioinformatics, 20(1), 233. https://doi.org/10.1186/s12859-019-2844-z

[16] Chowdhury, N. B., Alsiyabi, A., & Saha, R. (2022). *Characterizing the interplay of Rubisco and nitrogenase enzymes in anaerobic-photoheterotrophically grown Rhodopseudomonas palustris CGA009 through a genome-scale metabolic and expression model.* Microbiology Spectrum, 10(6), e01463-22. https://doi.org/10.1128/spectrum.01463-22

[17] Bianchi, L., Mannelli, F., Viti, C., Adessi, A., & De Philippis, R. (2010). *Hydrogen-producing purple non-sulfur bacteria isolated from the trophic lake Averno (Naples, Italy).* International Journal of Hydrogen Energy, 35(22), 12216–12223. https://doi.org/10.1016/j.ijhydene.2010.08.038

[18] Brettin, T., Davis, J. J., Disz, T., Edwards, R. A., Gerdes, S., Olsen, G. J., Olson, R., Overbeek, R., Parrello, B., Pusch, G. D., Shukla, M., Thomason, J. A., Stevens, R., Vonstein, V., Wattam, A. R., & Xia, F. (2015). *RASTtk: A modular and extensible implementation of the RAST algorithm for building custom annotation pipelines and annotating batches of genomes.* Scientific Reports, 5, 8365. https://doi.org/10.1038/srep08365

[19] Faria, J. P., Liu, F., Edirisinghe, J. N., Gupta, N., Seaver, S. M. D., Freiburger, A. P., Zhang, Q., Weisenhorn, P., Conrad, N., Zarecki, R., Song, H.-S., DeJongh, M., Best, A. A., Cottingham, R. W., Arkin, A. P., & Henry, C. S. (2023). *ModelSEED v2: High-throughput genome-scale metabolic model reconstruction with enhanced energy biosynthesis pathway prediction.* bioRxiv. https://doi.org/10.1101/2023.10.04.556561

[20] Kanehisa, M., Furumichi, M., Tanabe, M., Sato, Y., & Morishima, K. (2017). *KEGG: New perspectives on genomes, pathways, diseases and drugs.* Nucleic Acids Research, 45(D1), D353–D361. https://doi.org/10.1093/nar/gkw1092

[21] The UniProt Consortium. (2015). *UniProt: A hub for protein information.* Nucleic Acids Research, 43(D1), D204–D212. https://doi.org/10.1093/nar/gku989

[22] King, Z. A., Lu, J., Dräger, A., Miller, P., Federowicz, S., Lerman, J. A., Ebrahim, A., Palsson, B. Ø., & Lewis, N. E. (2016). *BiGG Models: A platform for integrating, standardizing and sharing genome-scale models.* Nucleic Acids Research, 44(D1), D515–D522. https://doi.org/10.1093/nar/gkv1049

[23] Mistry, J., Chuguransky, S., Williams, L., Qureshi, M., Salazar, G. A., Sonnhammer, E. L. L., Tosatto, S. C. E., Paladin, L., Raj, S., Richardson, L. J., Finn, R. D., & Bateman, A. (2021). *Pfam: The protein families database in 2021.* Nucleic Acids Research, 49(D1), D412–D419. https://doi.org/10.1093/nar/gkaa913

[24] Adessi, A., La Cava, E., & De Philippis, R. (2021). *Photosynthesis | Purple bacteria: Electron acceptors and donors*. In W. J. Lennarz & M. D. Lane (Eds.), *Encyclopedia of Biological Chemistry* (3rd ed., Vol. 2, pp. 305–314). Elsevier. https://doi.org/10.1016/B978-0-12-819460-7.00016-5

[25] Thiele, I., & Palsson, B. Ø. (2010). *A protocol for generating a high-quality genome-scale metabolic reconstruction.* Nature Protocols, 5, 93–121. https://doi.org/10.1038/nprot.2009.203

[26] Cantalapiedra, C. P., Hernández-Plaza, A., Letunic, I., Bork, P., & Huerta-Cepas, J. (2021). *eggNOG-mapper v2: Functional annotation, orthology assignments, and domain prediction at the metagenomic scale.* Molecular Biology and Evolution, 38(12), 5825–5829. https://doi.org/10.1093/molbev/msab293

[27] Ebrahim, A., Lerman, J. A., Palsson, B. Ø., & Hyduke, D. R. (2013). *COBRApy: COnstraints-based reconstruction and analysis for Python.* BMC Systems Biology, 7(1), 74. https://doi.org/10.1186/1752-0509-7-74

[28] Caspi, R., Billington, R., Keseler, I. M., Kothari, A., Krummenacker, M., Midford, P. E., Ong, W. K., Paley, S., Subhraveti, P., & Karp, P. D. (2020). *The MetaCyc database of metabolic pathways and enzymes: A 2019 update.* Nucleic Acids Research, 48(D1), D445–D453. https://doi.org/10.1093/nar/gkz862

[29] Lazzari, G. (2025). *Unraveling strain-specific metabolic diversity using genome-scale models: Development of computational methods and applications* [Doctoral dissertation, University of Verona]. UNITeSi. https://hdl.handle.net/20.500.14242/202822

[30] Brown, B., Wilkins, M., & Saha, R. (2022). *Rhodopseudomonas palustris: A biotechnology chassis. Biotechnology Advances, 60*, 108001. https://doi.org/10.1016/j.biotechadv.2022.108001

[31] Greetham, D. (2014). *Phenotype microarray technology and its application in industrial biotechnology. Biotechnology Letters, 36*(6), 1153–1160. https://doi.org/10.1007/s10529-014-1481-x

[32] Capson-Tojo, G., Batstone, D. J., Grassino, M., Vlaeminck, S. E., Puyol, D., Verstraete, W., Kleerebezem, R., Oehmen, A., Ghimire, A., Pikaar, I., Lema, J. M., & Hülsen, T. (2020). *Purple phototrophic bacteria for resource recovery: Challenges and opportunities. Biotechnology Advances, 43*, 107567. https://doi.org/10.1016/j.biotechadv.2020.107567

[33] Pemberton, J. M., Horne, I. M., & McEwan, A. G. (1998). *Regulation of photosynthetic gene expression in purple bacteria. Microbiology, 144*(2), 267–278. https://doi.org/10.1099/00221287-144-2-267

[34] Madigan, M. T., & Jung, D. O. (2009). An overview of purple bacteria: Systematics, physiology, and habitats. In C. N. Hunter, F. Daldal, M. C. Thurnauer, & J. T. Beatty (Eds.), *The purple phototrophic bacteria* (pp. 1–15). Springer. https://doi.org/10.1007/978-1-4020-8815-5_1

[35] Ali, S., Khan, S. A., Hamayun, M., & Lee, I.-J. (2023). The recent advances in the utility of microbial lipases: A review. *Microorganisms, 11*(2), 510. https://doi.org/10.3390/microorganisms11020510

[36] Bornscheuer, U. T. (2002). *Microbial carboxyl esterases: Classification, properties and application in biocatalysis. FEMS Microbiology Reviews, 26*(1), 73–81. https://doi.org/10.1111/j.1574-6976.2002.tb00503.x

[37] Chandel, N. S. (2021). *Lipid metabolism. Cold Spring Harbor Perspectives in Biology, 13*(10), a040576. https://doi.org/10.1101/cshperspect.a040576

[38] Pohanka, M. (2020). D-lactic acid as a metabolite: Toxicology, diagnosis, and detection. *BioMed Research International, 2020*, 3419034. https://doi.org/10.1155/2020/3419034

[39] Xiao, Z., & Xu, P. (2007). Acetoin metabolism in bacteria. *Critical Reviews in Microbiology, 33*(2), 127–140. https://doi.org/10.1080/10408410701364604

[40] Rubin, C. A., & Madigan, M. T. (1986). Amino acid and ammonia metabolism by the halophilic nonsulfur purple bacterium *Rhodospirillum salexigens. FEMS Microbiology Letters, 34*(1), 73–77. https://doi.org/10.1111/j.1574-6968.1986.tb01352.x

[41] Alfonso, M., Perewoska, I., & Kirilovsky, D. (2001). *Redox control of ntcA gene expression in* Synechocystis *sp. PCC 6803: Nitrogen availability and electron transport regulate the levels of the NtcA protein. Plant Physiology, 125*(2), 969–981. https://doi.org/10.1104/pp.125.2.969

[42] Ohlendorf, R., & Möglich, A. (2022). *Light-regulated gene expression in bacteria: Fundamentals, advances, and perspectives.* Frontiers in Bioengineering and Biotechnology, 10, 1029403. https://doi.org/10.3389/fbioe.2022.1029403

[43] Zeller, T., & Klug, G. (2006). *Thioredoxins in bacteria: Functions in oxidative stress response and regulation of thioredoxin genes. Naturwissenschaften, 93*(6), 259–266. https://doi.org/10.1007/s00114-006-0106-1

[44] Leigh, J. A., & Dodsworth, J. A. (2007). *Nitrogen regulation in bacteria and archaea. Annual Review of Microbiology, 61*, 349–377. https://doi.org/10.1146/annurev.micro.61.080706.093409

PART IV

General Conclusions

Production of waste is one of the main consequences of the linear economic model that has been prevalent throughout the 20th century and still is today. The volume and type of waste generated have increased steadily in recent decades, driven by economic development and the dogma on which it is based: extracting raw materials from the environment, transforming them into finished products, and finally disposing of them at the end of their useful life. The situation is further exacerbated by the fact that many products placed on the market have an extremely short life cycle, being designed for single use and destined primarily for landfill.

The circular economy aims to reverse this logic by extending the life cycle of products, both consumer goods and by-products of production processes, to reduce waste volumes, and consequently the extraction of raw materials and their associated environmental impact. Biorefineries are currently the most concrete tool for promoting the circularization of the economy in this context: they integrate biological, chemical, and physical processes that convert biomass, particularly agro-industrial waste, into a variety of chemical products, biomaterials, and energy. Microorganisms are the "engine" of these systems thanks to their ability to transform complex substrates into valuable molecules or provide useful precursors for further synthesis processes. Therefore, developing and optimizing biotechnological processes that can convert waste biomass into valuable products is a key strategy for transitioning to a sustainable, circular economic model.

This doctoral thesis aimed to explore the potential of purple non-sulfur bacteria (PNSB) to produce biohydrogen (bio-H_2) and polyhydroxybutyrate (PHB) from various agro-industrial and food waste streams. The high metabolic versatility of these bacteria, combined with their ability to operate at ambient temperatures and pressures without the need for costly or hazardous chemical processes, makes them ideal candidates for use as "microbial factories" in biorefineries.

The first chapter of the Results section demonstrated the feasibility of using bread waste as a raw material for PHB production through a combined process of dark fermentation (DF) and photofermentation (PF). DF, conducted with *Lactobacillus amylovorus* DSM 20532, enriched the substrate with organic acids, mainly lactate, generating an effluent suitable for subsequent PF. The integration of the substrate with digestate from an anaerobic digestion plant also reduced the need for chemical additives, providing macro and micronutrients essential for PNSB growth. Among the six strains tested, *Cereibacter johrii* Pisa7 proved to be the most promising for PHB growth and accumulation and was selected for scale-up experiments in a 5 L photobioreactor

equipped with selected lighting. Despite the expected decrease in yield at a larger scale, the results obtained are in line with those reported in the literature for similar volumes, confirming the scalability and potential industrial applicability of the process.

The second chapter of the Results section addressed the valorization of second cheese whey (SCW), a by-product of the dairy industry, for the simultaneous production of bio-H_2 and PHB by *Rhodopseudomonas palustris* 42OL in an integrated DF/PF system. The DF, conducted with a co-inoculum of *Lactococcus lactis* MK L84 and *Lacticaseibacillus paracasei* MK L49, produced an effluent rich in lactate, demonstrating that pH control is a determining factor for process efficiency. This study also highlighted the crucial role of light quality, particularly the emission spectrum, in modulating bio-H_2 and PHB yields, confirming that the correct selection of wavelengths can significantly improve photosynthetic efficiency and PNSB performance.

Overall, the first two experimental chapters highlighted how the high compositional variability of agro-industrial wastewater makes it impossible to adopt a single approach to its valorization. Each effluent requires a tailor-made strategy that includes appropriate pre-treatment, the definition of optimal bioreactor operating conditions, and the targeted selection of microbial strains. Among the operating parameters, light quality emerges as one of the most important, and often most overlooked, factors, the optimization of which maximizes the use of light radiation by PNSB and, consequently, the overall efficiency of the process.

The third chapter initiated the reconstruction of a genome-scale metabolic model (GEM) for *R. palustris* 42OL. This laid the foundations for future in silico simulations aimed at guiding metabolic engineering interventions. Although the completely manual approach was more time-consuming than automated methods, it ensured accuracy in the formulation and balancing of reactions, as well as in the definition of gene-protein-reaction associations. Meanwhile, phenotypic characterization using Biolog® microplates confirmed the high metabolic versatility of *R. palustris* 42OL. This revealed significant differences in substrate utilization under various metabolic regimes, especially under anaerobic light (AnL) conditions. These conditions are highly relevant for the biosynthesis of high-value molecules. While the reconstruction work is ongoing, the obtained reaction database provides a solid foundation for continuing the model and its future validation. This will enable metabolic bottlenecks to be identified and support the rational design of optimization strategies for producing bio-H_2 and PHB in PNSB.

In conclusion, this thesis has expanded our knowledge of the processes involved in valorizing agro-industrial waste through PNSB. It has also demonstrated the feasibility of converting various effluents into bio-H_2 and PHB using integrated DF-PF systems. Looking ahead, research efforts should focus on conducting Life Cycle Assessments (LCAs) to understand and quantify the overall energy balance of the process in greater depth. These analyses will be crucial for identifying critical areas and developing strategies to enhance efficiency and minimize energy impact, potentially through integration with renewable sources. The integrated approach combining experimentation, modelling, and environmental analysis, as outlined in this thesis, could serve as a reference for developing sustainable biorefineries that fully align with the principles of the circular economy.

PART V

Appendix

Chapter I

Recent Advances in Dark Fermentative Hydrogen Production from Vegetable Waste: Role of Inoculum, Consolidated Bioprocessing, and Machine Learning

Devu Pengadeth[1], Nitai Basak[1], Luca Bernabò[2], and Alessandra Adessi[2]

[1] Department of Biotechnology, Dr. B R Ambedkar National Institute of Technology Jalandhar, Jalandhar 144 008, India.

[2] Department of Agriculture, Food, Environment and Forestry (DAGRI), University of Florence, Piazzale delle Cascine, 18, 50144 Florence, Italy.

[*] Correspondence: basakn@nitj.ac.in

Manuscript published in **Environmental Science and Pollution Research** (6 December 2024)

https://doi.org/10.1007/s11356-024-35668-7

Abstract

Waste-centred-bioenergy generation have been garnering interest over the years due to environmental impact presented by fossil fuels. Waste generation is an unavoidable consequence of urbanization and population growth. Sustainable waste management techniques that are long term and environmentally benign are required to achieve sustainable development. Energy recovery from waste biomass via dark fermentative hydrogen production is a sustainable approach to waste management. Vegetable waste is generated in plenty over the food supply chain and being a rich source of carbon and other nutrients it has been studied for production of biohydrogen. This review aims to offer a comprehensive overview on the potential of vegetable waste as a feedstock for dark fermentative biohydrogen production. The hydrogen output from dark fermentative process is lower and additional strategies are required to improve the production. This review addresses the challenges generally encountered during dark fermentative hydrogen production using vegetable waste and the importance of methods such as bioaugmentation and application of extremophiles for process enhancement. The role of machine learning in the field of biohydrogen production is briefly discussed. The application of dark fermentative effluents for secondary valuable product generation and its contribution to the biohydrogen biorefinery is discussed as well.

Keywords

Bioaugmentation; biohydrogen; extremophiles; inhibitors; pretreatment; single-pot bioconversion

Abbreviations

ANFIS, Adaptive Neuro-Fuzzy Interference System; ANN, Adenosine triphosphate; ATP, Artificial neural network; CBP, Chemical oxygen demand; COD, Consolidated bioprocessing; Fd, Ferredoxin; FVW, Fruit and vegetable waste; GA, Genetic algorithm; GDOC, Groundnut deoiled cake; GHGs, Greenhouse gases; LAB, Lactic acid bacteria; MEC, Microbial electrolysis cell; MFC, Microbial fuel cell; MKLMA, Microbial kinetic with Levenberg–Marquardt; ML, Machine learning; MLPANN, Multilayer perception artificial neural network; NADP, Nicotinamide adenine dinucleotide phosphate; PHA, Polyhydroxyalkanoates; RF, Random forests; RSM, Response surface methodology; SVM, Support vector machines; VFA, Volatile fatty acids; VS, Volatile solids.

1. Introduction

Waste generation, specifically food waste, is an inevitable consequence of urbanization and anthropogenic activities. More than US$1 trillion worth of food is wasted every year, leading to economic and habitat loss due to food loss and conversion of natural ecosystems to agricultural land, respectively. The waste biomass being generated has a lasting effect on the environment, with food waste contributing about 8 to 10% of greenhouse gas (GHG) emissions. The food waste generated contains up to 62% fruit and vegetable waste (by mass), and these waste materials are generally subject to either open dumping and landfilling or are used as animal feed (United Nations Environment Programme 2024). Although these practices make use of the waste to a certain level, the environmental impact associated with their management still remains. Landfilling generates large amounts of methane, a potent GHG with 28 times greater global warming potential than carbon dioxide over a 100-year period (IEA 2024). The anaerobic decay of the organic wastes in the landfill leads to methane generation and its release to the environment. It has been estimated that up to 11% of anthropogenic CH_4 emissions occur from landfills (Singh et al. 2018; Kaza et al. 2018). Along with the landfill gas generation, the effluent generated from the decay can contaminate groundwater and could be a breeding point for potential disease-causing agents.

With the advent of the waste-centered circular economy approach, waste biomass is viewed as a nutrient-rich resource rather than a harmful byproduct. Waste generated in different sectors of the economy is utilized as a feedstock for the production of valuable products. This approach to waste remediation enables the establishment of sustainable waste management practices that are longer-term and ecofriendly. Vegetable waste has been studied for its potential as a feedstock for generation of diverse commercially important products such as biochar; bioactive compounds (pectin); bioenergy (biohydrogen, biomethane, and bioethanol); and biofertilizers. Biohydrogen, the carbon neutral and energy dense (143 GJ/tonne) bioenergy source, is produced from vegetable waste by dark and photo fermentative process with an anaerobic microorganism (Jayachandran et al. 2022). The gross calorific energy value of mixed vegetable waste (comprising of beetroot, broad beans, banana plantain, cabbage green beans onion, okra, potato, radish, and tomato) is 18.92 MJ/Kg (Prem Ananth Surendran and Shanmugam 2021), making it an efficient feedstock for biohydrogen production. In theory, the dark fermentative route can generate 20.83 mol H_2 from 1 kg COD (chemical oxygen demand) of vegetable waste with an energy output of 5906.97 kJ (1.6 kWh) via the acetic acid

fermentation pathway (Dahiya et al. 2018). However, in reality, the yield is much lesser due to cell metabolic requirements and the distribution of energy for the generation of unwanted byproducts. Nevertheless, the biological route of hydrogen production has displayed promising results and is considered as a sustainable alternative to fossil fuels thereby enabling environmentally benign waste management and renewable energy generation.

Dark fermentative hydrogen production from vegetable waste has been widely studied over the years (Mohan et al. 2009; Mohanakrishna et al. 2010a). The research in this area has demonstrated the potential of vegetable waste as an efficient feedstock for hydrogen producers. However, the biohydrogen yield from vegetable waste is lower, and researchers have opted for numerous methods to improve it. The pretreatment of vegetable waste to improve the yield of simpler sugars is a common practice to enhance the hydrogen production. Methods such as chemical pretreatment, namely acid and alkaline treatment, hydrothermal treatment, and enzymatic hydrolysis have been studied (Kumar and Mohan 2018). Although these processes help to improve the total carbohydrate concentration available for hydrogen producers, the majority of the pretreatment techniques generate byproducts that inhibit the growth of microorganisms (Bundhoo and Mohee 2016). An additional detoxification process would be required to remove the inhibitors that reduce the quantity of hydrogen produced, rendering the overall process costly. The cost of operation, transportation of goods, and many other factors determine the successful commercial application of the fermentation process. The biomass-based microbial production of hydrogen cost is estimated to be INR 813/Kg, €2.5 to 5.5/Kg by the European Union, and the US Department of Energy (DOE) has put forth a target lesser than $2/Kg for hydrogen production with $8/kWh for storage (DST 2020; EU 2020; DOE 2018). The feedstock cost is a critical factor that impacts the overall production cost; the application of waste as a potential substrate could help reduce the overall cost. Therefore, the selection of cost-effective routes and strategies that would improve the hydrogen production is needed. Recently, bioaugmentation and application of mixed microbial cultures and extremophiles with diverse metabolic capabilities have demonstrated good results. Additionally, the integration of machine learning technology with biohydrogen production can help to better understand the critical process parameters.

This review explores the advantages and limitations associated with the use of vegetable waste as a feedstock for dark fermentative hydrogen production. The limitations associated with the pretreatment methods are briefly discussed, and the

application of strategies such as extremophiles, bioaugmentation, single-pot conversion, and mixed culture biotechnology for enhancement of hydrogen yield is extensively explored. The role of machine learning and its application to dark fermentation are discussed in the context of vegetable waste. Further, vegetable waste and its part in the waste-centred-biorefinery route for generation of valuable products are explored.

2. Dark fermentation: a brief introduction

Dark fermentative hydrogen production is a promising route to hydrogen generation due to its high production rate, low-cost nature, and ability to handle versatile substrates (Srivastava et al. 2021; Mohanakrishna et al. 2023). The theoretical yield of hydrogen through dark fermentation is dependent on the type of anaerobic microorganisms that are used (Mathews and Wang 2009). Depending upon the metabolic pathway and end product generated by the microorganisms, the hydrogen yield will change; with the acetate pathway generating 4 mol of H_2 and the butyrate pathway producing 2 mol of H_2 per mol of glucose, respectively (Eqs. (1) and (2)) (Ahmad et al. 2024). Obligate anaerobes such as *Clostridium acetobutylicum* utilize dark fermentation via glycolysis to breakdown glucose into pyruvate and NADH. The pyruvate formed is then oxidized into acetyl-CoA and CO_2 by pyruvate ferredoxin oxidoreductase. This step requires the reduction of a ferredoxin (Fd). Acetyl-CoA is converted to acetyl phosphate, which results in the formation of ATP and acetate. Hydrogen gas is generated by the activity of hydrogenase, which oxidizes the reduced ferredoxin to regenerate the oxidized ferredoxin (Tenca et al. 2011; Sevinç et al. 2012). Further, hydrogen is produced at very low partial pressures (< 60 Pa) from the NADH formed during the earlier glycolysis. NADH is oxidized by the Fd reduction and an NADH-ferredoxin reductase (Mathews and Wang 2009). Dark fermentation in facultative anaerobes like Enterobacter aerogenes follows the oxidative conversion of pyruvate into formate and acetyl-CoA by the activity of pyruvate formate lyase. Hydrogen gas is formed by the conversion of formate into CO_2 and H_2 by hydrogenase enzymes. Acetyl-CoA is converted into acetyl phosphate resulting in the formation of ATP and acetate (Sevinç et al. 2012; Jayachandran et al. 2022).

Acetate pathway:

$$C_6H_{12}O_6 + 2H_2O \rightarrow 2CH_3COOH + 2CO_2 + 4H_2 \quad \Delta G^\circ = -126.0 \text{ KJ/mol} \tag{1}$$

Butyrate pathway:

$$C_6H_{12}O_6 \rightarrow CH_3CH_2CH_2COOH + 2CO_2 + 2H_2 \quad \Delta G^\circ = -214.3 \text{ KJ/mol} \tag{2}$$

3. Vegetable waste for production of value-added-products

Vegetable waste is generated from different sectors of the food supply chain in the form of peels, stems, rotten residues, and damaged produce (Fig. 1). The waste generated contains high COD and carbohydrate content and can be used for the production of a wide variety of products of commercial value. Prem Ananth Surendran and Shanmugam (2021) reported that a mixed vegetable waste comprising beetroot, broad beans, banana plantain, cabbage, green beans, onion, okra, potato, radish, and tomato waste contains 6.37% total solids. The organic solids are further classified as 82.81% volatile solids (VS) and 17.19% ash. The total soluble COD and moisture content of the waste were 1.58 g COD/g VS and 93.63% making it an efficient substrate for biohydrogen production. Vegetable waste generated can have simpler (easily biodegradable) and complex composition (lignocellulosic) based on the source of waste. Since waste generated can vary from time to time, characterization or composition analysis of the feedstock (physical, chemical, or biological) is important for the digestion process. Understanding the physio-chemical characteristics such as total fixed solids, ash content, volatile solids, pH, moisture content, and measure of cellulose, hemicellulose, nitrogen, starch, lignin, organic carbon, COD level before the fermentation proceeds is important for the overall digestion process to be successful (Singh et al. 2012). These factors will greatly influence the metabolic pathways of the hydrogen producers and essentially the end-product of the fermentation. Variations in the initial pH, sugar content, and presence of nutrients can have a greater influence on the fermentation route, and in order for hydrogen production to be successful, a good grasp on these physio-chemical characteristics of the waste is essential. Hence, while working with vegetable waste, it is important to characterize the substrate before proceeding with the fermentation.

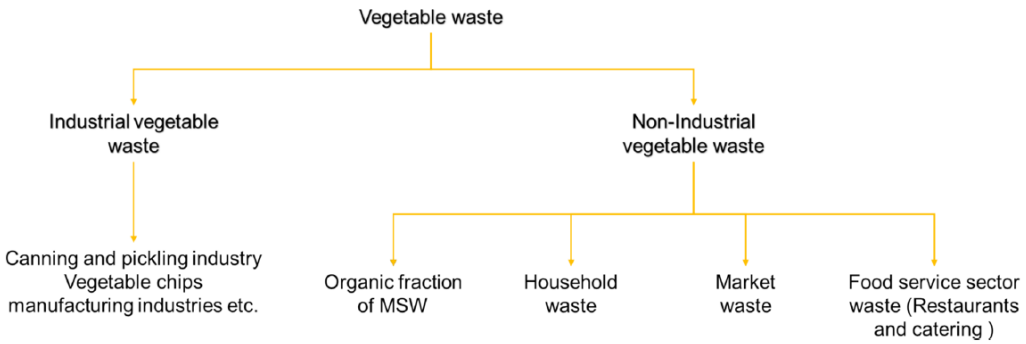

Figure 1. Schematic representation of different sources of vegetable waste

4. Limitations of feedstock pretreatment

The dark fermentative hydrogen production from vegetable waste has been extensively studied over the years (Panin et al. 2021; Martínez-Mendoza et al. 2022). The studies pertaining to vegetable waste have explored co-digestion with other feedstock, pretreatment of substrate, and nutrient supplementation to enhance the biohydrogen production. Feedstock pretreatment is commonly used to enhance the yield of simple sugars that in turn could be utilized by the hydrogen producers. The pretreatment methods are categorized into physical, mechanical, chemical, physio-chemical, and biological techniques. Briefly, the physical pre-treatment methods, such as thermal and microwave pre-treatment, treat the sample using different types of radiation, such as gamma rays, microwaves, and electron beams (Rajesh Banu et al. 2020). These treatments enhance the liquefaction of the substrate by heat generation, causing cell disruption and also breakage of the glycosidic linkages under standard pressure and temperature conditions. Mechanical pre-treatment, mainly ultrasonication, creates vacuum bubbles inside the substrate solutions due to pressure; these bubbles collapse, resulting in the phenomenon called cavitation that sends vibrations across the solution, causing cell disruption due to heat generation (Jiradechakorn et al. 2023). Chemical pre-treatment generally involves the hydrolysis of the substrate using concentrated or dilute acids (H2SO4 and HCl mainly) and alkalis (NaOH) (Rodríguez-Valderrama et al. 2020). Physio-chemical pre-treatments can be thermo-chemical, hot compressed water treatment, hydrothermal, and autoclave pre-treatment. Biological pre-treatments involve microbial and enzymatic treatment of the substrate to release the sugars to the solution for hydrogen producers to consume (Lo et al. 2009; Hitit et al. 2017). Microbial pretreatment can be carried out by either fungal or cellulolytic bacteria, while enzymes such as cellulases, hemicellulases, laccases, and xylanases are used for enzymatic treatment (Ni et al. 2006).

Among all these pre-treatment techniques, acid and alkaline hydrolysis are mostly used. In the majority of studies that dealt with food waste comprising of fruits, vegetables, and other organic wastes, acid and alkaline hydrolysis of the substrate have proven to be very efficient (Ramprakash and Muthukumar 2018). Acidic pre-treatments are carried out using hydrochloric acid (HCl), sulfuric acid (H_2SO_4), hydrogen peroxide (H_2O_2), and acetic acid (CH_3COOH) (Hafid et al. 2015). Acid hydrolysis of lignocellulosic vegetable waste (stems, stalk, and peels) is performed to efficiently remove the hemicellulose by breaking ether bonds in lignin/phenolic-carbohydrate complexes; the lignocellulosic components will breakdown into low energy compounds causing an increase in solubilisation and hydrolysis rate (Hafid et al. 2015). Whereas alkaline treatment using

sodium hydroxide (NaOH), calcium hydroxide (Ca (OH)2), or ammonia is mostly used for lignin hydrolysis. The hydrolysis takes place by the cleavage of ester bonds in the lignin/phenolic-carbohydrate complexes, followed by saponification of esters of the uronic bonds existing between hemicelluloses and lignin (Monlau et al. 2013). This causes the bulging of biomass, an increase in the internal surface area, and a reduction in the degree of polymerization. As a result, the lignin structure will be disrupted and can be separated from the raw material as a fraction rich in phenolic compounds. This increased pore size can facilitate the diffusion of hydrolytic enzymes (if combined with biological pre-treatment). Although acidic and alkaline pre-treatment improve hydrogen production by many folds, they become obsolete due to the neutralization of substrate required after the treatment and the by-products they generate. These pre-treatments of substrates also result in the formation of by-products like furan derivatives such as furfural and 5-hydroxymethylfurfural (5-HMF), phenolic compounds such as vanillin and syringaldehyde, and weak acids such as acetate (Bundhoo and Mohee 2016; Muñoz-Páez et al. 2019). These byproducts of pretreatments have often been observed to be toxic to microbial growth, decrease the hydrogen productivity, and reduce the quantity of hydrogen produced, rendering the process costly.

5. Strategies to improve hydrogen production from vegetable waste

5.1. Mixed microbial cultures

While considering dark fermentation from an economic point of view, optimum operational conditions are needed for the deployment of the biohydrogen process. Although pure strains have demonstrated substantial hydrogen production, for commercial application, pure cultures are not ideal. Vegetable waste generation vary as a result of geographical distribution, seasonal variations, and consumer demand. The pH of vegetable waste generally ranges between 4.0 and 4.8 (acidic range) (Tab. 1) and can be complex in nature. The lignocellulosic vegetable waste would require an initial hydrolysis treatment prior to fermentation. The accumulation of volatile fatty acids (VFA) upon fermentation can inhibit the bacteria activity as well. Hence, the characteristics of the inoculum are a key factor that influence the fermentation process. A mixed microbial culture with a broad enzymatic pool and metabolic capabilities is required to adapt with the complex waste and dynamic environment. Mixed cultures primarily anaerobic sludge have demonstrated efficient waste degradation and biohydrogen production from vegetable waste. The presence of diverse microbial communities in the mixed culture

offers efficient substrate utilization and ease in operational control and scale up (Mohanakrishna and Pengadeth 2024). However, the possibility of hydrogen consumption accompanied by methane and acetic acid generation by methanogenic and homoacetogenic bacteria is high. The unpredictable generation of unwanted byproducts in response to environmental changes is also plausible. This could be avoided by selective enrichment of microbial communities, but such techniques require additional energy input to the system.

Table 1. Dark fermentative hydrogen production from vegetable waste using mixed microbial inoculum

Feedstock	Composition of vegetable waste	Substrate characteristics	Inoculum	Comments	Hydrogen production	Reference
Composite vegetable waste	Tomato, potato, carrot, cabbage, brinjal, beet-root, okra, and coccinia residues	COD (with pulp): 57.6 g COD/L COD (without pulp): 52.0 g COD/L	Anaerobic mixed culture	Acetic acid (51.69 to 77.28%) and butyric acid were found in higher amounts	23.96 mmol/day	Mohan et al. 2009
FVW	Eggplant, carrot, tomato, cucumber, onion, radish, potato, capsicum, cabbage, pumpkin	COD: 111.5 ± 5.1 g/L Total carbohydrate: 78.9 ± 2.9 g/L pH: 4.6	Anaerobic digestate	Major organic acid was lactic acid, acetic acid, butyric acid, propionic acid and formic acid	49.5 NmL H_2/g VS_{fed}	Martínez-Mendoza et al. 2022
FVW	Radish, pepper, pumpkin, tomato, onion, potato, eggplant, carrot, cucumber, cabbage	COD: 9.5 g/L Total sugar: 0.818 g/L pH: 4.75 ± 0.1	Anaerobic mixed consortium	Acetic acid remained the dominant organic acid	10.23 mL $H_2/g_{vs\ added}$	
Fruit-vegetable and swine manure	Potato, Zucchini	TS: 133.0 ± 8.0 g/kg pH: 4.60 ± 0.10	Thermophilic inoculum	Acetic acid concentration (8.3 to 12.9 g acetic acid/kg	126 ± 22 mL H_2 g/ VS_{added}	Tenca et al. 2011
FVW	Radish, pepper, pumpkin, tomato, onion, potato, eggplant, carrot, cucumber, cabbage	—	Pre-treated inoculum	Acetic acid (13,023 mg/L) and isobutyric acid (7605 mg/L) were the major metabolites generated	23.53 NmL H_2 /g VS	
Vegetable waste	Leaf-shaped vegetable refuses and potato peels	TS%: 5.3 ± 0.1 VS%: 4.15 ± 0.07	Indigenous microflora	Mixed acid profile with acetate, lactate, butyrate etc	24 ± 2 L H_2/kg VS	Marone et al. 2014
Vegetable waste	Rotten potato, tomatoes, cabbage, carrot, brinjal, coccinia, okra, and beetroot	Soluble COD: 11.4 g/L Soluble reducing sugars: 2.8 g/L pH: 3.82	Anaerobic pre-treated inoculum	Acetic acid was dominant in the effluent	1.22 L H_2	Kumar and Mohan 2018
Vegetable waste + sewage	Unused/residual vegetables like tomato, potato, carrot, cabbage, brinjal, beet-root, okra, coccinia, etc	COD: 5.2 kg COD/m^3	Anaerobic mixed microflora	Acetic acid was dominate among other VFAs18.4	18.4 mmol H_2/day	Mohanakrishna et al. 2010a, b

*FVW fruit and vegetable waste

5.2. Extremophiles for single-pot bioconversion of substrate to hydrogen

The advancements in the field of biological hydrogen production have led to the transformation of biohydrogen production from a multi-vessel bioconversion process to a single-vessel approach termed consolidated bioprocessing (CBP). Although pre-treatment of vegetable waste helps to enhance the yield of hydrogen, the commercial-scale hydrogen production is hindered greatly by the high cost of substrate pre-treatment, followed by the removal of inhibitory compounds of pre-treatment. Hence, to decrease the cost of production, the identification and utilization of a suitable bacterium that can perform hydrolysis and biohydrogen production is needed. Thermophiles (60-75 °C) or hyperthermophiles (75-90 °C) that contain membrane-bound NADPH-dependent hydrogenase enzyme have been shown to produce higher yields of hydrogen. Thermophilic hydrogen fermentations using thermophilic bacteria such as *Caldicellulosiruptor saccharolyticus* (Pawar et al. 2013) and *Thermotoga maritima* (Saidi et al. 2018) have shown promising results for hydrogen production in comparison to the mesophilic ones. Higher yields under these conditions are due to the inactivation of hydrogen consumers such as methanogens and sulphate-reducing bacteria. Additionally, several thermophiles can produce hydrogen from both pentose and hexose sugars (Bibra et al. 2018).

Taking into account the capability of thermophilic strains in converting complex wastes to simple sugars and producing hydrogen, the single pot approach or CBP is more attractive in comparison with the multi-vessel dark fermentation (Fig. 2). In CBP, enzyme production, feedstock saccharification, hydrolysis, and fermentation all take place without the additional need for substrate pretreatment. This will not only reduce the use of costly pre-treatment methods but also offer the complete utilization of the substrate without waste generation. Bibra et al. (2018) in their study on biohydrogen production using thermophiles via single-pot bioconversion of prairie cordgrass demonstrated the use of a thermophilic consortium for hydrogen production from lignocellulosic biomass. The thermophilic consortium utilized both glucose and xylose at 60 °C and produced 2.2 mmol H_2/g of prairie cordgrass. Hasyim et al. (2011) studied the feasibility of producing biohydrogen from sago starch in wastewater using a thermophilic mixed culture enriched from a hot spring. Thermophiles such as *T. saccharolyticum*, *T. thermosulfurigenes*, and uncultured *Thermoanaerobacterium* sp. were the predominant hydrogen producers in the mixed thermophilic culture, and a maximum hydrogen yield of 422 mL H_2/g starch was obtained. Pawar et al. (2013) demonstrated biohydrogen production from wheat straw

hydrolysate using *Caldicellulosiruptor saccharolyticus* DSM 8903 and observed a maximum production rate of 5.2 L H_2/L/Day.

Therefore, the application of thermophilic bacterium or thermophilically derived enzymes that are thermostable for hydrogen production and pretreatment of vegetable waste can greatly contribute towards the commercial applicability of the fermentation process. Single-pot bioconversion or CBP is a promising area of research that can turn the tide in the fermentative biohydrogen production from lignocellulolytic-based waste. In-depth studies on the role of metabolic pathways associated with the extremophiles can help to understand the microbial behavior under specific conditions.

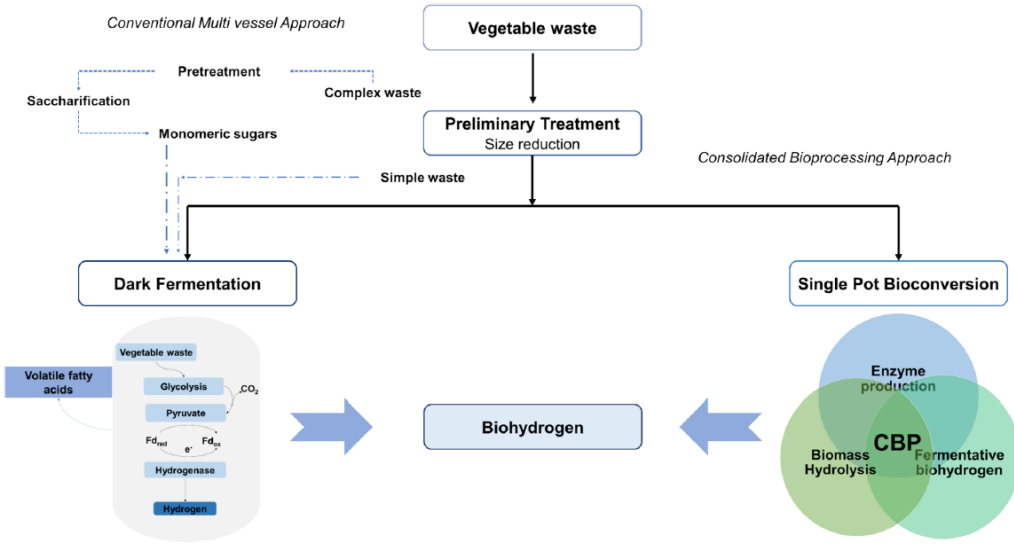

Figure 2. Schematic comparison of dark fermentation and single pot conversion process for biohydrogen production.

5.3. Indigenous microbial communities

Most of the studies on vegetable used an anaerobic inoculum that required a pre-treatment to inactivate the methanogens that consume hydrogen produced during fermentation. As aforementioned, substrate and inoculum pre-treatment require additional energy. Vegetable waste or any waste biomass in itself contains abundant indigenous microflora, which are capable of producing hydrogen. In nature, waste biomass self-decompose under room temperature if the required conditions are met (Marone et al. 2014). This principle allows natural selection to take place by controlling the reactor operating conditions. Biohydrogen production by self-fermentation without any substrate pre-treatment and inoculum but using the indigenous microbes within the substrate has been studied. Yokoyama et al. (2007) in the study on hydrogen production from a dairy cow waste slurry examined hydrogen production by batch culture using the

microflora naturally existing within the slurry in a temperature range of 37 to 85 °C. They observed hydrogen-producing moderate and extremophiles such as *Clostridium thermocellum* and *Caldanaerobacter subterraneus* in the slurry. If the suitable operating conditions are provided, the self-fermenting potential of waste biomasses can help to decrease the initial pretreatment cost associated with hydrogen production. In another study, Kim et al. (2011) demonstrated a similar simple method to naturally induce hydrogen production from food waste by controlling the operation temperature. They cultivated the food waste at a temperature range of 35 to 60 °C with a 5 °C interval without the addition of any inoculum or any pretreatment. Successful hydrogen production was achieved in the food waste incubated at a range of 50–60 °C with a hydrogen yield of 1.79 mol H_2/mol hexose added. Hydrogen producers such as *Clostridium sp*., *Acetanaerobacterium elongatum*, and *Caloramater indicus* were predominantly present in fermentation. Marone et al. (2014) demonstrated the potential of vegetable waste as a substrate and source for microflora for hydrogen production in their study on dark fermentation on two different substrates made of leaf-shaped vegetable refuse (V) and leaf-shaped vegetable refuse plus potato peels (VP). From batch experiments under two different mesophilic anaerobic conditions (28 °C and 37 °C), they were able to isolate and identify different hydrogen producers such as those belonging to the family *Enterobacteriaceae* (γ-proteobacteria) and *Streptococcaceae* (firmicutes). Apart from this, they also found four different genera namely *Pectobacterium*, *Raoultella*, *Rahnella*, and *Lactococcus,* that were not previously reported as HPB from glucose. A hydrogen yield of 1.6–2.2 mol H_2/mol glucose added was observed from low glucose concentration of 1 g/L.

From the literature overview (Shimizu et al. 2008; Kim et al. 2009), hydrogen production by self-fermentation is achieved without the addition of an external inoculum or by pre-treatment of substrate but by carefully controlling the important operating parameters such as pH and temperature to enhance the growth of hydrogen producers and suppressing the activity of hydrogen consumers. Apart from the dependency of hydrogen production on the operating pH and temperature, the microbial analysis, especially by Kim et al. (2011) revealed the temperature-based vulnerability of lactic acid bacteria (LAB) and the role of high temperature in suppressing the same. LAB are present in most forms of food products, and owing to their unique metabolic characteristics and antibiotic functions, they suppress the growth of other microbes and impede hydrogen production. Hence, by carefully monitoring the operating temperature and pH, self-fermentation of

vegetable waste can help in reducing the pre-treatment requirements and can help to enrich the indigenous microbes within the substrate to enhance the hydrogen production.

5.4. Bioaugmentation

Enrichment of the indigenous microbial communities helps to improve the hydrogen production, and the application of bioaugmentation in this context is advantageous. Bioaugmentation is the practice of supplementing the existing inoculum with specific microbes to improve the substrate utilization efficiency, promote microbial growth towards hydrogen production, and reduce the initial lag phase (Mohan et al. 2007). In the study by Marone et al. (2012) on hydrogen production from vegetable waste, enhancement of biohydrogen production was achieved by bioaugmentation with indigenous microbial communities, namely *Buttiauxella sp*. 4, *Rahnella sp*. 10, and *Raoultella sp*. 47. The individual strains enriched from vegetable waste was supplemented to the self-fermentative biohydrogen process. The study observed that all the individual bacterial inocula promoted hydrogen yield and the production rate. Indigenous microbial communities *Buttiauxella sp*. 4, *Rahnella sp*. 10, and *Raoultella sp*. 47 demonstrated potential for hydrogen production from cellulolytic hydrolysates as well. Yang et al. (2016) observed a shift in the metabolic pathway of native microbial communities towards hydrogen production upon bioaugmentation of anaerobic granular sludge with *Hydrogenispora ethanolica* LX-B. The hydrogen production improved within a range of 2.3 to 3.5 mmol H_2/gVS. In another study by Mohan et al. (2007), the effect bioaugmentation on enhancing the hydrogen production in an anaerobic sequencing batch biofilm reactor (AnSBBR) was studied using a selectively enriched anaerobic mixed consortium. Bioaugmentation improved the reactor performance while the microbes persisted in the system until the end of the operation, imparting specific functional characteristics to the native species. Villanueva-Galindo and Moreno-Andrade (2021) observed an improved hydrogen production of 84.5 mL H_2/g VS and decreased lag phase from food waste upon bioaugmentation of anaerobic sludge with Bacillus subtilis culture. Therefore, the application of bioaugmentation to the dark fermentative process can help in enhancing the performance of the hydrogen producers. A synthetic consortium with individual microbes performing selective functions can be developed by studying the properties of the augmented inoculum.

5.5 Machine learning in biohydrogen production

When biohydrogen production from complex feedstocks, such as vegetable waste, is studied, control over the process is challenged by the diverse and variable nature of the feedstock. When mixed cultures are used as the biocatalyst, the variability increases, and this would make it difficult to identify the operational parameters involved and the community dynamics existing within the system. Hence, mathematical models would fail to optimize the nonlinear and complex relationships that exist in dark fermentation. Modelling of biohydrogen is the cornerstone for scale-up and optimization of the dynamic biohydrogen generation system (Wang et al. 2021a; Kumar Sharma et al. 2022). Machine learning (ML) based statistical tools such as Artificial neural networks (ANNs), Random forests (RF), Adaptive neuro-fuzzy inference system (ANFIS), Genetic algorithm (GA), and Support vector machines (SVMs) have shown great potential in hydrogen-related technologies over the past few years (Tab. 2). The diverse algorithms enable accurate prediction of the expected outcomes by pooling through the databases (Kazemi et al. 2020; Hosseinzadeh et al. 2020; Vendruscolo et al. 2020).

ML, being a data-driven method, is independent of the complex interconnections that exist in the mathematical models. Unlike the conventional methods where the stoichiometry and background mechanisms are considered, ML's entire approach is based on publicly accessible online data or old recording of the procedure and being a data-driven method; the algorithms can handle the complex multivariate data and predict non-linear connection (Kumar Sharma et al. 2022). Apart from this, it maps the non-linear input–output connections and does not necessarily require a general understanding of stoichiometry or background mechanisms. ML algorithm-based biohydrogen prediction generally follows a trend. For a dark fermentative biohydrogen production from waste biomass, for example, vegetable waste, the initial inputs and the outputs of the fermentation are used to predict the performance, optimize, and predict the outcome of the process. Based on the objective of the process, the models (ANN, SVM, RF, and GA) with the help of the existing data available in literature will reduce the variables of the process and generate the expected results of the fermentation. Wang et al. (2021a) compared and evaluated three different modelling techniques, namely the multilayer perception artificial neural network (MLPANN), the response surface methodology (RSM), and the microbial kinetic with Levenberg–Marquardt algorithm (MKLMA) for dark fermentation. In the study, a robust paradigm was proposed for modelling the major metabolic intermediates during dark fermentation for biohydrogen production. From the study, it was conferred that with respect to the data, the MKLMA model requires a longer

Table 2. Different machine learning models used in biohydrogen production

ML algorithms	Function	Application in biohydrogen production	Reference
Support vector machine (SVM)	Nonlinear mapping to develop a model to train or classify data accurately	Hydrogen yield prediction and process optimization	Kazemi et al. 2020; Mahata et al. 2020; Hosseinzadeh et al. 2022
Random forest (RF)	Decision tree construction followed by forest development using bootstrap samples from original data source	Asses the change in microbial community and correlate parameters with biogas production Models for hydrogen production prediction	Vendruscolo et al. 2020; Bagherzadeh et al. 2021; Pandey et al. 2023
Artificial neural network (ANN)	Computing tools called neuron control the environment and backpropagation method predict the outcome of the process by making use of a large data pool	Predict, control, and monitor H_2 production, and hydrogen production rate Predict and monitor VFA production kinetic	Nasr et al. 2013; El-Shafie 2014; Hosseinzadeh et al. 2020; Wang et al. 2021b
Genetic algorithm (GA)	Stochastic search technique to evaluate multiple options at once	Global optimization in biohydrogen production Investigate effect of operational parameters on fermentation	Prakasham et al. 2011; Wang et al. 2021b; Pandey et al. 2023

computing time in comparison to the MLPANN model. The MLPANN model, being a soft computing approach, has the added advantage of being faster in implementing the kinetic correlations between the key metabolic intermediates.

In another study by Wang et al. (2021b) on dark fermentation, optimization of the process was demonstrated by a novel hybrid approach that combined ANNs with RSM. The methodology applied helped in the analysis of critical operational parameters such as the carbon sources (from potato peel wastes and starchy wastes); pH; microbial load on hydrogen production; concentration of the intermediate metabolites (acetic acid, propionic acid, etc.); and the metal cofactor Fe0. Apart from this, the hybrid model demonstrated the generation of 106.2 cm^3/g hydrogen under the optimal operational conditions. Mahata et al. (2020) in their study on the improvement of dark fermentative hydrogen production from organic wastes using acidogenic mixed consortia, used ML techniques such as ANN and SVM. The experimental results of biohydrogen production from starchy wastewater supplemented with groundnut de-oiled cake (GDOC) were analyzed by RSM, ANN, and SVM. From their studies, they demonstrated that the SVM model, a previously less explored model, had similar prediction capability in comparison with RSM and ANN. Apart from that, they combined the ML techniques with GA and particle swarm optimization (PSO) to estimate the optimal

process parameters. The SVM-based model showed a 2.1-fold hydrogen production in comparison to the unoptimized process.

ML algorithms offer potential as a faster prediction tool for biohydrogen production by taking into account the nonlinear interactions between the operational parameters. Models such as ANN that are simple and could imitate the structures of the biological neural networks will clarify the intricate connections that exist between numerous components of the fermentation process and would prove useful in the prediction of optimum operational conditions. The research in this field is in its nascent state and requires in-depth studies to contribute towards the optimization of process parameters. Additionally, research should be directed to studying the effect of inhibitors on fermentation, along with the development of the optimal process conditions for maximum yield of biohydrogen.

6. Limitations, future direction, and biohydrogen-biorefinery

In spite of having a high hydrogen production rate (192 m^3 $H_2/m^3 \cdot d$), dark fermentative biohydrogen production technology is not commercialized for bioenergy generation due to low hydrogen yield. The maximum hydrogen yield observed is around 2 mol H_2/mol hexose because of thermodynamic limitations, and it accounts for only 20% of substrate electrons. This would imply that 60-70% of electrons are trapped within the carboxylate end products and 10 to 20% electrons for cell growth (biomass-associated and utilization-associated electron) (Lee et al. 2022). Hence, considering the dark fermentative process from an economic perspective, the practical implementation of the biohydrogen production units would be costly. Therefore, post-hydrogen production from the carboxylate would play a major role in commercializing dark fermentation technology. The integration of microbial electrolysis cell (MEC) with dark fermentation can help to counter these challenges. MECs, being versatile technology, produce hydrogen in the cathodic compartment by making use of the carboxylate fraction of dark effluent in the anodic compartment (Magdalena et al. 2023). The anode colonized by exoelectrogenic bacterial communities capable of carboxylate metabolism would help to generate hydrogen with a maximum production rate of 18 m3 H2/m3-d. Up to 6 mol H2/mol hexose can be generated when MEC is combined with the dark fermentation process (Lee et al. 2022).

The VFA generated from the dark fermentation would serve as low-cost carbon source for microalgal cultivation and photo fermentative hydrogen production and as precursors

for the production of secondary metabolites such as polyhydroxyalkanoates (PHA), and 1,3-propanediol (1,3-PD) (Kora et al. 2023) (Fig. 3). Dark fermentative hydrogen production, although has higher production rate, yields lower hydrogen molecules in comparison with the photo fermentative route of hydrogen production. The fermentative effluent serves as a simpler carbon source for photo-fermentative bacteria such as the purple non-sulfur bacteria belonging to *Rhodobacteraceae* and *Rhodospirillaceae* family for hydrogen generation in the presence of light under anaerobic conditions (Rao and Basak 2022; Sen et al. 2024). Although photo-fermentative hydrogen production from VFAs have been explored, their dependency on sunlight can restrict their application. The residual carbon fraction of the effluent could also serve as the primary substrate for exoelectrogenic microbes in bioelectrochemical systems such as microbial fuel cells (MFC), bioelectricity production as well (Mohanakrishna et al. 2010b). Similarly, the effluent would be an efficient alternative to nutrient media for commercially relevant microalgal growth and biomass generation. Microalgal cultivation in the organic acid-rich effluent contributes greatly towards the vision of microalgae-centred-waste-biorefinery. Microalgae, the photosynthetic microorganism, is considered a powerhouse of lipids, carbohydrates, proteins, and other nutrients and has potential applications in the biodiesel, nutraceutical, and bioenergy fields, and would enable energy recovery and effluent treatment simultaneously. Several secondary metabolite productions occur from the harvested algal biomass, thereby setting off a chain of diverse product generation (Chiranjeevi and Venkata Mohan 2017). One of the most prominent routes to acidogenic effluent utilization is its application in the generation of PHAs, the emerging alternative to petroleum-based plastics (Martinez et al. 2016; Tamang and Nogueira 2021; Lagoa-Costa et al. 2022). The microbial generation of these polyesters has been extensively studied, and a PHA generation ranging between 30 and 70% have been observed from fermentative effluent by mixed and pure bacterial cultures namely *Bacillus tequilensis*, *Cupriavidus necator*, *Pseudomonas oleovorans*, *Alcaligenes eutrophus*, and many more (Venkateswar Reddy and Venkata Mohan 2012; Aremu et al. 2021; Khatami et al. 2022).

Hence, the integration of multiple unit operations can help in the profitability of the dark fermentative process. As aforementioned, the utilization of fermentative effluents, mixed microbial cultures, and extremophiles with diverse metabolic capabilities can improve the prospects of the process. However, further in-depth studies on the dynamics between the microbial communities and their influence on the end product generation is required. Although synergic interactions yield effective results, the presence of diverse

bacterial communities could also induce feedstock related competition and antagonism as well (Mohanakrishna and Pengadeth 2024). With the recent advancements in synthetic biology, the keystone species in the mixed cultures can be identified and could be further modelled to direct their metabolism towards hydrogen production by metabolic pathway manipulation. The development of synthetic cultures with known hydrogen producers would offer a better understanding of the intricate pathways involved in byproduct generation. Further studies on extremophiles and their integration with genetic engineering can help to develop bacterial strains capable of carrying out substrate hydrolysis and hydrogen production simultaneously to avoid the expensive pretreatment methods (Byrne et al. 2021). The addition of machine learning tools in biohydrogen processes has paved the way for researchers in understanding the process parameters and their influence on hydrogen production; however, the studies on ML pertaining to vegetable waste is scarce in the literature and need further exploration. The studies on hydrogen production from vegetable waste are mostly restricted to batch systems. However, for commercial deployment of production units, continuous fermentation set-ups are required, and research is needed in this direction.

Figure 3. Schematic diagram on biohydrogen biorefinery utilizing the acidogenic effluents from dark fermentation.

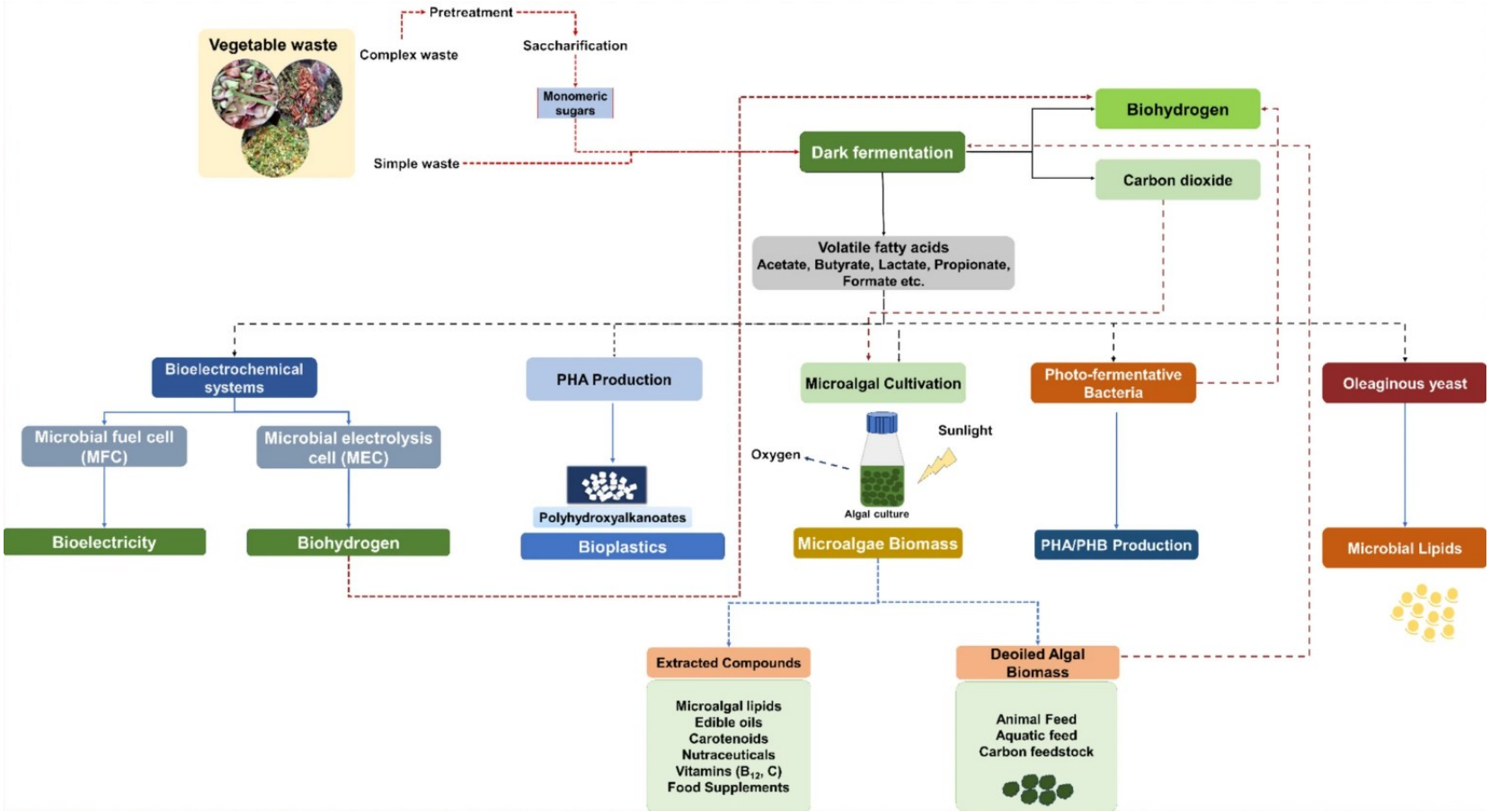

7. Conclusion

Dark fermentative hydrogen production from vegetable waste is an attractive solution for waste management and sustainable energy generation. This review explored the recent strategies to improve hydrogen production from vegetable waste with emphasis on bioaugmentation and mixed cultures. The advantages of extremophiles for the single-pot conversion of feedstock to hydrogen were reviewed. One of the major setbacks in dark fermentation is the formation of unwanted byproducts; the application of these effluents for secondary value-added products would help to improve the development of full-scale fermentation set-ups. With process integration, green hydrogen generation and its implementation within the framework of the circular bioeconomy could be achieved.

Acknowledgements

The authors are thankful to the Ministry of Education (MoE), Govt of India for bestowing the first author with the postgraduation fellowship. The authors are extremely grateful to the facilities and support provided by the Department of Biotechnology, Dr. B R Ambedkar National Institute of Technology, Jalandhar, India. The paper is a result of the existing collaboration in the frame of Memorandum of Understanding (MoU) Of Cultural and Scientific Cooperation between the Dr. B. R. Ambedkar National Institute of Technology, Jalandhar, India and the University of Florence, Italy.

Author contributions

Devu Pengadetha has contributed towards conceptualization and designing of the work, material preparation, data collection, analysis, and manuscript preparation. Nitai Basak has contributed towards conceptualization and designing of the work, data analysis, and manuscript preparation, revision of manuscript, and overall supervision of the project. Luca Bernabò has contributed for data analysis and revision of manuscript. Alessandra Adessi has contributed to the study's conception, design and revision of manuscript. All authors read and approved the final manuscript.

References

Ahmad A, Rambabu K, Hasan SW, Show PL, Banat F (2024) Biohydrogen production through dark fermentation: recent trends and advances in transition to a circular bioeconomy. *Int J Hydrogen Energy* 52:335–357. https://doi.org/10.1016/j.ijhydene.2023.05.161

Aremu MO, Ishola MM, Taherzadeh MJ (2021) Polyhydroxyalkanoates (PHAs) Production from volatile fatty acids (VFAs) from organic wastes by *Pseudomonas oleovorans*. *Fermentation* 7:287. https://doi.org/10.3390/fermentation7040287

Bagherzadeh F, Mehrani M-J, Basirifard M, Roostaei J (2021) Comparative study on total nitrogen prediction in wastewater treatment plant and effect of various feature selection methods on machine learning algorithms performance. *J Water Process Eng* 41:102033. https://doi.org/10.1016/j.jwpe.2021.102033

Bibra M, Kumar S, Wang J, Bhalla A, Salem DR, Sani RK (2018) Single pot bioconversion of prairie cordgrass into biohydrogen by thermophiles. *Bioresour Technol* 266:232–241. https://doi.org/10.1016/j.biortech.2018.06.046

Bundhoo MAZ, Mohee R (2016) Inhibition of dark fermentative biohydrogen production: a review. *Int J Hydrogen Energy* 41:6713–6733. https://doi.org/10.1016/j.ijhydene.2016.03.057

Byrne E, Björkmalm J, Bostick JP, Sreenivas K, Willquist K, Niel EdWJV (2021) Characterization and adaptation of *Caldicellulosiruptor* strains to higher sugar concentrations, targeting enhanced hydrogen production from lignocellulosic hydrolysates. *Biotechnol Biofuels* 14:210. https://doi.org/10.1186/s13068-021-02058-x

Chiranjeevi P, Venkata Mohan S (2017) Diverse acidogenic effluents as feedstock for microalgae cultivation: dual phase metabolic transition on biomass growth and lipid synthesis. *Bioresour Technol* 242:191–196. https://doi.org/10.1016/j.biortech.2017.04.059

Dahiya S, Kumar AN, Shanthi Sravan J, Chatterjee S, Sarkar O, Venkata Mohan S (2018) Food waste biorefinery: sustainable strategy for circular bioeconomy. *Bioresour Technol* 248:2–12. https://doi.org/10.1016/j.biortech.2017.07.176

DOE (2018) DOE hydrogen and fuel cell program. https://www.nrel.gov/docs/fy19osti/73353.pdf. Accessed 23 Aug 2024

DST (2020) Department of Science and Technology, India country status report on hydrogen and fuel cells. https://dst.gov.in/collationindias-hydrogen-fuel-cells-research-status-launched. Accessed 21 Aug 2024

El-Shafie A (2014) Neural network nonlinear modeling for hydrogen production using anaerobic fermentation. *Neural Comput Appl* 24:539–547. https://doi.org/10.1007/s00521-012-1268-8

EU (2020) A hydrogen strategy for a climate-neutral Europe. Communication from the commission to the European parliament, the council, the European economic and social committee and the committee of the regions

Hafid HS, Rahman NA, Md Shah UK, Baharudin AS (2015) Enhanced fermentable sugar production from kitchen waste using various pretreatments. *J Environ Manag* 156:290–298. https://doi.org/10.1016/j.jenvman.2015.03.045

Hasyim R, Imai T, O-Thong S, Sulistyowati L (2011) Biohydrogen production from sago starch in wastewater using an enriched thermophilic mixed culture from hot spring. *Int J Hydrogen Energy* 36:14162–14171. https://doi.org/10.1016/j.ijhydene.2011.04.211

Hitit ZY, Lazaro CZ, Hallenbeck PC (2017) Single stage hydrogen production from cellulose through photo-fermentation by a coculture of *Cellulomonas fimi* and *Rhodopseudomonas palustris*. *Int J Hydrogen Energy* 42:6556–6566. https://doi.org/10.1016/j.ijhydene.2016.12.035

Hosseinzadeh A, Zhou JL, Altaee A, Baziar M, Li D (2020) Effective modelling of hydrogen and energy recovery in microbial electrolysis cell by artificial neural network and adaptive network-based fuzzy inference system. *Bioresour Technol* 316:123967. https://doi.org/10.1016/j.biortech.2020.123967

Hosseinzadeh A, Zhou JL, Altaee A, Li D (2022) Machine learning modeling and analysis of biohydrogen production from wastewater by dark fermentation process. *Bioresour Technol* 343:126111. https://doi.org/10.1016/j.biortech.2021.126111

IEA (2024) Global methane tracker 2024. IEA, Paris. https://www.iea.org/reports/global-methane-tracker-2024. Accessed 23 Aug 2024

Jayachandran V, Basak N, De Philippis R, Adessi A (2022) Novel strategies towards efficient molecular biohydrogen production by dark fermentative mechanism: present progress and future perspective. *Bioprocess Biosyst Eng* 45:1595–1624. https://doi.org/10.1007/s00449-022-02738-4

Jiradechakorn T, Chuetor S, Kirdponpattara S et al (2023) Performance of combined hydrochemo-mechanical pretreatment of rice straw for bioethanol production. *Energy Rep* 9:180–185. https://doi.org/10.1016/j.egyr.2023.08.081

Kaza S, Yao LC, Bhada-Tata P, Van Woerden F (2018) What a waste 2.0: a global snapshot of solid waste management to 2050. *Urban Development*; © Washington, DC: World Bank. http://hdl.handle.net/10986/30317. Accessed 18 Aug 2024

Kazemi P, Giralt J, Bengoa C, Steyer J-P (2020) Data-driven fault detection methods for detecting small-magnitude faults in anaerobic digestion process. *Water Sci Technol* 81:1740–1748. https://doi.org/10.2166/wst.2020.026

Khatami K, Perez-Zabaleta M, Cetecioglu Z (2022) Pure cultures for synthetic culture development: next level municipal waste treatment for polyhydroxyalkanoates production. *J Environ Manag* 305:114337. https://doi.org/10.1016/j.jenvman.2021.114337

Kim D-H, Kim S-H, Shin H-S (2009) Hydrogen fermentation of food waste without inoculum addition. *Enzyme Microb Technol* 45:181–187. https://doi.org/10.1016/j.enzmictec.2009.06.013

Kim D-H, Wu J, Jeong K-W, Kim MS, Shin HS (2011) Natural inducement of hydrogen from food waste by temperature control. *Int J Hydrogen Energy* 36:10666–10673. https://doi.org/10.1016/j.ijhydene.2011.05.153

Kora E, Patrinou V, Antonopoulou G, Ntaikou I, Tekerlekopoulou AG, Lyberatos G (2023) Dark fermentation of expired fruit juices for biohydrogen production followed by treatment and biotechnological exploitation of effluents towards bioplastics and microbial lipids. *Biochem Eng J* 195:108901. https://doi.org/10.1016/j.bej.2023.108901

Kumar AN, Mohan SV (2018) Acidogenic valorization of vegetable waste for short chain carboxylic acids and biohydrogen production: influence of pretreatment and pH. *J Clean Prod* 203:1055–1066. https://doi.org/10.1016/j.jclepro.2018.08.198

Lagoa-Costa B, Kennes C, Veiga MC (2022) Influence of feedstock mix ratio on microbial dynamics during acidogenic fermentation for polyhydroxyalkanoates production. *J Environ Manag* 303:114132. https://doi.org/10.1016/j.jenvman.2021.114132

Lee H-S, Xin W, Katakojwala R, Mohan SV, Tabish NMD (2022) Microbial electrolysis cells for the production of biohydrogen in dark fermentation–a review. *Bioresour Technol* 363:127934. https://doi.org/10.1016/j.biortech.2022.127934

Lo Y-C, Saratale GD, Chen W-M, Bai M-D, Chang J-S (2009) Isolation of cellulose-hydrolytic bacteria and applications of the cellulolytic enzymes for cellulosic biohydrogen production. *Enzyme Microb Technol* 44:417–425. https://doi.org/10.1016/j.enzmictec.2009.03.002

Magdalena JA, Pérez-Bernal MF, Bernet N, Trably E (2023) Sequential dark fermentation and microbial electrolysis cells for hydrogen production: volatile fatty acids influence and energy considerations. *Bioresour Technol* 374:128803. https://doi.org/10.1016/j.biortech.2023.128803

Mahata C, Ray S, Das D (2020) Optimization of dark fermentative hydrogen production from organic wastes using acidogenic mixed consortia. *Energy Convers Manag* 219:113047. https://doi.org/10.1016/j.enconman.2020.113047

Marone A, Massini G, Patriarca C, Signorini A, Varrone C, Izzo G (2012) Hydrogen production from vegetable waste by bioaugmentation of indigenous fermentative communities. *Int J Hydrogen Energy* 37:5612–5622. https://doi.org/10.1016/j.ijhydene.2011.12.159

Marone A, Izzo G, Mentuccia L, Massini G, Paganin P, Rosa S, Varrone C, Signorini A et al (2014) Vegetable waste as substrate and source of suitable microflora for bio-hydrogen production. *Renew Energy* 68:6–13. https://doi.org/10.1016/j.renene.2014.01.013

Martinez GA, Rebecchi S, Decorti D, Domingos JMB, Natolino A, Daniel DR, Bertin L, Caria DP, Faya F (2016) Towards multipurpose biorefinery platforms for the valorisation of red grape pomace: production of polyphenols, volatile fatty acids, polyhydroxyalkanoates and biogas. *Green Chem* 18:261–270. https://doi.org/10.1039/C5GC01558H

Martínez-Mendoza LJ, Lebrero R, Muñoz R, García-Depraect O (2022) Influence of key operational parameters on biohydrogen production from fruit and vegetable waste via lactate-driven dark fermentation. *Bioresour Technol* 364:128070. https://doi.org/10.1016/j.biortech.2022.128070

Mathews J, Wang G (2009) Metabolic pathway engineering for enhanced biohydrogen production. *Int J Hydrogen Energy* 34:7404–7416. https://doi.org/10.1016/j.ijhydene.2009.05.078

Mohan SV, Mohanakrishna G, Veer Raghavulu S, Sarma PN (2007) Enhancing biohydrogen production from chemical wastewater treatment in anaerobic sequencing batch biofilm reactor (AnSBBR) by bioaugmenting with selectively enriched kanamycin resistant anaerobic mixed consortia☆. *Int J Hydrogen Energy* 32:3284–3292. https://doi.org/10.1016/j.ijhydene.2007.04.043

Mohan SV, Mohanakrishna G, Goud RK, Sarma PN (2009) Acidogenic fermentation of vegetable based market waste to harness biohydrogen with simultaneous stabilization. *Bioresour Technol* 100:3061–3068. https://doi.org/10.1016/j.biortech.2008.12.059

Mohanakrishna G, Pengadeth D (2024) Mixed culture biotechnology and its versatility in dark fermentative hydrogen production. *Bioresour Technol* 394:130286. https://doi.org/10.1016/j.biortech.2023.130286

Mohanakrishna G, Kannaiah Goud R, Mohan SV, Sarma PN (2010a) Enhancing biohydrogen production through sewage supplementation of composite vegetable based market waste. *Int J Hydrogen Energy* 35:533–541. https://doi.org/10.1016/j.ijhydene.2009.11.002

Mohanakrishna G, Mohan SV, Sarma PN (2010b) Utilizing acidrich effluents of fermentative hydrogen production process as substrate for harnessing bioelectricity: an integrative approach. *Int J Hydrogen Energy* 35:3440–3449. https://doi.org/10.1016/j.ijhydene.2010.01.084

Mohanakrishna G, Sneha NP, Rafi SM, Sarkar O (2023) Dark fermentative hydrogen production: potential of food waste as future energy needs. *Sci Total Environ* 888:163801. https://doi.org/10.1016/j.scitotenv.2023.163801

Monlau F, Aemig Q, Trably E, Hamelin J, Steyer JP, Carrere H (2013) Specific inhibition of biohydrogen-producing *Clostridium* sp. after dilute-acid pretreatment of sunflower stalks. *Int J Hydrogen Energy* 38:12273–12282. https://doi.org/10.1016/j.ijhydene.2013.07.018

Muñoz-Páez KM, Alvarado-Michi EL, Buitrón G, Valdez-Vazquez I (2019) Distinct effects of furfural, hydroxymethylfurfural and its mixtures on dark fermentation hydrogen

production and microbial structure of a mixed culture. *Int J Hydrogen Energy* 44:2289–2297. https://doi.org/10.1016/j.ijhydene.2018.04.139

Nasr N, Hafez H, El Naggar MH, Nakhla G (2013) Application of artificial neural networks for modeling of biohydrogen production. *Int J Hydrogen Energy* 38:3189–3195. https://doi.org/10.1016/j.ijhydene.2012.12.109

Ni M, Leung DYC, Leung MKH, Sumathy K (2006) An overview of hydrogen production from biomass. *Fuel Process Technol* 87:461–472. https://doi.org/10.1016/j.fuproc.2005.11.003

Pandey AK, Park J, Ko J, Joo HH, Raj T, Singh LK, Singh N, Kim SH (2023) Machine learning in fermentative biohydrogen production: advantages, challenges, and applications. *Bioresour Technol* 370:128502. https://doi.org/10.1016/j.biortech.2022.128502

Panin S, Setthapun W, Elizabeth Sinsuw AA, Sintuya H, Chu CY (2021) Biohydrogen and biogas production from mashed and powdered vegetable residues by an enriched microflora in dark fermentation. *Int J Hydrogen Energy* 46:14073–14082. https://doi.org/10.1016/j.ijhydene.2020.09.246

Pawar SS, Nkemka VN, Zeidan AA, Murto M, Niel EWJV (2013) Biohydrogen production from wheat straw hydrolysate using *Caldicellulosiruptor saccharolyticus* followed by biogas production in a two-step uncoupled process. *Int J Hydrogen Energy* 38:9121–9130. https://doi.org/10.1016/j.ijhydene.2013.05.075

Prakasham RS, Sathish T, Brahmaiah P (2011) Imperative role of neural networks coupled genetic algorithm on optimization of biohydrogen yield. *Int J Hydrogen Energy* 36:4332–4339. https://doi.org/10.1016/j.ijhydene.2011.01.031

Prem Ananth Surendran S, Shanmugam P (2021) Correlation between empirical formulae based stoichiometric and experimental methane potential and calorific energy values for vegetable solid wastes. *Energy Rep* 7:19–31. https://doi.org/10.1016/j.egyr.2020.10.071

Rajesh Banu J, Merrylin J, Mohamed Usman TM, Kannah RY, Gunasekaran M, Kim SH, Kumar G (2020) Impact of pretreatment on food waste for biohydrogen production: a review. *Int J Hydrogen Energy* 45:18211–18225. https://doi.org/10.1016/j.ijhydene.2019.09.176

Ramprakash B, Muthukumar K (2018) Influence of sulfuric acid concentration on biohydrogen production from rice mill wastewater using pure and coculture of *Enterobacter aerogenes* and *Citrobacter freundii*. *Int J Hydrogen Energy* 43:9254–9258. https://doi.org/10.1016/j.ijhydene.2018.03.198

Rao R, Basak N (2022) Sequential dark-photo batch fermentation and kinetic modelling for biohydrogen production using cheese whey as a feedstock. *Appl Biochem Biotechnol* 194:3930–3960. https://doi.org/10.1007/s12010-022-03958-w

Rodríguez-Valderrama S, Escamilla-Alvarado C, Magnin J-P, Rivas-Garcia P, Valdez-Vazquez I, Rios-Leal E (2020) Batch biohydrogen production from dilute acid hydrolyzates of fruits-and-vegetables wastes and corn stover as co-substrates. *Biomass Bioenergy* 140:105666. https://doi.org/10.1016/j.biombioe.2020.105666

Saidi R, Liebgott PP, Gannoun H, Gaida LB, Miladi B, Hamdi M, Bouallagui H, Auria R (2018) Biohydrogen production from hyperthermophilic anaerobic digestion of fruit and vegetable wastes in seawater: simplification of the culture medium of *Thermotoga maritima*. *Waste Manag* 71:474–484. https://doi.org/10.1016/j.wasman.2017.09.042

Sen AS, Rao R, Basak N (2024) CFD modelling of hydrodynamics and temperature distribution during photo fermentative biohydrogen generation from cheese whey effluent in cylindrical bioreactor. *Int J Hydrogen Energy* 60:740–755. https://doi.org/10.1016/j.ijhydene.2024.02.207

Sevinç P, Gündüz U, Eroglu I, Yücel M (2012) Kinetic analysis of photosynthetic growth, hydrogen production and dual substrate utilization by *Rhodobacter capsulatus*. *Int J Hydrogen Energy* 37:16430–16436. https://doi.org/10.1016/j.ijhydene.2012.02.176

Sharma AK, Ghodke PK, Goyal N, Nethaji S, Chen WH (2022) Machine learning technology in biohydrogen production from agriculture waste: recent advances and future perspectives. *Bioresour Technol* 364:128076. https://doi.org/10.1016/j.biortech.2022.128076

Shimizu S, Fujisawa A, Mizuno O, Kameda T, Yoshioka T (2008) Fermentative hydrogen production from food waste without inocula. In: *AIP Conference Proceedings*. American Institute of Physics 987(1):171–174. https://doi.org/10.1063/1.2896968

Singh A, Kuila A, Adak S, Bishai M, Banerjee R (2012) Utilization of vegetable wastes for bioenergy generation. *Agric Res* 1:213–222. https://doi.org/10.1007/s40003-012-0030-x

Singh CK, Kumar A, Roy SS (2018) Quantitative analysis of the methane gas emissions from municipal solid waste in India. *Sci Rep* 8:2913. https://doi.org/10.1038/s41598-018-21326-9

Srivastava N, Srivastava M, Abd-Allah EF, Singh R, Hashem A, Gupta VK (2021) Biohydrogen production using kitchen waste as the potential substrate: a sustainable approach. *Chemosphere* 271:129537. https://doi.org/10.1016/j.chemosphere.2021.129537

Tamang P, Nogueira R (2021) Valorisation of waste cooking oil using mixed culture into short- and medium-chain length polyhydroxyalkanoates: effect of concentration, temperature and ammonium. *J Biotechnol* 342:92–101. https://doi.org/10.1016/j.jbiotec.2021.10.006

Tenca A, Schievano A, Perazzolo F, Adani F, Oberti R (2011) Biohydrogen from thermophilic co-fermentation of swine manure with fruit and vegetable waste: maximizing stable production without pH control. *Bioresour Technol* 102:8582–8588. https://doi.org/10.1016/j.biortech.2011.03.102

United Nations Environment Programme (2024) *Food waste index report 2024. Think eat save: tracking progress to halve global food waste.* Nairobi. https://www.unep.org/resources/publication/food-waste-index-report-2024. Accessed 24 Aug 2024

Vendruscolo ECG, Mesa D, Rissi DV, Meyer BH, Pedrosa FdO, Souza EMd, Cruz LM (2020) Microbial communities network analysis of anaerobic reactors fed with bovine and swine slurry. *Sci Total Environ* 742:140314. https://doi.org/10.1016/j.scitotenv.2020.140314

Venkateswar Reddy M, Venkata Mohan S (2012) Influence of aerobic and anoxic microenvironments on polyhydroxyalkanoates (PHA) production from food waste and acidogenic effluents using aerobic consortia. *Bioresour Technol* 103:313–321. https://doi.org/10.1016/j.biortech.2011.09.040

Villanueva-Galindo E, Moreno-Andrade I (2021) Bioaugmentation on hydrogen production from food waste. *Int J Hydrogen Energy* 46:25985–25994. https://doi.org/10.1016/j.ijhydene.2020.11.092

Wang Y, Tang M, Ling J, Wang Y, Liu Y, Jin H, He J, Sun Y (2021a) Modeling biohydrogen production using different data driven approaches. *Int J Hydrogen Energy* 46:29822–29833. https://doi.org/10.1016/j.ijhydene.2021.06.122

Wang Y, Yang G, Sage V, Xu J, Sun G, He J, Sun Y (2021b) Optimization of dark fermentation for biohydrogen production using a hybrid artificial neural network (ANN) and response surface methodology (RSM) approach. *Environ Prog Sustain Energy* 40:e13485. https://doi.org/10.1002/ep.13485

Yang Z, Guo R, Shi X, He S, Wang L, Dai M, Qiu Y, Dang X (2016) Bioaugmentation of *Hydrogenispora ethanolica* LX-B affects hydrogen production through altering indigenous bacterial community structure. *Bioresour Technol* 211:319–326. https://doi.org/10.1016/j.biortech.2016.03.097

Yokoyama H, Waki M, Moriya N, Yasuda T, Tanaka Y, Haga K (2007) Effect of fermentation temperature on hydrogen production from cow waste slurry by using anaerobic microflora within the slurry. *Appl Microbiol Biotechnol* 74:474–483. https://doi.org/10.1007/s00253-006-0647-4

Chapter II

Photofermentative Production of Poly-β-hydroxybutyrate (PHB) by Purple Non-Sulfur Bacteria using Olive Oil By-products

Gianmarco Mugnai[1,2], Luca Bernabò[1], Giulia Daly[1], Elisa Corneli[1,3] and Alessandra Adessi[1]*.

[1] Department of Agriculture, Food, Environment and Forestry (DAGRI), University of Florence, Piazzale delle Cascine, 18, 50144 Florence, Italy.

[2] Department of Agricultural, Food and Environmental Sciences, University of Perugia, Borgo XX Giugno, 74, 06121 Perugia, Italy.

[3] PhotoB. Srl, Via Montecalvi, 3, San Casciano in Val Di Pesa, 50026 Florence, Italy.

* Correspondence: alessandra.adessi@unifi.it; Tel.: +39-0552755534

Manuscript published in **Bioresources and Bioprocessing** (24 March 2025)

https://doi.org/10.1186/s40643-025-00856-x

Abstract

This study evaluated the ability of six purple non-sulfur bacteria (PNSB) to convert olive oil by-products into poly-β-hydroxybutyrate (PHB). Strains were first independently cultivated in synthetic media with different carbon sources (acetic, lactic and malic acid) to assess their physiology and PHB production. Subsequently, their growth and PHB production using ingested pâté olive cake (IPOC) as a substrate were investigated. Transmission electron microscopy (TEM) observations were conducted on strains cultivated on IPOC to investigate their cell morphologies and inclusion bodies presence and size. *Rhodopseudomonas palustris* strains accumulated up to 6.8% w PHB/w cells with acetate and 0.86% w PHB/w cells with a daily productivity of 0.54 mg PHB L^{-1} culture d^{-1} on IPOC. In contrast, *Cereibacter johrii* and *Cereibacter sphaeroides* reached 58.64% w PHB/w cells and 65.45% w PHB/w cells with acetate, respectively, while *C. sphaeroides* achieved 21.48% w PHB/w cells and a daily productivity of 10.85 mg PHB L^{-1} culture d^{-1} when cultivated on IPOC. All strains exhibited growth and PHB accumulation in both synthetic media and IPOC substrate. Specifically, *R. palustris* strains 42OL, AV33 and CGA009 displayed growth capability in all substrates, while *C. johrii* strains 9Cis and PISA 7, and *C. sphaeroides* F17 showed promising PHB synthesis capabilities. TEM observations revealed that *R. palustris* strains, with smaller cell and inclusion body sizes, exhibited lower PHB accumulations, while *C. johrii* and *C. sphaeroides* strains, characterized by larger cells and inclusion bodies, demonstrated higher PHB production, recognizing them as promising candidates for PHB production using olive oil by-products. Further investigations under laboratory-scale conditions will be necessary to optimize operating parameters and develop integrated strategies for simultaneous PHB synthesis and the co-production of value-added products, thereby enhancing the economic feasibility of the process within a biorefinery framework.

Keywords

Rhodopseudomonas palustris; *Cereibacter sphaeroides*; *Cereibacter johrii*; ingested pâté olive cake (IPOC); biopolymers; resource recovery.

Highlights

- Growth and poly-β-hydroxybutyrate (PHB) production of Purple Non-Sulfur Bacteria (PNSB) on synthetic media predict their performance on olive oil by-products.
- Ingested pâté olive cake (IPOC) is a suitable substrate for PHB production.
- *R. palustris* strains utilized IPOC for cell growth, whereas *C. johrii* and *C. sphaeroides* synthesized PHB.
- 21.48% PHB/cell weight was accumulated by *C. sphaeroides* F17 on IPOC.
- Growth data and PHB production of the poorly described species *C. johrii* are reported.

Introduction

Third-generation feedstock, such as microbes, are emerging as promising biopolymer sources to replace petrochemical plastics, offering significant advantages by not competing with human food or animal feed and not requiring arable land or freshwater resources (Amadu et al. 2021). A sustainable and eco-friendly type of microbial bioplastics is polyhydroxyalkanoates (PHAs), which are biodegradable polymers obtained from microbial fermentation. Poly-β-hydroxybutyrate (PHB) is the most extensively studied PHA and can be produced by a wide variety of bacterial strains using renewable biomasses as substrates, and is degradable by several aerobic and anaerobic microorganisms (McAdam et al. 2020; Monroy and Buitrón 2020). PHB exhibits mechanical properties similar to conventional thermoplastics (Monroy and Buitrón 2020; Sirohi et al. 2021), with a melting temperature of 177 °C, a glass transition temperature of 2 °C, a tensile strength of 43 MPa, and approximately 60% crystallinity (McAdam et al. 2020; Sirohi et al. 2021). These physical and chemical properties demonstrate the wide range of possible applications: in agriculture (as fertilizer or for agrochemicals release), in the medical sector (such as in surgical sutures and long-term drug carriers), and in packaging industries (such as molded containers and food packaging materials) (McAdam et al. 2020; Monroy and Buitrón 2020; Sirohi et al. 2020, 2021; Montiel-Corona and Buitrón 2021).

A group of photosynthetic bacteria, called Purple Non-Sulfur Bacteria (PNSB), are capable of accumulating PHB (Adessi et al. 2017; Monroy and Buitrón 2020). The most studied PNSB species for PHB production include *Cereibacter sphaeroides* (formerly *Rhodobacter sphaeroides*), *Rhodopseudomonas palustris*, *Rhodobacter capsulatus*, *Rhodobacter sulfidophilus*, and *Rhodospirillum rubrum* (Argun and Kargi 2011; Adessi et al. 2017; Hördt et al. 2020). The new genus *Cereibacter* has been reported according to Hördt et al. (2020); therefore, in this work, all genera and species will be referred to by the current nomenclature, even when reporting literature published before 2020.

Microbial PHB is produced as a storage compound during starvation and accumulated in intracellular inclusions (McAdam et al. 2020; Monroy and Buitrón 2020; Fradinho et al. 2021). Several factors affect PHB production, including the type of strain, substrate, temperature, C/N ratio, nutrient concentrations, light fluxes, and pH (Sedlacek et al. 2019).

During the photofermentation process, Purple Non-Sulfur Bacteria (PNSB) can produce hydrogen or PHB using carbon substrates, including organic acids,

carbohydrates, or wastewaters and effluents deriving from other processes, such as dark fermentation (Argun and Kargi 2011; Adessi et al. 2017; Monroy and Buitrón 2020). The sustainability of fermentative processes mainly depends on the type of substrate employed as the carbon source (Adessi et al. 2017; Sirohi et al. 2020; Bhatia et al. 2021; Montiel-Corona and Buitrón 2021). Agricultural and food-processing residues represent low-cost, abundant, and renewable biomasses, providing a useful substrate for microbial growth due to their non-toxic properties and high nutrient and carbon content, including volatile fatty acids (VFAs) and simple sugars. Since the carbon source for bacterial PHB production accounts for about half of the total production costs (Brown et al. 2020), using these feedstocks as substrates can significantly reduce economic costs and environmental impact, thereby enhancing the profitability and sustainability of PHB production (Adessi et al. 2017; Monroy and Buitrón 2020; Sirohi et al. 2020, 2021; Bhatia et al. 2021). The most investigated no-cost agro-industrial wastes for PHB production using PNSB include lignin (Brown et al. 2020), agro-industrial residues (Corneli et al. 2016), cheese whey (Carlozzi et al. 2021), winery wastewater (Policastro et al. 2020), municipal solid waste (Luongo et al. 2017), digested sludge (Touloupakis et al. 2023), and olive mill wastewater (Carlozzi et al. 2019b). These studies demonstrate the metabolic flexibility of PNSB in efficiently utilizing different waste streams, highlighting their role as a promising and eco-friendly biotechnological tool for waste valorization within a bio-based and circular economy framework.

The effluent from the olive oil industry is considered one of the most polluting wastes in the Mediterranean basin due to its high salt concentration (EC 5-10 mS cm^{-1}), high acidity (pH 4-5), high biological and chemical oxygen demand (BOD and COD of 100,000 and 220,000 mg L^{-1}, respectively), and high content of polyphenols (Aharonov-Nadborny et al. 2018). The main by-products generated from the olive oil process are olive mill wastewater (OMW) and olive pomace or pâté olive cake (POC) (Foti et al. 2022). Although recent studies have demonstrated that OMW is an interesting substrate for green energy production (Mugnai et al. 2021) and biopolymers (Carlozzi et al. 2019b; Corneli et al. 2016; Padovani et al. 2016), the application of olive cake as a substrate for photofermentative processes is still lacking. POC, generated by olive oil extraction using a multiphase decanter, contains high levels of bioactive compounds such as fatty acids, proteins, and carbohydrates, representing a suitable matrix for biotechnological applications in a biorefinery perspective (Foti et al. 2022). These advantages have led to the use of POC as a valuable feedstock for anaerobic digestion, which can be conducted

in one- or two-phase systems to produce biogas and digestate. In a two-stage process, the initial stage produces an ingestate called ingested pâté olive cake (IPOC), enriched in organic acids such as acetic, propionic, and butyric acids, which serve as essential carbon and energy sources for the metabolism of PNSB.

The aim of this study was to select Purple Non-Sulfur Bacteria (PNSB) strains able to produce poly-β-hydroxybutyrate (PHB) using olive oil by-products as feedstock for sustainable bioplastics production. To achieve this goal, the experimental plan was divided into two main steps. First, the molecular identification and physiological characterization of six PNSB strains were performed using a synthetic growth medium with different single carbon sources (acetic, lactic, and malic acid), evaluating their biomass and PHB production. Second, the growth capability and PHB production of the six selected strains were investigated using ingested pâté olive cake (IPOC) as substrate

The strains used in this study include *Rhodopseudomonas palustris* strain 42OL, strain AV33, and CGA009, selected based on prior knowledge of their metabolic versatility and ability to use wastes for growth (Bianchi et al. 2010; Adessi et al. 2012, 2018). Three additional strains, *Cereibacter sphaeroides* strain F17, *Cereibacter johrii* strain PISA 7, and strain 9Cis, which have never been tested before, were selected considering the different ecological niches from which they were isolated-spanning from various wastewater treatment plants (F17 and 9Cis) to a nature reserve lacustrine area (PISA 7). The ability to thrive under different environmental conditions, including limited nutrient availability, confers a competitive advantage and drives the development of distinct metabolic traits influenced by their ecological niches. We hypothesize that the ecological niche of isolation and the life-history strategies of each strain represent critical factors that could contribute to the identification and selection of new promising strains for PHB accumulation from agro-industrial waste.

2. Materials and Methods

2.1. Strains identification

Relevant information on PNSB strains used in this study is listed in Tab. 1. The selection criteria for the strains investigated in this study were based on prior knowledge of their metabolic versatility and the ecological niches of their isolation, which could confer different metabolic traits. All strains are preserved in agar slants in the collection of the Department of Agriculture, Food, Environment and Forestry (University of Florence, Italy). After DNA extraction, the bacterial 16S rRNA region (V3–V4) was

amplified using a *GeneAmp PCR System 9700* (Applied Biosystems, UK) with the following primers: 27F and 1837R (Marchesi et al. 1998). The DNA was subsequently purified using the GeneJet PCR Purification Kit (Thermo Fisher Scientific Inc.) and its purity assessed spectrophotometrically (*NanoDrop ND-1000*, Thermo Scientific, Wilmington, USA). The rRNA sequences were obtained by an external sequencing service (CIBIACI, Florence, Italy) and identified against the NCBI nucleotide sequence database. The most similar sequences were exported, and the sequence alignment (*MUSCLE*) was generated using MEGA11 (Tamura et al. 2021). Phylogenetic tree reconstruction was performed using the neighbor-joining method (Saitou and Nei 1987). The robustness of the phylogenetic inference was estimated using the bootstrap method with 1,000 pseudo-replicates.

Table 1. List of used strains, isolation substrates and localities

Species	Isolation substrates	Isolation locality
Rhodopseudomonas palustris strain 42OL	Sugar refinery waste treatment pond	Castiglion Fiorentino, Arezzo, Italy
Rhodopseudomonas palustris strain AV33	Trophic lake	Averno, Italy
Rhodopseudomonas palustris strain CGA009	Chloramphenicol-resistant derivative of R. *palustris strain* CGA001	American Type Culture Collection (ATCC), US
Cereibacter johrii strain 9Cis	Dairy wastewater	Bologna, Italy
Cereibacter johrii strain PISA 7	Lake	San Rossore, Pisa, Italy
Cereibacter sphaeroides strain F17	Wastewater lagoon	Florence, Italy

2.2. Inoculum and batch photofermentation assays using synthetic media

Photofermentation was carried out using pure cultures of each strain. The strains were previously activated in 250 mL bottles at 25 °C with a light intensity of 150 µmol (photons) m^{-2} s^{-1} using malic RPN medium composed of: malic acid 2.0 g L^{-1}; yeast extract 0.2 g L^{-1}; K_2HPO_4 0.5 g L^{-1}; K_2PO_4 0.3 g L^{-1}; $MgSO_4 \cdot 7H_2O$ 0.4 g L^{-1}; NaCl 0.4 g L^{-1}; $CaCl_2 \cdot 2H_2O$ 0.075 g L^{-1}; ferric citrate 0.005 g L^{-1}; NH_4Cl 0.5 g L^{-1}. Trace elements were supplied by adding 10 mL L^{-1} of a solution containing: $ZnSO_4 \cdot 7H_2O$ 10 mg L^{-1}; $MnCl_2 \cdot 4H_2O$ 3 mg L^{-1}; H_3BO_3 30 mg L^{-1}; $CoCl_2 \cdot 6H_2O$ 30 mg L^{-1}; $CuCl_2 \cdot 2H_2O$ 1 mg L^{-1}; $NiCl_2 \cdot 6H_2O$ 2 mg L^{-1}; $Na_2MoO_4 \cdot 2H_2O$ 30 mg L^{-1}. All the above-cited salts were purchased from Sigma-Aldrich (USA).

The pH of the medium was adjusted to 6.8 using 2 M NaOH, both prior to and following autoclaving, with measurements performed using a pH-meter (*XS Instruments*, Italy).

The strains were grown until reaching a cell concentration of 400 mg L^{-1} to carry out the subsequent inoculation in RPN media containing different carbon sources: acetic acid (3.6 g L^{-1}) and lactic acid (1.8 g L^{-1}). The photofermentation batch assay was carried out

under anaerobic conditions using rubber-stoppered glass bottles (100 mL). Each bottle was filled with 100 mL of RPN medium with an initial cell concentration of 100 mg L^{-1} as cell dry weight (CDW). Bottles were kept at 25 °C with a light intensity of 150 µmol (photons) m^{-2} s^{-1}, supplied by a warm white LED lamp, for 14 days. Samples (2 mL per replicate) were collected three times per week, from the beginning to the end of the experiment, for determining biomass growth by spectrophotometric measurements of the optical density at 660 nm (OD_{660}) and bacteriochlorophyll a (BChl*a*) content. At the end of the experiments, samples were collected to determine CDW (15 mL per replicate), and aliquots (60 mL per replicate) were stored at –20 °C until the determination of the intracellular PHB content.

2.3. Batch photofermentation assays using ingested pâté olive cake (IPOC)

IPOC is a dark fermented effluent, obtained from the first phase of a two-phase anaerobic digestion process. The effluent was provided by *Frantoio Oleario Cassese Domenico*, located in Villa Castelli, Brindisi, Italy. The dark fermented effluent was centrifuged for 30 min at 3800 × g (22 °C) to separate the solid fraction. The suspension was then diluted with distilled water in a 1:2 v/v ratio. The concentrations of lactic and acetic acids in the IPOC were determined using a Varian ProStar HPLC chromatograph equipped with an Aminex 87H column maintained at 65 °C, a 20 µL injection loop, a UV detector (λ = 210 nm), and a refractive index (RI) detector. The eluent was 0.01 N H_2SO_4 (*Carlo Erba*, Milan, Italy) at a flow rate of 0.6 mL min^{-1}. The concentrations of metals and other inorganic compounds were determined through inductively coupled plasma–optical emission spectrometry (ICP-OES) (*Thermo Scientific™ iCAP™ 7400*, USA), following the IRSA 3010 (conventional acid mineralization) and IRSA A-3020 (determination of chemical elements by plasma emission spectroscopy) methods. The pH of IPOC was measured with a *pH-meter* (*XS Instruments*, Italy), checked before autoclaving, and adjusted to a value of 6.14 after autoclaving. The ammonium concentration was determined using the Nessler method (Adessi et al. 2012), with the *Ammonia High Range Reagent Kit HI93733-03* and the *HI93733 Photometer for Ammonium Determination* (*Hanna Instruments, Inc.*). The PNSB strains were grown using acetic RPN medium at 24 °C under continuous light until reaching a cell concentration of 400 mg L^{-1}. The biomass was then centrifuged for 20 min at 2000 × g, and the pellets were re-suspended with the IPOC substrate to a final volume of 100 mL, with an initial cell concentration of 100 mg L^{-1} CDW. The photofermentation batch assay

was carried out under anaerobic conditions using rubber-stoppered glass bottles (100 mL) equipped with a needle to allow the outflow of hydrogen possibly produced during fermentation. To avoid contamination, each needle was equipped with a 0.2 µm Nucleopore filter (*Whatman International Ltd.*, Maidstone, England). The bottles (100 mL) were kept at 25 °C under a light intensity of 150 µmol (photons) m^{-2} s^{-1} for 30 days. Bacterial growth was investigated by determining BChl*a* at the starting point (T_0; day 0) and at the end of the experiment (T_{30}; day 30). The PHB produced by PNSB was determined at the end (T_{30}) of the experiment.

2.4. Analytical methods

Biomass growth was measured in terms of optical density at a wavelength of 660 nm (OD_{660}), bacteriochlorophyll *a* (BChl*a*) content, and cell dry weight (CDW). Culture turbidity (optical density) was measured spectrophotometrically at 660 nm (OD_{660}) using a UV-3100PC UV–Vis spectrophotometer (Varian, Mulgrave, Australia). BChl*a* was determined according to Carlozzi and Sacchi (2001). Each sample was centrifuged at 4000 × g for 10 min, and the supernatant was removed. BChl*a* was extracted from the cell pellet using an acetone/methanol (7:2) mixture. The samples were incubated at 4 °C for 30 min and then centrifuged again at 4000 × g for 10 min. BChl*a* content was determined by measuring the absorbance at 775 nm (ε = 75 mM^{-1} cm^{-1}) with a Varian Cary 50 UV–Visible spectrophotometer (Varian, Mulgrave, Australia). CDW was expressed as the change in dry weight (Δ dry weight) from T_0 to T_{14}, where T_0 represents the cell dry weight after inoculation and T_{14} indicates the cell dry weight at the end of the experiments. Determination of CDW was carried out in triplicate using 5 mL culture samples, filtered through pre-weighed 0.45 µm membranes (Fisher Scientific International, Inc., Pittsburgh, PA, USA), dried at 105 °C for 3 h, and weighed on an analytical balance (Sartorius AG, Göttingen, Germany).

The intracellular content of poly-β-hydroxybutyrate (PHB) was determined in the form of crotonic acid by HPLC, according to De Philippis et al. (1992b). Briefly, acid cellular hydrolysis was carried out to convert PHB into crotonic acid. At the end of the batch assay, a 60 mL sample from each 100 mL bottle was harvested. The sample was centrifuged at 2000 × g for 10 min; the pellet was resuspended with 1 mL of distilled water and then dried at 50 °C overnight. Dried cells were weighed, and 3 mL of pure sulfuric acid was added to each screw-cap glass test tube. Subsequently, the tubes were heated at 105 °C for 30 min, cooled on ice for 10 min, and diluted to 3% with distilled

water. The solution in each tube was filtered and centrifuged at 16,000 × g for 5 min. The supernatant was then analyzed using HPLC for PHB quantification. The crotonic acid concentration was determined using a Varian ProStar HPLC system equipped with an Aminex 87H column maintained at 65 °C. The system utilized a 20 µL injection loop, UV detector (λ = 210 nm), and refractive index (RI) detector. The eluent was 0.01 N H_2SO_4 (Carlo Erba, Milan, Italy) at a flow rate of 0.6 mL min^{-1}. The equations for calculating the PHB yield, determined based on crotonic acid concentration, are provided in detail in Supplementary Material, Appendix 1.

2.5. Transmission electron microscopy (TEM)

TEM observations were performed at the end of the 30-day photofermentation batch experiments on the IPOC substrate. Bacterial cells were treated with 2.5% (w/v) glutaraldehyde at 4 °C, then suspended twice in phosphate buffer (PBS, 0.1 M, pH 7.0) for 15 min each, and treated with 1% osmium tetroxide (pH 7.0) for 1 h. Subsequently, the samples were suspended with PBS and dried. The samples were then rehydrated in a graded ethanol series (25%, 50%, 70%, 80%, 90%, and 100%) for 10 min each. Spurr's epoxy resin was used to infiltrate and embed the samples. The resin infiltration was performed in propylene oxide for 10 min using a 2:1 propylene oxide/resin solution, followed by a 1:1 propylene oxide/resin mixture for a minimum of 1 h, and finally a 1:2 propylene oxide/resin mixture from 1 h to overnight. The samples were then sectioned and post-stained with uranyl acetate and lead citrate. TEM images were acquired with a Philips CM12 transmission electron microscope (*Philips Electronics*, Amsterdam, The Netherlands) equipped with CRYO-GATAN UHRST 3500 technology and a digital camera.

2.6. Statistical analysis

All the analyses were conducted in experimental triplicates (N = 3); a minimum number of three instrumental replicates (n = 3) was always used for each measurement. To determine whether the results were significantly different, data were analyzed using one-way and two-way analysis of variance (ANOVA) at 95% confidence level, followed by Tukey's honest significant difference (HSD) post hoc test and Bonferroni post hoc test. Results were considered statistically significant at $p < 0.05$. Prior to ANOVA, all data were checked for normality assumptions using the D'Agostino-Pearson normality test and for homogeneity of variances using Bartlett's test. Statistical analyses were performed using GraphPad Prism version 9.00 (*GraphPad Software*, California, USA).

3. Results

3.1. Strains identification

The phylogenetic tree (Fig. 1) revealed three major clusters: (i) strain F17, which showed a high similarity to the type strain *Cereibacter sphaeroides* strain DSM 158^T; (ii) strain 9Cis and strain PISA 7, which showed a high similarity with the type strain *Cereibacter johrii* strain JA192^T; (iii) strain 42OL, strain AV33, and strain CGA009, which exhibited a high similarity to the type strain *Rhodopseudomonas palustris* strain ATCC 17001^T.

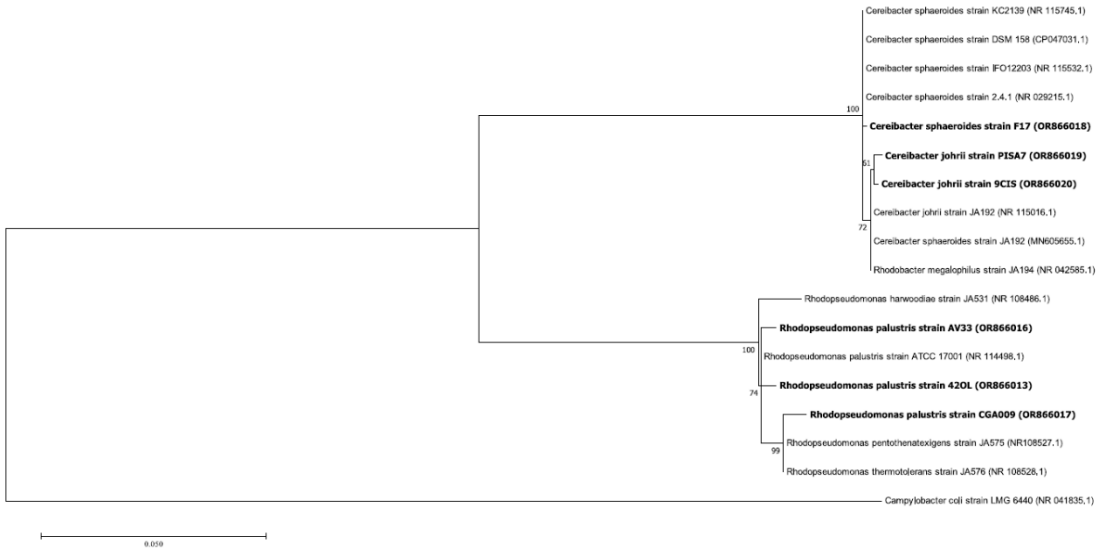

Figure 1. Phylogenetic tree analysis of sequences of the 16S rRNA regions. The numbers given on branches are frequencies (> 50%) with which a given branch appeared in 1000 bootstrap replications. The scale indicates the number of expected substitutions accumulated per site. The tree is rooted with *Campylobacter coli* strain LMG 6440. Type strains used in this study: *Cereibacter sphaeroides* strain DSM 158^T, *Rhodopseudomonas palustris* strain ATCC 17001^T, *Cereibacter johrii* strain JA192^T.

3.2. Batch photofermentation assays using synthetic media

The behaviors of the six selected strains during photoautotrophic growth on RPN medium using different single carbon sources (acetic, lactic, and malic acids) are represented in Fig. 2. *Rhodopseudomonas palustris* strain 42OL showed the highest values of OD_{660}, BChl*a*, and CDW, expressed as Δ dry weight (T_{14}-T_0), in the RPN medium with lactate, followed by the RPN medium enriched with malic acid (Fig. 2a, b, c). The lowest biomass accumulation was obtained with acetate RPN (Fig. 2a; c). *R. palustris* strain AV33 showed the highest value of BChl*a* after 5 days under lactic RPN (Fig. 2d), while no significant differences were observed in the growth of this strain on

RPN with acetic and malic acid in terms of OD_{660}, BChl*a*, and CDW by the end of the experiment (Fig. 2d, e, f).

Rhodopseudomonas palustris strain CGA009 followed a similar trend to *R. palustris* strain 42OL, showing no significant differences between the RPN with acetic acid and the RPN with malic acid, except for the BChl*a* content at the end of the experiment (Fig. 2g, h, i). The highest OD_{660}, BChl*a*, and CDW values were observed in the presence of lactate. *Cereibacter johrii* strain PISA 7 showed the most effective growth and metabolic activity when cultured in RPN with lactic acid, as indicated by higher OD_{660}, BChl*a* content, and CDW after 14 days (Fig. 2j, k, l). *C. johrii* strain 9Cis showed higher OD_{660} values after 12 days in the RPN medium with lactic acid (Fig. 2m), a trend further supported by the determination of BChl*a* content and CDW (Fig. 2n, o). *Cereibacter sphaeroides* strain F17 exhibited greater growth on the substrate enriched with acetic acid compared to the other organic acids tested, as evidenced by OD_{660}, BChl*a*, and CDW measurements (Fig. 2p, q, r).

The highest PHB content (Fig. 3), volumetric production, and daily productivity (Table 3) were detected in *Cereibacter sphaeroides* strain F17 (65.45 ± 6.08% w PHB/w cells), followed by *C. johrii* strain PISA 7 (58.64 ± 8.28% w PHB/w cells) and *C. johrii* strain 9Cis (48.18 ± 1.92% w PHB/w cells). These strains also demonstrated notable PHB accumulation when cultured in the synthetic medium with lactic acid. On the other hand, the three *Rhodopseudomonas palustris* strains accumulated low amounts of intracellular PHB, and only when grown with acetic acid as the carbon source. In particular, *R. palustris* strain CGA009 showed a PHB content of 6.87 ± 0.90% w PHB/w cells when grown on RPN with acetic acid, while *R. palustris* strain AV33 showed a content of 2.05 ± 0.33% w PHB/w cells under the same growth conditions (Fig. 3). Similarly, the PHB volumetric production and daily productivity (Tab. 3) were very low for all the *R. palustris* strains.

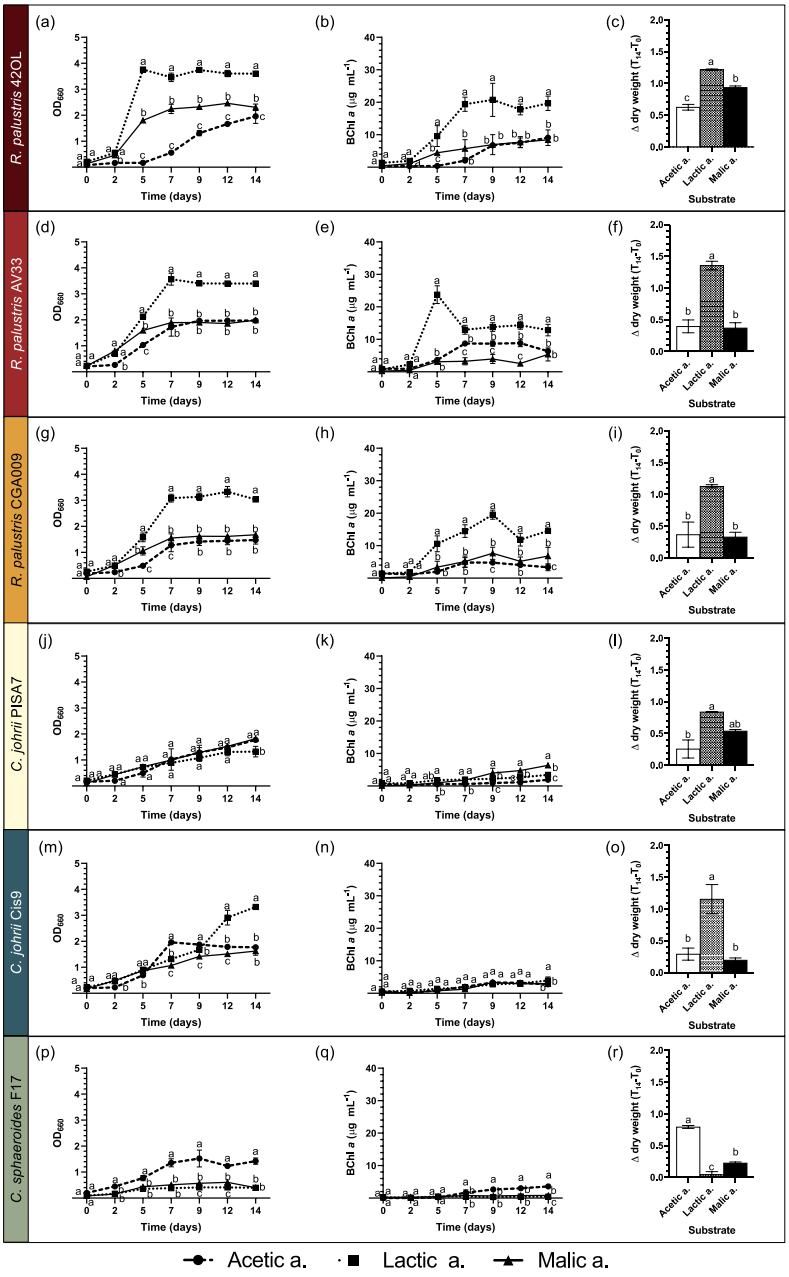

Figure 2. Optical density at 660 nm (OD_{660}), bacteriochlorophyll a (BChl*a*) content, and Δ dry weight (T_0-T_{14}), representing biomass change from T_0 to T_{14} days, measured during the growth of *Rhodopseudomonas palustris* strain 42OL (a, b, c), *R. palustris* strain AV33 (d, e, f), *R. palustris* strain CGA009 (g, h, i), *Cereibacter johrii* strain PISA 7 (j, k, l), *C. johrii* strain 9Cis (m, n, o), and *Cereibacter sphaeroides* strain F17 (p, q, r) in RPN medium with different carbon sources (acetic ●, lactic ■ , and malic ▲ acids). Results are the means of three replicates (N = 3), with error bars indicating the standard deviation (SD). Differences in the growth of each strain using different carbon sources (acetic, lactic, and malic acids) at each sampling day (OD_{660}, BChl*a*) or from T_0 to T_{14} days (Δ dry weight T_0-T_{14}) were evaluated using one-way ANOVA followed by Tukey's honest significant difference (HSD) post hoc test. Different lowercase letters indicate significant differences ($p < 0.05$).

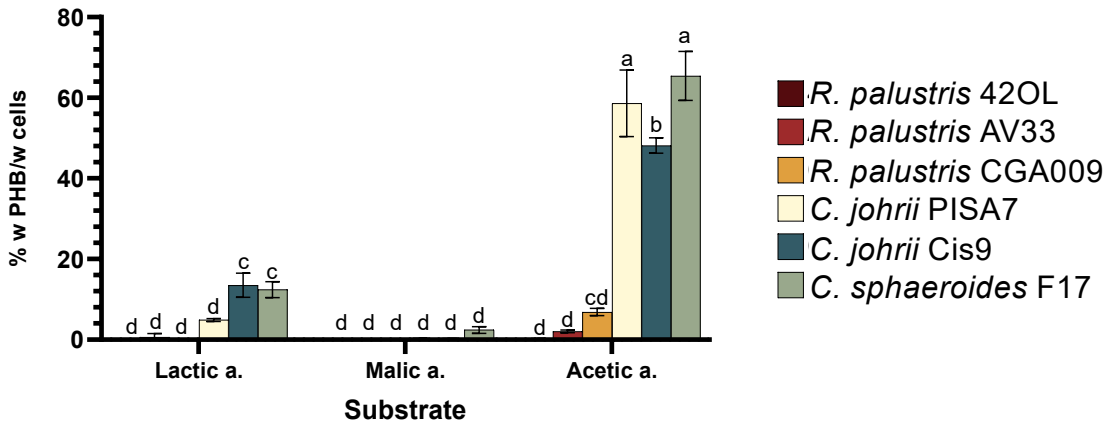

Figure 3. Intracellular poly-β-hydroxybutyrate (PHB) concentration measured at the end of the photofermentation batch assay (14-day) using RPN medium with different carbon sources (acetic, lactic, and malic acids) conducted on *R. palustris* strain 42OL, *R. palustris* strain CGA009, *R. palustris* strain AV33, *C. johrii* strain 9Cis, *C. johrii* strain PISA 7, *C. sphaeroides* strain F17. Results are the means of three replicates ($N = 3$), with error bars indicating the standard deviation (SD). Differences in PHB content among the six different strains using the three different carbon sources on the RPN medium were evaluated using one-way ANOVA followed by the Turkey's honest significance test (HSD). Different lowercase letters indicate significant differences ($p < 0.05$).

3.3. Growth capability and PHB production using IPOC

The composition of IPOC was shown in Table 2. The dark fermented effluent contained 0.73 g L^{-1} of acetic acid, 1.37 g L^{-1} of NH_4^+, a C/N ratio of 0.25 and a pH of 6.14. The compositions of metals and ions in IPOC showed a high content of K (221.54 ± 15.4 g L^{-1}), followed by Na (8.50 ± 0.18 g L^{-1}), Ca (2.49 ± 0.86 g L^{-1}), Fe (1.03 ± 0.01 g L^{-1}), S (0.25 ± 0.07 g L^{-1}), Mg (0.22 ± 0.03 g L^{-1}) and Si (0.19 ± 0.01 g L^{-1}) (Tab. 2). The suitability of IPOC for supporting the growth and PHB production of the six selected strains was investigated. *R. palustris* strain 42OL, *R. palustris* strain AV33 and *R. palustris* strain CGA009 showed a significant increase of BChl*a* content from the beginning (T_0; day 1) to the end (T_{30}; day 30) of the batch fermentation experiments (Fig. 4a). In contrast, *C. sphaeroides* strain F17, *C. johrii* strain PISA 7, and *C. johrii* strain 9Cis did not exhibit any variation of their BChl*a* content. On the other hand, the PHB content at the end of the experiment was significantly higher in the batch fermentation experiment inoculated with *C. sphaeroides* strain F17 (21.48 ± 2.43 % w PHB/w cells), followed by *C. johrii* strain PISA 7 (10.16 ± 2.26 % w PHB/w cells) and *C. johrii* strain 9Cis (9.71 ± 2.19 % w PHB/w cells) (Fig. 4b). Conversely, strains belonging to the *R. palustris* species showed a PHB content lower than 1.02 % w PHB/w cells. The PHB

volumetric production and daily productivity (Table 3) were in accordance with the trend described.

TEM observations, conducted after 30 days, revealed the presence of small granules of PHB in the cytoplasm as insoluble inclusions across all analyzed samples (Fig. 5). Among the *R. palustris* species, strain 42OL showed cells 0.86 ± 0.20 µm wide with granules with 0.14 ± 0.05 µm of diameters (Fig. 5a). Instead, *R. palustris* strain AV33 displayed a smaller cell size of 0.76 ± 0.28 µm wide with inclusion bodies size of 0.17 ± 0.04 µm (Fig. 5b). *R. palustris* strain CGA009 exhibited large cell size (1.11 ± 0.33 µm wide) and similar PHB granules size of 0.16 ± 0.04 µm (Fig. 5c). *C. johrii* strain PISA 7 exhibited a cell size of 1.23 ± 0.35 µm wide, with a comparatively larger size of PHB of 0.31 ± 0.02 µm (Fig. 5d). On the other hand, *C. johrii* strain 9Cis displayed a larger cell size of 1.45 ± 0.32 µm wide, with PHB granules measuring 0.24 ± 0.05 µm (Fig. 5e). Meanwhile, *C. sphaeroides* strain F17 showed a cell size of 1.44 ± 0.35 µm wide, and its PHB particles were notably larger (0.59 ± 0.05 µm) than the other PNSB inclusions bodies analyzed (Fig. 5f).

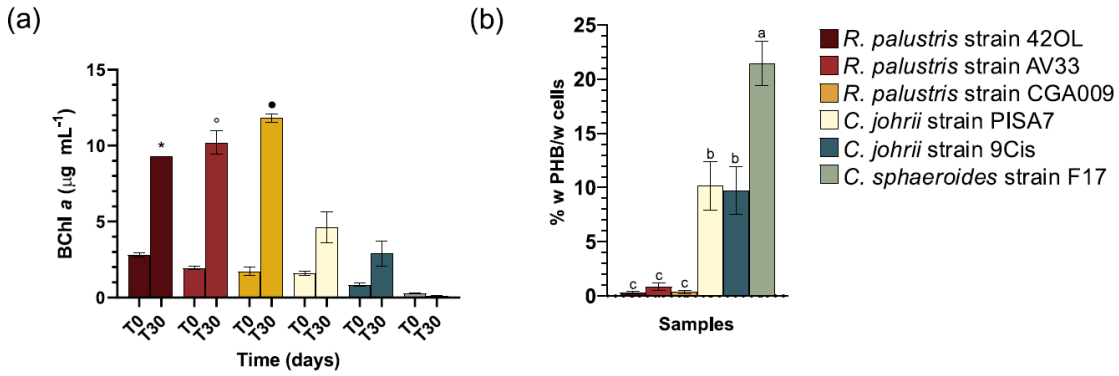

Figure 4. (a) Bacteriochlorophyll *a* content (BChl *a*) measured after inoculation (T_0; day 1) and at the end of the experiment (T_{30}; day 30) using *R. palustris* strain 42OL, *R. palustris* strain AV33, *R. palustris* strain CGA009, *C. johrii* strain PISA 7, *C. johrii* strain 9Cis, and *C. sphaeroides* strain F17 grown on IPOC substrate. Results are the means of three replicates (N = 3), with error bars indicating the standard deviation (SD). Differences in BChl *a* content between time points (T_0 and T_{30}) were evaluated using two-way ANOVA followed by Bonferroni's post-hoc test. Different symbols indicate significant differences ($p < 0.05$) in BChl *a* content between T_0 and T_{30} for each strain. (b) Intracellular poly-β-hydroxybutyrate (PHB) contents measured at the end of the 30-day photofermentation batch experiment on IPOC substrate using *R. palustris* strain 42OL, *R. palustris* strain AV33, *R. palustris* strain CGA009, *C. johrii* strain 9Cis, *C. johrii* strain PISA 7, and *C. sphaeroides* strain F17. Results are the means of three replicates (N = 3), with error bars indicating the standard deviation (SD). Differences in PHB content among the six different strains were evaluated using one-way ANOVA followed by Tukey's honest significance difference (HSD) test. Different lowercase letters indicate significant differences ($p < 0.05$).

Table 2. Composition of ingested pâté olive cake (IPOC).

Compounds	Concentration (g L^{-1})
Lactic acid (g L^{-1})	Nd
Acetic acid (g L^{-1})	0.73 (±0.01)
NH_4^+	1.37 (±0.31)
B	Nd
Ca	2.49 (±0.86)
Cd	Nd
Co	Nd
Cr	Nd
Cu	Nd
Fe	1.03 (±0.01)
K	221.54 (±15.4)
Mg	0.22 (±0.03)
Mn	Nd
Mo	Nd
Na	8.50 (±0.18)
Ni	Nd
S	0.25 (±0.07)
Si	0.19 (±0.01)
Zn	Nd

Results are expressed as mean ± standard deviation (SD), $n = 3$

* *nd* not detected

Table 3. Volumetric PHB final production (mg PHB L_{cult}^{-1}) and daily productivity (mg PHB L_{cult}^{-1} d^{-1}) for all strains grown on RPN synthetic media containing acetate, lactate or malate as carbon sources and on ingested pâté olive cake (IPOC)

Substrate →	Acetate		Lactate		Malate		IPOC	
Strain ↓	$mg_{PHB}\ L_{cult}^{-1}$	$mg_{PHB}\ L_{cult}^{-1}\ d^{-1}$	$mg_{PHB}\ L_{cult}^{-1}$	$mg_{PHB}\ L_{cult}^{-1}\ d^{-1}$	$mg_{PHB}\ L_{cult}^{-1}$	$mg_{PHB}\ L_{cult}^{-1}\ d^{-1}$	$mg_{PHB}\ L_{cult}^{-1}$	$mg_{PHB}\ L_{cult}^{-1}\ d^{-1}$
R. palustris strain 42OL	1.28 (±0.34)	0.09 (±0.02)	0.27 (±0.05)	0.02 (±0.01)	0.37 (±0.11)	0.03 (±0.01)	1.60 (±1.18)	0.11 (±0.08)
R. palustris strain AV33	17.27 (±2.91)	1.23 (±0.21)	1.18 (±0.90)	0.08 (±0.06)	0.38 (±0.34)	0.03 (±0.02)	6.41 (±2.74)	0.54 (±0.20)
R. palustris strain CGA009	40.69 (±6.13)	2.91 (±0.44)	0.72 (±0.08)	0.05 (±0.00)	0.21 (±0.14)	0.02 (±0.01)	2.39 (±0.85)	0.17 (±0.06)
C. johrii strain 9Cis	339.73 (±7.87)	24.26 (±0.56)	70.47 (±39.00)	5.03 (±2.78)	1.75 (±1.06)	0.13 (±0.08)	68.70 (±18.42)	4.83 (±1.85)
C. johrii strain PISA 7	373.89 (±55.11)	26.71 (±3.94)	25.89 (±4.19)	1.85 (±0.30)	1.71 (±1.31)	0.12 (±0.09)	73.44 (±11.78)	4.97 (±0.98)
C. sphaeroides strain F17	399.50 (±54.77)	28.54 (±3.91)	14.48 (±1.82)	1.03 (±0.13)	5.10 (±2.38)	0.36 (±0.17)	151.98 (±21.05)	10.85 (±1.50)

Results are expressed as mean ± standard deviation (SD), $n = 3$

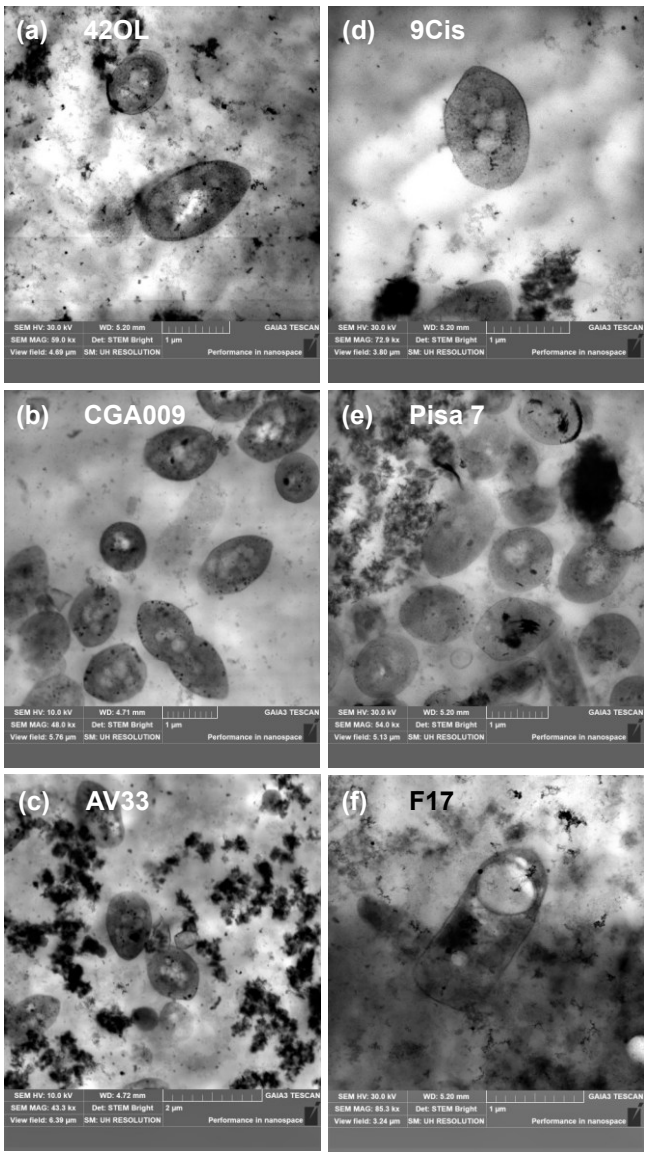

Figure 5. Transmission electron microscopy images of the inclusion bodies obtained from batch photofermentation experiments conducted using *R. palustris* strain 42OL (a), *R. palustris* strain AV33 (b), *R. palustris* strain CGA009 (c), *C. johrii* strain PISA 7 (d), *C. johrii* strain 9Cis (e) and *C. sphaeroides* strain F17 (f) at the end of the 30-day photofermentation batch experiments on IPOC substrate.

5. Discussion

The application of PNSB for PHB production has recently been expanded to strains originally investigated for hydrogen production. Their use for PHB production is supported by the knowledge previously gained regarding their physiological properties, metabolic traits, optimal growth conditions, biomass production, and carbon-to-biomass conversion efficiency during hydrogen production experiments. *R. palustris* strains 42OL, AV33 and CGA009 were primarily studied for hydrogen production (Bianchi et al.

2010; Adessi et al. 2012, 2018). Despite they are members of the same cluster and all show high adaptability to different substrates, the results obtained in this study clearly demonstrated a more efficient substrate assimilation when lactic acid was the C source, resulting in rapid cell growth. These results were also supported by the work of Dipasquale et al. (2015), where the authors found that lactate was the preferred substrate for high yield hydrogen production in combined dark-photo fermentation systems using *R. palustris* 42OL.

Among the *R. palustris* strains, the highest content of PHB was produced by the strain CGA009, which was associated with the lowest BChl a content, when acetate was used as carbon source. Indeed, the results obtained with *R. palustris* strain CGA009 showed that this strain converts acetate into PHB rather than increasing biomass, as previously noted by Carlozzi et al. (2019a) and Liebergesell et al. (1991) using *Rhodopseudomonas* sp. S16-VOGS3 and *R. palustris* 1850, respectively. Similar findings were also documented by Wu et al. (2012), utilizing *R. palustris* WP3-5, where acetate was identified as the most favorable substrate for PHB synthesis.

The low PHB accumulation by the *R. palustris* strain 42OL grown using synthetic media with different carbon sources was also confirmed by other studies, where the bacterium was cultured indoors and outdoors, using freely suspended or immobilized cells (De Philippis et al. 1992a; Vincenzini et al. 1997; Carlozzi and Sacchi 2001). Conversely, *C. sphaeroides* has been extensively documented for its ability to produce more PHB than *R. palustris* species (Monroy and Buitrón 2020). Examining the substrate preferences, our results suggested that *C. sphaeroides* strain F17 grown in the RPN medium with malate as a carbon source produced lower PHB compared to the results achieved by Yigit et al. (1999), 2.40% and 19.8% w PHB/w cells, respectively. In contrast, the results obtained using lactate were very similar to those reached by Khatipov et al. (1998) using *C. sphaeroides* RV.

In addition, it is also remarkable that the results obtained from growing the same strain with acetic acid in RPN medium revealed that this carbon source not only yielded the highest PHB content but also promoted the highest cell growth, demonstrating a significant advantage over all other substrates. One plausible explanation for this phenomenon is the easy conversion of acetate into acetyl-CoA, a key precursor in the formation of PHB, as proposed by Karthikeyan et al. (2015). In particular, comparing the PHB accumulated by *C. sphaeroides* strain F17 using acetate as carbon source with other studies (Liebergesell et al. 1991; Khatipov et al. 1998; Kemavongse et al. 2008; Kim et

al. 2011), it is worth mentioning that its production is very promising. Especially, PHB content obtained in this study by employing NH_4Cl, yeast extract, and acetate (65.45% w PHB/w cells), are higher than those reported by Khatipov et al. (1998) and Kim et al. (2011); which were 40% and 54% w PHB/w cells, respectively, obtained using ammonium and ammonium sulfate. However, a comparable yield was achieved by Liebergesell et al. (1991), with values of 63% and 69.9% w PHB/w cells in *C. sphaeroides* Y and *C. sphaeroides* 17,023, respectively, while Kemavongse et al. (2008) obtained a PHB yield of 87% w PHB/w cells using *C. sphaeroides* U7. Therefore, according to Khatipov et al. (1998) acetic acid constitutes the main carbon source promoting PHB accumulation, significantly enhanced under stress conditions, in *C. sphaeroides* (Touloupakis et al. 2021).

Although several studies have been conducted on *Rhodopseudomonas* sp. and *C. sphaeroides*, limited information is available on the species *C. johrii* (Hördt et al. 2020). The *C. johrii* strains PISA 7 and 9Cis exhibit high similarity across most of the sequenced regions of the 16S rRNA gene; however, their PHB production differs significantly depending on the different carbon sources. In particular, *C. johrii* strain PISA 7 displayed a significantly higher accumulation of PHB when grown on RPN supplemented with acetic acid, whereas PHB accumulation was comparatively lower when lactic acid was used as the carbon source, in contrast to the *C. johrii* strain 9Cis. These differences were also confirmed by growth profile results, expressed in terms of OD_{660}, BChl*a* and CDW. *C. johrii* strain PISA 7 exhibited higher BChl*a* and CDW contents when grown on lactic and malic acid as carbon sources. In contrast, *C. johrii* strain 9Cis showed higher growth performances on the lactic acid-enriched substrate.

Since malate and lactate can easily enter the TCA cycle and satisfy the cell energy needs, unlike acetate, it would be interesting to investigate the potential applications of these two new strains of *C. johrii* not only for the PHB accumulation but also for hydrogen production processes (Kars and Gündüz 2010).

Overall, metabolic profiles indicate different nutrient aptitudes among the selected six strains using culture media enriched with malic, acetic, and lactic acid. The *R. palustris* strains showed similar metabolic pattern, with lactic acid identified as the optimal carbon source for biomass production. However, despite stable growth across different single carbon sources, *R. palustris* strains displayed low PHB accumulation, likely due to unsuitable growth conditions for promoting PHB production. Therefore, a potential strategy to enhance PHB production is to use a multi-step cultivation process with

different nutrient conditions, starting with nutrient-sufficient conditions, followed by a stage of nitrogen or magnesium limitation (Corneli et al. 2016), concluding with a final stage of sulfur deficiency (Carlozzi et al. 2019a). Conversely, under the same culture conditions, *C. johrii* strains PISA 7 and 9Cis, as well as *C. sphaeroides* strain F17, exhibited limited growth but enhanced PHB accumulation. This preference for PHB production over biomass synthesis may reflect species-specific bacterial adaptations. This shift may result from a complex interplay of factors, including genetic diversity, enzyme specificity, regulatory networks, metabolic pathway flexibility, and evolutionary processes (Amadu et al. 2021). All these factors contribute to the ecological niche specialization of bacterial strains and their capacity to adapt to diverse environments.

Despite the strains exhibited a cluster-associated trend in terms of nutritional traits, growth aptitudes, and PHB productions, their characterization in pure culture and synthetic media provides several advantages, such as identifying favorable conditions to promote PHB production. On the contrary, the bioconversion of complex agro-industrial waste into valuable products requires multiple investigations into both strain capabilities and substrate composition to define the optimal conditions for successful bioconversion. In this study, based on the insights obtained from the synthetic batch experiment, the same strains were fed with ingested pâté olive cake (IPOC) to produce PHB through the photo-fermentative process.

The dark fermented effluent from the first phase of a two-phase anaerobic digestion process contained 0.73 g/L (12.00 mM) of acetic acid. Although this concentration is significantly lower than the recommended 50 mM needed to promote efficient PHB production (Monroy and Buitrón, 2020), the results obtained with the strains *C. johrii* strain PISA 7, 9Cis, and *C. sphaeroides* F17 are very promising. In contrast, strains of the *R. palustris* genus displayed a significant increase in BChl*a* content, favoring biomass production rather than PHB accumulation. The volatile fatty acids (VFAs) content in the dark fermented effluent is similar to that reported by Corneli et al. (2016) using ensiled olive pomace, as well as the PHB produced by the strains *C. johrii* PISA 7 and 9Cis. The lower VFA concentration in both these studies, compared to that of the substrate used in Padovani et al. (2016), is likely due to the high contents of phenols and furans in the solid fraction of IPOC and ensiled olive pomace (eOP), which are commonly identified as inhibitors of the acidogenesis phase of anaerobic digestion (Vavouraki et al. 2020; Caroca et al. 2021).

Another important operating parameter that could affect PHB production is the C/N ratio. Indeed, the high content of NH_4^+ (1.37 g/L) in the IPOC substrate reduced this ratio to 0.25, a value that is 120-fold lower than the recommended level for effective PHB synthesis (Monroy and Buitrón, 2020).

It is well known that the limitation or the absence of elements such as phosphorus and magnesium enhance PHB production (Corneli et al. 2016; Montiel-Corona and Buitrón, 2021; Sali and Mackey 2021). Results of ICP-OES analysis (Table 2) indicated that the Mg^{2+} content in the acetic RPN medium is about 79.8% higher than those in the IPOC substrate, acting as a limiting factor that could trigger PHB accumulation. However, this Mg^{2+} concentration is higher than that reported in ensiled olive pomace by Corneli et al. (2016). In literature, there is a lack of data regarding the influence of potassium, sodium and calcium on PHB production by PNSB. In IPOC, potassium concentrations were 270 times greater than those in the acetic RPN medium, sodium 53 times higher, and calcium levels were over 33 times higher than in the synthetic medium. Such elevated concentrations of calcium, sodium and potassium may affect cellular osmotic balance and could potentially reduce the ability of PNSB to produce PHB (Obruca et al. 2017). Furthermore, the high concentration of trace metals, such as Fe, which is more than 200 times higher in IPOC than in acetic RPN medium, can also negatively affect the PHB yield (Monroy and Buitrón, 2020).

Overall, different strains adopted different metabolic strategies when fed with the IPOC substrate, likely driven by highly specialized metabolic pathways shaped by the selective pressures of their ecological niches. Strains belonging to *R. palustris* (strains 42OL, CGA009 and AV33) used the IPOC substrate through a replicative metabolism, increasing their biomass during the incubation. In contrast, the *C. johrii* strains PISA 7 and 9Cis, along with *C. sphaeroides* F17, promoted PHB metabolism by converting carbon sources into precursors that were then polymerized to form PHB granules within the cells. The distinct metabolic strategies adopted by the different strains in this study were confirmed by transmission electron microscopy (TEM) micrographs. *R. palustris* strains exhibited smaller cells with small inclusion bodies, while *C. johrii* strains PISA 7 and 9Cis displayed larger cells containing PHB granules twice the size of those observed in *R. palustris*. Notably, *C. sphaeroides* strain F17 showed the largest cell size and the most substantial PHB granules among all the examined PNSB, providing comprehensive insight into their distinctive metabolic behaviors. Furthermore, the volumetric production, daily productivity and PHB content achieved in this study with *C. sphaeroides* strain F17

(21.48 ± 2.43% w PHB/w cells) represent the basis for a promising biotechnological application, exceeding previously reported content for untreated IPOC, including Corneli et al. (2016; 11.54 ± 0.64% w PHB/w cells), Padovani et al. (2016; 9.0% w PHB/w cells), and Carlozzi et al. (2019b; 15.7% w PHB/w cells). These findings highlight the remarkable capability of *C. sphaeroides* strain F17 in bioconverting complex waste substrates. The differences in PHB accumulation observed for *C. sphaeroides* strain F17 when comparing the synthetic media and IPOC may be linked to the specific metabolic behaviors of this strain or to the effects of certain IPOC-derived compounds that influence PHB synthesis through distinct mechanisms. These findings highlight the need for further investigation into the molecular and biochemical mechanisms underlying strain-specific responses to complex substrates such as IPOC.

The current work used an integrated approach of phylogenetic analysis, metabolic characterization and morphological evaluation to identify strains suitable for waste valorization through PHB accumulation. While photosynthetic bacteria offer standard advantages, such as reduced aeration requirements and the ability to utilize a wide range of waste substrates, phylogenetic analysis and metabolic characterizations conducted on synthetic media and in pure culture provide predictive insights into their performance on complex substrates, such as IPOC. Furthermore, the morphological characterization of the strains using TEM observation conducted directly on the selected PNSB strains grown on the complex IPOC substrate offers a significant advantage. This approach provides valuable information on cell dimensions and inclusion body sizes, which are strictly associated with the PHB yields. It also highlights the adaptability of the strains during growth in IPOC, which is among the most inhibitory substrates for microbial growth in the Mediterranean basin due to its high content of phenolic and antimicrobial compounds. These findings enhance our understanding of strain-specific responses and their capacity for PHB accumulation.

In addition, growing these strains on the IPOC substrate also presents several challenges. High concentrations of ammonium and phenolic compounds in IPOC can inhibit acetic acid production, thereby limiting PHB accumulation. Additionally, elements such as iron, potassium, and calcium present in IPOC may interfere with PHB synthesis, highlighting the necessity for targeted optimization strategies to enhance metabolic performance. Despite these limitations, the PHB yield achieved in this study with *C. sphaeroides* strain F17 highlights its suitability as a valuable candidate for producing PHB and other substances of economic interest.

6. Conclusion

The bioconversion of olive mill wastes into high-value bioproducts, specifically PHB, using six strains from three distinct species (*R. palustris*, *C. sphaeroides*, and *C. johrii*), has provided significant insight into their metabolic capabilities and bioconversion potential. The dual aptitudes of these strains, characterized by their replication strategies and PHB production capabilities, along with their distinct morphological traits, have provided paramount information for identifying promising candidates for further investigation. Among these, *C. sphaeroides* strain F17 and the novel *C. johrii* strains 9Cis and PISA 7 have emerged as interesting candidates for future research.

Future laboratory-scale studies should focus on optimizing the growth conditions and PHB production of these strains by investigating the effects of key parameters, such as temperature, pH, and nutrient concentrations. Parallel efforts should focus on the optimization of treatments for the IPOC substrate to mitigate potential inhibitory factors, including high concentrations of phenols, iron, calcium, potassium, and nitrogen, while enhancing the availability of acetic acid.

These laboratory-scale efforts must finally be validated on the pilot scale, where productivity and production costs are assessed to establish the feasibility of future industrial applications. This comprehensive approach will lay the foundations for the development of an efficient and economically viable biorefinery process.

Acknowledgements

The Authors would like to acknowledge Dr. Maria Cristina Salvatici at CE.M.E., CNR, Florence, Italy for the electron micrographs and MIOOLIO Frantoio Oleario Cassese Domenico for providing the IPOC.

Author contributions

GM: Conceptualization; Formal Analysis, Methodology, Data Curation, Writing-Original Draft, Writing-Review & Editing; LB: Formal Analysis, Methodology, Writing-Original Draft, Writing-Review & Editing; GD: Formal Analysis, Writing-Review & Editing; EC: Conceptualization, Writing-review&editing; AA: Conceptualization, Supervision, Writing-review&editing.

References

Adessi A, McKinlay JB, Harwood CS, De Philippis R (2012) *A Rhodopseudomonas palustris nifA* mutant produces H_2 from NH_4^+-containing vegetable wastes.* Int J Hydrogen Energy* 37:15893–15900. https://doi.org/10.1016/j.ijhydene.2012.08.009

Adessi A, Corneli E, De Philippis R (2017) Photosynthetic purple non sulfur bacteria in hydrogen producing systems: new approaches in the use of well known and innovative substrates. In: Hallenbeck PC (ed) *Modern Topics in the Phototrophic Prokaryotes*, 1st edn. Springer, Cham, pp 321–350

Adessi A, Venturi M, Candeliere F et al (2018) Bread wastes to energy: sequential lactic and photo-fermentation for hydrogen production. *Int J Hydrogen Energy* 43:9569–9576. https://doi.org/10.1016/j.ijhydene.2018.04.053

Aharonov-Nadborny R, Tsechansky L, Raviv M, Graber ER (2018) Mechanisms governing the leaching of soil metals as a result of disposal of olive mill wastewater on agricultural soils. *Sci Total Environ* 630:1115–1123. https://doi.org/10.1016/j.scitotenv.2018.02.270

Amadu AA, Qiu S, Ge S et al (2021) A review of biopolymer (Poly-β-hydroxybutyrate) synthesis in microbes cultivated on wastewater. *Sci Total Environ* 756:143729. https://doi.org/10.1016/j.scitotenv.2020.143729

Argun H, Kargi F (2011) Bio-hydrogen production by different operational modes of dark and photo-fermentation: an overview. *Int J Hydrogen Energy* 36:7443–7459. https://doi.org/10.1016/j.ijhydene.2011.03.116

Bhatia SK, Otari SV, Jeon JM et al (2021) Biowaste-to-bioplastic (polyhydroxyalkanoates): conversion technologies, strategies, challenges, and perspective. *Bioresour Technol* 326:124733. https://doi.org/10.1016/j.biortech.2021.124733

Bianchi L, Mannelli F, Viti C et al (2010) Hydrogen-producing purple non-sulfur bacteria isolated from the trophic lake Averno (Naples, Italy). *Int J Hydrogen Energy* 35:12216–12223. https://doi.org/10.1016/j.ijhydene.2010.08.038

Brown B, Immethun C, Wilkins M, Saha R (2020) *Rhodopseudomonas palustris* CGA009 polyhydroxybutyrate production from a lignin aromatic and quantification via flow cytometry. *Bioresour Technol Rep* 11:100474. https://doi.org/10.1016/j.biteb.2020.100474

Carlozzi P, Sacchi A (2001) Biomass production and studies on Rhodopseudomonas palustris grown in an outdoor, temperature controlled, underwater tubular photobioreactor. *J Biotechnol* 88:239–249. https://doi.org/10.1016/S0168-1656(01)00280-2

Carlozzi P, Giovannelli A, Traversi ML et al (2019a) Poly-3-hydroxybutyrate and H_2 production by *Rhodopseudomonas sp*. S16-VOGS3 grown in a new generation photobioreactor under single or combined nutrient deficiency. *Int J Biol Macromol* 135:821–828. https://doi.org/10.1016/j.ijbiomac.2019.05.220

Carlozzi P, Seggiani M, Capperucci A et al (2019b) Hydroxytyrosol rich-mixture from olive mill wastewater and production of green products by feeding *Rhodopseudomonas sp*. S16-FVPT5 with the residual effluent. *J Biotechnol* 295:28–36. https://doi.org/10.1016/j.jbiotec.2019.02.006

Carlozzi P, Giovannelli A, Traversi ML, Touloupakis E (2021) Poly(3-hydroxybutyrate) bioproduction in a two-step sequential process using wastewater. *J Water Process Eng* 39:101700. https://doi.org/10.1016/j.jwpe.2020.101700

Caroca E, Serrano A, Borja R et al (2021) Influence of phenols and furans released during thermal pretreatment of olive mill solid waste on its anaerobic digestion. *Waste Manage* 120:202–208. https://doi.org/10.1016/j.wasman.2020.11.027

Corneli E, Adessi A, Dragoni F et al (2016) Agroindustrial residues and energy crops for the production of hydrogen and poly-β-hydroxybutyrate via photofermentation. *Bioresour Technol* 216:941–947. https://doi.org/10.1016/j.biortech.2016.06.046

De Philippis R, Ena A, Guastiini M et al (1992a) Factors affecting poly-β-hydroxybutyrate accumulation in cyanobacteria and in purple non-sulfur bacteria. *FEMS Microbiol Lett* 103:187–194. https://doi.org/10.1016/0378-1097(92)90309-C

De Philippis R, Sili C, Vincenzini M (1992b) Glycogen and poly-β-hydroxybutyrate synthesis in *Spirulina maxima*. *J Gen Microbiol* 138:1623–1628. https://doi.org/10.1099/00221287-138-8-1623

Dipasquale L, Adessi A, d'Ippolito G et al (2015) Introducing capnophilic lactic fermentation in a combined dark-photo fermentation process: a route to unparalleled H_2 yields. *Appl Microbiol Biotechnol* 99:1001–1010. https://doi.org/10.1007/s00253-014-6231-4

Foti P, Pino A, Romeo FV et al (2022) Olive pomace and pâté olive cake as suitable ingredients for food and feed. *Microorganisms* 10:1–12. https://doi.org/10.3390/microorganisms10020237

Fradinho J, Allegue LD, Ventura M et al (2021) Up-scale challenges on biopolymer production from waste streams by purple phototrophic bacteria mixed cultures: a critical review. *Bioresour Technol*. https://doi.org/10.1016/j.biortech.2021.124820

Hördt A, López MG, Meier-Kolthoff JP et al (2020) Analysis of 1,000+ type-strain genomes substantially improves taxonomic classification of *Alphaproteobacteria*. *Front Microbiol*. https://doi.org/10.3389/fmicb.2020.00468

Kars G, Gündüz U (2010) Towards a super H_2 producer: improvements in photofermentative biohydrogen production by genetic manipulations. *Int J Hydrogen Energy* 35:6646–6656. https://doi.org/10.1016/j.ijhydene.2010.04.037

Karthikeyan OP, Chidambarampadmavathy K, Cirés S, Heimann K (2015) Review of sustainable methane mitigation and biopolymer production. *Crit Rev Environ Sci Technol* 45:1579–1610. https://doi.org/10.1080/10643389.2014.966422

Kemavongse K, Prasertsan P, Upaichit A, Methacanon P (2008) Poly-β-hydroxyalkanoate production by halotolerant *Rhodobacter sphaeroides* U7. *World J Microbiol Biotechnol* 24:2073–2085. https://doi.org/10.1007/s11274-008-9712-8

Khatipov E, Miyake M, Miyake J, Asada Y (1998) Accumulation of poly-β-hydroxybutyrate by *Rhodobacter sphaeroides* on various carbon and nitrogen substrates. *FEMS Microbiol Lett* 162:39–45. https://doi.org/10.1016/S0378-1097(98)00099-8

Kim MS, Kim DH, Son HN et al (2011) Enhancing photo-fermentative hydrogen production by *Rhodobacter sphaeroides* KD131 and its PHB synthase deleted-mutant from acetate and butyrate. *Int J Hydrogen Energy* 36:13964–13971. https://doi.org/10.1016/j.ijhydene.2011.03.099

Liebergesell M, Hustede E, Timm A et al (1991) Formation of poly(3-hydroxyalkanoates) by phototrophic and chemolithotrophic bacteria. *Arch Microbiol* 155:415–421. https://doi.org/10.1007/BF00244955

Luongo V, Ghimire A, Frunzo L et al (2017) Photofermentative production of hydrogen and poly-β-hydroxybutyrate from dark fermentation products. *Bioresour Technol* 228:171–175. https://doi.org/10.1016/j.biortech.2016.12.079

Marchesi JR, Sato T, Weightman AJ et al (1998) Primer für 16S rRNA. *Appl Environ Microbiol* 64:795–799

McAdam B, Fournet MB, McDonald P, Mojicevic M (2020) Production of polyhydroxybutyrate (PHB) and factors impacting its chemical and mechanical characteristics. *Polymers* 12:1–20. https://doi.org/10.3390/polym12122908

Monroy I, Buitrón G (2020) Production of polyhydroxybutyrate by pure and mixed cultures of purple non-sulfur bacteria: a review. *J Biotechnol* 317:39–47. https://doi.org/10.1016/j.jbiotec.2020.04.012

Montiel-Corona V, Buitrón G (2021) Polyhydroxyalkanoates from organic waste streams using purple non-sulfur bacteria. *Bioresour Technol*. https://doi.org/10.1016/j.biortech.2020.124610

Mugnai G, Borruso L, Mimmo T et al (2021) Dynamics of bacterial communities and substrate conversion during olive-mill waste dark fermentation: prediction of the metabolic routes for hydrogen production. *Bioresour Technol* 319:124157. https://doi.org/10.1016/j.biortech.2020.124157

Obruca S, Sedlacek P, Mravec F et al (2017) The presence of PHB granules in cytoplasm protects non-halophilic bacterial cells against the harmful impact of hypertonic environments. *N Biotechnol* 39:68–80. https://doi.org/10.1016/j.nbt.2017.07.008

Padovani G, Carlozzi P, Seggiani M et al (2016) PHB-rich biomass and $BioH_2$ production by means of photosynthetic microorganisms. *Chem Eng Trans* 49:55–60. https://doi.org/10.3303/CET1649010

Policastro G, Luongo V, Fabbricino M (2020) Biohydrogen and poly-β-hydroxybutyrate production by winery wastewater photofermentation: effect of substrate concentration and nitrogen source. *J Environ Manage* 271:111006. https://doi.org/10.1016/j.jenvman.2020.111006

Saitou N, Nei M (1987) The neighbor-joining method: a new method for reconstructing phylogenetic trees. *Mol Biol Evol* 4:406–425

Sali S, Mackey HR (2021) The application of purple non-sulfur bacteria for microbial mixed culture polyhydroxyalkanoates production. *Rev Environ Sci Biotechnol* 20:959–983. https://doi.org/10.1007/s11157-021-09597-7

Sedlacek P, Slaninova E, Koller M et al (2019) PHA granules help bacterial cells to preserve cell integrity when exposed to sudden osmotic imbalances. *N Biotechnol* 49:129–136. https://doi.org/10.1016/j.nbt.2018.10.005

Sirohi R, Prakash Pandey J, Kumar Gaur V et al (2020) Critical overview of biomass feedstocks as sustainable substrates for the production of polyhydroxybutyrate (PHB). *Bioresour Technol* 311:123536. https://doi.org/10.1016/j.biortech.2020.123536

Sirohi R, Kumar Gaur V, Kumar Pandey A et al (2021) Harnessing fruit waste for poly-3-hydroxybutyrate production: a review. *Bioresour Technol* 326:124734. https://doi.org/10.1016/j.biortech.2021.124734

Tamura K, Stecher G, Kumar S (2021) MEGA11: molecular evolutionary genetics analysis version 11. *Mol Biol Evol* 38:3022–3027. https://doi.org/10.1093/molbev/msab120

Touloupakis E, Poloniataki EG, Ghanotakis DF, Carlozzi P (2021) Production of biohydrogen and/or poly-β-hydroxybutyrate by *Rhodopseudomonas sp.* using various carbon sources as substrate. *Appl Biochem Biotechnol* 193:307–318. https://doi.org/10.1007/s12010-020-03428-1

Touloupakis E, Chatziathanasiou A, Ghanotakis DF et al (2023) Poly(3-hydroxybutyrate) production by *Rhodopseudomonas sp.* S16-VOGS3 cells grown in digested sludge. *Environ Technol Innov* 30:103058. https://doi.org/10.1016/j.eti.2023.103058

Vavouraki AI, Zakoura MV, Dareioti MA, Kornaros M (2020) Biodegradation of polyphenolic compounds from olive mill wastewaters (OMW) during two-stage anaerobic co-digestion of agro-industrial mixtures. *Waste Biomass Valorization* 11:5783–5791. https://doi.org/10.1007/s12649-019-00887-4

Vincenzini M, Marchini A, Ena A, De Philippis R (1997) H_2 and poly-β-hydroxybutyrate, two alternative chemicals from purple non-sulfur bacteria. *Biotechnol Lett* 19:759–762. https://doi.org/10.1023/A:1018336209252

Wu CW, Whang LM, Cheng HH, Chan KC (2012) Fermentative biohydrogen production from lactate and acetate. *Bioresour Technol* 113:30–36. https://doi.org/10.1016/j.biortech.2011.12.130

Yigit DÖ, Gündüz U, Türker L et al (1999) Identification of by-products in hydrogen producing bacteria; *Rhodobacter sphaeroides* O.U. 001 grown in the wastewater of a sugar refinery. *J Biotechnol* 70:125–131. https://doi.org/10.1016/S0168-1656(99)00066-8

Appendix 1: calculation of polyhydroxybutyrate (PHB) content based on crotonic acid concentration.

This calculation aims to estimate the percentage of PHB in a sample, based on the concentration of crotonic acid obtained from High-Performance Liquid Chromatography (HPLC) analysis. This approach involves a stoichiometric conversion and adjustment for water loss.

Methodology

Assumptions and definitions.

A. Let X be the concentration of crotonic acid detected in the sample.
B. Molar mass value:
   - Crotonic acid ($MW_{\text{crotonic acid}}$) = 86.09 g/mol
   - 3-hydroxybutyric acid ($MW_{\text{3-hydroxybutyric acid}}$) = 104.11 g/mol

Calculation step.

1. Calculate moles of crotonic acid based on X:

$$Moles\ of\ crotonic\ acids\ = \frac{X}{MW_{crotonic\ acid}}$$

2. Assume moles of 3-hydroxybutyric acid are equivalent:

$$Moles\ of\ 3-\text{hydroxybutyric acid}\ = \frac{X}{MW_{crotonic\ acid}}$$

3. Calculate the concentration of 3-hydroxybutyric acid in mg/L:

$$\text{Concentration of } 3-\text{hydroxybutyric acid}\ =\ \text{X}\ \times \frac{MW_{3-hydroxybutyric\ acid}}{MW_{crotonic\ acid}}$$

4. Adjust for sample volume. Assuming the sample volume was 100 mL (as opposed to 1L), adjust the concentration accordingly:

$$\text{Mass of 3hydroxybutyric acid in 100 mL} =$$

$$= \text{X} \times \frac{MW_{3-hydroxybutyric\ acid}}{MW_{crotonic\ acid}} \times \frac{100\ mL}{1000\ mL}$$

5. Adjust for water loss using a proportion to account for water molecule (half a water molecule)

$$0.043 : 0.036 = \text{Mass of 3-hydroxybutyric acid in 100 mL} : Y$$

Solving for Y (mg of PHB in 100 ml), the corrected PHB mass:

$$Y = \frac{0.036 \times \text{Mass of } 3-\text{hydroxybutyric acid in 100 mL}}{0.043}$$

6. Calculate PHB content on Dry Cell Weight basis. Given a dry cell weight of cells W (e.g., 165 mg), calculate the PHB %:

$$PHB\ \%\ (Dry\ Weight) = \frac{Y}{W} \times 100$$

This calculation is a stoichiometric approach for estimating PHB content based on crotonic acid concentration and is suitable for conditions where crotonic acid is a reliable marker for PHB breakdown.